Reservoir Rock Geostatistics and Well-to-Well Tracer Tests by Simulations and Laboratory Experiments

Saleem Ghous Khan Ghori

Submitted in Partial Fulfillment
of the Requirements for the Degree of
Doctor of Philosophy in Petroleum Engineering

New Mexico Institute of Mining and Technology
Socorro, New Mexico
May, 1992

Acknowledgments

This author is greatly indebted to his adviser Dr. John P. Heller for his continuous advice, guidance and encouragement during the course of this research.

I also wish to thank the members of my thesis committee, Dr. Allan Gutjahr, Dr. Ashok Singh, Dr. William Lyons and Dr. James Smoake for their advice and encouragement.

Special thanks to Sandra Ishmael for her continuous support and work for this thesis. I also acknowledge my colleagues for their helpful discussion and suggestions. Deep gratitude is also expressed to James McLemore and Tariq Ahsan for their assistance in the experimental work.

The authors thank the New Mexico Petroleum Recovery Research Center for supporting this work. Financial contributions for this work were furnished, as part of their support for a broader project, by the PRRC, the New Mexico Research and Development Institute, the U.S. Department of Energy, and a consortium of corporations including the Abu Dhabi National Reservoir Research Foundation, AMOCO Production Company, ARCO Oil and Gas, BP Exploration Company, Chevron Oilfield Research, Oxy Oil and Gas, CONOCO, Japan National Oil Corporation, JAPEX Research Center, Marathon, Petro-Canada Resources, and Texaco. Their support is gratefully acknowledged.

Finally, for their everlasting love and support regardless of their physical absence, I dedicate this work to my parents Ghous Mohammed Khan, Saeeda Perveen, and to my sister Rani.

Table of Contents

List of Figures

List of Tables

Abstract

Tracer tests have been widely used in the petroleum industry in determining qualitative information about underground reservoirs, such as the existence of flow barriers, directional flow paths, etc. This paper describes a basis on which well-to-well tracer tests can be used to obtain quantitative information about the geostatistical parameters (variance and correlation scale) of permeability. Both theoretical and experimental results are presented.

In the theoretical work, a catalogue of tracer production curves for different sets of geostatistical parameters and several flooding patterns is produced. These are computed with the help of a new numerical technique that is stable and devoid of any numerical dispersion. The effects of variance of the natural logarithm of the permeability (ranging from .14 to 2.25), the dimensionless correlation scale (ranging from .2 to .5) and of numerous realizations, are quantified. The general effect of areal heterogeneity is that multiple peaks appear in the output tracer concentration curve, even when the flow is confined to a single layer. An increase in variance generally increases the number of prominent peaks in the output concentration profile, decreases the time between the emergence of peaks and increases the time span of the occurence of the tracer. An increase in correlation scale generally decreases the number of peaks. By using a sufficient number of permeability realizations, an attempt is made to assess the variance and correlation length of the permeability field from the tracer and output concentration curves.

In the experimental work, a slab of rock (Arizona Flagstone) that could represent a quarter of five-spot pattern is selected. A simple minipermeameter is used to measure areal permeability on grids of points on both top and bottom surfaces of the rock. A tracer test is performed and the tracer output concentrations are measured at six intervals along the depth of the rock at the production well. Six different types of concentration curves were obtained, which shows that downhole sampling of the tracer is important in achieving adequate information about the reservoir rock. Permeabilities measured from the minipermeameter are used as input into the simulator. The numerical production curves are then compared with

the experimental profiles. The occurrences of similar patterns of multiple peaks confirm8CD that well-to-well tracer tests can be used to estimate the geostatistical parameters of the permeability field.

Assessment of reservoir property distribution from the known data is one of the major purposes of geostatistical methods. In this work, a new linear and unbiased estimation method is presented. The new method is based on the conditioning of the source points in the *source point method* and is called the *conditioned source point method* (CSPM). The new method is compared with the kriging method by using a set of permeability data that was measured with a minipermeameter device. The CSPM is compared for computer efficiency, incorporation of anisotropy in the estimated field, relative error, variograms and spatial distribution of high and low permeability values.

Results have shown that, like kriging, the CSPM can be used in the conditional simulation method (CS) in the sense that the desired variograms are reproduced in the simulated fields. There is an improvement in CPU time of more than 300% over the conventional CS method. The simulated fields from CSPM produce variograms that are close to experimental variograms. The spatial distribution of the highs and lows are comparable in both the two methods. The method can easily produce anisotropic fields and is a good substitute for methods like kriging.

1 Introduction

It has been recognized that heterogeneity of the reservoir is one of the most important characteristics that influence oil recovery. This is especially true in enhanced oil recovery projects (EOR) where displacement patterns are more critical (Lasseter, et al., 1986; Weber, 1986). The most important aspect of reservoir heterogeneity may be the spatial permeability variations. It is impossible to quantify this by single values, but the spatial distribution can be described by probabilistic theory (Journel and Huijbregts, 1978; Matheron, 1973; Marsily, 1984). Unfortunately, not enough actual field permeability data is available to define the spatial permeability variation statistically. In general, to characterize the heterogeneity of a reservoir, one needs to know not only the parameters of the distribution (the mean and variance) but also the parameters describing the auto-correlation of nonuniformities in the field. The correlation structure, in fact, has been observed at different scales from pore level to interwell distance (Bahralolom and Heller, 1989; Goggin, et al., 1989).

Radioactive or chemical tracers have long been used in reservoir floods to give information about reservoir and flow characteristics (Wagner, 1977; Carpenter, et al., 1954; Strum and Johnson, 1951). This information is usually obtained from the tracer breakthrough profile at the production well. The profiles at multiple production wells have also been studied extensively (Lichtenberger, 1990). In a flooding pattern, tracer output concentration at the well is the summation of tracer responses from many streamlines that constitute the flow geometry inside the reservoir. In addition, the tracer flow is affected by dispersion which is mainly due to tortousity of the flow paths at the microscopic scale and the variation in permeability of the reservoir rock. Operating engineers use output concentration at the production well to predict the behavior of the reservoir qualitatively, (Wagner, 1977) but these tests do not reveal quantitative information about the permeability heterogeneity. A great deal of information is lost in surface sampling of the tracer. With the help of laboratory tracer experiments, we show that quantitative information can be obtained with multiple subsurface sampling of the tracer.

Mathematically, the two dimensional flow of a miscible tracer is described by the well-known convective-dispersion equation.

$$\frac{\partial C}{\partial t} = -\frac{\mathbf{u}}{\phi S_w}\nabla C + \nabla \cdot \mathbf{D} \cdot \nabla C \tag{1.1}$$

where u = Darcy velocity, in the x direction; ϕ = porosity; $\mathbf{D}$ = dispersion tensor. For a non-uniform flow field where the Darcy velocity and dispersion coefficients are functions of position, Eq. (1.1) becomes a second-order partial differential equation in three independent variables (x, y, t) with variable coefficients. Even in two dimensions, the exact analytical or numerical solutions for a nonuniform flow field are not available. Existing numerical simulation procedures can show instability problems or suffer from numerical dispersion, especially on a large field scale (Peaceman and Rachford, 1962; Fanchi, 1983). Several techniques are described in the literature (Chaudhari, 1971; Stone and Brian, 1963; Larson, 1982; Garder, et al., 1963; Laumbach, 1975) that attempt to minimize the effect of numerical dispersion, but its elimination has not been completely achieved.

This study imparts a better understanding of the effect of geostatistical parameters (variance and correlation length) permeability on the displacement of a miscible tracer in flooding patterns such as the five-spot, the staggered line drive, and the direct line drive. A single component, single phase, miscible tracer with unit mobility ratio for numerical computations is considered. The formation is assumed to have only a single layer.

The computations are performed in several steps. In the first of these steps, a synthesized permeability field is generated by the Source Point Method (SPM) (Heller, 1972). Secondly, an efficient computer simulator is used to obtain solutions to pressure equations for the Darcy velocity. The source point method is modified to include the effect of anisotropy in the generated fields. A new numerical method is presented to compute the changing fluid composition for the solution of the convective-dispersion equation. This numerical technique was originated by Heller (1986), who applied the technique to a one dimensional radial flow problem. After the application of this technique, the tracer concentration curves of the pro-

duced fluid are then computed to see the effect of two parameters (variance and correlation length) of the permeability distribution and of the dispersivity of the rock. It has been observed that tracer output concentration curves are also affected by realizations (seed values in the generation of random numbers) of the generated permeability field. Therefore, an attempt is made to quantify the effect of realizations on the tracer output concentration curves. In the laboratory, a tracer experiment is performed in two stages. In the first stage, permeability at both top and bottom surfaces of a rock sample (Arizona Flagstone representing a quarter of five-spot pattern) are measured with the help of a minipermeameter device. A single phase, single component, miscible tracer test is then performed. Finally, both numerical and experimental results are compared and analyzed.

Determination of the geostatistical parameters is helpful in the geostatistical techniques, such as kriging and conditional simulation. In this study, conditional simulation with a new estimation method is presented in the last chapter.

2 Literature Review

This chapter presents the literature relevant to this study. The chapter is divided into four main sections. In the first section, literature related to the interpretation of reservoir rocks from a tracer test is presented. The second part discusses the mechanism of tracer flow in a porous media. In this part, the origin of equations that describe mixing of tracers and their solutions, both analytical and numerical, for linear and non-linear geometries are covered. The third section discusses the literature which concerns the importance and quantification of the permeability heterogeneity. This survey gives an overall view of quantifying reservoir heterogeneity by researchers in the soil science, hydrology and petroleum industries. In the fourth section, field applications and limitations of the geostatistical methods are presented. The last section provides the summary of this chapter.

2.1 Interpretation from Tracer Tests

Two kinds of tracers have been used to evaluate underground oil and water formations. These tests can be radioactive or chemical, depending upon the type of formation, the fluid, and the availability of tracers. Chemical tracers are detected by simply taking a sample at the well head; whereas, radioactive tracers are detected through a well logging tool. The tracer tests conducted are usually of two types, 1) well-to-well (interwell tests), in which a tracer is injected in an injection well and detected at the production well, or 2) single well tests in which the tracer is injected into a well and is allowed to react with the formation fluid before being detected from the same well.

The necessary characteristics of a good tracer material were described by Carpenter et al. (1952). The material should

- be susceptible to quantitative determination at very low concentrations,
- either be entirely absent of natural waters, or else contain only trace quantities
- not react with the input or connate waters to form a precipitate,
- not be adsorbed by reservoir rocks,
- be cheap and readily available,

- be soluble with water to an extent that the required concentration may be introduced at the injection well.

Carpenter used boron in the form of borax ($Na_2B_4O_71OH_2O$) and boric acid (H_3BO_3) as tracers to determine water channelling in three different formations. Wagner (1977) gave a complete list of the information that can be attained by tracer tests. This list is useful in the design, control, and interpretation of subsequent tertiary oil recovery processes applied in the oil field. This comprehensive information is given as follows:

Volumetric Sweep.

The volume of fluid injected at an injection well following injection of the tracer, till the breakthrough of that tracer at a producing well, shows the volumetric sweep efficiency between that pair of wells. Small breakthrough volumes relative to interwell pore volume indicate a fracture or high permeability streak, and give an idea of the volume of that channel.

Identification of Offending Injectors.

Different tracers can be used to determine the injectors responsible for early breakthrough in specific producers, so that a remedial treatment can be applied to seal a channel.

Directional Flow Trends.

When different tracers are injected at different injection wells, the directional flow trends are identified by early tracer breakthrough at the producers located along the preferential flow direction.

Delineation of Flow Barriers.

If an injected tracer does not show a response at a producer, it shows the existence of a flow barrier or a sealing fault between that pair of wells.

Relative Velocities of Injected Fluids.

When different fluids are injected with different tracers at an injection well, the relative velocities of these fluids can be measured from the individual tracer arrival times at offset producers. The early arrival of one of the tracer fluids indicates that

the early arriving fluid has contacted less of the reservoir than the late arriving fluid. This shows a need to alter one of the injected fluids to improve sweep efficiency and mobility control.

Evaluation of Sweep-Improvement Treatments.

After a remedial treatment has been done, the success or failure of the treatment can be evaluated by performing a tracer test again.

Strum and Johnson (1951) determined qualitatively the applicability of certain chemicals in tracing the progress of flood waters through the underground oil reservoirs. Three different tracers were used: brine, fluorescein, and a surface-active compound. These tracers were first tested on the laboratory cores, then applied to the Pennsylvanian Bradford Third Sand Formation. They showed that many adverse conditions such as crevices, fissures or directional permeability can be detected by these tests. These can be determined from a study of time elapsing between the injection of the tracer and its appearance in the surrounding producing wells. Recently Hutchins et al. (1991) and Taylor et al. (1989) demonstrated the proper selection and usage of chemicals and radionuclides for tracer testing. They reported the limitations and precautions for individual chemicals that were applied to several field cases. For radioactive tracers, the environmental aspects and precautions were discussed. Lichtenberger (1991) presented the results of interwell tracer tests performed in the McClesky sandstone with a polymer flood operation. The main purpose of the tests were to delineate the fluid migration, measure the residual oil saturation, and compare the tracer performance by co-injection.
Recently, tracer tests have been used to determine quantitative information about the reservoir rock, for example, determination of average permeability in a particular layer. This has been achieved by the use of numerical reservoir simulation (Allison, et al., 1991; Kazemi and Shinta, 1991).

2.2 Mechanism of Tracer Flow

As indicated above, the flow of an ideal tracer through the reservoir follows that of the fluid to be traced, whether this is the injected water or some other displacing

fluid. That flow, or convection, is in accord with the pressure field in the reservoir. In addition, the tracer distribution is continuously modified by hydrodynamic dispersion during the time it remains in the porous rock. Mathematically, the flow of a miscible tracer is described by the well-known Convective-Dispersion equation

$$\frac{\partial C}{\partial t} = -\frac{\mathbf{u}}{\phi S_w}\nabla C + \nabla \cdot \mathbf{D} \cdot \nabla C \tag{2.1}$$

Here, $\mathbf{D}$ is the second order symmetric tensor which represents the coefficient of dispersion for the fluid matrix system (Bear, 1961; de Jong, 1958). Even for a homogeneous and isotropic system, dispersion is direction dependent. Dispersion also contains both molecular diffusion and convective mixing in an inseparable form. Therefore, it is possible to express dispersion (Heller, 1986; Blackwell, 1962; Perkins and Johnston, 1963) as

$$D_L = \frac{D_m}{\phi F} + \frac{\lambda_L |\mathbf{u}|}{\phi} \tag{2.2}$$

where λ_L is the dispersivity constant in the longitudinal direction. In the transverse direction λ_L will be replaced by λ_T. In equation (2.1) $\mathbf{u}$ is the Darcy velocity vector and for a non-uniform field can be obtained by the solution of a *pressure equation*, which reduces to the Laplace equation for a homogeneous formation. The Darcy flow results from the pressure gradient imposed on the system at production and injection wells drilled into a formation, and by the density differences of the flowing fluids. In general, convective flow mainly depends upon the well arrangements and operating conditions, such as flow rates of the wells and the pressures imposed on them.

2.2.1 Analytical Solutions of Convective-Dispersion Equation

For a linear flow system, where Darcy velocity is a constant, Aronofsky and Heller (1957) solved the convective-dispersion equation in one dimension. They solved the following continuity equation for the fluid concentration

$$D_L \frac{\partial^2 C}{\partial x^2} - v\frac{\partial C}{\partial x} = \frac{\partial C}{\partial t} \tag{2.3}$$

with

$$C(0,t) = C_o$$

$$C(x,0) = 0$$
$$C(x,0) = 0$$
$$C(\infty,t) = 0 \qquad (2.4)$$

where,

C = concentration of displacing fluid, mass fraction

D_L= effective mixing coefficient, L^2/T

v = interstitial velocity, L/T

(Darcy velocity divided by porosity)

The Aronofsky-Heller solution is

$$\frac{C(x,t)}{C_o} = 1/2\left[\text{erfc}\left(\frac{x-vt}{2\sqrt{D_L t}}\right) + \exp\left(\frac{vx}{D_L}\right)\text{erfc}\left(\frac{x+vt}{2\sqrt{D_L t}}\right)\right] \qquad (2.5)$$

Ogata and Banks (1961) solved Eq. 2.1 using the same type of boundary conditions. Brigham et al. (1961) performed experiments on miscible displacement for both consolidated and unconsolidated sandstone. They studied the effects of fluid velocity, bead size, viscosity ratio, and pack diameter as the length of the mixed zone. They concluded that the mixing phenomenon in displacements with unfavorable viscosity ratio no longer follows the error function type solution. They also discovered that the dispersion is more effective in consolidated as compared to unconsolidated sand.

Besides longitudinal dispersion, a similar but less effective mixing, known as transverse dispersion, occurs perpendicular to the direction of mean flow. In recognition of the experimentally observed difference between the effective dispersion coefficients parallel and perpendicular to flow, the equation for the conservation of mass of dispersing substance (Scheidegger, 1961), can be written as

$$\frac{\partial C}{\partial t} = -\frac{u}{\phi}\frac{\partial C}{\partial x} + D_L\frac{\partial^2 C}{\partial x^2} + D_T\left(\frac{\partial^2 C}{\partial y^2} + \frac{\partial^2 C}{\partial z^2}\right) \qquad (2.6)$$

Here, x is measured in the direction of the Darcy's velocity u, and y and z in two mutually perpendicular directions transverse to it. A detailed experimental

evaluation of transverse dispersion is given by Blackwell (1962). He used calcium chloride as a tracer to measure the mixing coefficient for a different range of flow rates, fluid

viscosities, column length, and sand grain sizes. Mass transport by molecular diffusion was found more important for transverse mixing than for longitudinal mixing. At high flow rates, transverse dispersion was found to be smaller by a factor of about twenty-four compared to the mixing in the flow direction.

So far we have considered linear flow, which assumes a constant value of velocity, and consequently of dispersion inside a porous media. For other geometries, such as radial flow or flow in a five-spot pattern, the velocity is a function of position, and consequently the dispersion coefficient is a variable. For these complex geometries the convective-dispersion equation becomes a second-order differential equation with variable coefficients, which makes it very difficult if not impossible to derive an analytical solution to describe mixing in non-uniform flow fields. The two-dimensional flow system will be more difficult, because this system will include transverse along with longitudinal dispersion. Several approximate analytical solutions are, however, available which describe mixing in radial flow systems with good accuracy. The general equation describing the spatial and time distribution of a tracer (Hoopes and Harleman, 1965) in terms of r and θ coordinates, without molecular diffusion, can be written as

$$\frac{\partial C}{\partial t} + \frac{A_q}{r}\frac{\partial C}{\partial r} = \lambda_L \frac{A_q}{r}\frac{\partial^2 C}{\partial r^2} + \lambda_T \frac{A_q}{r}\frac{\partial^2 C}{\partial \theta^2} \tag{2.7}$$

where $A_q = Q/2\pi h\phi$, and $\lambda's$ are defined in Eq. 2.2.

If we assume that the concentration distribution is symmetrical with respect to θ so that no lateral concentration gradient develops, then Eq. 2.7 reduces to

$$\frac{\partial C}{\partial t} + \frac{A_q}{r}\frac{\partial C}{\partial r} = \lambda_L \frac{A_q}{r}\frac{\partial^2 C}{\partial r^2} \tag{2.8}$$

Raimondi et al. (1959) gave a solution to Eq. 2.8 with a modified dispersion form. The approach is based upon the assumption that dispersion in comparison with convection has a negligible influence on the tracer distribution and becomes small in comparison to the local convective effect as the tracer moves away from the source. For the continuous injection of a tracer of constant concentration, C_o, their solution was

$$\frac{C}{C_o} = 1/2 \text{ erfc } \left(\frac{r^2/2 - A_q t}{\sqrt{4/3\lambda_L r^3 + \frac{D_m}{A_q} r^4}} \right) \tag{2.9}$$

Ogata (1958) obtained a solution to Eq. 2.8 in integral form for the case where the tracer is introduced when $t = 0$ at $r = r_w$ is maintained constant for $t > 0$. This integral solution is too complicated to evaluate analytically. A numerical integration of the integral would be required. Gelhar and Collins (1971) developed a general approximate analytic solution for longitudinal dispersion in steady flows with variations in velocity along streamlines. By transforming the convective-dispersion equation into a convected coordinate system and using the boundary layer approximation, the governing equation was reduced to a simple diffusion equation. The effects of the variation of longitudinal velocity and dispersion coefficient were incorporated implicitly through two integral transformations. When this general solution was applied to a radial flow, it generated the same approximate solutions as proposed by Raimondi et al. (1959). An approximate solution was given by Baldwin (1966) in both radially diverging and converging situations. The approach was based on the assumption that the growth of the length of the mixed zone in a radial displacement was a linear sum of two effects: fluid movement (distance traveled) and the geometry of the system (divergence or convergence of stream lines). The distance effects were obtained from the mixing equation for a linear system. The geometry effects were derived from the consideration of material balance, as the volume of the dispersed zone had to remain constant at a given point regardless of the geometry of the system. Thus, for diverging flow

$$\frac{C}{C_o} = 1/2 \text{ erfc} \left(\frac{r^2 - \bar{r}_1^2}{2\sqrt{4/3\lambda_L r^3}} \right) - 1/2 \text{ erfc} \left(\frac{r^2 - \bar{r}_2^2}{2\sqrt{4/3\lambda_L r^3}} \right) \tag{2.10}$$

and for diverging-converging flow Eq. (2.10) becomes

$$\frac{C}{C_o} = 1/2 \text{ erfc} \left(\frac{r^2 - \bar{r}_1^2}{2\sqrt{4/3\lambda_L (r_e^3 - r^3)}} \right) - 1/2 \text{ erfc} \left(\frac{r^2 - \bar{r}_2^2}{2\sqrt{4/3\lambda_L (r_e^3 - r^3)}} \right) \tag{2.11}$$

where,

r = radial distance, L

r_e = radius of the radial element, L

$\bar{r}_1$ = radius of back of the slug, L

$\bar{r}_2$ = radius of front of the slug, L

Brigham (1974) used the same idea for different types of geometries. He showed that by breaking the flow system into segments in which width was a linear function of distance, and by repeated use of his solution, mixing could be computed for a variety of geometries. An expression for mixing in a general stream tube was also developed in his paper.

Tang and Babu (1979), Moench and Ogata (1981), and Chen (1985) used the Laplace transformation for the solution of Eq. 2.8 with a velocity dependent dispersion.

The five-spot pattern is the most commonly used flood pattern for the recovery of oil. A considerable amount of work has already been done to simulate the pattern numerically or analytically for an immiscible case (Schafer-Perini, 1990). For a miscible case, though the complexity of the flow in the pattern is less, the literature is limited. Brigham and Smith (1965) performed a quantitative analysis on tracer dilution curves for developed five-spot patterns. They approximated the flow as radial in the pattern, and devised an equation for the tracer breakthrough curve by combining the tracer dispersion (longitudinal) effects with the areal sweep effects. Equations were also developed to predict the time of tracer breakthrough and peak concentration of the tracer. This approximation, however, introduced errors in the computation of arrival times for the different streamlines.

Abbaszadeh (1983) produced useful approximate analytical solutions for different developed patterns with a mobility ratio of one. The derivation of his equations was accomplished by combining the tracer dispersion (longitudinal) effects with the areal sweep effects for any type of developed pattern. For tracer dispersion effects, he used the same concept as given by Lau et al. (1959), Baldwin (1966), and Brigham (1973). By integrating individual stream tube tracer concentration, analytical expressions were obtained which define the tracer breakthrough curves for several developed patterns. For areal-sweep effects, exact analytical equations were obtained in the form of elliptic integrals which describe several pattern breakthrough

curves. This study shows that the tracer breakthrough curves from a homogeneous system depend upon the geometry, pattern size, and dispersion constant of the formation rock. This study did not include transverse dispersion, or the velocity independent component of both the longitudinal and transverse dispersion that is due to molecular diffusion. Fig. 2.1 through Fig. 2.3 shows the tracer concentrations for five-spot, staggered line drive, and direct line drive for different values of the peclet number (a/α). Due to geometric effect, three different types of output concentration profiles were obtained.

2.2.2 Numerical Solutions of Convective-Dispersion Equation

A great deal of work has been performed on the numerical solution of the convective-dispersion equation. In these studies the differential equation is replaced by the finite difference analogues. In general, three types of finite difference schemes are employed.

Explicit Method: This requires known concentration values at the previous time level, and the concentration at the next time level is solved explicitly. The size of the grid spacing and the time increment for an explicit scheme are restricted to very small values by the stability criteria. This makes the numerical scheme impractical for large field problems in terms of the computer time requirement.

Implicit Method: The spatial derivatives are evaluated at time t_{n+1} instead of at t_n. Thus, concentration is obtained implicitly by solving a system of equations.

Crank-Nicholson Method: This type of implicit difference analogue for the C-D equation can be obtained by replacing the spatial derivatives by the average of the second difference quotient at both the old and new time levels. This method also produced a system of simultaneous equations.

Besides these three methods, there are some other methods and techniques available in the literature. All these methods require a time stability criteria that makes them numerically stable or unstable, depending upon the type of finite difference scheme. Another complication to the numerical solutions of the convective-dispersion equation arises due to the presence of numerical dispersion. Numerical dispersion in the finite difference computation methods is an effective dispersion caused by the finite

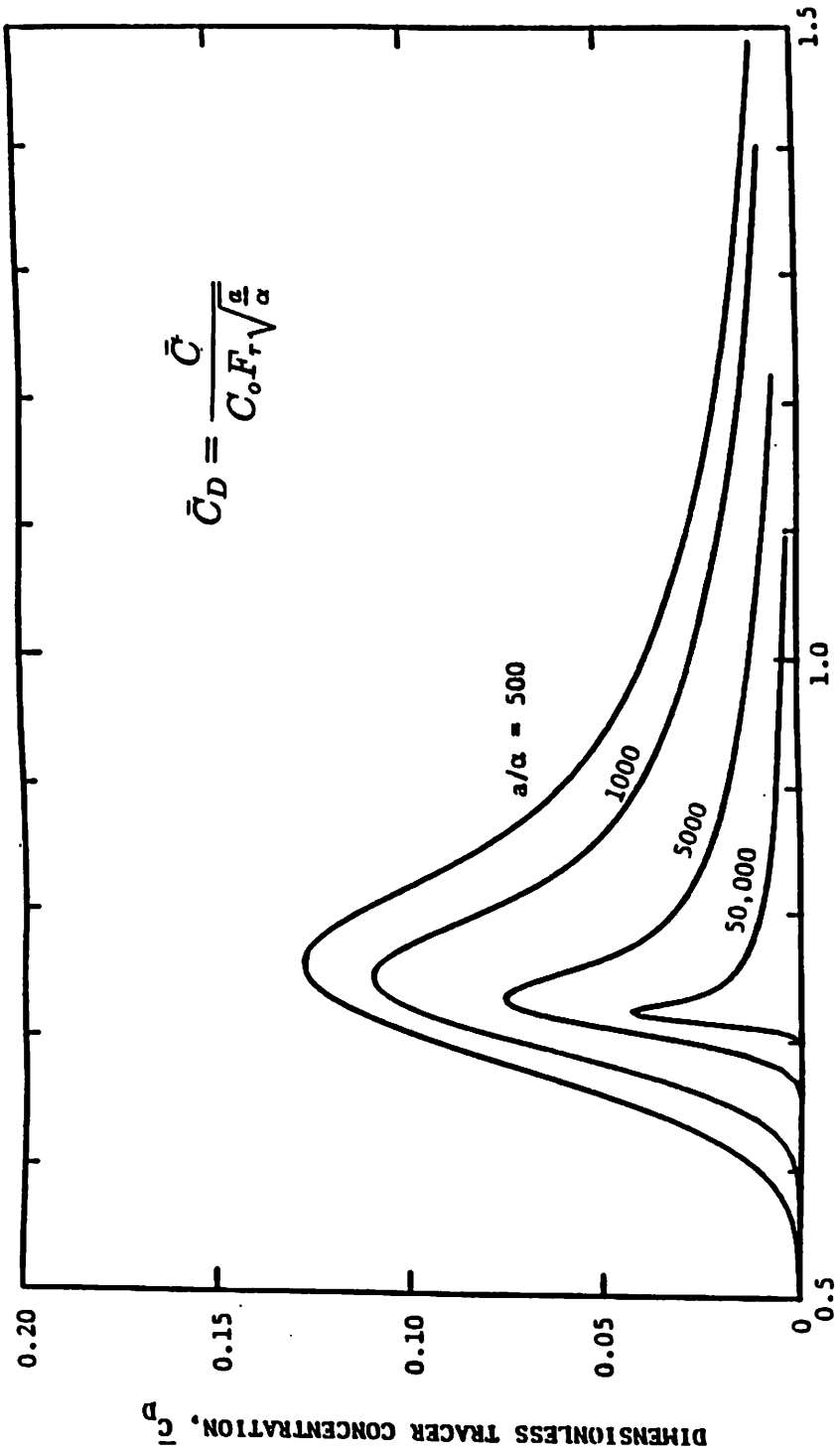

Fig. 2.1 Dimensionless Tracer Concentration vs Pore Volume Injected, Five-spot Pattern. (After Abbaszadeh and Brigham, 1983)

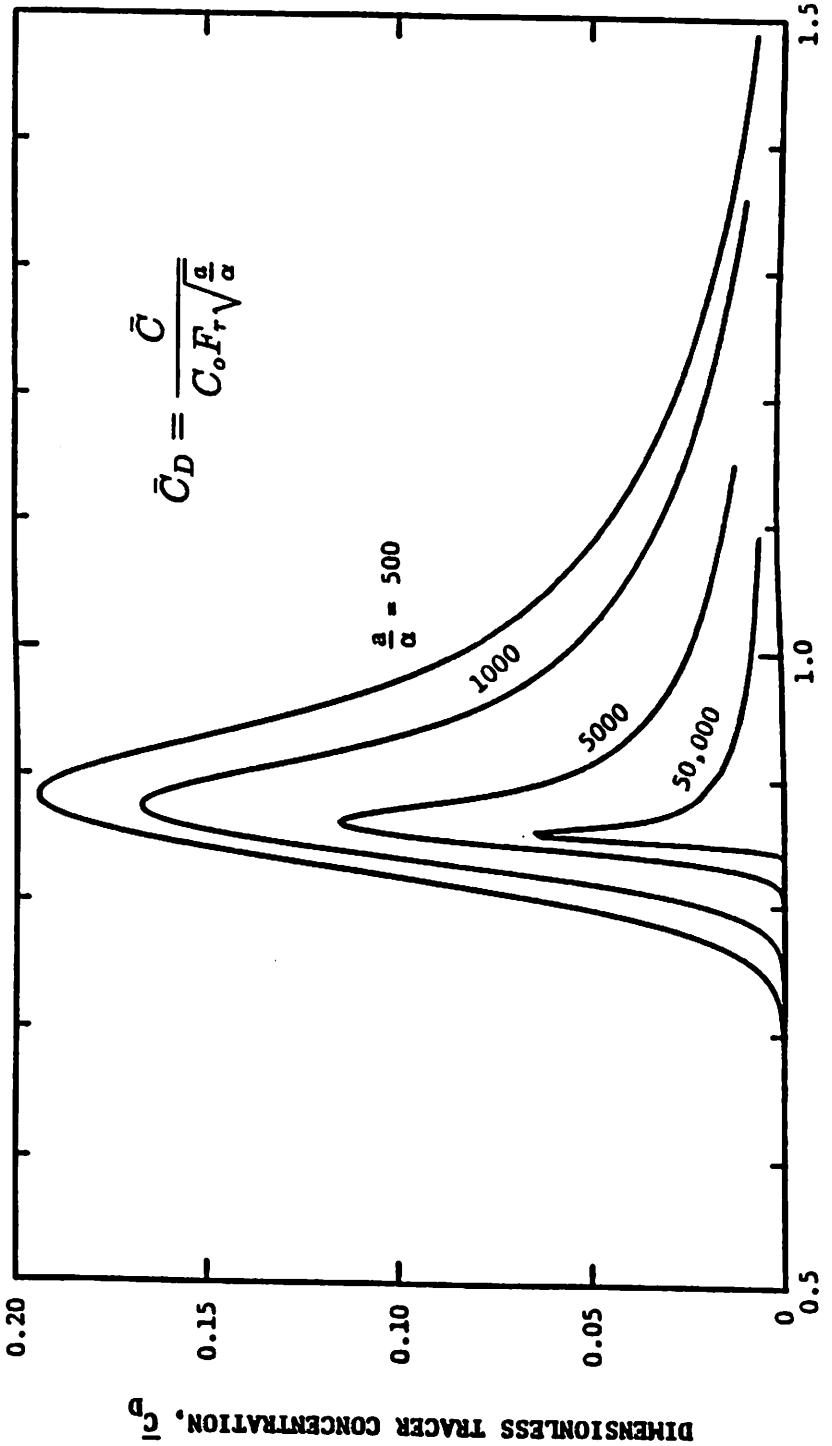

Fig. 2.2 Dimensionless Tracer Concentration vs Pore Volume Injected, Staggered Line Drive. (After Abbaszadeh and Brigham, 1983)

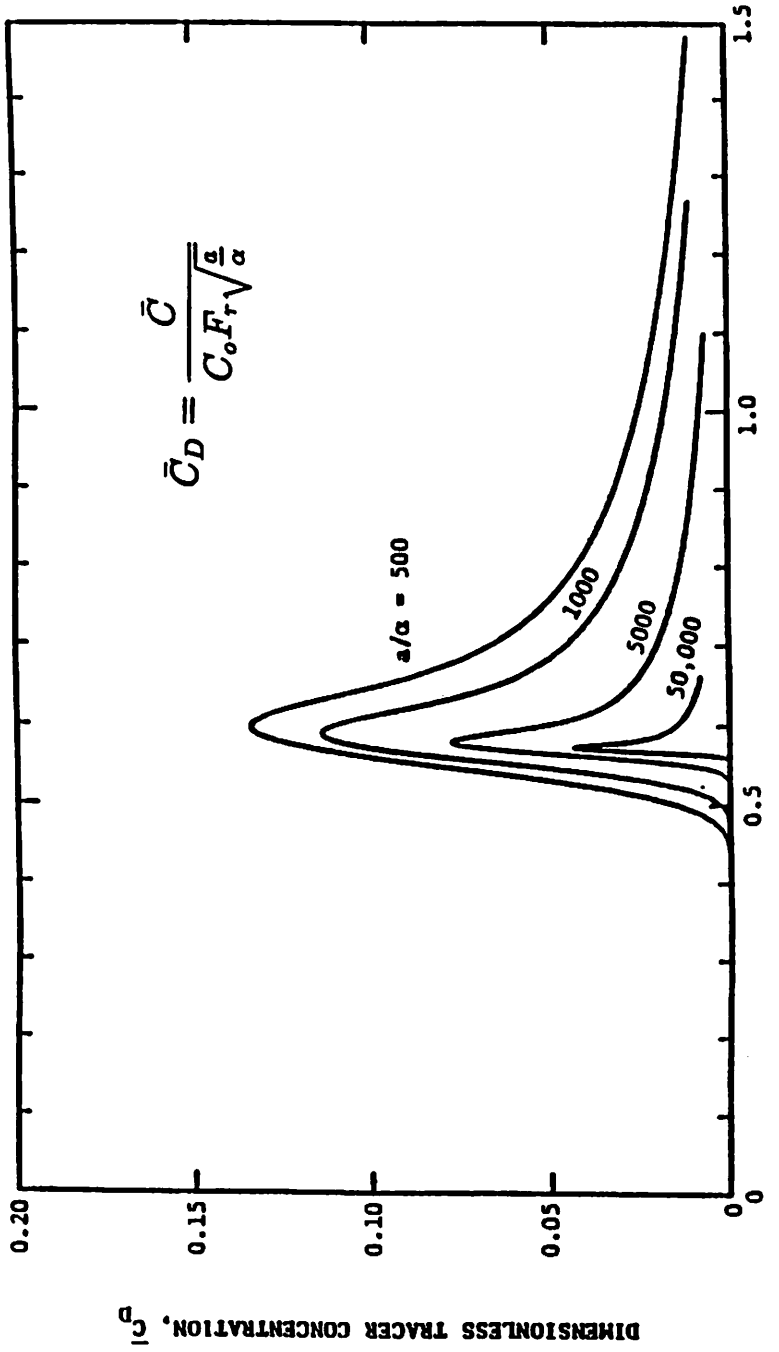

Fig. 2.3 Dimensionless Tracer Concentration vs Pore Volume Injected, Direct Line Drive. (After Abbaszadeh and Brigham, 1983)

difference approximations that uses only a limited number of terms in the Taylor series expansion. It produces dispersion in the displacement front even when the physical dispersion coefficients are set equal to zero. Usually, the major part of the numerical dispersion occurs due to the finite difference approximation of the first order derivatives ($\partial C/\partial t, \partial C/\partial x$). This problem gets severe when simulating large scale field problems, where a large grid block size is the only choice, due to computer efficiency.

Peaceman (1977) analyzed different finite difference schemes for instability and numerical dispersion. Through some example calculations, he summarized that the convective-dispersion equation would either show numerical dispersion or some oscillatory behavior, and that up to some extent, trade off between one or the other can be obtained by some higher order methods. It is in general not possible to make both disappear except if the grids are refined, which is limited by practical considerations.

Garder, Peaceman, and Pozzi (1964) used the method of characteristics to improve the numerical solution of the same problem. In addition to the usual division of the two-dimensional space into rectangles by grid lines, they introduced a set of moving points. Each moving point had associated with it a concentration, which varies with time. The velocities at each time step were obtained by the method given by Peaceman and Rachford (1959). Each moving point was then moved to a new location using the local velocity and the time increment. Each rectangle of the grid was assigned a new concentration equal to the average of the concentrations of the moving points in it. This concentration in each rectangle was modified by dispersion in two dimensions, and the change in concentration was then applied to all moving points within the rectangle. This method reduced numerical dispersion to some extent.

Stone and Brian (1963) made a thorough analysis of a numerical scheme to solve Eq. 2.2. They used six points, involving three, adjacent-space locations at two time levels. They assigned arbitrary weighting coefficients in the convective and time terms, and determined their magnitude so that the numerical solution approaches

the analytical solution. They also proposed an iterative scheme with three cycles per time step to improve the solutions. Stone and Brian's method requires much less computer time and storage than the method of characteristic, because one does not have to deal with the moving points. The one-dimensional problem solved by Garder, Peaceman, and Pozzi (1964) was computed by the Stone and Brian scheme for comparison. The results had the same degree of accuracy as those presented by Garder et al. (1964).

Lantz (1971) gave a quantitative determination of the truncation error of a one dimensional C-D equation. Table 2.1 gives the summary of these truncation errors for different finite difference schemes. In the table it was assumed that the truncation errors are negligible for higher order derivatives.

In a later work Fanchi (1983) extended the work of Lantz to two and three dimensions and evaluated quantitative values of numerical dispersion for different finite difference schemes. He found that besides smearing, numerical dispersion can rotate the principal flow axis. This implies that even if the principal direction of dispersion is the flow direction (dispersion tensor with off diagonal terms equal zero), the numerical dispersion puts back the cross derivative terms (i.e. the off diagonal terms of the dispersion tensor are no longer zero) that were eliminated. A decrease in time step was suggested to minimize this problem.

Chaudhari (1971) used a second order difference scheme for the first order derivatives. Solutions produced by this method became oscillatory at concentrations near one and zero. These oscillations were removed artificially by reducing the incoming and outgoing numerical dispersion. He applied this technique to the one and two dimensional convective-dispersion equations.

Saad et al. (1990) used a third order differencing scheme to the C-D equation. They compared their results with the Chaudhari method, and showed that the proposed scheme has reduced the numerical dispersion, and the computation time was reduced effectively. Although a good comparison of the numerical with an analytical solution was reported, the peclet number was less than 250 in their analysis.

Heller (1986) formulated a useful numerical method for the radial flow problem,

Difference Form		Error Forms	
Spatial	Time	Miscible	Immiscible
BD	Explicit	$(\Delta\xi-\Delta\tau)/2$	$\frac{df_w}{dS_w}(\Delta\xi-\frac{df_w}{dS_w}\Delta\tau)/2$
CD	Explicit	$-\Delta\tau/2$	$-\left(\frac{df_w}{dS_w}\right)^2\Delta\tau/2$
BD	Implicit	$(\Delta\xi+\Delta\tau)/2$	$\frac{df_w}{dS_w}(\Delta\xi+\frac{df_w}{dS_w}\Delta\tau)/2$
CD	Implicit	$\Delta\tau/2$	$\left(\frac{df_w}{dS_w}\right)^2\Delta\tau/2$

Table 2.1 Truncation Errors for Different One Dimensional Finite Difference Schemes. (After Lantz, 1971)

which has been extended in this study to give solution for the five-spot pattern. He solved the problem in terms of equations of motion of the isoconcentration lines. The tracer slug was divided into some number of points lying on isoconcentration surfaces. Each isoconcentration point was subjected to the influence of convection and dispersion, and the numerical calculations were directed towards keeping track of their positions. This method did not require any detailed assumption about the outer boundary conditions. A one-dimensional radial flow problem with longitudinal dispersion and molecular diffusion at low flow velocities was considered. The results were not compared with any of the analytical solutions, though useful analysis about the behavior of displacement fronts in radial geometry were described.

2.3 Flow of Fluids in Heterogeneous Porous Media

It has been recognized now that without any exception, the properties of the porous media are not homgeneous, but rather heterogeneous. The most important parameter in the reservoir heterogeneity, at least for flow and displacements, is its permeability. The variations in other parameters, for example porosity and reservoir thickness are either negligible or unimportant with respect to the flow characteristics of the fluid in the media. The variability in the permeability is as much as four orders of magnitude. Whereas the variability in the porosity generally follows changes in permeability, the amount of the change is much smaller (Warren and Price 1961). In light of this, the literature survey presented here is only concerned with the heterogeneity of permeability (or/hydraulic conductivity) in the underground reservoirs.

Perhaps the first real attempt to study the variation in permeability was presented by Law (1944). In his work, the permeability variation was described by a log normal distribution function. Muskat (1948) assumed both log normal and exponential distribution functions in describing the stratification of a formation; also, Stiles (1949) and Dykstra and Parsons (1950) presented the influence of stratification on water flood performances.

Warren et al. (1961) measured the permeability values in cores obtained from 14 wells. They compared the average of the permeabilities with effective permeability

obtained from the pressure build up test, and suggested that the geometric average is the most probable value in the random heterogeneous reservoir. Later, Warren and Price (1961) studied a 3-dimensional model of homogeneous permeability blocks. The permeability of the individual elements follows some specific distribution function, for example, log normal, skewed log normal and exponential. In their model, the amount of heterogeneity decreases with the increase in the number of elements, and vice versa. They investigated the effect of the permeability variations on both steady state and transient flow. They did not quantitatively define the spatial correlation of the permeability field.

Freeze (1975) presented a 1-D stochastic model for heterogeneous porous media. He used a Monte Carlo simulation technique to solve a boundary value problem and showed that the degree of uncertainty associated with the hydraulic head increases with the increase in the degree of nonuniformity in the porous media. Though, the hydraulic conductivities that were generated assumed a multivariate normal distribution, the spatial correlation structure was not considered. Later, Smith and Freeze (1979) used a first order nearest neighbor stochastic process model to introduce spatial correlation in a 1-D random stochastic permeable model. In a subsequent paper Smith and Freeze extended this work to a two dimensional steady state flow in a bounded domain. They showed that the ratio of the integral scale (correlation length) of conductivity to the distance between the boundary points is a fundamental parameter in the analysis of the behavior of heterogeneous porous media.

For a stationary random field with mean zero, it is possible to represent a stochastic process by a complex stochastic field through a Fourier Stieltjes integral, which decomposes the process into uncorrelated random components. These random components in turn give the spectral density function, which is the distribution of the variance of the stationary field. Bakr et al. (1978) presented hydraulic conductivity as a spatial stochastic process with a certain covariance structure and by applying spectral theory the solution of the hydraulic head perturbation was evaluated. By using the Fourier Stieltjes representation, the flow equation was solved

for the spectrum of head in terms of the spectrum of hydraulic conductivity. The analysis produces functional relationships between the wave number spectrum of the hydraulic conductivity perturbations and the spectrum of the hydraulic head in the flow system. From these spectra relationships covariances of the hydraulic head were obtained by using assumed covariances for the conductivity perturbation. They generated one and three dimensional hydraulic conductivities and showed that the variance in the resulting hydraulic head is reduced by an order of magnitude in three dimensions compared to the one dimensional case. In the second paper of this series, Gutjahr et al. (1978) investigated the importance of the normality of the Ln K process and the dimensionality of the flow system.

2.3.1 Dispersion in Heterogeneous Porous Media

A physical quantity that describes the mixing of fluids is the dispersion coefficient. The larger term of this coefficient is proportional to the velocity of the fluids; the constant of proportionality is called the dispersivity distance. This distance is defined by Eq. 2.2 for packs or columns containing uniformly sized grains, and is a microscopic parameter that depends upon the particle size and the tortousity of the flow paths through the pores. A unit-mobility ratio displacement in such a rock shows relatively smooth fronts, and the length of the mixing zone grows as the square root of the average distance traveled. The permeability heterogeneity of reservoir rock is usually defined on a macroscopic scale (such as the size of a grid block in a field simulator), and may introduce channeling and additional mixing. A displacement dominated by channeling shows complex behavior and a unique relationship between the growth of the mixing zone and the distance traveled often can not be defined. Lake et al. (1989) stated, however, that the mixing in a channeling-dominated reservoir grows linearly in proportion to the average distance traveled. They also pointed out that the mixing due to the dispersion alone is small compared to the mixing by channeling, and that the dependency between these two mechanisms is unknown.

Warren and Skiba (1964) used a Monte Carlo model to study the flow of a miscible displacement in a three dimensional porous media. They found that the amount of

macroscopic dispersion depends upon the scale of heterogeneity in the permeability and its distribution. Their investigation suggests that the experiments performed in laboratory cores do not give a valid measure of macroscopic dispersion. They also concluded that the effect of porosity variations on macroscopic dispersion is second order with respect to the effect of permeability variations.

Smith and Schwartz (1980) used a nearest-neighbor stochastic process to generate a two dimensional spatially auto-correlated hydraulic conductivity field in the flow of miscible displacement. Their model accounted for macroscopic dispersion not as a large scale diffusion process, but as mixing caused by the variability in hydraulic conductivity. They showed that the important parameters that controlled mass transport are the variance of log conductivity, and the magnitude and anisotropy of the integral scale. They also concluded that the mean convective velocity of the tracer particles, and the extent of the macroscopic dispersion, reflect the effect of the conductivity distribution. The effect of microscopic dispersion is of secondary importance. In a following paper, Smith and Schwartz (1981) extended the transport analysis in the ground water to consider layering, hydraulic anisotropy and chemical processes. They showed that anisotropy can limit the size of the region through which a miscible fluid is likely to spread. Other parameters, such as porosity and the cation exchange process, influence only the magnitude of the velocity. The variations in these parameters are of secondary importance.

Gelhar and Axness (1983) used spectral theory to represent macroscopic dispersion in a three dimensional heterogeneous flow system. They showed that for an isotropic reservoir, a macroscopic longitudinal dispersivity is independent of the microscopic dispersivity, but the macroscopic transverse dispersivity is controlled by the microscopic dispersivity. For an arbitrarily oriented anisotropic conductivity covariance, all the components of the macroscopic dispersivity were found to be convectively controlled.

Schwartz (1977) used a hypothetical medium in which blocks of lower conductivity were inserted into somewhat homogeneous blocks. He analyzed the effect of permeability variation on the dispersivity and suggested that the magnitude of dispersion

is proportional to the permeability contrast. He concluded that the large field scale dispersivities are significantly higher than those measured in laboratory core samples, and assignment of a constant dispersivity value in a heterogeneous medium is not valid.

Kelkar and Gupta (1988) presented the effect of the permeability variation on the evaluation of the effective dispersivity. A base (microscopic) dispersivity was used in the simulator. By comparing the simulated results with a one dimensional analytical solution, the effective dispersivity was measured. They found that for an areal heterogeneity, the effective dispersivity increases with the correlation length. For a relatively small correlation length the effective dispersivity was found to be comparable with the base dispersivity.

Heravi (1988) perhaps was the first to show the effect of areal permeability heterogeneity on production breakthrough curves, in a quarter of a five-spot pattern. The author did not include the effect of dispersive mixing. Later, Schafer-Perini (1990) gave a detailed analysis of pressure field, velocity field, and displacement patterns in heterogeneous developed oil field containing thirty six injectors and twenty five producers. The author also did not consider any inherent dispersive effects. Schafer-Perini compared the effect of using a quarter of a five-spot pattern to the same pattern in the field of repeated five-spots. Although the difference in the displacement fronts and capture zones between the truncated and the full five-spot was shown substantially different, the breakthrough curves obtained from a quarter five-spot pattern has basically the same characteristics as all of the breakthrough curves compiled in the full domain simulation. The author indicated that by assuming symmetry and modeling only a quarter of five-spot pattern, the results may be misleading and should be accepted with caution.

2.4 Field Application of Geostatistical Methods

Assessment of reservoir heterogeneity from the available field data is a major concern of operating engineers for a successful planning of enhanced oil recovery projects. Recently, development of high speed computers has made it possible to simulate large reservoirs with a fine grid system. Our ability to predict flow performance is

now limited by the knowledge of reservoir properties at the specified grid system in the simulator.

For the past two decades, the theory of geostatistics has achieved special attention due to its ability to characterize reservoir rock in a probability framework. Geostatistical techniques have been used in the mining industry for the past forty years. Its application in reservoir engineering has been a question in the oil industry due to the lack of available data. The data is usually obtained by well testing, well logging and laboratory core analysis.

2.4.1 Generation of random permeability/porosity field

One of the most necessary requirements in reservoir characterization is the generation of a random field for porosity and permeability. This is based on the fact that field data available from well logging, well testing, and core analysis is generally not sufficient for characterization of the field. A complete description of the reservoir by conditional simulation methods requires the use of synthetic random fields. Earlier in such random generators, though they assumed a multivariate normal distribution, the spatial correlation structure was not considered (Warren and Price, 1961; Freeze, 1975). Later studies (Matheron, 1973) demonstrated that reservoir properties show a correlation structure; i.e., the permeability is not totally random and is dependent on the neighboring permeability values. The correlation scales differ from one reservoir to Several geostatistical techniques have been developed to generate random fields for stochastic stationary processes.

The Turning Band Method (TBM) was developed by Mantoglou and Wilson in 1982 from an earlier version originated by Matheron (1971). This method, although efficient with respect to computer time and storage, shows regular trends of high or low permeability streaks (McKay, 1988; Sultan, 1992), which is an artifact of the method. The second method is called the Fast Fourier Transform Method (FFTM) and was originated by Gutjahr (1989). This method employs the classical theory of Fourier analysis. The method is efficient in the sense that a desired 2-D field (of specific variance and correlation scales) can be obtained; in addition the amount of anisotropy can be taken into account. The only drawback in this method is that a

larger computer storage capacity and time is required. The last method is called the Source Point Method (SPM) and was developed by Heller in 1972. The method uses the inverse square law assumption, is the fastest to compute, and requires much less computer storage as compared to the other methods. Some researchers have stated that the desired correlation length in the SPM cannot be prespecified (Arya, 1986). The method also has other limitations: it is not clear how anisotropy may be incorporated. The only variogram shape available is similar to the spherical model. All these methods have a further common limitation; that a single overall variance and correlation scale of the property distribution is obtained. It has been suggested in many studies that the reservoir heterogeneity shows a different behavior at different scales of measurements. It has been observed that fractal distributions can be used to describe the properties of porous media, for example, permeability (Emanuel et al. 1987), fracture network (Barton et al., 1987), viscous fingering (Fanchi and Christiansen, 1989), and pore surfaces. One of the most important characteristics of fractal methods is the ability to take into account correlation length at many different scales of measurement. The knowledge of heterogeneity at different scales is very important in the simulation and prediction of the performance of enhanced oil recovery. The scaling phenomena in reservoirs can be divided into four different classes. These are the microscopic scale (few pores in the porous media), macroscopic scale (laboratory cores), megascopic scale (size of grid blocks for large field models), and the gigascopic scale (the scale of the reservoir). For situations where only interwell data is available, it is difficult to measure the variability at a smaller scale, for example, at the size of the grid block. With the assumption of fractal distribution characteristics, the property distribution can be computed at any scale.

The methods mentioned above can generate a random field for a porosity/ permeability field. It is necessary to find the evidence for fractal distribution in the reservoir. If such data does exist, then the use of fractal distribution is more appropriate. If the analysis shows no fractal distribution, then the next criteria depends on the need of anisotropy conditions. If anisotropy in the generated field is required,

then the FFTM should be used; otherwise, the SPM is very efficient for generating an isotropic random field. The TBM, in our opinion, has a low rating because it shows artificial, undesired streaks in the property distribution (Mckay, 1988; Sultan, 1992).

2.4.2 Interpolation Techniques

To predict the performance of a reservoir through simulation, it is necessary to assume the value of properties such as permeability at every specified grid point. The size of the grid block is much smaller than the spacing between the data available (interwell distance). To predict the property at grid blocks, some sort of interpolation of data is required.

Chopra et al. (1990) presented two types of interpolation techniques: conventional and geostatistical. In the conventional method, three types of techniques were used.

1. Triangulation: In this technique, the known data points are joined to form a mesh of triangles. The unknown point, within a mesh is joined to the corners of the triangle, and the areas of the new triangle are computed. A contour map can then be drawn from it. This method gives non-unique results because different configurations of triangles can be selected.

2. Piecewise linear least squares: The value $z(m,n)$ at a grid point (m,n) is calculated as

$$z(m,n) = A(x - x_m) + B(y - y_n) + C \tag{2.12}$$

The constants A, B, and C are computed by minimizing the least square error of the plane.

3. Piecewise linear least square with corrector: This method uses the same technique as the previous one, and then follows with an adjustment to smooth and remove sharp irregularities from the grid. An octant from the known data values is selected, and the $z(x,y)$ is lowered or raised to pass through all eight of the selected control points.

4. Quadratic projection method: The equation of the surface is described as

$$z(u,v) = A(u-x)^2 + B(u-x)(v-y) + C(v-y)^2 + D(u-x) + E(v-y) + z_i \quad (2.13)$$

where z_i is the known location. In the geostatistical technique, Chopra et al. (1990) used kriging, and compared it with the conventional methods.

5. Kriging: This method performs spatial modeling through the use of variance size of analysis between the known and predicted value, and is dependent on the assumption of probabilistic modeling. It estimates an unknown Z_o^* at other locations in terms of the known values by the formula

$$Z_o^* = \sum_{i=1}^{n} \lambda_o^i z_i \quad (2.14)$$

with the weight function λ to have unbiased condition as

$$\sum_{i=1}^{n} \lambda_o^i = 1 \quad (2.15)$$

This technique also computes the error of estimation or variance as

$$\sigma_o{}^2 = -\sum_{i=1}^{n}\sum_{j=1}^{n} \lambda_o^i \lambda_o^j \gamma(x_j - x_i) + 2\sum_{i=1}^{n} \lambda_o^i \gamma(x_i - x_o) \quad (2.16)$$

where, $\gamma's$ are the semi-variograms. This equation is minimized, and the resulting system of kriging equations is solved for $\lambda's$.

Chopra et al. (1990) in their paper, applied techniques (2) through (5) to a sandstone reservoir. The reservoir contains shales with alternating sands. They applied these techniques to the data of permeability thickness (kh). The comparisons of the techniques were based on the cross-validation of the data. In the cross-validation technique, a known point is removed from the data set. This value is then computed by any of the methods mentioned, and compared with the actual value.

In the conventional technique, the piecewise linear least square method with corrector showed the best results. The criteria was the standard estimate of error associated in each of the techniques. The limitations of all the conventional techniques are 1) the computed transmissivity values do not preserve the correlation

structure, and 2) an estimate of uncertainty associated with each estimated value is not provided.

Kriging techniques require estimation of the variogram of known data. Chopra et al. performed analysis of variograms on the kriging results. By fitting variogram models with the experimental variogram, they studied the nugget effect and directional variograms. After comparing with the geological data, the directional variograms were found more useful. In both cases of omnidirectional and directional models, the nugget effect tends to smooth the data by adding a randomly fluctuating component. The results of conventional techniques were found similar to the results obtained using isotropic variograms with zero nugget. Chopra et al. stated two factors contributing to the similarity: 1) the conventional technique implicitly assumes an isotropic structure, and 2) strong near neighbor correlation structure is introduced in the piecewise linear least square method with corrector. The kriging technique did not produce any peaks or valleys usually associated with the conventional technique. In conclusion, the kriging technique is more informative than the conventional techniques because it provides an error variance map, by which one can assess risk in the development of decisions based on maps of estimated values. The drawbacks of kriging are 1) the data generated is smoother than the natural geological data occurring, and 2) the error of variance is higher when less data is available. The next section presents another geostatistical technique, which is called conditional simulation.

6. Conditional Simulation:

Conditional simulation is one of the most advanced geostatistical tools in reservoir characterizations. The process of conditional simulation takes one of the random fields produced by any of the methods mentioned in section 2, and forces it to pass through the known data values and the appropriate locations. Conditional simulation reproduces more closely the true variability of the field under consideration. The simulated values: 1) vary stochastically and follow the same variogram generated from the real data, and 2) honor the given data. Conditional simulation techniques require 1) adequate data available (well testing, well logging, coring),

2) a random field generator (SPM, FFTM, fractal), and 3) a kriging algorithm for unconditional path and the real data.

Out of hundreds of realizations of a conditional simulation, one or more realizations might possibly approximate the true paths. Conditional simulation, however, is not applied to estimate the true path but to produce realizations that have the same degree of variability as the true path. The kriging residual, that is the difference between the unconditional path and the kriged unconditional path has only small scale variability. The amount of small scale variability is then added back to the kriged surface of the known data to produce a distribution that satisfies the variogram. Since the kriged surface of the known data and the kriging residual are independent of one another, different realizations of the kriging residual can be used to produce different realizations satisfying the variogram.

Fogg and Lucia (1990) gave a precise use of conditional simulation for estimating discontinuous interwell permeability patterns. The technique was applied to Dune Field, Crane County, Texas. The detailed permeability data were estimated by using an approximate correlation between interparticle porosity (measured from geophysical logs), particle size, and permeability. Both vertical and horizontal spatial correlation structures were estimated. In the horizontal variography procedure, variograms were also constructed in different directions. This was necessary to confirm any trends or anisotropy that can be visualized by geologic interpretation. Figure 2.4(a) and 2.4(b) show their fitting of the variograms with two different spherical models. As can be seen from the figure, two entirely different correlation lengths can be assumed. This analysis shows that insufficient field data can give misleading results. After fitting the theoretical variogram to the experimental one, the overall variance and correlation length were computed. Conditional simulations of permeability were run for a total of 200 realizations in each simulation. They showed that the permeability generated with the conditional simulation was different than kriging or deterministic methods by having isolated high or low permeable zones between the wells. The generated permeability field, after conditioning, was then used in the simulation of water flooding. The water flooding also incorporated

the effect of infill drilling.

Fogg and Lucia (1990) used a fine scale grid spacing in both horizontal and vertical directions to capture the permeability variation at a smaller scale in their simulation of water flooding. They showed that with a stochastically-generated permeability field, and with existing well spacing, recovery efficiency will be no greater than 40 to 55 percent. By adding two infill wells, the recovery efficiency generally increased by at least 27 to 32 percentage points. They also showed the effect of different realizations used in the conditional simulation method. Unrealistic realizations were discarded on the basis of unrealistically produced WOR's.

As mentioned earlier, scaling is an important aspect of the reservoir characterization. It has been found in laboratory and field experiments that a porous media shows a different flow behavior at different scales of measuring reservoir properties, such as permeability. In a reservoir simulation, the values of a reservoir permeability are required at the scale of grid block size. But the data usually available, for an areal flow, is at the scale of well spacings. The kriging technique, when employed in this case, shows unnecessary smoothing. The conditional simulation, on the other hand, provides a better picture of the property variation by using unconditional realizations (with the same variance and correlation as the real data) than kriging techniques. In order to evaluate the influence of property variation on the flow processes, we need the property distribution at all scales of variability that is close to reality. Hewett and Behrens (1988) used conditional simulation with fractals to describe the variability of property at all scales. They suggested the use of conditional simulations of permeability fields. Such fields will honor measured data and produce similar variability and spatial correlations of the permeability as exists in the field. Once a good representation of the permeability is known, the effective dispersivity may then be calculated as

$$\lambda = \rho_v^2 \delta \tag{2.17}$$

where, λ is the effective dispersivity (dispersion coefficient divided by velocity), ρ_v is the coefficient of variation of the permeability distribution and δ is the correlation

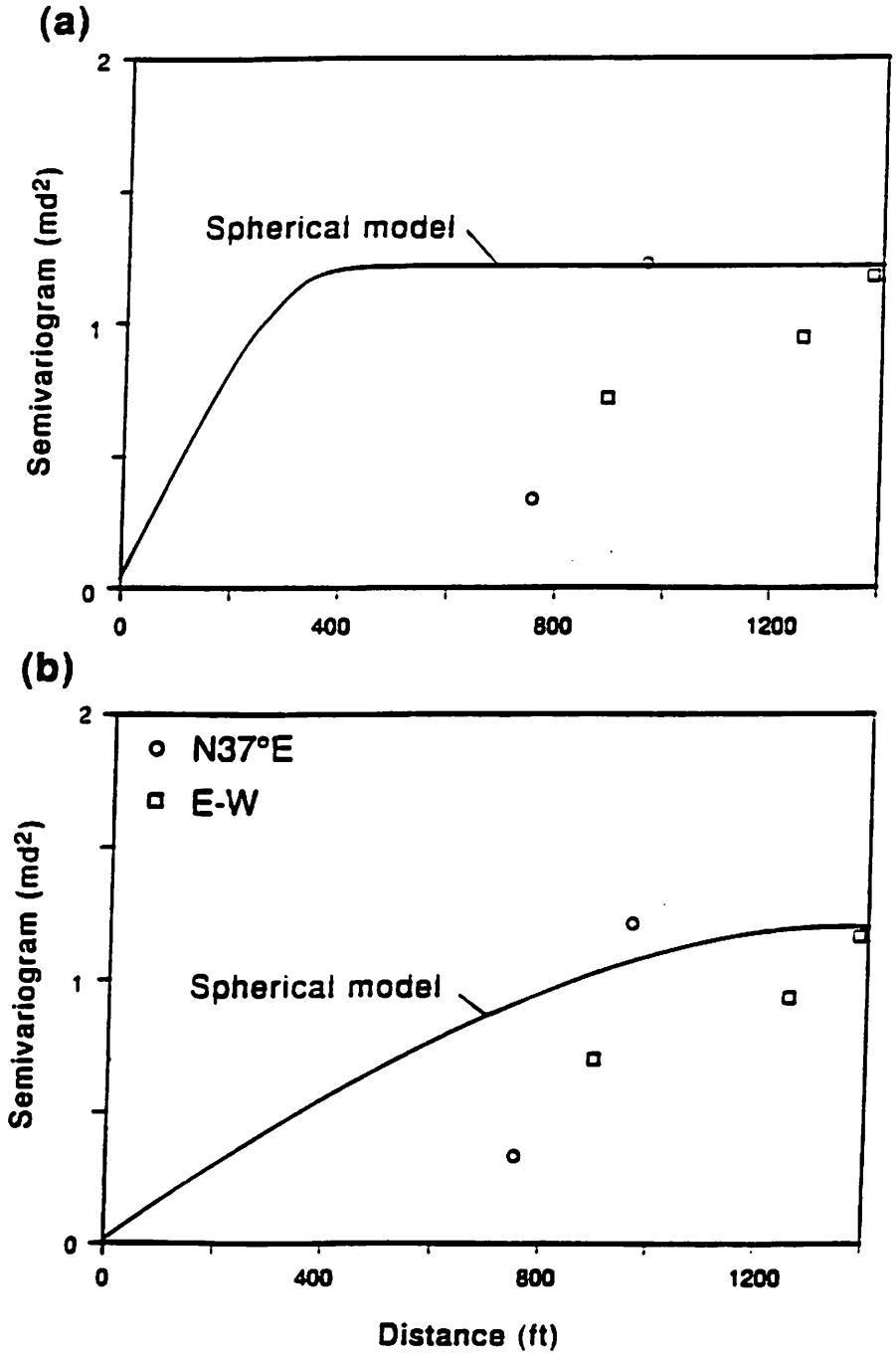

Fig. 2.4 Horizontal Variogram Models (γ) Used to Generate Stochastic Simulations of Permeability between Two Wells. Two Different Ranges for γ_s are Assumed and are Used in the Simulations: (a) 400 ft, Representing Poor Continuity, and (b) 13,00 ft, Representing Good Continuity. (After Fogg and Lucia, 1990)

length. This relationship of the effective dispersivity can be used to characterize the influence of permeability heterogeneity on dispersive mixing.

One of the major problems in the aforementioned geostatistical techniques is the lack of interwell data. Generally, the vertical data is adequate, but the horizontal, or the areal information between the wells is not sufficient. This problem creates complexity in the construction of variograms. A true variogram from a field is the key to a good approximation by the kriging or conditional simulations.

2.5 Summary

From the preceding literature survey, it is evident that knowledge of the reservoir heterogeneity (especially permeability) is very important in the recovery of oil. Although it is impossible to compute actual values of permeability at the specified grid of a reservoir simulator; the statistical variation of permeability can be evaluated by geostatistical techniques. For a good approximation, these techniques (for example kriging and conditional simulation) require adequate data available from the field. Unfortunately, field sampling is not sufficient, especially in the horizontal direction where the data is only available at the scale of well spacing. Variograms constructed from this type of data can give misleading estimates of the geostatistical parameters (variance and correlation length) of the permeability. An incorrect estimate of the variogram can in turn give unacceptable results from any interpolation technique (Fogg and Lucia, 1990). Therefore, a true estimate of the geostatistical parameters of the rock property is the key to a successful interpretation of the reservoir heterogeneity.

Tracer tests have been widely used in the oil industry and hydrology to obtain qualitative information about the reservoir rock, for example delineation of flow barriers, preferential flow paths, etc. In this study, an attempt is made to show that well-to-well tracer results can be used to assess the variance and correlation length of the permeability distribution. To verify this concept, numerical as well as experimental verification is required. Existing numerical schemes either have instability problems or show numerical dispersion. Therefore, a good numerical scheme of the solving C-D equation is essential. Laboratory experiments can be used

to confirm the theoretical results since sufficient field data is usually not available to prove or disprove them.

3 Miscible Tracers in Oil Field Flooding Patterns

3.1 Introduction

Mathematically, the flow of a miscible tracer in a reservoir is described by the well-known convective-dispersion (C-D) equation. The exact analytical or numerical solutions for a nonuniform flow field are not available. Existing numerical simulation procedures can show instability problems or suffer from numerical dispersion, especially on a large field scale (Peaceman and Rachford, 1962; Fanchi, 1983). Several techniques are described in the literature (Chaudhari, 1971; Stone and Brian, 1963; Larson, 1982; Garder, et al., 1963; Laumbach, 1975) that attempt to minimize the effect of numerical dispersion, but its elimination has not been completely achieved.

This chapter presents a new numerical method of solving (C-D) equation for displacement of miscible tracers in flooding patterns such as the five-spots, the staggered line drive, and the direct line drive. More emphasis is given to five-spot because they are widely used, and because the different behavior shown by other flooding patterns are only due to the geometry of that particular pattern. A single component, single phase, miscible tracer with unit mobility ratio for numerical computations is considered. The formation is assumed to have only a single layer. The new numerical technique considers both convection and physical dispersion during flow of the tracer and approaches the solution differently then do conventional finite difference methods. An equation of motion, which contains both Darcy and dispersive terms, allows tracking of isoconcentration lines. This numerical method is stable and avoids any numerical dispersion.

The chapter is divided into three main sections. The first section presents the theory of mixing in a five-spot pattern for unit-mobility case. A qualitative analysis of the flow mechanism in five-spot pattern is presented. The second section presents equations that describe the miscible/immiscible flow of a tracer slug. The equation of motion of the isoconcentration lines is also derived in this section. By using tensor analysis, the equation of motion is first derived in a general curvilinear coordinate system, and then in an orthogonal (Φ, Ψ) coordinate system. Finally, the proposed

numerical technique to solve the convective-dispersion equation is presented.

3.2 Mixing Mechanism in Flooding Patterns

Most waterfloods use existing wells for producers and injectors to make a particular pattern. If the wells are drilled on a square grid, a five-spot will result if any side of the square grids are converted into injection wells. Theoretical considerations, if the formation is assumed to be homogeneous, provide symmetry properties in a system of wells like a five-spot pattern. For a heterogeneous formation, the permeabilities for all four quarters of the five-spot pattern are assumed to come from the same distribution. Further, the flow rates at each of the four production wells of the pattern are kept constant at one fourth of the total injection. In a heterogeneous formation, the streamlines may follow the path outside the four boundaries of the truncated five-spot quadrant (Schafer-Perini, 1990). In a truncated pattern, only the streamlines close to the no flow boundaries are incorrectly modeled (Schafer Perini, 1990). Therefore, the effect of using a quadrant of a five-spot may alter mostly the production at long times after breakthrough. For the purpose of analysis here, only one quarter of a five-spot pattern is considered.

The transport of a tracer in the porous medium at unit mobility ratio is subjected to convection and dispersion. Both of these are modified considerably by the presence of channeling due to permeability heterogeneity. Convection represents the gross movement of fluids in the system, keeping the sharp front between displacing and displaced fluids. For example, Fig. 3.1 shows the front locations for the leading and trailing isoconcentration lines of a tracer slug in a homogeneous formation, at four different values of the pore volume injected. Because it was assumed in the calculation that produced Fig. 3.1 that there was no dispersive mixing, the separation between the first and last isoconcentration lines can hardly be seen. This is because the spreading tendency of the isoconcentration lines is zero. The tracer output concentration at the production well, as shown in Fig. 3.2, is considerably less then 100%. The dilution of the output tracer concentration is due to the geometric effect of the five-spot pattern. Due to the geometric effect, the majority of the streamlines entering the production well at any given time carry fluid which

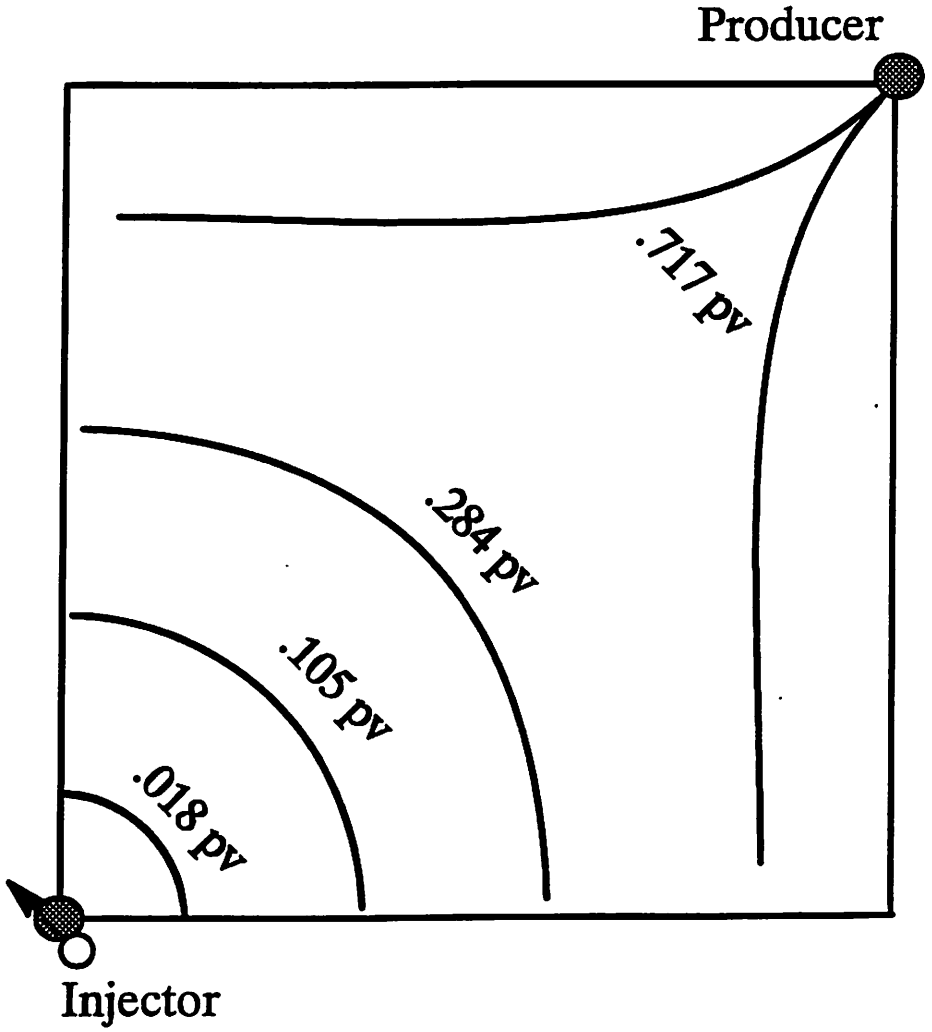

Fig. 3.1 Front Locations of First and Last Isoconcentration Lines of Tracer Slug with no Dispersion (Homogeneous Case).

has zero concentration.

Fig. 3.3 shows the same case with the inclusion of dispersive mixing. The dispersive mixing has increased the separation between two isoconcentration lines. The separation of the leading and trailing isoconcentration lines is obvious in Fig. 3.3. The corresponding tracer profile shows more dilution due to the effect of dispersive mixing, as shown in Fig. 3.4. It is to be noted that in both the cases of a homogeneous formation, the tracer output concentration at the production well has only one peak. As shown in Fig. 3.5, for a heterogeneous case, where the permeability varies in space, the front locations for the leading and trailing isoconcentration lines will be irregular. In this case, the tracer profile (Fig 3.6) is even more diluted, and multiple peaks occur due to the spatial permeability variation.

It is clear from the above discussion that the mixing of a tracer in a flooding pattern is influenced by the geometry (convective effects), dispersion and the permeability heterogeneity. The dispersion employed here refers to the dispersive mixing at a macroscopic level. Its effect is usually much smaller (Lake et al., 1989) than is the mixing caused by channeling. In the present work, we will study the effect of all three factors that influence the flow of a miscible tracer through oil field flooding patterns, i.e., 1) the geometric effect, 2)variability of permeability, and 3) macroscopic dispersivity.

3.3 Flow/Displacement Equations in Flooding Patterns

The production of tracer flow requires the calculation of the convective term, which for a steady-state flow, is a function of position alone. The following assumptions have been made to describe fluid movement.

1. Formation is isotropic, but assumed to be either heterogeneous or homogeneous.
2. Fluids are incompressible, and gravity, and capillary effects are neglected.

The Darcy velocity in differential form can be written as

$$-\mathbf{u} = \frac{k}{\mu}\nabla P \tag{3.1}$$

where, ∇P is the pressure gradient.

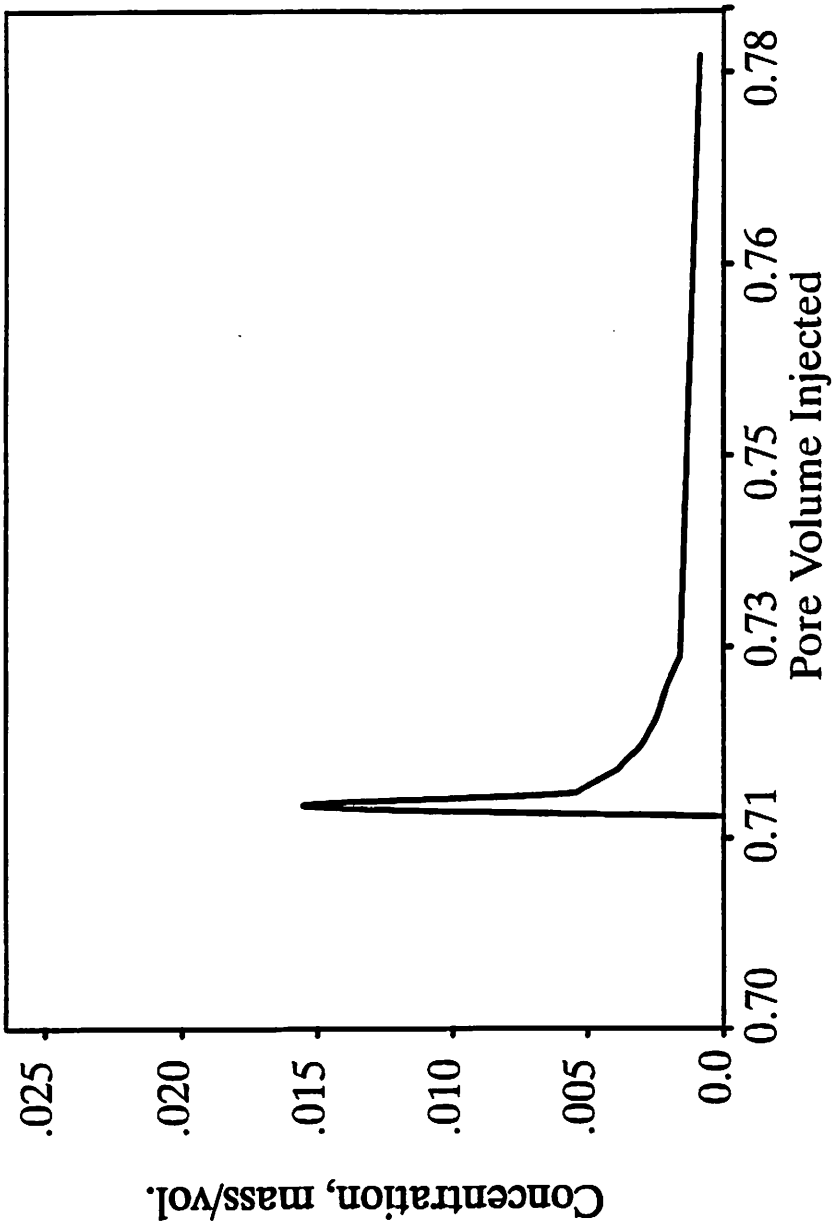

Fig. 3.2 Integrated Output Concentration Profile of Tracer Slug with no Dispersion (Homogeneous Case).

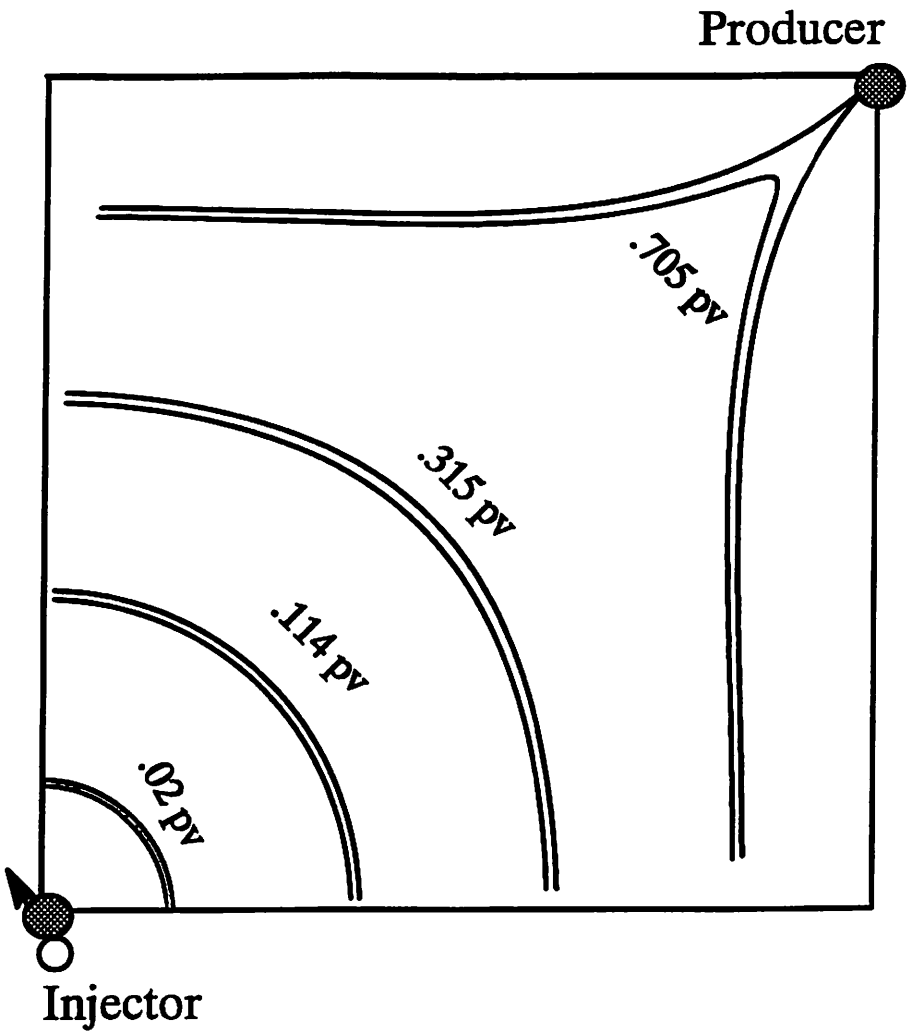

Fig. 3.3 Front Locations of First and Last Isoconcentration Lines of Tracer Slug, $a/\lambda_L = 500$ (Homogeneous Case).

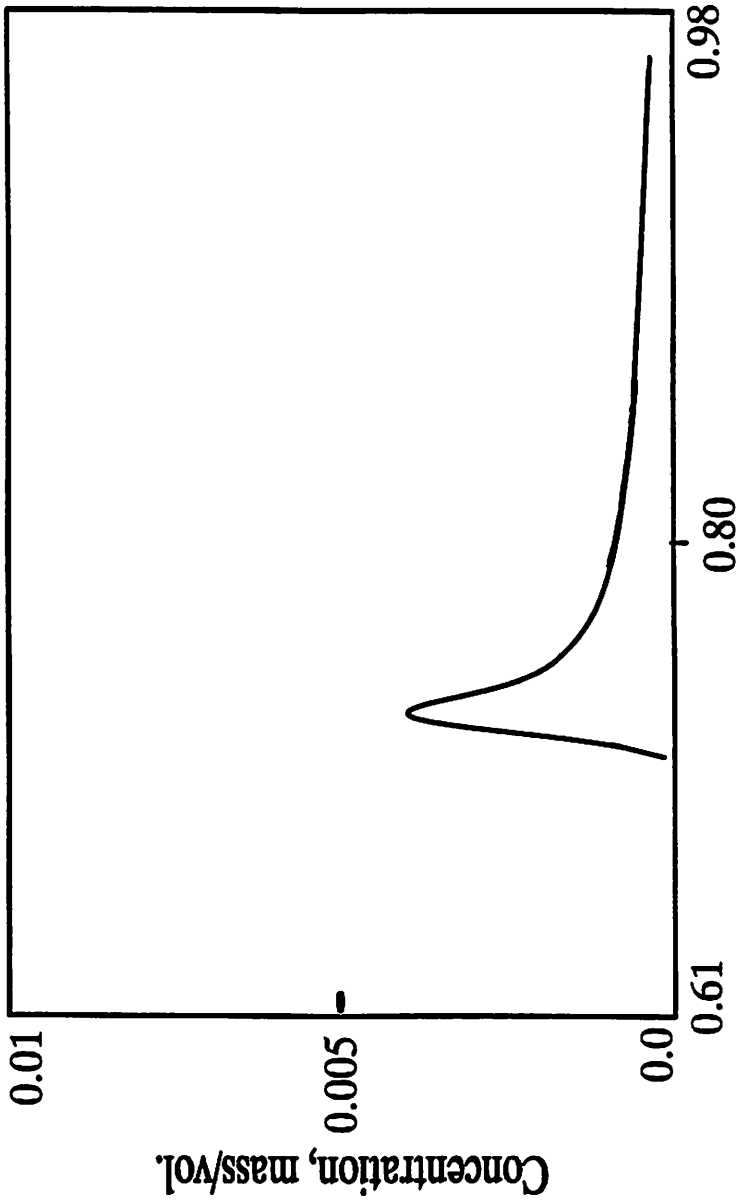

Fig. 3.4 Integrated Output Concentration Profile of Tracer Slug, $a/\lambda_L = 500$ (Homogeneous Case).

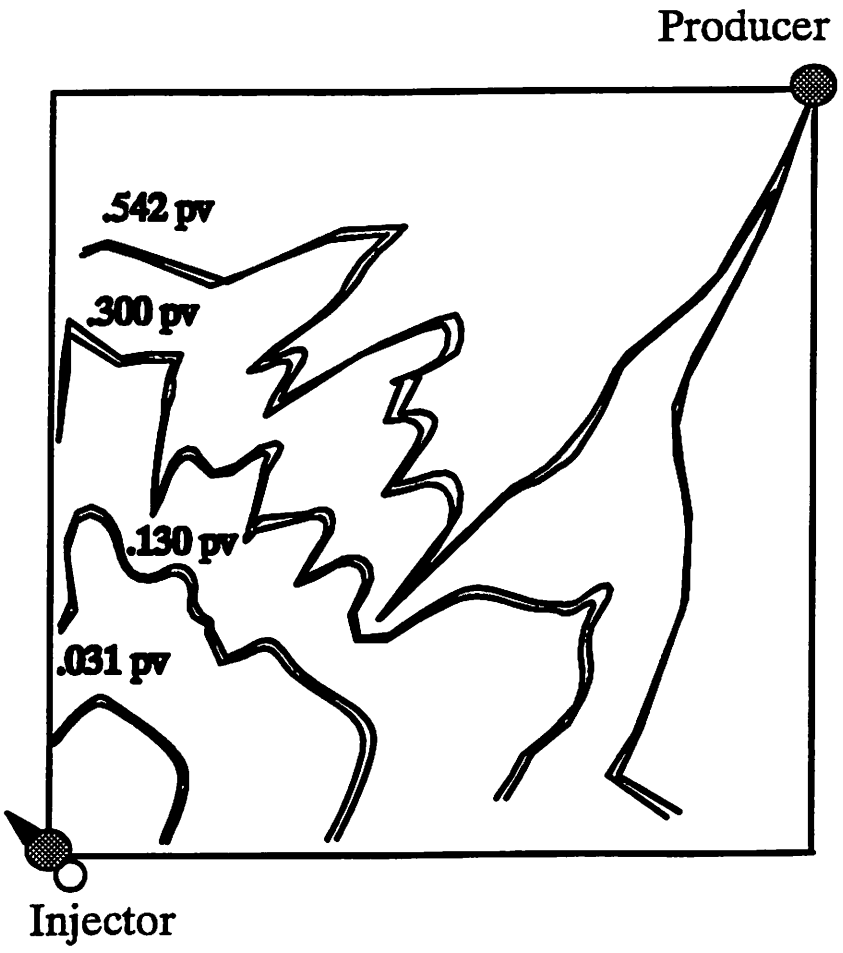

Fig. 3.5 Front Locations of First and Last Isoconcentration Lines of Tracer Slug, $a/\lambda_L = 500$, $\sigma^2 = 1.12$, $\lambda_D = 0.2$.

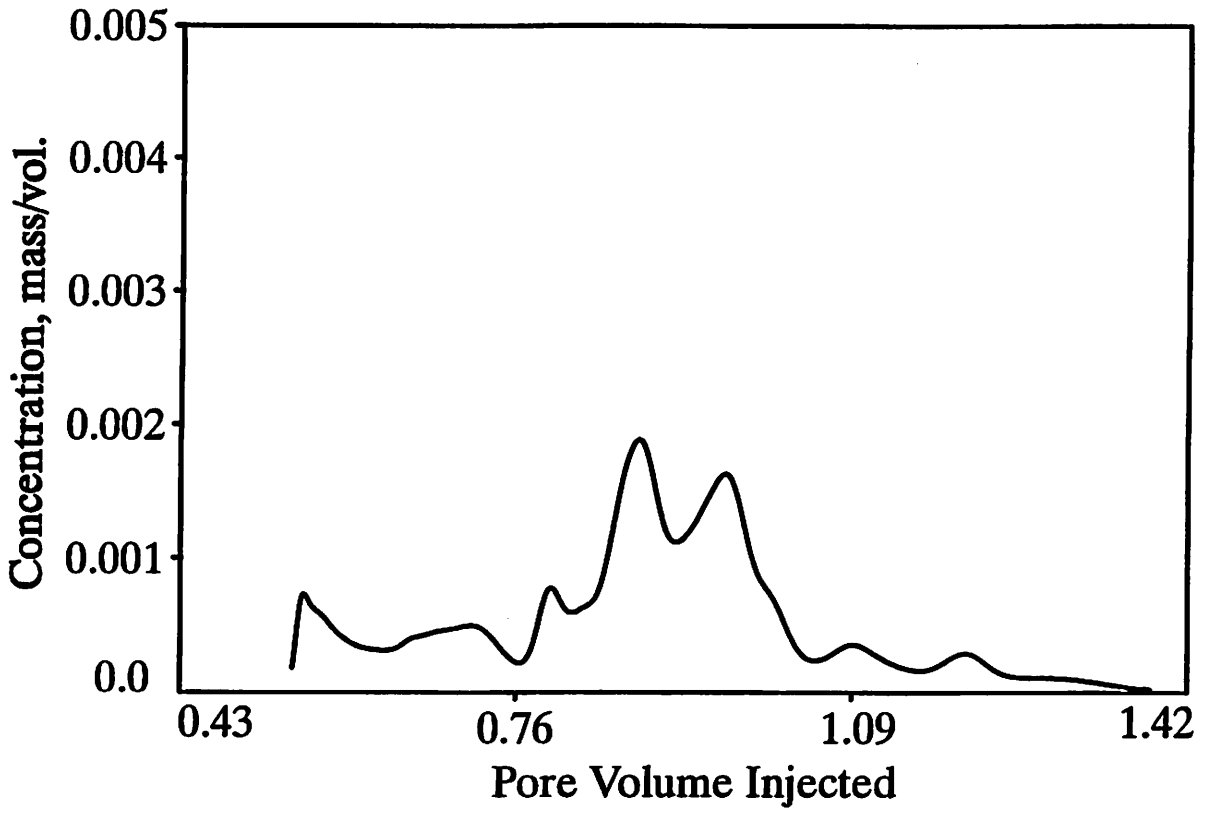

Fig. 3.6 Integrated Output Concentration Profile of Tracer Slug, $a/\lambda_L = 500$, $\sigma^2 = 1.12$, $\lambda_D = 0.2$.

While the fluid density remains constant, the gravitational forces are neglected in Eq. 3.1. Additionally, if the fluid viscosity, μ, and permeability, k, are not functions of position, and if the fluid is incompressible, then Eq. 3.1 can be reduced by taking the divergence, which produces Laplace's partial differential equation in pressure

$$\nabla^2 P = 0 \tag{3.2a}$$

Solutions to this equation can be easily obtained if the function P or the normal component of its gradient is given on the boundary. In cases where the boundary cannot be represented analytically, numerical techniques are available by which P can be evaluated at the mesh points of grids covering the region of interest. In cases where permeability is a function of position, the simplification that led to Eq. 3.2a cannot be used, and the divergence of Eq. 3.1 becomes

$$\nabla^2 P + \nabla P \cdot \nabla lnK = 0 \tag{3.2b}$$

No general analytical solutions to Eq. 3.2b are available; it can only be solved numerically. The pressure equation (Eq. 3.2b) deals with values of the permeability and of the gradient of permeability at the specified grid points. In practice, the permeability values are only known at well locations. Geostatistical techniques are therefore employed to estimate probable values of the permeabilities at the grids of a reservoir simulator. The next chapter describes the techniques and computations of the permeability field. After the solution of Eq. 3.2 has been obtained, the velocity distribution can be easily obtained from Eq. 3.1. For a constant density fluid, pressure can be equated to a function as $\xi = P/\rho + gz$, where the second term can be neglected in an areal flow situation. Replace $\rho\xi$ by Φ, where Φ is now defined as the potential function and has units of pressure.

Instead of observing pressure variations and computing velocity from them, it is possible to observe the computed Darcy streamlines in a steady flow through a porous medium, and then to compute the fluids velocities from these observations. The streamline is to be understood as an average concept because it is impossible to label a single fluid particle and observe its motion. In the flow domain at any

instant of time, a velocity vector with a definite direction can be easily defined on a point. At that point, the instantaneous curves that are at every point tangent to the direction of the velocity are called streamlines (Fig. 3.7). The mathematical expression defining a streamline (Bear, 1972) is therefore $\mathbf{u} \times d\mathbf{r} = 0$ and we can write

$$\frac{dx}{u_x} = \frac{dy}{u_y} \qquad \text{or} \qquad u_y\,dx - u_x\,dy = 0 \tag{3.3}$$

The solution of Eq. 3.3 can be written as

$$\zeta = \zeta(x, y) = \text{constant for a particular streamline} \tag{3.4}$$

This evaluates the instantaneous geometry of the streamlines. If we write Eq. 3.3 as $dy/dx = u_y/u_x = f(x, y)$, it follows that the direction of a streamline at a point is given by the angle $\theta = \tan^{-1} f(x, y)$. This is the angle between the tangent to the curve and the x-direction at any point. If we define the total derivative of Eq. 3.4 as

$$d\zeta = \frac{\partial \zeta}{\partial x}\,dx + \frac{\partial \zeta}{\partial y}\,dy = u_x\,dy - u_y\,dx = 0$$

then

$$u_x = \frac{\partial \zeta}{\partial y} \quad ; \quad u_y = -\frac{\partial \zeta}{\partial x}$$

Replacing ζ as $k\Psi/\mu$, where Ψ is known as the stream function, the velocity equations using the Cauchy-Riemann principle can be written as

$$u_x = \frac{k}{\mu}\frac{\partial \Psi}{\partial y} = \frac{k}{\mu}\frac{\partial \Phi}{\partial x} \quad ; \quad u_y = \frac{-k}{\mu}\frac{\partial \Psi}{\partial x} = \frac{-k}{\mu}\frac{\partial \Phi}{\partial y} \tag{3.5}$$

It can be proved easily that the lines of constant Φ and Ψ are orthogonal (Bear, 1972).

3.3.1 Miscible Displacement

Miscible displacement is not strictly "piston-like", but is accompanied by the dispersive mixing of flowing fluids at the displacement front, which in turn is the result of hydrodynamic dispersion and small-scale permeability variations. A mathematical description of dispersive mixing of fluids in porous media is described in this section.

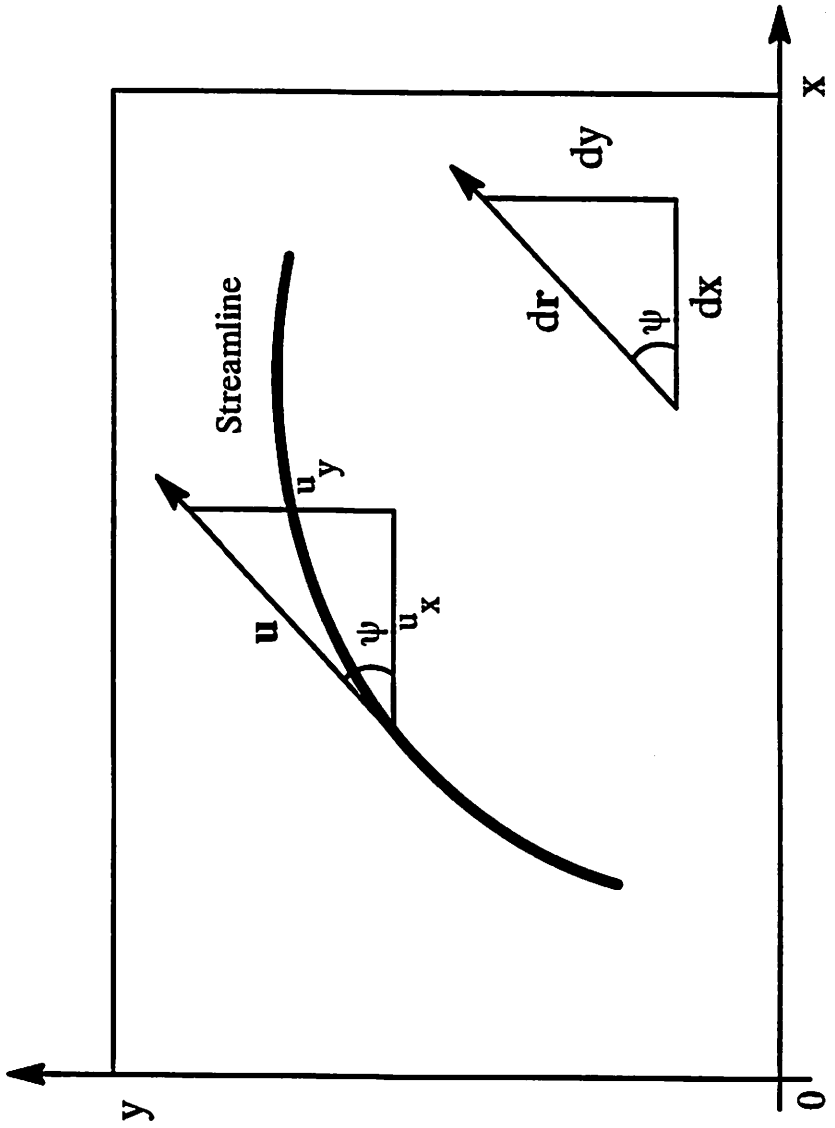

Fig. 3.7 Velocity and Position Components of Streamlines.

In flow through porous media, a tracer will occupy a larger portion of the flow domain due to dispersive mixing than it would occupy with the average flow alone. This mixing mechanism is called hydrodynamic dispersion.

The hydrodynamic dispersion depends upon: a) microscopic geometry of the pore space and consequent spatial velocity variations, b) molecular diffusion that tends to reduce variations in tracer concentration within the liquid phase, and c) interaction between the liquid and solid phases.

There are two basic phenomena involved in hydrodynamic dispersion: 1) convection and 2) molecular diffusion. The hydrodynamic dispersion due to convection is often referred to as mechanical dispersion, which is caused by the variations in local velocity both in magnitude and direction, along the tortuous flow path. This type of inhomogeneity is on a microscopic scale; whereas, on a macroscopic scale, variations in average permeability are also responsible for the mixing of tracer. The mixing introduced by the permeability variation is dominant over dispersive mixing (Ghori and Heller, 1990). Mechanical dispersion can be further classified into two components, namely longitudinal dispersion in the average-flow direction and transverse dispersion normal to the average-flow direction. Experiments show that the magnitude of transverse dispersion is approximately 20 to 50 times less than the longitudinal dispersion (Perkins and Johnson 1963; Blackwell, 1962) if the velocities are high enough that the convective components of the dispersion coefficients are much greater than the diffusive part.

3.3.2 Derivation of Equation of Motion

In this section, equations are derived which describe the flow of a tracer slug through a porous rock. In the development of the equations, the following assumptions are made:

1. A steady-state flow condition has been established in the pattern prior to the injection of the tracer slug.
2. There is only one mobile fluid-phase in the system, which is the same as that of the tracer slug.

3. The tracer does not adsorb on the formation rock, or into any immobile fluid phase.
4. The tracer does not react with either the formation fluid or the formation matrix.
5. The half-life of the tracer is long enough (if it is a radioactive tracer) so that it does not decay appreciably during flow and prior to breakthrough.
6. The tracer slug has the same mobility as the displaced and displacing fluid.
7. The tracer slug size is small compared to the volume of the pattern.

The flow of tracer fluids through the porous system with the same mobility is equivalent to a single-phase displacement. In a steady-state flow of a single-phase fluid, one pressure field is enough to describe the entire system. As a consequence, the streamlines and isopotential lines for the system are unaffected by the location of the displacement fronts. For convenience, such flow systems can be divided into several unvarying stream-tubes, and the fluid flow in each can be studied.

The state of displacement of a miscible fluid in a porous medium is specified by two macroscopic variables, a vector $\mathbf{u}$, a function of the coordinate which is described by the Darcy velocity, and a scalar C, which represents the concentration of displacing fluid ranging from 0 to 1. The variation of concentration of a displacing fluid and velocity field are related as

$$\frac{\partial C}{\partial t} = -\frac{\mathbf{u}}{\phi S_w}\nabla C + \nabla \cdot \mathbf{D} \cdot \nabla C \tag{3.6}$$

Here, $\mathbf{D}$ is the second order symmetric tensor which represents the coefficient of dispersion for the fluid matrix system. Even for a homogeneous and isotropic system, dispersion is direction dependent. As discussed earlier, that dispersion contains molecular diffusion and convective mixing in an inseparable form, therefore it is useful to express dispersion (Blackwell, 1962; Perkins and Johnston, 1963; and Heller, 1986) as

$$D_L = \frac{D_m}{\phi F} + \frac{\lambda_L |\mathbf{u}|}{\phi} \tag{3.6a}$$

where λ_L is the dispersivity constant in the longitudinal direction. In the transverse direction, λ_L will be replaced by λ_T as pointed out before λ_L/λ_T is in the order of 30.

3.3.3 Motion of the Isoconcentration Surfaces in Two Dimensions

The description of the two-state variables $(\mathbf{u}, C)$ in miscible displacement may be given in terms of the motion of a family of isoconcentration surfaces. The concentration is represented by a scalar function of two quantities, space and time $C(\mathbf{r},t)$, the total derivative of which is

$$dC = \nabla C \cdot d\mathbf{r} + \frac{\partial C}{\partial t} dt \tag{3.7}$$

The substantive time derivative of concentration can then be written as

$$\frac{DC}{Dt} = \nabla C \cdot \frac{d\mathbf{r}}{dt} + \frac{\partial C}{\partial t} \tag{3.8}$$

About a test point that is moving with a given isoconcentration surface, the substantive time derivative of concentration (along an isoconcentration surface) will be zero. Replacing $d\mathbf{r}/dt$ by a vector $\mathbf{v}$, equation (3.8) becomes

$$\mathbf{v} \cdot \nabla C = -\frac{\partial C}{\partial t} \tag{3.9}$$

Here $\mathbf{v}$ is the displacement velocity vector or front velocity vector of the isoconcentration surface. Combining equation (3.6) and (3.9) we get

$$\mathbf{v} \cdot \nabla C = \frac{\mathbf{u}}{\phi S_w} \cdot \nabla C - \nabla \cdot \mathbf{D} \cdot \nabla C \tag{3.10}$$

The dot product on the $L.H.S$ of Eq. 3.10 can be identified as a scalar v which is the local velocity of the isoconcentration lines, perpendicular to the concentration gradient. Again similar to a convective-dispersion equation (Eq. 3.6), Eq. 3.10 also has a convective part and a dispersive part. The convective term (which is proportional to the Darcy velocity vector $\mathbf{u}$) can be computed either from Eq. 3.2a (homogeneous case) or from Eq. 3.2b (heterogeneous case). For the dispersive part

in Eq. 3.10 a modification is required to deal with the tensorial nature of dispersion. In a one-dimensional flow system, Eq. 3.10 can be solved numerically quite easily. For a multidimensional flow system, however, Eq. 3.10 can be solved numerically if the flow vector is parallel to one of the coordinates of the flow system. In most multidimensional miscible displacements, for example flow in a five-spot, the flow vectors are not simply oriented with respect to the coordinate axis. Although most of the reservoir problems can be simulated on rectangular grids, there are many instances in which the geometry of the reservoir is suitable to a curvilinear coordinate system. For example, an areal flow in a five-spot pattern can be described by the grid, produced by the family of streamlines Ψ = constant and isopotential lines Φ = constant. These are shown in Fig. 3.8 for a homogeneous reservoir. In a heterogeneous formation, the family of Darcy streamlines, although much less smooth, are still the lines of constant Ψ. The equipotential lines, similarly, are still locally perpendicular to the streamlines. By using tensorial analysis the equation of motion of the isoconcentration lines can be written in a Φ and Ψ coordinate system (Appendix A) as

$$v_\Phi \frac{\partial C}{\partial \Phi} + v_\Psi \frac{\partial C}{\partial \Psi} = \frac{u}{\phi}\frac{\partial C}{\partial \Phi} - \frac{1}{h}\left[\frac{\partial}{\partial \Phi}\left(D_L \frac{\partial C}{\partial \Phi}\right) + \frac{\partial}{\partial \Psi}\left(D_T \frac{\partial C}{\partial \Psi}\right)\right] \qquad (3.11a)$$

This is the equation of motion of isoconcentration surfaces in a two dimensional ($\Phi - \Psi$) coordinate system. This analytic expression is used directly in the two-dimensional miscible displacement of a tracer in porous media. The method involves injecting a tracer of a *rampup and rampdown* shape with concentration distribution values assigned to this ramp ranging from 0 to 1. This concentration profile is divided into seventeen isoconcentration lines or points. Each isoconcentration line is subjected to the influence of convection and dispersion, and outward or front velocity is calculated by the equations

$$v_\Phi = \frac{u}{\phi} - \frac{\frac{1}{h}\left[\frac{\partial}{\partial \Phi}\left(D_L \frac{\partial C}{\partial \Phi}\right)\right]}{\frac{\partial C}{\partial \Phi}} \qquad (3.11b)$$

in the longitudinal direction, and

$$v_\Psi = -\frac{\frac{1}{h}\left[\frac{\partial}{\partial\Psi}\left(D_T\frac{\partial C}{\partial\Psi}\right)\right]}{\frac{\partial C}{\partial\Psi}} \tag{3.11c}$$

in the transverse direction. The resultant velocity of the front is then,

$$v = \sqrt{(v_\Phi^2 + v_\Psi^2)} \tag{3.11d}$$

3.4 Numerical Method

The numerical computations have been divided into three major parts. The first section computes the pressure field and the Darcy velocity; the second part computes the velocity of the isoconcentration lines, v; and the last section calculates the integrated output concentration profile that would be observed at the production well. The computation has been coded in Fortran 77 in Appendix D.

3.4.1 Determination of Darcy Velocity

The equation of motion of the isoconcentration lines requires computed values of the Darcy velocity along prespecified streamlines. While this velocity can be obtained analytically for the homogeneous case by solution of the Laplace equation, there exists no general analytical solution in fields where the permeability varies arbitrarily from point to point. As noted previously, if the spatial permeability pattern is known or can be approximated, the pressure field can be computed numerically by solution of an equation similar to that of Laplace:

$$\nabla^2 P + \nabla P \cdot \nabla lnK = 0 \tag{3.2b}$$

For a two-dimensional isotropic system containing both injectors and producers, Eq. 3.2b can be written as

$$\frac{\partial}{\partial x}(K(x,y)\frac{\partial p}{\partial x}) + \frac{\partial}{\partial y}(K(x,y)\frac{\partial p}{\partial y}) + q(x,y,p) = 0 \tag{3.12}$$

$$0 \le x \le XL, \quad 0 \le y \le YL$$

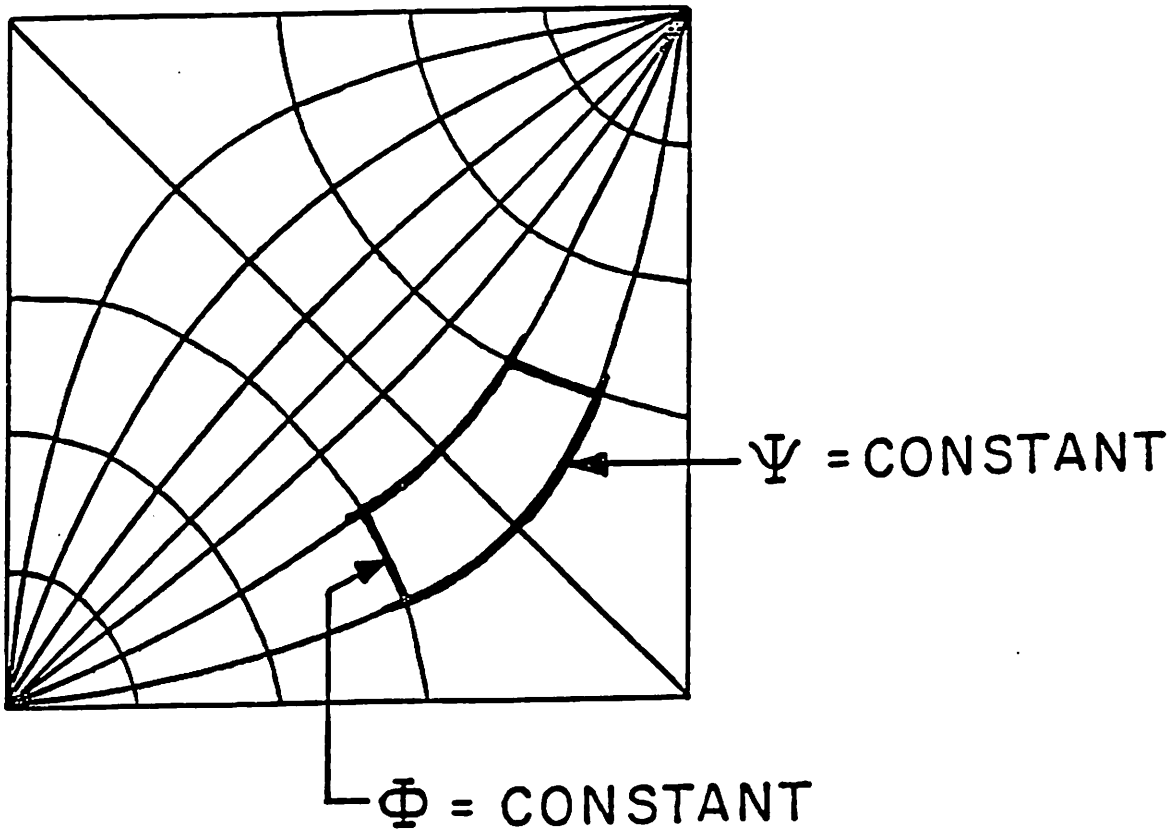

Fig. 3.8 Curvilinear Coordinates
in a Five-Spot Pattern.

where, q(x,y,p) represent the sources and the sinks (depending on whether q is negative or positive) and is a function of position and the pressure at that location. If no flow is specified as the condition at the outer boundaries then

$$\frac{\partial p}{\partial x} = 0 \quad at\ x = 0\ and\ x = XL\ for\ 0 \geq y \leq YL$$
$$\frac{\partial p}{\partial y} = 0 \quad at\ y = 0\ and\ y = YL\ for\ 0 \geq x \leq XL \tag{3.13}$$

A *point centered* grid system was used as shown in Fig. 3.9. For an irregular grid system the derivatives in Eq. 3.12 can be written as

$$\frac{\partial}{\partial x}(K\frac{\partial p}{\partial x}) \approx \frac{K_{i+1/2,j}\frac{P_{i+1,j}-P_{ij}}{x_{i+1}-x_i} - K_{i-1/2,j}\frac{P_{ij}-P_{i-1,j}}{x_i-x_{i-1}}}{x_{i+1/2} - x_{i-1/2}} \tag{3.14a}$$

$$\frac{\partial}{\partial y}(K\frac{\partial p}{\partial y}) \approx \frac{K_{i,j+1/2}\frac{P_{i,j+1}-P_{ij}}{y_{j+1}-y_j} - K_{i,j-1/2}\frac{P_{ij}-P_{i,j-1}}{y_j-y_{j-1}}}{y_{j+1/2} - y_{j-1/2}} \tag{3.14b}$$

Now define

$$\Delta x = x_{i+1/2} - x_{i-1/2}$$

$$\Delta y = y_{j+1/2} - y_{j-1/2}$$

where, $x_{i+1/2}$ and $y_{i+1/2}$ etc. represent the center of the grid blocks as shown in Fig. 3.9. Eq. 3.12 can be written as

$$\frac{K_{i+1/2,j}\frac{P_{i+1,j}-P_{ij}}{x_{i+1}-x_i} - K_{i-1/2,j}\frac{P_{ij}-P_{i-1,j}}{x_i-x_{i-1}}}{\Delta x}$$

+

$$\frac{K_{i,j+1/2}\frac{P_{i,j+1}-P_{ij}}{y_{j+1}-y_j} - K_{i,j-1/2}\frac{P_{ij}-P_{i,j-1}}{y_j-y_{j-1}}}{\Delta y} = q(x_i, y_j, P_{ij}) \tag{3.15}$$

Let

$$KX_{i+1/2,j} = \frac{K_{i+1/2,j}\Delta y_j}{x_{i+1} - x_i}$$

$$KY_{i,j-1/2} = \frac{K_{i,j-1/2}\Delta x_j}{y_j - y_{j-1}}$$

etc., and

$$Q_{ij} = \Delta x_i \Delta y_j q(x_i, y_j, P_{ij})$$

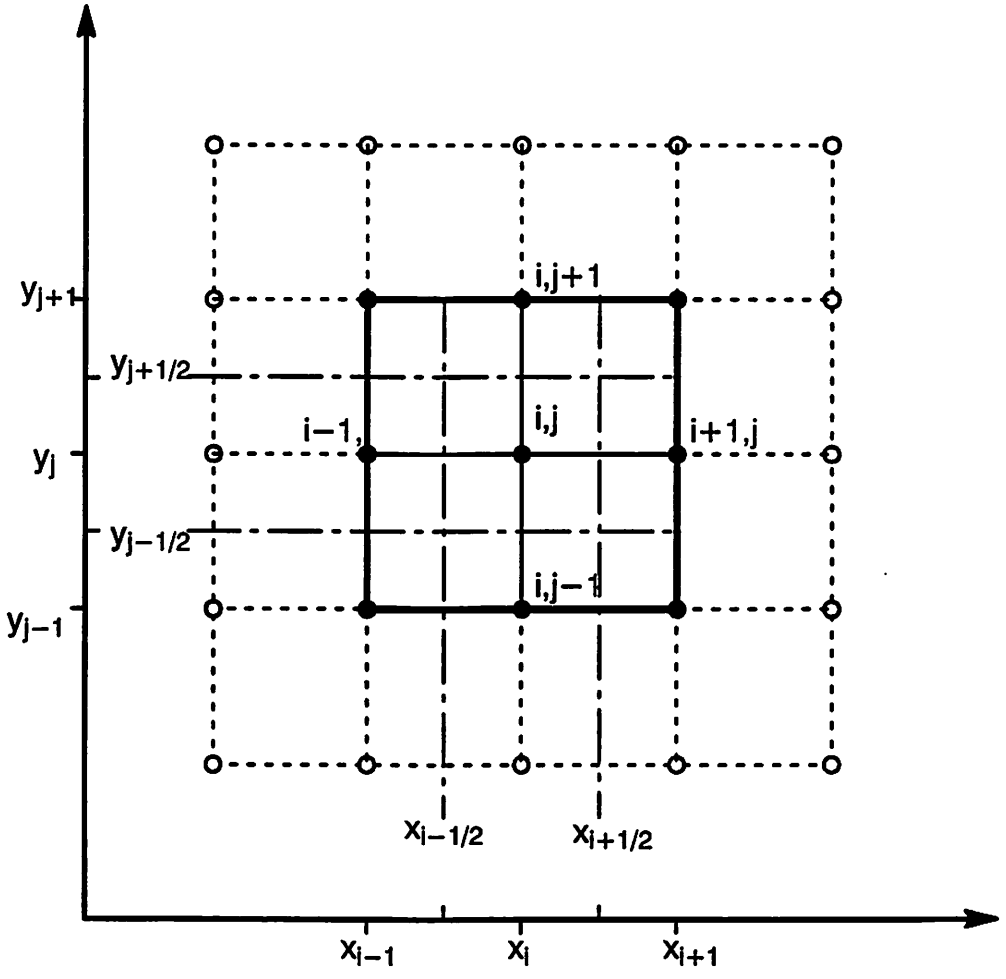

Fig. 3.9 Point Centered Grid System
Used in the Solution of Pressure Equation.

Now, substitute these expressions in Eq. 3.15 and multiply through by $\Delta x_i\ \Delta y_j$. Following (Peaceman, 1977), we get:

$$-KX_{i+1/2,j}(P_{i+1,j} - P_{ij}) + KX_{i-1/2,j}(P_{ij} - P_{i-1,j})$$

$$-KY_{i,j+1/2}(P_{i,j+1} - P_{ij}) + KY_{i,j-1/2}(P_{ij} - P_{i,j-1}) = Q_{ij} \qquad (3.16)$$

where, Q_{ij} represents the injection rate or the production rate. The no flow boundary conditions for a point center grid are

$$P_{0,j} = P_{2,j},\ \ P_{NX+1,j} = P_{NX-1,j} \quad 1 \leq j \leq NY$$

$$P_{i,0} = P_{i,2},\ \ P_{i,NY+1} = P_{i,NY-1} \quad 1 \leq i \leq NX \qquad (3.17)$$

For a two dimensional flow domain, Eq. 3.16 and Eq. 3.17 generate a system of I × J equations with I × J unknowns, P_{ij}. This system of equations is called a *pentadiagonal matrix* and is usually sparse, i.e. most of the elements of the matrix are generally zero. To solve this system of equations, a successive over relaxation (SOR) method is used.

3.4.2 Solution of Equation of Motion

As mentioned earlier, instead of solving the Convective-Dispersion equation in the present study, we will solve the Equation of Motion of the Isoconcentration Lines (EOM). Solution of this equation requires a different technique than a conventional finite difference method. This section describes the technique of solving the EOM and appendix D includes the computer code written in Fortran 77.

The numerical technique employed here has eliminated the use of any type of outer boundary conditions. This is because we have computed the Darcy streamlines which contain tracer slug, and the movement of the tracer slug is followed along these streamlines. Nevertheless, an initial condition is required to start the computations of tracer band movements. It is presumed that the actual tracer band is initially introduced as a flat topped slug with ramps on the outer edges, as shown in Fig. 3.10a. The thickness or the extent in the flow direction of the flat top portion depends upon the amount of tracer injected into the pattern. This type of input

profile was first introduced by Heller in 1986 to calculate dispersion in a radial pattern. The "*ramp up ramp down*" input profile is somewhat more realistic than a step-input profile and can be used in Eq. 3.11 since it never involves an infinite value for the concentration gradient. The step input profile has an infinite concentration gradient, and the sharp corners at the top of the slug have infinite values of second derivatives. This situation can hardly be met in a real physical problem, especially when a water-soluble tracer is injected into a reservoir filled with water. But the major reason for the assumed initial slug with a shape shown in Fig. 3.10a is that the computational difficulties will be less. In fact, the method described cannot be used if the initial slug shape is described as an infinite-slope, rectangular slug. The slopes of the ramps can be made as near to vertical as desired. The initial profile has discontinuities only in the second derivative, where they do not interfere with the calculations, as shown in Fig. 3.10c. It was assumed that the tracer slug size is much smaller than the size of the flow domain, and, because of the stability of the calculations, it turns out that the final results are not appreciably influenced by the assumed values of the width of the ramps. The width of the ramps at the front and rear edges of the initial slug have been used here as 0.4 feet.

The initial or starting time is not zero, but is assigned a value that is equal to the fill up time of a circular region of radius S_{cen} around the well bore

$$T_{\text{init}} = \frac{\pi S_w h_f \phi S_{\text{cen}}^2}{Q} \tag{3.18}$$

where,

S_{cen} = distance from the center of the well to the center of the concentration profile, L.

Initially the concentration profile is described by seventeen isoconcentration points equally divided up and down the initial ramps. At each point the displacement velocity is calculated using Eq. 3.11. The evolution of the tracer slugs can be explained in terms of distances between isoconcentration lines and is described below:

There are two distinct effects on the shape of the concentration profile. First is the

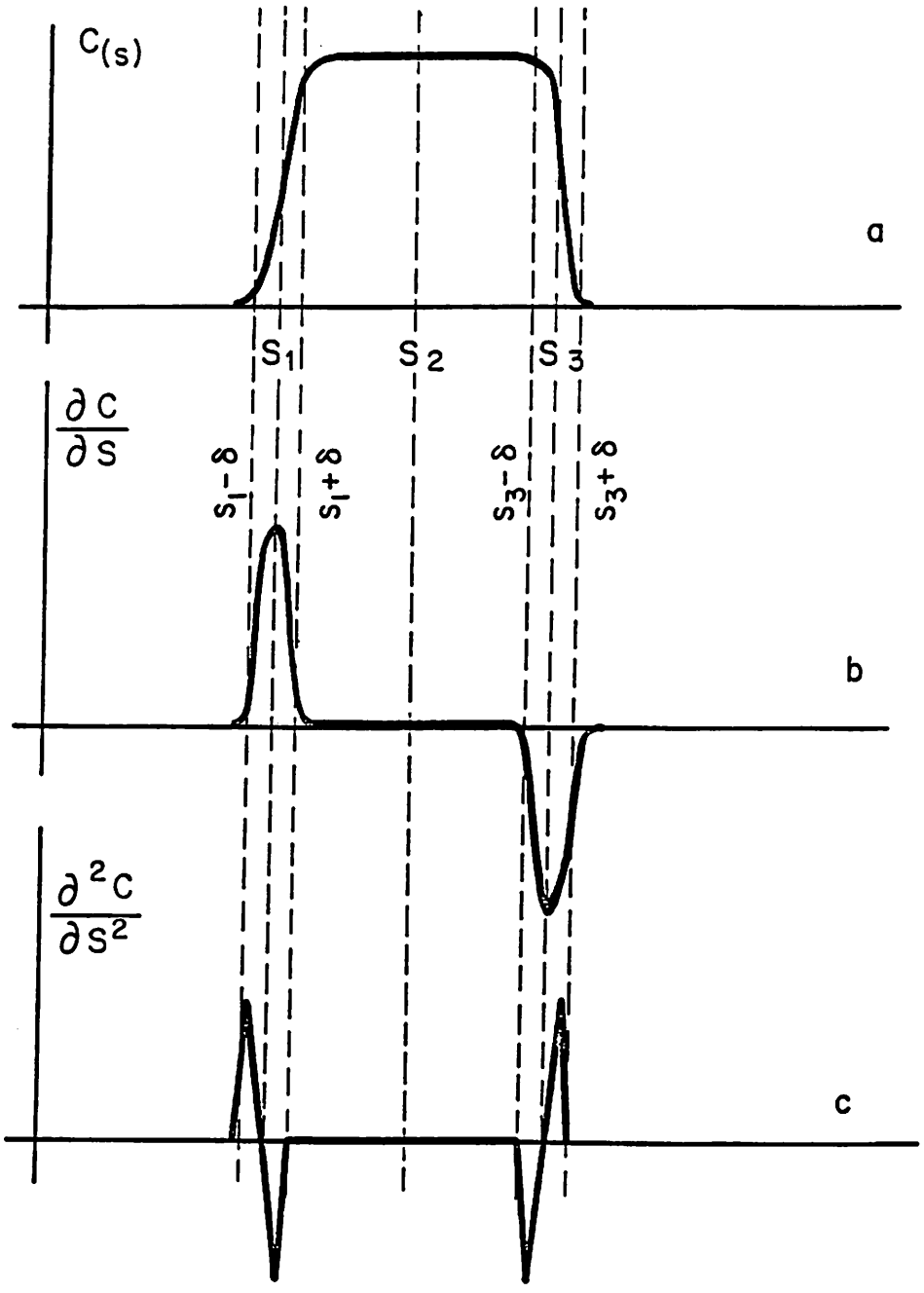

Fig. 3.10 Tracer Slug and Derivatives
During Early Flattop Stage.

effect of the geometry of the flooding pattern. On each streamline (which extends from the injector to the producer), the flow velocity reaches a minimum somewhere near the middle of the distance between wells, and increases again beyond this point. The initial decrease of velocity with distance from the injector causes the isoconcentration lines to draw closer together, and the increasing velocity during later stages causes the slug to widen again. Second is the effect of the longitudinal dispersion of the tracer which always tends to spread the slug. Only the first half of the flow domain of a flooding pattern is considered to explain these effects.

Due to geometric effects, the isoconcentration line at S_1 moves more rapidly than do those at S_3, and the distance between them decreases. Opposed to this, there is the effect of longitudinal dispersion, which tends to spread out the front. This phenomenon can be well explained by Fig. 3.10 and Eq. 3.11. The first and second derivatives of concentration at $(S_1 - \delta)$ are both positive. Therefore velocity of an isoconcentration line at $(S_1 - \delta)$ will be less than that at S_1. At $(S_1 + \delta)$ on the other hand, the first derivative of concentration is still positive; whereas, the second derivative goes negative. This makes the velocity of isoconcentration lines at $(S_1 + \delta)$ greater than those at S_1. In the early part of the flow, the geometric effects are more powerful than the dispersive influences, the slope of the inward sides of the concentration profile at S_1 will decrease, and the slope at $(S_1 + \delta)$ will increase. Similarly, the isoconcentration line at $(S_3 + \delta)$ will move faster than at S_3; whereas, at $(S_3 - \delta)$ it will move slower so the tracer slug becomes narrower. As the front proceeds further into the formation, the isoconcentration lines at $(S_1 + \delta)$ and $S_3 - \delta$ will move closer, and a time will be reached when the dispersion effects will become dominant. At this time the widening of the negative and positive spikes of $\frac{\partial C}{\partial S}\left(= \frac{1}{h}\frac{\partial C}{\partial \Phi}\right)$ will decrease until they begin to influence each other. At that time the flat top will disappear, and the maximum concentration will start to decrease. The top will resemble a parabolic shape. The shapes of this concentration profile with its first and second derivatives are given in Fig. 3.11. It is shown that at this stage, the first derivative goes through 0 at S_2; whereas the second derivative is no longer 0. The velocity of isoconcentration line at S_2 is indeterminate,

because the peak concentration becomes less than the value originally assigned to this line. It is obvious that the velocity at the peak and at 50% isoconcentration points are not influenced by dispersion and only move with convection velocity. Calculation of the tracer peak concentration and tracer band-width are given in the later sections. Following is the discussion about numerical accessories needed in the present numerical scheme.

3.4.2.1 Approximation of Derivatives

In addition to the assignment of values to the parameters in Eq. 3.11, this requires that some approximation scheme be adopted by which the first and second derivatives of concentration may be computed in both $\Phi - \Psi$ directions. Finite difference approximations, which are derived from a Taylor Series Expansion, are widely used in petroleum reservoir simulation. Though, for convenience the isoconcentration lines in the initial *rampsup and rampdown* concentration profile are equally spaced, the successive positions of these points/lines can be irregularly spaced. Moreover, it would be of practical use to refine the grids, near the well bores, due to the sharp concentration gradients and high flow velocities in the region. It would also be useful to make the grids coarser where there is less concentration gradient; thus resulting in an irregular grid spacing for the system. In the present scheme, in cases where transverse dispersion is included, the grids are equally spaced in the Ψ-direction; whereas, they are unequally spaced in the Φ-direction.

Concentration Gradient in Φ-direction

The scheme applied here is based on the approximation of the expanded form of the differential operator

$$A_d(C_i) = D_L \frac{\partial^2 C}{\partial \Phi^2} + \frac{\partial D_L}{\partial \Phi} \frac{\partial C}{\partial \Phi}$$

where A_d is the differential operator.

This scheme was applied to petroleum engineering problems for the first time by Heller (1986), and is given as

$$\mathcal{L}(C_i) = \frac{2D_{Li}}{\Delta\Phi_+ + \Delta\Phi_-} \left[\frac{C_{i+1} - C_i}{\Delta\Phi_+} - \frac{C_i - C_{i-1}}{\Delta\Phi_-} \right] + \frac{D_{Li+1} - D_{Li-1}}{\Delta\Phi_+ + \Delta\Phi_-} \cdot \frac{C_{i+1} - C_{i-1}}{\Delta\Phi_+ + \Delta\Phi_-} \tag{3.19}$$

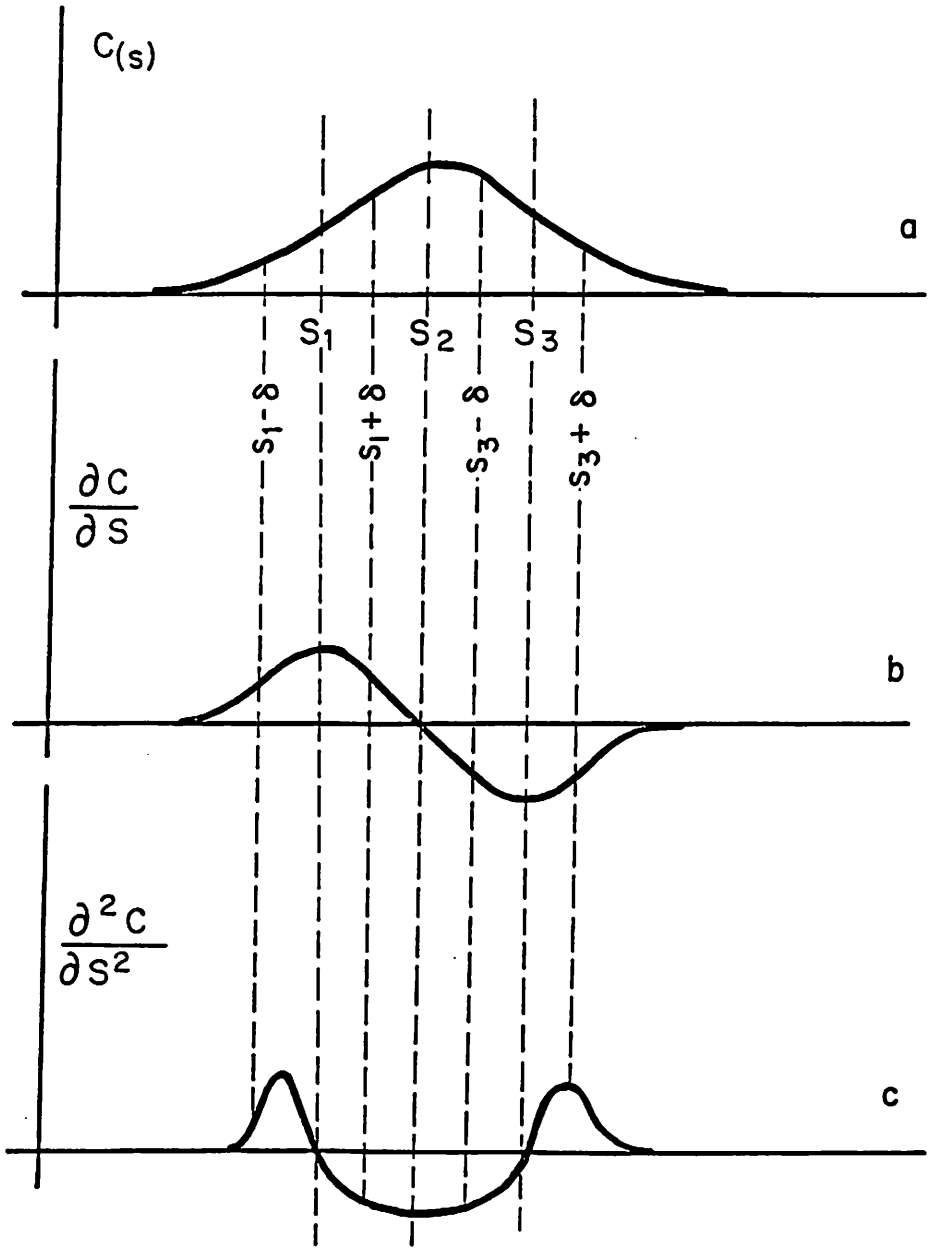

Fig. 3.11 Tracer Slug and Derivatives
After Flattop Stage is Past.

where,

$\mathcal{L}$ = the difference operator

$\Delta\Phi_+ = \Phi_{i+1} - \Phi_i$

$\Delta\Phi_- = \Phi_i - \Phi_{i-1}$

The local discretization error associated with this scheme (Settari and Aziz, 1972) is

$$\begin{aligned} e(C_i) = &- \frac{(\Delta\Phi_+ - \Delta\Phi_-)}{6}[2D_L C''' + 3(D'_L C')']_i \\ &- \frac{1}{12}\frac{\Delta\Phi_+^3 + \Delta\Phi_-^3}{\Delta\Phi_+ + \Delta\Phi_-}[D_L C^{iv} + 2D'_L C''' + 3D''_L C'' + 2D'''_L C']_i \\ &+ \frac{(\Delta\Phi_+ - \Delta\Phi_-)}{4} D''_L C'' + 0(\Delta\Phi^3) \end{aligned} \tag{3.20}$$

It is to be noted that this scheme is derived directly in terms of the values of D_L at the grid points and is of order $0(\Delta\Phi)$. This scheme for approximating derivatives is consistent (Settari and Aziz, 1972), which means that for $\|\Delta\Phi\| \rightarrow 0$ the difference operator converges to differential operator. Subroutine DERPHI in Appendix D calculates the concentration gradient in the longitudinal direction.

A Similar approach can be used in the computation of derivatives in the transverse direction, i.e., in the Ψ direction. In a previous study (Ghori, 1988), it was found that the effect of the transverse concentration gradient had a negligible effect as compared to the concentration gradient in the longitudinal direction. Therefore, in the present study, the transverse dispersion has been taken as zero unless otherwise specified.

3.4.2.2 Time Stability

Once the velocities of isoconcentration lines have been computed, their new positions are obtained by using a suitable time step. The time step criterion is important in terms of the stability of the numerical scheme. By definition, a numerical algorithm is considered stable if any errors introduced at some stage of computation do not amplify during subsequent computations. Two kinds of errors may be amplified if the numerical scheme is unstable.

Round-off Errors: This is caused by the finite accuracy of the computer performing the operations.

Truncation Errors: This error is due to the approximation of the derivatives by

using finite difference schemes.

The finite difference approximations are obtained by truncating higher order terms in a Taylor Series expansion. Other types of errors can be due to the approximation of initial and boundary conditions (Aziz and Settari 1978). In general, if an error E_0 introduced by initial conditions magnifies with time, the numerical scheme is called *unstable.*

The present numerical scheme is unconditionally stable. Therefore, a local inaccuracy (a bump on the concentration profile), caused by a previous error in the calculation of velocity will damp out in the next iteration, if a suitable time step is used.

In the near vicinity of the well bore, there are large concentration gradients and high-flow velocities. Tracer flow is dominated by convection, and dispersive effects are less. Therefore, it is desirable to use a smaller time step near the well bore.

The next position of the isoconcentration lines can be obtained from the first two terms of the expansion of the Taylor series

$$\begin{aligned} S_i(t+\Delta t) &= S_i(t) + \frac{dS_i}{dt}\Delta t + \frac{d^2S_i}{dt^2}\frac{(\Delta t)^2}{2} + \frac{d^3S_i}{dt^3}\frac{(\Delta t)^3}{6} + \cdots \\ &\approx S_i(t) + v_i\Delta t + v_i\frac{\partial v_i}{\partial S}\frac{(\Delta t)^2}{2} \end{aligned} \tag{3.21}$$

The flow near the injection well is essentially radial; therefore, the magnitude of Darcy velocity can be written as

$$u = \frac{Q}{2\pi h_f S S_w}$$

using this expression in Eq. 3.11 and neglecting the dispersive term, we get

$$= \frac{Q}{2\pi h_f \phi S S_w} \tag{3.22}$$

and

$$\frac{\partial v}{\partial S} = -\frac{Q}{2\pi h_f \phi S^2 S_w} \tag{3.23}$$

If the time increment is small enough, the higher order terms of Eq 3.21 will be negligible. Therefore if it is arbitrarily assumed that the magnitude of the third term

in Eq 3.21 is less than one hundredth of that of the second term, by substituting Eq. 3.22 and 3.23 in Eq. 3.21, we obtain the inequality

$$\Delta t < 0.04 \frac{\pi h_f \phi S^2 S_w}{Q} \tag{3.24}$$

This time step is used near production/injection wells and is denoted as DTA in subroutine DELTIM. As the flood proceeds, Δt may be safely increased in order to save computer time.

An additional restriction on the size of the time interval arises from the requirement of numerical stability of the dispersive process. The dispersive mixing involved here is itself quite stable. In the numerical computations, the sign of the velocity of the isoconcentration line will be such as to decrease the amplitude of any irregularity in the profile. But if too large a time interval is chosen, then there will be over-correction of any such irregularities in the profile, and successive positions of isoconcentration lines would oscillate with increasing amplitude, resulting in numerical instability.

Although in the present numerical scheme, the dispersion process is two-dimensional, a one-dimensional analysis which can easily be extended to a two dimensional case is presented to determine the critical time interval.

By neglecting the convective term in Eq. 3.11, the next position of the isoconcentration line in one dimension can be written as

$$v_i \Delta t = h \Delta \Phi_i = -\frac{1}{h} \left[D_L \frac{\frac{\partial^2 C}{\partial \Phi^2}}{\frac{\partial C}{\partial \Phi}} \right] \Delta t \tag{3.25}$$

We will examine the increment in $h\Phi_i$(or S_i) in the Φ-direction along a streamline. Utilizing the approximation of the first and second derivatives of concentration from Eq. 3.19 into Eq. 3.25

$$\Delta \Phi_i = -\frac{1}{h^2} D_L \left[\frac{2 \left[\frac{1}{\Phi_{i+1} - \Phi_i} - \frac{1}{\Phi_i - \Phi_{i-1}} \right]}{(\Phi_{i+1} - \Phi_{i-1}) \left(\frac{1}{\Phi_{i+1} - \Phi_i} + \frac{1}{\Phi_i - \Phi_{i-1}} \right)} \right] \Delta t \tag{3.26}$$

If the isoconcentration lines are equally incremented, a profile with a small amount of curvature would be represented (Fig. 3.12) by the following position of $(i-1)$, i

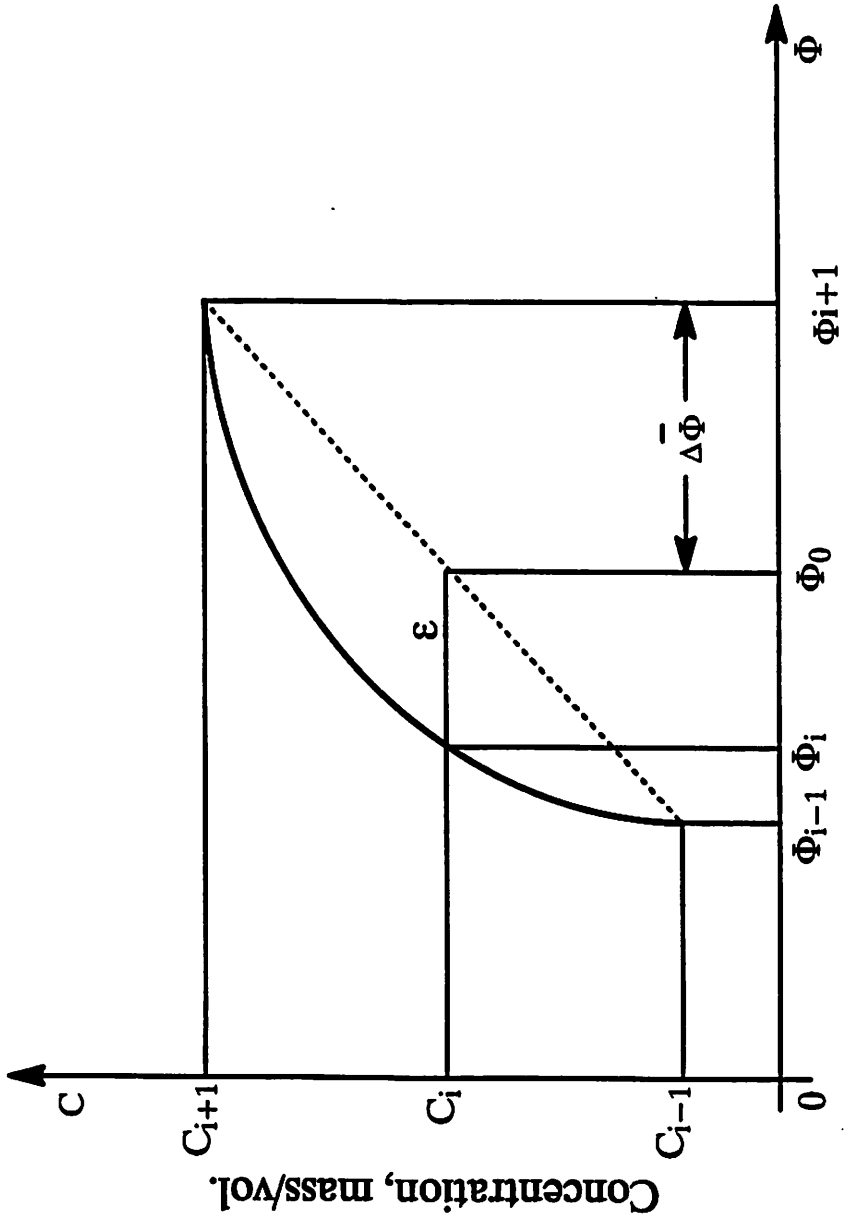

Fig. 3.12 Curvature Between Three Isoconcentration Points.

and $(i+1)$ isoconcentration lines

$$\begin{aligned} \Phi_{i-1} &= \Phi_0 - \Delta\bar{\Phi}_i \\ \Phi_i &= \Phi_0 + \epsilon \\ \Phi_{i+1} &= \Phi_0 - \Delta\bar{\Phi}_i \end{aligned} \tag{3.27}$$

where Φ_0 is the true coordinate location at which the curve formed by the two isoconcentration points is devoid of curvature, $\Delta\bar{\Phi}$ is the spacing of isoconcentration points in the profile, and ϵ represents the measure of the curvature of the concentration distribution. Substituting Eq. 3.27 in Eq. 3.26, we get

$$\Delta\Phi_i = -\frac{1}{h^2}\frac{2D_L\epsilon\Delta t}{(\Delta\bar{\Phi}_i)^2} \tag{3.28}$$

Thus, to prevent the oscillation behavior described above, and to ensure stability, the magnitude of the calculated increment $\Delta\Phi$ must never be so great that it would change the sign of the original curvature. Therefore

$$\frac{1}{h^2}\frac{2D_L\epsilon\Delta t}{(\Delta\bar{\Phi}_i)^2} < \epsilon$$

and

$$\Delta t \leq \frac{h^2}{2}\frac{(\Delta\bar{\Phi}_i)}{D_L}$$

for a two-dimensional dispersion process, we can write

$$DTB = \Delta t \leq \frac{h^2}{2}\left(\frac{(\Delta\bar{\Phi}_i)^2}{D_L} + \frac{(\Delta\bar{\Psi}_i)^2}{D_T}\right) \tag{3.29}$$

where $\Delta\bar{\Psi}$ is the spacing in the Ψ-direction. As long as the time interval is kept less than this, the calculations should remain stable. A third time interval, DTC, is imposed only for convenience, so that the time increment will not grow so large in the later stage of computer run that the detail is lost in simulation.

3.4.2.3 Computation of Tracer Peaks and Widths

To calculate the peak concentration, a technical approach is employed. From the theory of statistics, it has been shown (Scheidegger, 1960) that the concentration distribution will evolve into a normal density function given by:

$$C(x,t) = \frac{1}{\sqrt{4\pi D_L t}}\exp\left\{\frac{(x-\bar{x})^2}{4D_L t}\right\} \tag{3.30}$$

where $\bar{x}$ is the mean of the normal distribution curve. Expanding Eq. 3.30 as

$$C(x,t) = \frac{1}{\sqrt{4\pi D_L t}}\left(1 - \frac{(x-\bar{x})^2}{4D_L t} + \frac{(x-\bar{x})^4}{2!(4D_L^2 t^2)} - \cdots\right) \tag{3.31}$$

If we consider some points that are close to the peak value of C at the mean $\bar{x}$, then the higher order term can be easily neglected from Eq. 3.31, and after rearranging we can write

$$(x-\bar{x})^2 = -4D_L t\left(C_{(x,t)} - \frac{1}{\sqrt{4\pi D_L t}}\right) \tag{3.32}$$

It is obvious from Eq. 3.32 that points in the near neighborhood of the mean $\bar{x}$, represent a parabola. The peak concentration can be easily calculated from this parabola as

$$C_{peak} = \frac{C_1 + C_2}{2} \tag{3.33}$$

where

$$\begin{aligned} C_1 &= C_{JL} - \frac{(C_{JL} - C_{JL-1})(C_{cen} - C_{JL})^2}{(S_{cen} - S_{JL-1})^2 - (S_{cen} - S_{JL})^2} \\ C_2 &= C_{JR} - \frac{(C_{JR} - C_{JR+1})(C_{cen} - C_{JR})^2}{(S_{cen} - S_{JR-1})^2 - (S_{cen} - S_{JR})^2} \end{aligned} \tag{3.34}$$

The terms on the right hand side of Eq. 3.34 are shown in Fig 3.13. Subroutine `TPEAK` in Appendix D calculates the peak concentration on each streamline.

As the computation proceeds, the middle isoconcentration lines gradually approach each other, rounding the corners of the flat-top of the initial concentration distribution. Eventually this flat-top disappears and `GONE` (an integer variable in the computer program) is set to one. As the flow proceeds, the middle isoconcentration lines again approach each other as the peak concentration decreases. A moment will come when the isoconcentration lines at S_{JL} and S_{JR} no longer exist. At this time two isoconcentration lines are lost, the succeeding isoconcentration lines are assigned as JL and JR on the concentration profile, and variable `GONE` is incremented by one. A subroutine `REDO` keeps track of the variable `GONE`. When it has declined to a critical value, it doubles the number of the isoconcentration lines by putting new ones between each of the remaining lines. In addition to the calculation of peak concentration at different times, the thickness of the tracer band in the flow

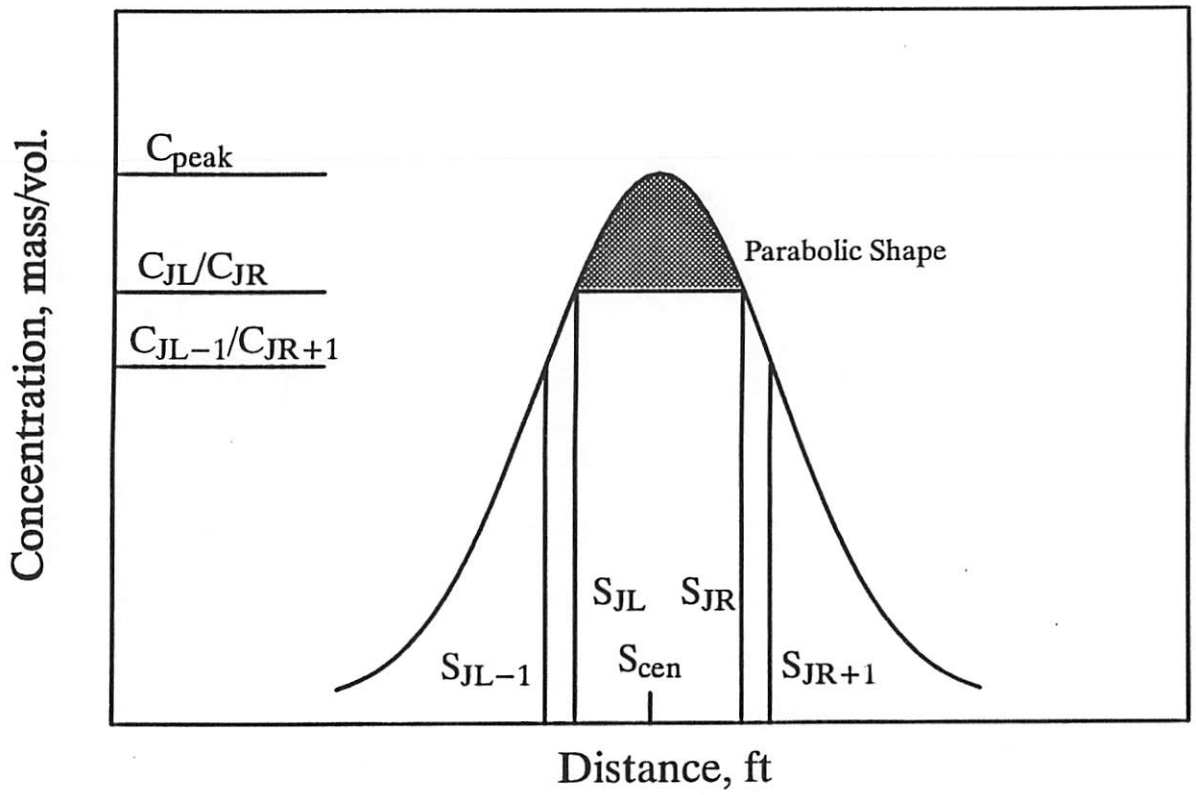

Fig. 3.13 Concentration Profile with a Parabolic Shape at the Top.

direction is also calculated. Subroutine BWIDTH calculates the width between the 50% concentration of the tracer band.

3.4.2.4 Convergence

In the section on stability criteria, we discussed that if the errors introduced by *round-off errors* or *truncation errors* do not amplify during subsequent computations, the numerical scheme is stable. By convergence we mean that the results of the method approach the analytical values as Δt and $\Delta\Phi$ both approach zero, or in other words, for a convergent difference scheme, the truncation error converges to zero as $\Delta\Phi$ and Δt both approach zero. This shows that stability and convergence are related properties. This result has been introduced in Lax's Equivalence Theorem: *For a consistent approximation, stability is a necessary and sufficient condition for convergence.* This theorem is of great practical use, because it is relatively easy to calculate the stability criteria; whereas, the direct proof of convergence is usually quite difficult for most practical problems. However, the theorem is valid only for 'properly posed' problems. Some non-linear problems may not satisfy this condition. In those cases, convergence cannot be guaranteed by stability (Aziz and Settari, 1974). The present numerical scheme is consistent and stable. Therefore, by Lax's Theorem, it should converge to the analytical solution of Eq. 3.6.

Another approach to assuming convergence is to show that the mass is conserved. The present numerical scheme does conserve mass as can be seen by the comparison with the analytical solution given by Abbaszadeh and Brigham, 1983 (see chapter 5) for the homogeneous case. The proposed numerical scheme computes the velocity of the isoconcentration lines, and discusses the error that might be introduced in the computations of these velocities. Therefore, a technical approach is employed that keeps the successive locations of the isoconcentration lines from dragging away from their true positions. It turns out that if we minimize the error in the computation of the front locations then the mass will remain constant during computations. This technique is discussed in the following paragraphs.

The volume of the tracer band can be calculated as

$$V = h_f \phi S_w \int_1^{NIS} w(\Phi,\Psi) C(\Phi,\Psi)\, dS(\Phi,\Psi) \qquad (3.35)$$

where,

$w(\Phi, \Psi)$ = width of the streamtube, L

h_f = thickness of the homogeneous formation, L

NIS = total number of isoconcentration points in a concentration profile.

The width of the streamtube at some location can be related to the velocity of the fluid at that point by:

$$w(\Phi, \Psi) = \frac{q}{u h_f S_w} \tag{3.36}$$

where, q = injection rate into the streamtube, L^3/t.

Therefore, if the volume V is kept constant, it is equivalent to keeping mass constant. A cubic spline interpolation is used to calculate the integral in Eq. 3.35. Subroutine `VOLUME` in Appendix D calculates the volume of the tracer band within each streamtube.

Volume is controlled after some number of computations of the successive positions of the isoconcentration lines. Subroutine `CRECTV` controls the volume of the tracer band. Any change in volume would be adjusted by this subroutine. If, for example, the volume has reduced, it will increase the volume by stretching the distance on the concentration profile from the center of it. The new concentration profile would then be

$$S_i = S_i + ALP \times VC(S_i - S_{cen}) \tag{3.37}$$

where,

VC = volume-correction factor.

ALP = a constant, depends on current and previous values of the volume correction factor.

S_{cen} = mean of the concentration profile.

The volume-correction factor can be calculated as

$$VC = 1 - V/V_{in} \tag{3.38}$$

where,

V = average volume of all the streamtube under consideration.

V_{in} = volume input at the injection well.

It is obvious that if VC is negative, the volume has increased from the original volume input. Therefore, by Eq. 3.37, it will decrease the volume by shrinking the points on the concentration profile. On the other hand, if VC is positive, it will stretch the concentration profile. The technique used here is reminiscent of a thermostat mechanism to control temperature.

3.5 Integrated Output Concentration Profile

The third section of the computer simulator computes the output tracer concentration to be observed at the producing well. The previous computation gave means to compute concentration profiles along each of the streamlines that enter the production well as a function of time. At any particular time, the overall effluent tracer concentration, $\bar{C}(t)$, from the system would then be given by the integral:

$$\bar{C}(t) = \frac{\int_0^{\pi/2} q(\Psi) C(\Psi, t)\, d\Psi}{q_t/4} \tag{3.39}$$

where $C(\Psi, t)$ is the concentration that enters the production well from a streamline, at a time t, and $q(\Psi)$ is the flow rate on that streamline. Although the flood front consists of infinite number of streamlines, this can be approximated for a computer by a smaller number. Originally, 89 streamlines are used in the solution of EOM. For the integrated output concentration, the number of streamlines are then increased by the method describe below.

The first step in the computation of the integrated output concentration is to approximate the curves of concentration versus time of the tracer slug on all the individual streamlines, by the equation,

$$C(\Psi, t) = C_p(\Psi) e^{(-[t-\bar{t}(\Psi)]^2)/2\sigma_t^2(\Psi)} \tag{3.40}$$

where,

$C(\Psi, t)$ = Concentration on streamline Ψ at time time t.

$C_p(\Psi)$ = Peak concentration on streamline Ψ.

$\bar{t}(\Psi)$ = Time to peak concentration on streamline Ψ.

$\sigma_t^2(\Psi)$ = Variance of the arrival time of isoconcentration lines on streamline Ψ.

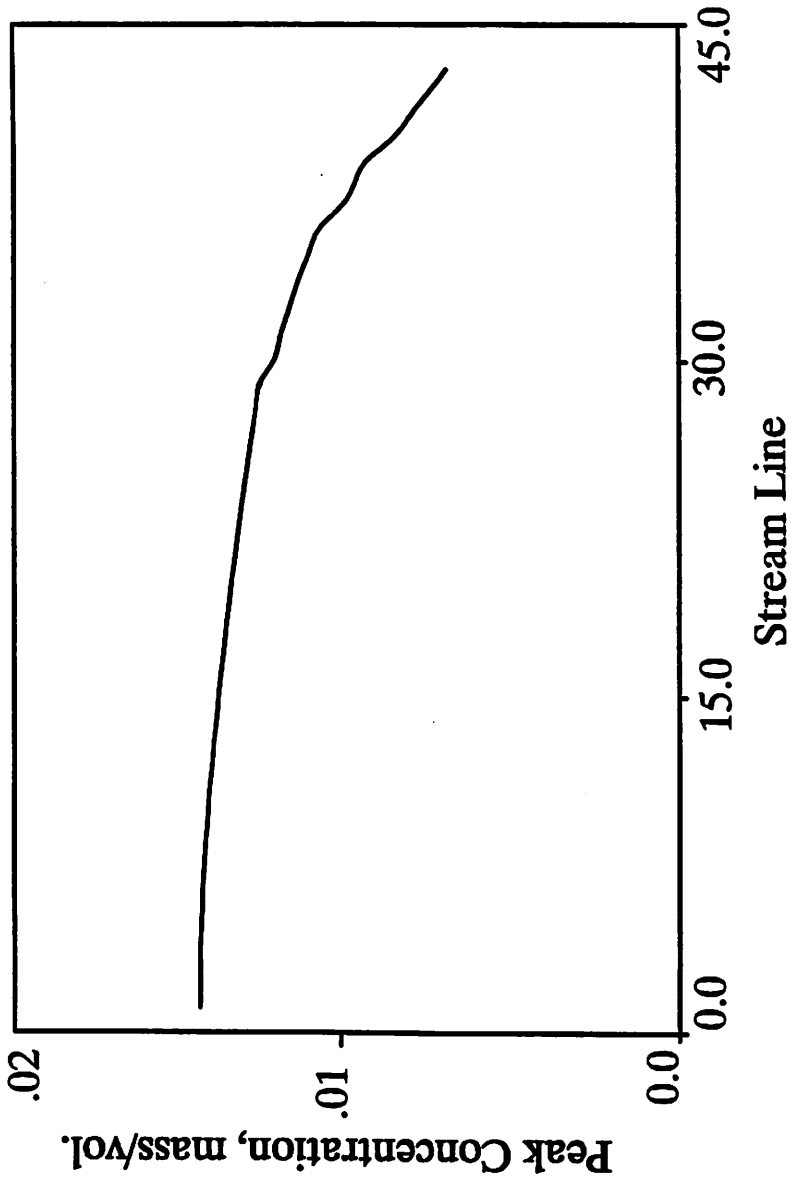

Fig. 3.14 Peak Concentration Occurrence on Streamlines ψ, $\lambda_L = 0.6$, $\sigma^2 = 0.6$, $\lambda_D = 0.2$.

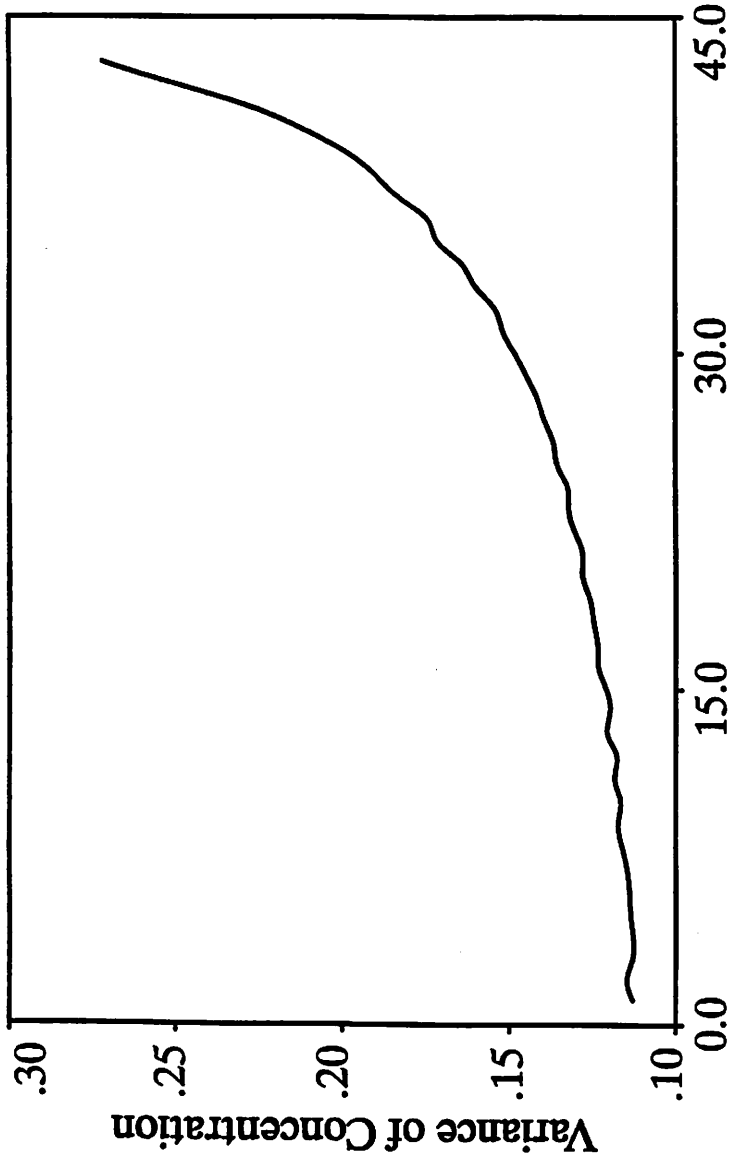

Fig. 3.15 Variances of the Concentration Distribution on Streamlines Ψ, $\lambda_L = 0.6$, $\sigma^2 = 0.6$, $\lambda_D = 0.2$.

Figure 3.14 to 3.16 show the plot of the peak concentration, $C_p(\Psi)$, the variance, $\sigma_t^2(\Psi)$ and the time to peak concentration, $\bar{t}(\Psi)$ versus the streamline number, respectively. The streamlines are numbered sequentially, according to their breakthrough at the production well. In the next step, ten streamlines are added between the existing pairs, thus making the total number of streamlines 889. By using the cubic spline interpolator the quantities, $C_p(\Psi)$, $\sigma_t^2(\Psi)$, and $\bar{t}(\Psi)$ are then interpolated on all the streamlines, and the concentration for each streamline is computed from Eq. 3.40. Finally, the integrated output concentration is then computed from Eq. 3.39. This procedure gives a smooth output concentration curve, free of anomalous peaks due to the fairly small number of streamlines that are actually followed. The relative smoothness of the curves in these three figures indicate that this approximation procedure is appropriate.

3.6 Summary and Conclusions

In this chapter, a new numerical method of solving (C-D) equation, for the displacement of miscible tracers in oil field flooding patterns, is presented. The numerical technique considers both convection and physical dispersion during flow of the tracer and approaches the solution differently then do conventional finite difference methods. An equation of motion, which contains both Darcy and dispersive terms, allows tracking of isoconcentration lines. Following conclusions can be drawn from this study:

1. The proposed numerical method is stable and is expected to avoid any numerical dispersion.
2. The method does not require any outer boundary condition or solution of matrices like the conventional finite difference methods.
3. The method can take into account the effect of both longitudinal and transverse dispersion along with their components of molecular diffusion at low flow velocity.
4. The method can be easily extended to three dimensional field problem.

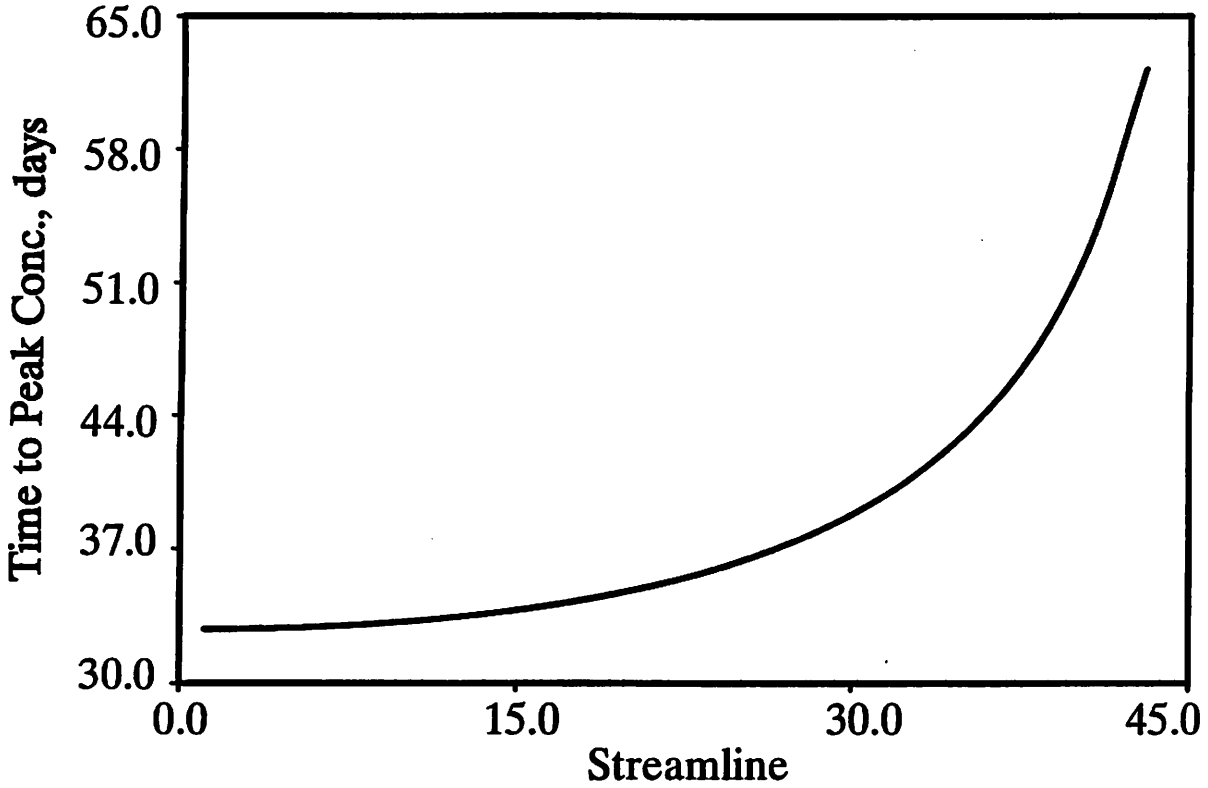

Fig. 3.16 Time to the Peak Concentration on Streamlines, i. $\lambda_L = 0.6$, $\sigma^2 = 0.6$, $\lambda_D = 0.2$.

4. An Efficient Method of Generating Random Permeability Field

4.1 Introduction

It has been recognized in the petroleum industry that permeability and porosity of a reservoir rock are not constant but vary in space. Similarly in the mining industry the concentration of ore deposits is not uniform throughout the formation. Knowledge of permeability and porosity is essential for a good prediction of the oil recovery process by numerical reservoir simulation. It is almost impossible to compute the permeability/porosity at the scale of the grid blocks of a reservoir simulator (Ghori and Heller, 1990). Therefore, to simulate natural variability, synthetic permeability fields are generated in a probabilistic framework. The variations of these properties are not totally random but show some correlation structure. Several methods of generating random permeability fields are available in the literature (Smith and Freeze, 1979; Mantoglou and Wilson, 1982; Gutjahr, 1989). The method developed here was first presented by Heller (1972) and is called the source point method (SPM).

The first section of this chapter gives a brief introduction to the theory of probability and geostatistics, which is further extended to include the theory of regionalized variables; i.e., spatial statistics. The necessary assumptions for the permeability generator are also stated. The method of generating random permeability by Heller is presented next. In the subsequent section, it is shown that the correlation length in the SPM can be prespecified. Finally, the SPM is modified to include the effect of anisotropy in the generated field.

4.2 Theory of Probability and Geostatistics

The concept of probability of a particular event of an experiment gives one an intuition or feeling about the outcome of the occurrences of that event. For example, the probability in the outcome of rolled die that a one will occur is $\frac{1}{6}$. The occurence of numbers on the die is a random process. When a random experiment is performed, we are not often interested in all the details of the experimental result but only in the value of some numerical quantity determined by the result. For instance, if two dice are thrown and we are interested only in the sum of the total of the two

occurrences, and are not really concerned about the values of the individual dice; the sum can then be considered as random variable. Another example can be given by the concept of determining the flowing ability of an underground geological formation. The flowing ability may depend on many factors such as grain and pore size, interconnectedness of the pores, the cementation of the grains, the type of formation etc. While some of these factors can be determined others cannot. The permeability is a numerical quantity that reflects all the factors that influence the ability of fluids to be forced to flow through a porous media. If the underground geologic formation exhibits variation in space, we can then associate probability values with the permeability. Thus permeability can be conceptualized as a numerically valued function on probability space and can be considered as a random variable. A random variable can either be continuous or discrete depending on the function of its distribution.

A distribution function contains most of the probabilistic information about a random variable X. It can be defined as the probability of all the possible numerical values of the random variable less than some tabulated value ($F(x) = P(X \leq x)$). If $F(x)$ is differentiable then we can define $f(x) = dF(x)/dx$; i.e., the probability density function. Similarly, if $X_1, X_2, ...X_n$ are n random variables, then

$$F(x_1, x_2, ...x_n) = P(X_1 \leq x_1, X_2 \leq x_2, ...X_n \leq x_n) \tag{4.1}$$

is called their joint distribution function. For differentiable joint distribution functions we can define

$$\partial^n F(x_1, x_2, ..x_n)/\partial x_1, \partial x_2, ..\partial x_n = f(x_1, x_2, ...x_n) \tag{4.2}$$

as a joint density function. Statistical independence of these variables implies that knowledge of one random variable does not give any information about the others. However, if $X_1, X_2, ..., X_n$ have joint density, we can obtain joint density of any subset of these by integrating over the excluded variables. Thus,

$$f_{X_1}(x_1) = \int_{-\infty}^{+\infty} f(x_1, x_2) dx_2 \tag{4.3}$$

is called the marginal density of X_1. This definition of the random variables will not give joint densities. To obtain joint densities, the concept of conditional probability, which is the basis of the phenomenon called the stochastic processes is employed . The concept of conditional probability is very important in probability theory. The reason is that we are often interested in calculating probabilities when some partial information concerning the result of the experiment is available, or in recalculating them if additional information is given. In addition, it is easy to compute the probability of an event by conditioning on the occurrence or nonoccurrence of a secondary event. Hence, if X_1 and X_2 are two discrete random variables, then the conditional distribution function of X_1 given X_2 can be defined as

$$P_{X_1}(x_1|x_2) = \frac{P(X_1 = x_1, X_2 = x_2)}{P(X_2 = x_2)} \tag{4.4}$$

Similarly the conditional density function of X_1 given X_2 can be given as

$$f_{X_1}(x_1|x_2) = \frac{f(x_1, x_2)}{f_{X_2}(x_2)} \tag{4.5}$$

One of the most important concepts in probability is the expectation of a random process $z(x)$, denoted as $E[Z(X)]$, also called the mean of the random variable. The expected value also referred to as the first order moment. The second order moment is called the variance of the random variable, and is given as

$$var[z(X)] = E[Z(X)]^2 - (E[Z(X)])^2 \tag{4.6}$$

By definition, the variance shows how far apart the $z(x)$ would be from its mean value on the average. For the case of the joint probability distribution, if two random variables $Z_1(x)$ and $Z_2(x)$ have the variances at the point x_1 and x_2, then they also have a covariance which is a function of two locations x_1 and x_2 and written as

$$cov[Z(x_1), Z(x_2)] = E[Z(x_1), Z(x_2)] - \mu_1\mu_2 \tag{4.7}$$

where, μ_1 and μ_2 are the mean of the random variables, $Z_1(x)$ and $Z_2(x)$, respectively.

In case of statistically independent random variables, the covariance will be zero; it becomes the variance of the random variable distribution if computed at the same location. Random variables follow some probability distributions; two commonly used distributions are discussed below.

Normal Distribution

A normal distribution is the most commonly used distribution. It is bell-shaped and is symmetric about the mean μ and variance σ^2 (Fig. 4.1). It is usually denoted as $X \sim N(\mu, \sigma^2)$ and its density is

$$f(x) = \frac{1}{\sqrt{2\pi}\sigma} e^{[-(x-\mu)^2/2\sigma^2]}$$
$$-\infty < x < +\infty \tag{4.8}$$

Lognormal Distribution

It has been often experienced that many geological features do not follow a normal distribution but rather their logarithms tend to be normally distributed. This is most notably the case for the permeability distribution, in many formations. The shape of the distribution is not symmetric but rather skewed (Fig. 4.1). The equation of the density of lognormal distribution is

$$f(x) = \frac{1}{x\beta_l\sqrt{2\pi}} e^{[-1/2(\frac{log\gamma_l - logx}{\beta_l})^2]} \tag{4.9}$$

The parameters that usually describe the lognormal distribution are the median of the distribution, which is $\gamma_l = e^{(\alpha_l)}$, if α_l is average of the logarithms, and β_l their standard deviation (David, 1977). Examples of variables that have a lognormal distribution are ore of gold and the permeability of porous media. The expected value of a lognormal process $V(x)$ with respect to a normal random process $W(x)$ can be written as

$$V(x) = e^{W(x)} \tag{4.10}$$

$$E[V(x)] = e^{\frac{(\mu_w + \sigma_{w2})}{2}} \tag{4.11}$$

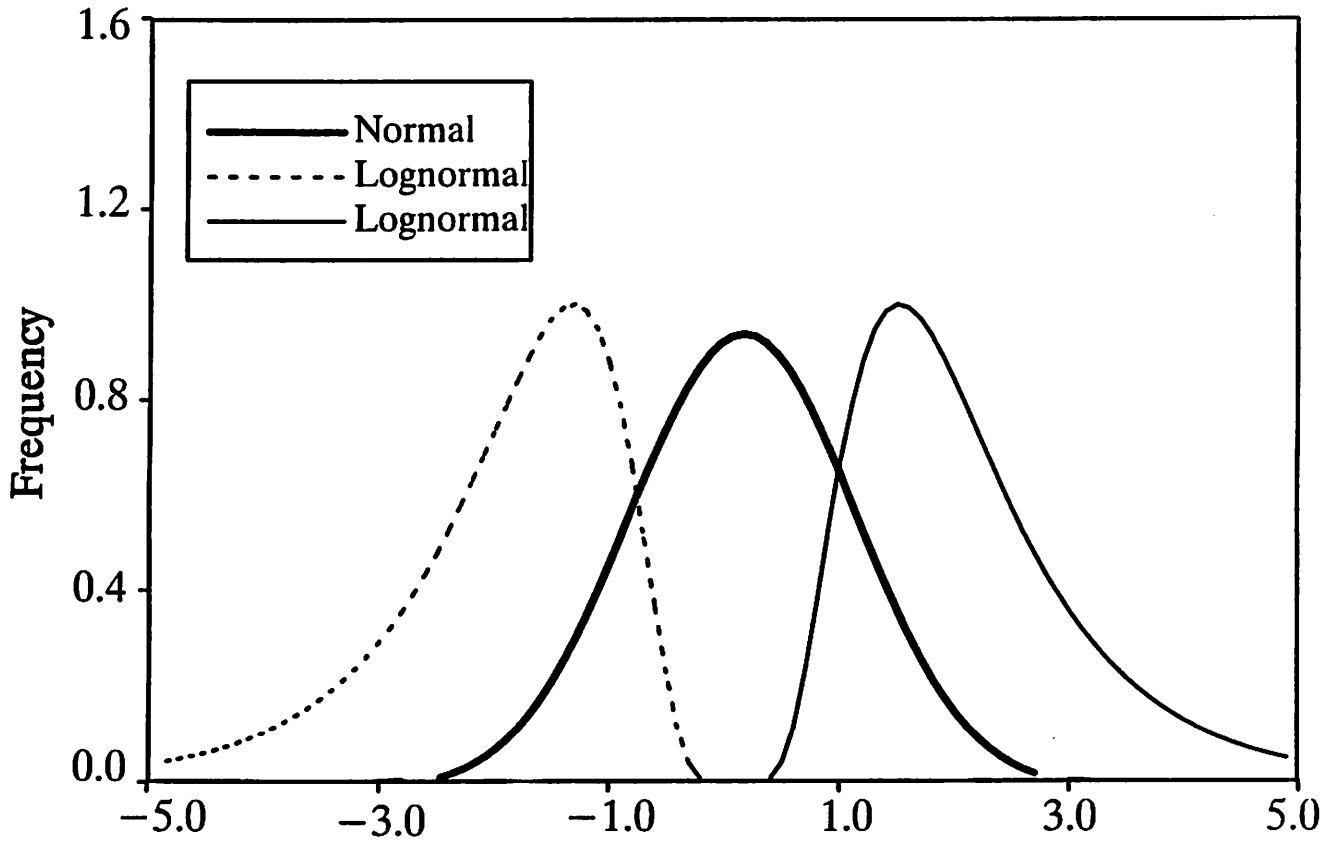

Fig. 4.1 Plot of Property Distributions for Normal and Two Lognormal Distributions (Skewed Left and Right).

This brief discussion of the theory of probability will lead us to understand the behavior of a process which varies in space (or time). The physical examples are the permeability, porosity, reservoir thickness etc., which vary in space, and weathering, which varies in time. To deal with these kinds of problems, stochastic methods are used because they deal with the study of dependent random variables and are well suited for the variability of the physical properties in space. Because only one realization for a particular domain is available, the main difficulty is to justify the equivalence of the distribution law for the spatial and ensemble statistics. Geostatistics offers a useful tool for studying and evaluating the spatial behavior of a random variable, which is also called the theory of 'regionalized variables'.

4.3 Theory of regionalized variables

If x is a point in space and $Z(x)$ is the value of a function at that point, then the function can be considered as a regionalized variable. Permeability, porosity, grade of an ore etc. are the regionalized variables because they vary with the location of the coordinates in space. Of course, in studying flow properties, one has to define these with respect to some space averaging at a particular location. The basic idea of the theory is that a function, $z(x)$, at location x, is only one realization of a random function, $Z(x)$. In other words, we can imagine a stochastic process defined in space; a realization which has a unique specific value at each point. By this consideration the physical, spatial properties can be evaluated under a probabilistic framework. Physical properties in space are not independent. On the contrary, they follow some structure defined by the spatial law of the phenomenon. Therefore, for a spatial random process that has only one realization and has correlation structure, some assumptions are necessary to make this concept useful.

The Second Order Stationary Assumption

Stationarity assumes that any statistical property of the medium is invariant under translation. An alternate condition is called weakly stationary and involves only the first two moments. The assumption has two conditions

$$E[Z(x)] = \mu \tag{4.12}$$

i.e., expected value is constant throughout the medium and

$$C(h) = cov[Z(x), Z(x+h)] = E[Z(x)Z(x+h)] - \mu^2 \tag{4.13}$$

where h is the lag distance. It is to be noted from Eq. 4.13 that the covariance is the function of separation distance only. In other words, stationarity implies that all the probability distribution functions of the random process $Z(x)$ are the independent of translation and does not rule out effect of rotation of the coordinate axes.

The Ergodic Assumption

Ergodicity implies that statistics of a single realization in space are equivalent in terms of probability density function (pdf) to the ensemble of all possible realizations. In other words, by observing the variability in a large enough sample space of the property, it is possible to determine the pdf of the random process for all the possible realizations.

The Intrinsic Assumption

It has been observed in some cases that the variance of the permeability increases with the size of the porous media. Matheron (1973) proposed the intrinsic hypothesis to deal with this problem. The hypothesis assumes that even if the variance of the random field $z(x)$ is not finite the variance of the first increment of $z(x)$ is finite, and this increment is weakly stationary

$$E[Z(x+h) - Z(x)] = \mu \tag{4.14}$$

and for zero mean,

$$var[Z(x+h) - Z(x)] = 2\gamma(h) \tag{4.15}$$

is a function of the lag distance h only. Here $\gamma(h)$ is called the semivariogram. In general, for a stationary process, the variogram is simply the symmetric translation of the covariance function

$$\gamma(h) = cov(0) - cov(h) \tag{4.16}$$

4.4 Generation of a Random Permeability Field

The main objective of this study is to quantify the effects of a statistical variation of the permeability. This can be achieved by comparing the output concentration profiles at the production well (after a tracer injection at the injector) in homogeneous and heterogeneous reservoirs. The computation method can be checked by comparing the results obtained from the simulator with those of the tracer production curve from a real field; the permeability distribution of which had been input to the simulator. In practice, enough permeability data are not available to make a complete statistical analysis. Therefore, synthetic permeability data are generated to use as input in the simulator. The method used here was first presented by Heller (1972) and is called the source point method (SPM). This method generates a random but somewhat "smooth" permeability field that is continuous every where in the mathematical sense.

The SPM requires generating $3 \times N_{sp}$ (where N_{sp}=number of source points) random numbers. The first two N_{sp} numbers, generated from a uniform distribution, are used to compute x and y coordinates of the "source points" in the field. The last N_{sp} numbers are generated from a normal distribution. These represent the log-permeabilities at the location of the source points. The source points will turn out to be local minima or maxima of the permeability values in the field. An inverse square assumption is then used to compute the log-permeability values at specified grid points as

$$S_g(N,M) = \frac{\sum_{j=1}^{N_{sp}} \frac{s_j}{(x_j - x_g(N))^2 + (y_j - y_g(M))^2}}{\sum_{j=1}^{N_{sp}} \frac{1}{(x_j - x_g(N))^2 + (y_j - y_g(M))^2}} \tag{4.17}$$

where,

N_{sp} = the number of source points

s_j = normally distributed random numbers
extremum of the log-permeability of the j^{th} point

x_j, y_j = uniform random numbers representing coordinates

of the j^{th} point

x_g, y_g = coordinates of the specified grid points

$S_g(N, M)$ = permeability exponent (log-k) at grid point (N,M)

Figures 4.2(a) and 4.2(b) show the log permeability surfaces for realizations that were computed using $N_{sp} = 50$ and $N_{sp} = 250$, respectively. It is obvious from these figures that the permeability field is more variable when a larger number of the source points (N_{sp}) is used. It can also be seen that the scale of the correlation structure is inversely related to N_{sp}. The log-permeability distribution obtained by this method follows a normal distribution. The permeability values at each grid point are then calculated as

$$k(N, M) = k_0 e^{\sigma S_g(N,M)} \tag{4.18}$$

where, k_0 is the base permeability and σ is the parameter defining the width of the permeability distribution. With this method, it is possible to generate a random permeability field with some correlation structure. The correlation length can be computed from the number of source points as will be seen in the next section.

4.4.1 Correlation Length in SPM

The correlation length or the integral scale of a second order stationary stochastic process is the lag distance at which the values at two locations are marginally dependent on each other. The permeabilities at points which are further apart than the correlation length are not noticeably correlated with each other. The correlation length of a process can be computed from, the autocovariance function, the autocorrelation function or from the variogram. The experimental covariance function for a second order stationary process can be given as

$$cov(l) = \frac{1}{N(l)} \sum_{j=1}^{N(l)} (z(j) - \bar{z})(z(j+l) - \bar{z}) \tag{4.19}$$

where $N(l)$ is the number of samples at lag distance l. The covariance function has its maximum value at zero lag, which is the variance of the random process. It decreases gradually from its maximum value to achieve an asymptotic value. Generally, the correlation length is evaluated by computing the length at which the

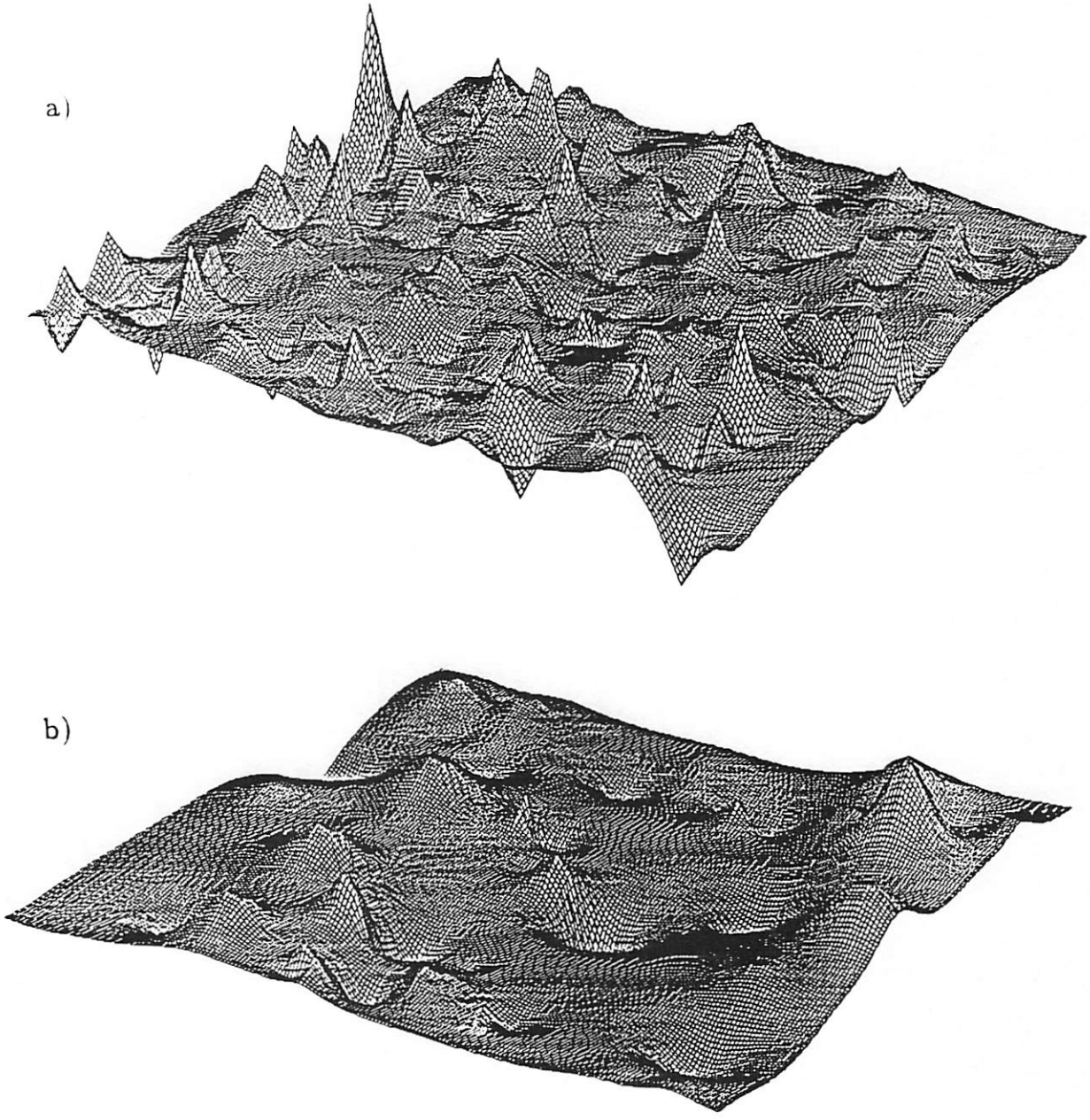

Fig. 4.2 Permeability Surfaces
for a) $N_{sp} = 250$; b) $N_{sp} = 50$.

curve crosses zero. The autocorrelation function is a covariance function normalized over the variance of the process,

$$C_{auto}(l) = \frac{cov(l)}{cov(0)} \tag{4.20}$$

The correlation length has also been evaluated, from an autocorrelation function by computing the area under the curve or by using an e^{-1} fold drop. The experimental semi-variogram can be evaluated by the formula,

$$\gamma(l) = \frac{1}{2N(l)} \sum_{j=1}^{N(l)} [(z(j) - z(j+l)]^2 \tag{4.21}$$

It often happens that a semi-variogram increases from 0 lag, reaching an asymptotic value called the "sill" of the variogram, which is the variance of the process. The correlation length in a semi-variogram is the lag distance at which it gets to the sill value.

In summary, the purpose of all these methods is to show the spatial structure of a second order stationary process, i.e., the variance and the correlation length can be computed.

Previous authors have reported that the correlation length in the SPM cannot be prespecified. An approximate relationship is developed which is described below.

Fig. 4.3 shows five semi-variograms of the log permeabilities (LnK) , generated from SPM, for different values of N_{sp}. We observed from this figure that as the number of source points increases, the correlation length decreases and vice versa. We noticed that even though the permeability was generated from a theoretical method; the curves in this figure do not exhibit smooth behavior. We made an attempt to account for the theory of conditional probability, and computed conditional covariances of the generated permeabilities from the SPM as described in the next section.

4.4.2 Conditional Covariance in SPM

The conditional covariance of a permeability field generated by the SPM can be evaluated by computing the covariance of LnK at the location of one source point,

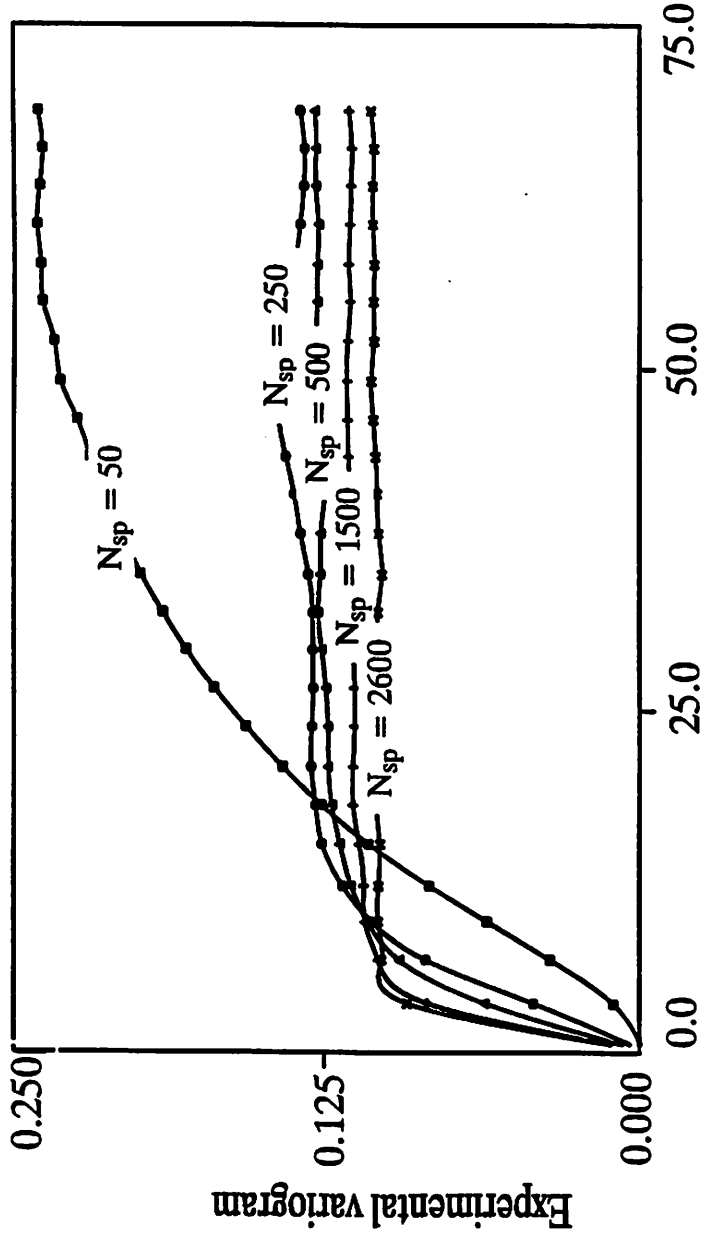

Fig. 4.3 Semi-variogram of the Log Permeabilities (*LnK*) for Different Values of N_{sp}.

given the locations of the rest of the source points (Gutjahr, 1990). The inverse square generating formula (Eq. 4.17) in the SPM can also be written as

$$S_g(N,M) = \sum_{j=1}^{N_{sp}} s_j w_j(N,M,\widehat{x}\widehat{y}) \tag{4.22}$$

where,

$$w_j = \frac{\dfrac{1}{(x_j - x_g(N))^2 + (y_j - y_g(M))^2}}{\displaystyle\sum_{k=1}^{N_{sp}} \frac{1}{(x_k - x_g(N))^2 + (y_k - y_g(M))^2}} \qquad j = 1,..N_{sp}$$

and,

$$\sum_{j=1}^{N_{sp}} w_j = 1 \qquad\qquad \sum_{j=1}^{N_{sp}} w_j^2 \neq 1 \tag{4.23}$$

where x and y's are the coordinates of the source point. For a fixed location of the source point (x,y), the conditional covariance can be written as

$$cov[S_g(N,M), S_g(N',M')|_{\widehat{x}\widehat{y}}] =$$

$$cov\Big[\sum_{j=1}^{N_{sp}} s_j w_j(N,M,\widehat{x}\widehat{y}), \sum_{k=1}^{N_{sp}} s_k w_k(N',M',\widehat{x}\widehat{y})\Big] =$$

$$\sum_{j=1}^{N_{sp}} {\sigma_j}^2 \Big[w_j(N,M,\widehat{x}\widehat{y}), w_j(N',M',\widehat{x}\widehat{y})\Big] \tag{4.24}$$

where

$${\sigma_j}^2 = \begin{cases} cov[s_j, s_k] & \text{if j = k} \\ 0 & \text{if j} \neq \text{k} \end{cases}$$

The locations of the source points change from one realization to the other, therefore the above conditional covariance was calculated for several realizations and the average value of these gave the desired covariance function. Fig. 4.4 shows the auto-correlation function for different values of the N_{sp}. The correlation lengths were here calculated by taking the e^{-1} fold drop. The correlation length were then plotted against the quantity $\sqrt{\frac{area}{N_{sp}}}$ as shown in Fig. 4.5. The *area* is referred to the actual area of the domain, and it has the dimension of L^2. Fig. 4.5 shows a straight

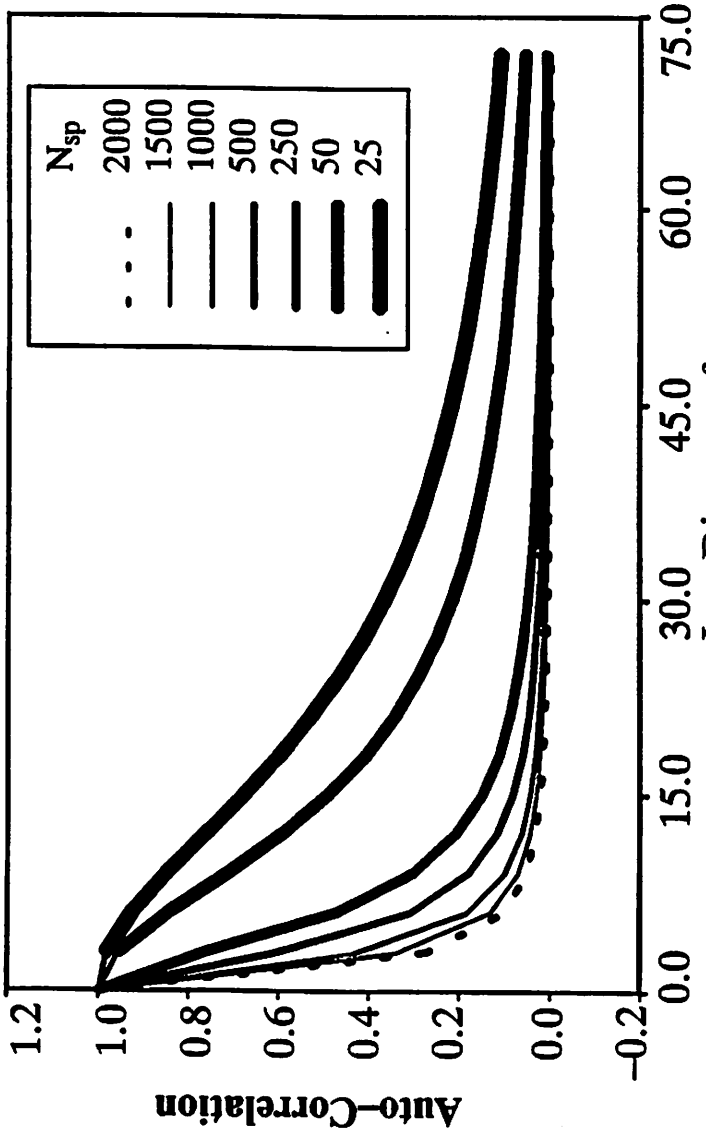

Fig. 4.4 Autocorrelation Function for Different Values of N_{sp}.

line with slope approximately equal to one, confirming that the correlation length in the SPM can be approximately prespecified as

$$L_c = \sqrt{\frac{area}{N_{sp}}} \tag{4.24a}$$

In another approach, the conditional covariance function is avoided, and the correlation lengths, for different values of the source points, are simply calculated from the semivariograms of each case. Again the correlation lengths are plotted against the quantity $\sqrt{\frac{area}{N_{sp}}}$. A least square method is used to obtain a best fit of a straight line with the equation

$$L_c = 2.0\sqrt{\frac{area}{N_{sp}}} \tag{4.24b}$$

Based on several numerical experiments, we suggest that the constant 2 should be included in the calculation of correlation lengths by the SPM. Here, the difference in the value of the constant is plainly a result of the way one chooses to define the L_c. The e^{-1} drop gave a constant 1, whereas measuring the distance to attainment of the sill in variograms, the constant becomes 2.

4.5 SPM for Anisotropic Fields

The property distributions of many physical regional variables such as ore grades or reservoir permeability are not generally isotropic. The permeability anisotropy has long been supposed to be one of the most important factors in determining the recovery efficiency of reservoirs (Dykstra and Parson, 1957; Weber, 1986). Therefore, it is necessary for a random generator to simulate property distribution with a desired anisotropy in a particular direction. Other methods such as FFTM and TBM are capable of incorporating anisotropy in the generated field, however SPM has been unable to produce anisotropic fields. In this section, a modified form of the SPM is described that can generate anisotropic fields. To produce a particular anisotropy, an empirical relationship is developed in which the desired correlation lengths in any direction can be used as input.

The modified generating formula for the source point method in a three dimensional anisotropic media can be written as

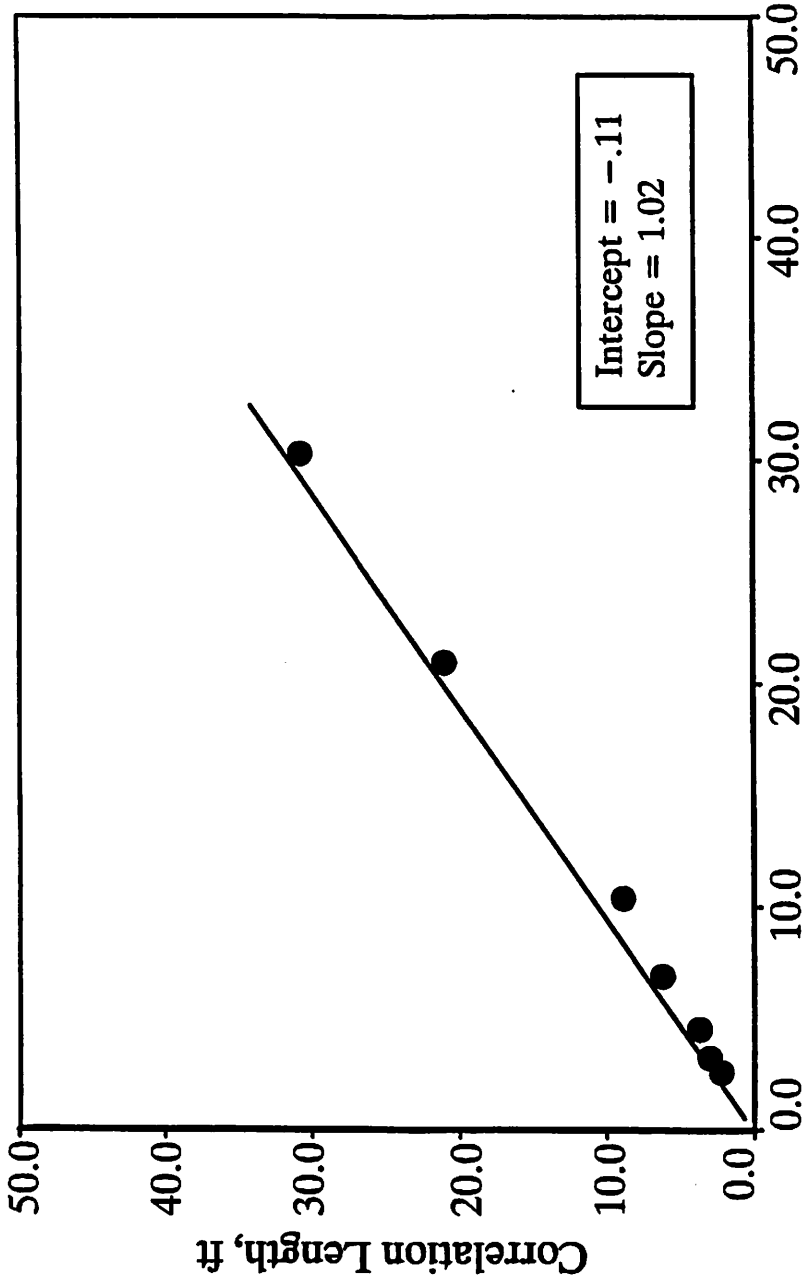

Fig. 4.5 Plot of Correlation Lengths vs $(area/N_{sp})^{1/2}$.

$$S_g(N,M,K) = \frac{\sum_{j=1}^{N_{sp}} \frac{s_j}{\alpha^2(x_j - x_g(N))^2 + \beta^2(y_j - y_g(M))^2 + \gamma^2(z_j - z_g(K))^2}}{\sum_{j=1}^{N_{sp}} \frac{1}{\alpha^2(x_j - x_g(N))^2 + \beta^2(y_j - y_g(M))^2 + \gamma^2(z_j - z_g(K))^2}} \quad (4.25)$$

where α, β, γ are the coefficients of anisotropy. The other variables are same as stated before. The procedure of generating the random field is also same as for the isotropic case. A difference lies only in presenting the correlation length in different directions. A two dimensional analysis of an anisotropic field generated by the SPM is described below.

The ratio of correlation length L_x/L_y is dependent on the ratio β/α (i.e., the ratio of the coefficients of anisotropy). To evaluate the relationship between these two quantities, a catalogue of the conditional covariance of the generated field by the SPM is computed. These conditional covariances are constructed with different values of the ratio β/α and for several sets of N_{sp}. Fig 4.6 shows the autocorrelation function in the x direction for three values of β/α when $N_{sp} = 100$.

The correlation lengths are computed by taking the e^{-1} fold drop of these curves as shown in Fig. 4.6. Fig. 4.7 shows the autocorrelation function in the y direction for the same values of the ratio β/α and of N_{sp}. We see that with the increase of β/α the correlation length in the x direction increases, while in the y direction it decreases. When α is equal to β, the correlation lengths in both the x and y directions are equal. Table 4.1 shows the values of L_x/L_y for several values of β/α for five sets of N_{sp}. It is apparent from the table that for a constant β/α, and with the increase of N_{sp}, the ratio L_x/L_y tends toward unity. This can be justified, since the effect of anisotropy is less effective for medium with small correlation lengths. Fig. 4.8 shows the plot of the ratio β/α vs L_x/L_y for the five sets of N_{sp}. It is apparent that the slopes of these curves increase with the increase of N_{sp}. If the curves are approximated by straight lines, their equations are:

$$\frac{L_x}{L_y} = \left(\frac{\beta}{\alpha}\right)^{f(N_{sp})} \quad (4.26)$$

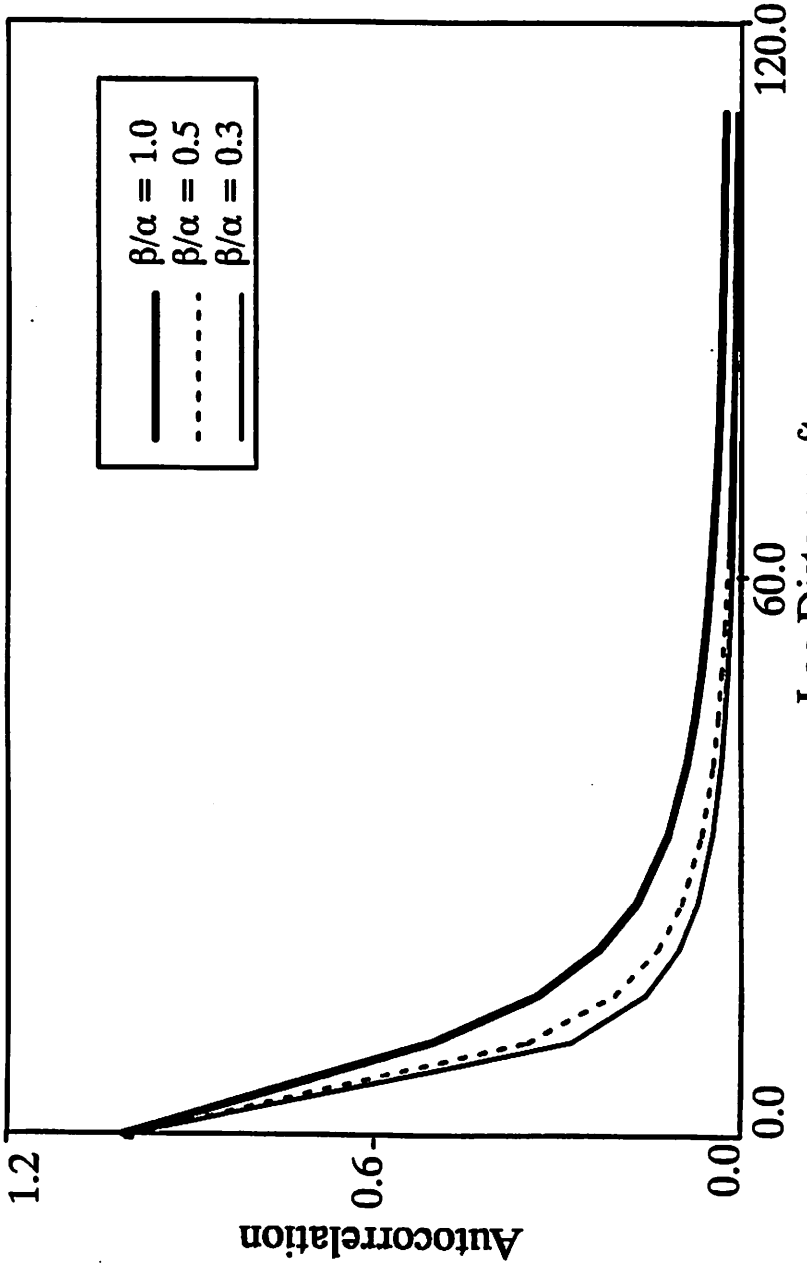

Fig. 4.6 Plot of Autocorrelation Function in the x Direction vs Lag Distance for Three Different Values of β/α.

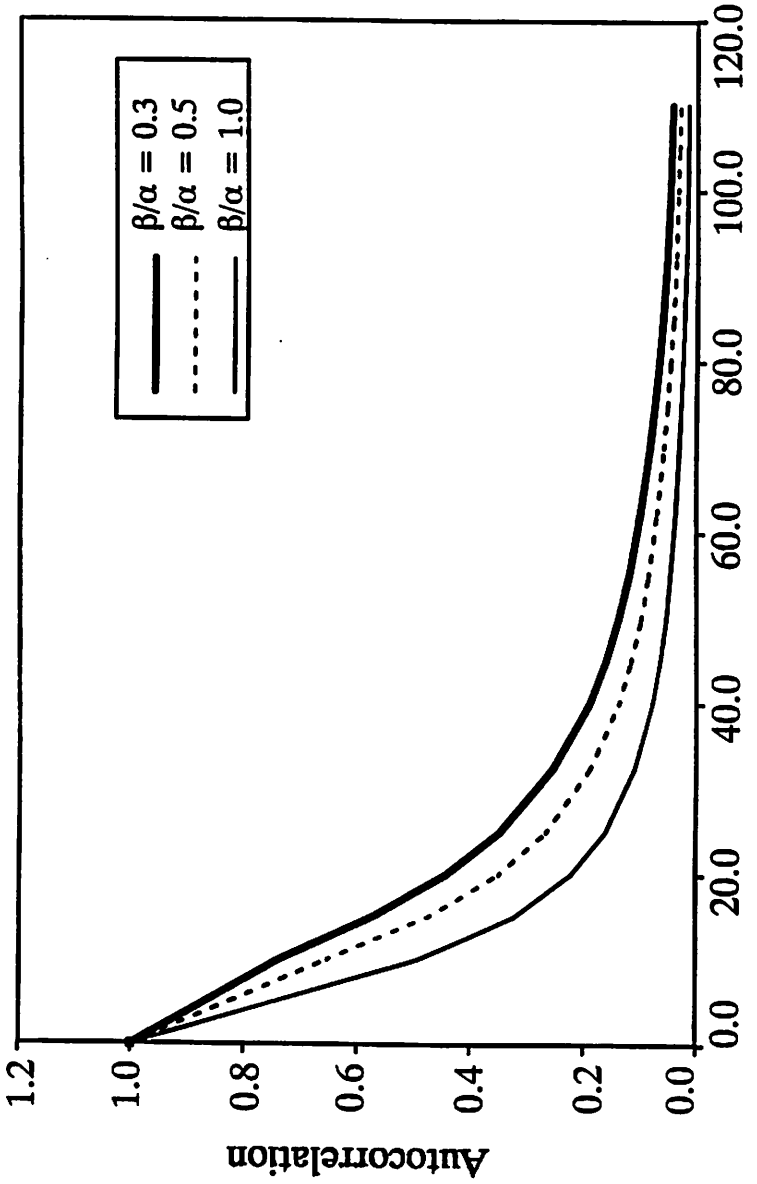

Fig. 4.7 Plot of Autocorrelation Function in the *y* Direction vs Lag Distance for Three Different Values of β/α.

Nsp / β / α	Lx / Ly				
	25	50	100	200	400
0.333	*0.244*	*0.377*	*0.548*	*0.713*	*0.832*
0.364	*0.275*	*0.410*	*0.579*	*0.737*	*0.847*
0.400	*0.312*	*0.450*	*0.614*	*0.762*	*0.863*
0.446	*0.359*	*0.500*	*0.653*	*0.790*	*0.881*
0.500	*0.419*	*0.552*	*0.698*	*0.821*	*0.899*
0.571	*0.498*	*0.621*	*0.751*	*0.855*	*0.919*
0.667	*0.606*	*0.710*	*0.815*	*0.8945*	*0.942*
0.800	*0.763*	*0.830*	*0.895*	*0.941*	*0.968*
1.000	*1.009*	*1.000*	*1.000*	*1.000*	*0.999*

Table 4.1 Table of L_x/L_y for Several Values of β/α for Five Sets of N_{sp}.

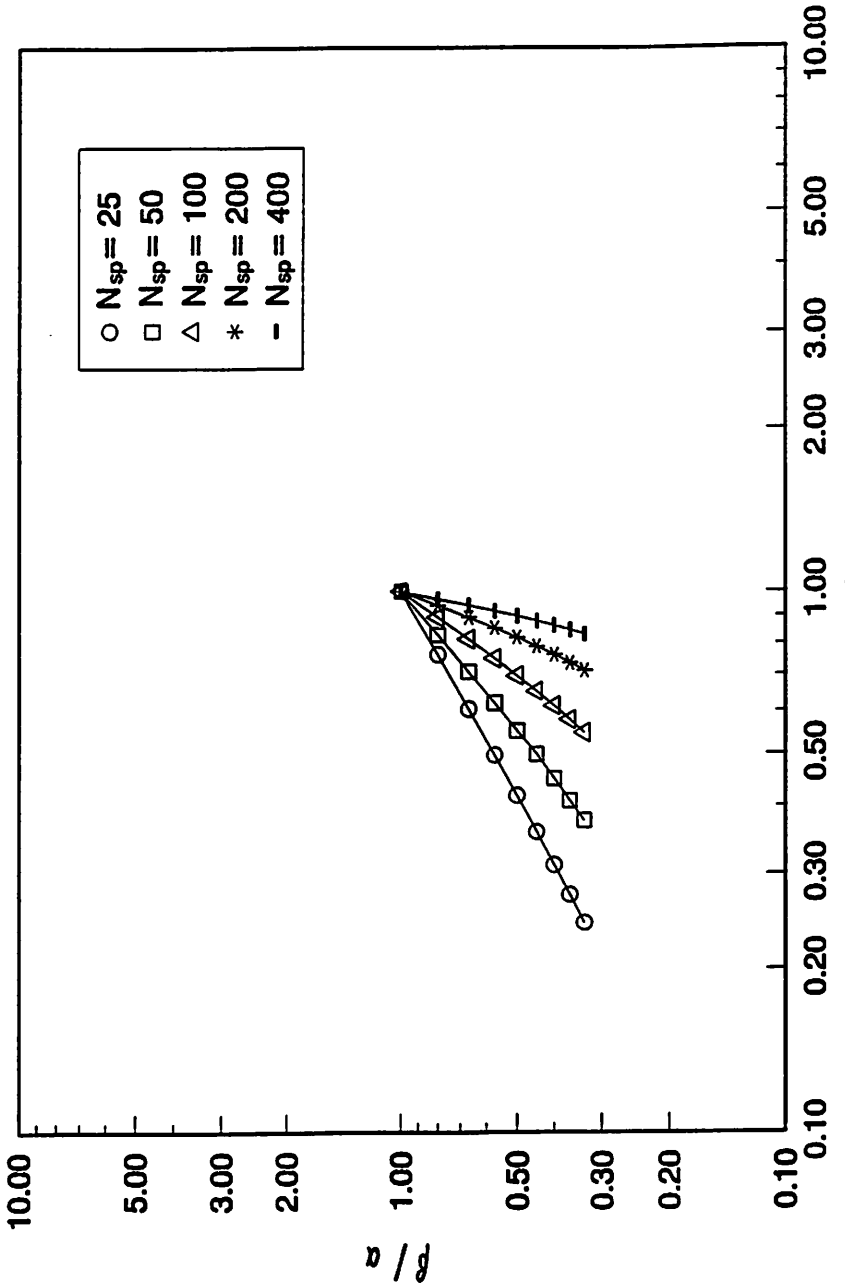

Fig. 4.8 Plot of the Ratio β/α vs L_x/L_y for the Five Sets of N_{sp}.

The next step is to evaluate the function $f(N_{sp})$. From Fig. 4.8 the slopes $f(N_{sp})$ of each curve for a particular N_{sp} is computed. Fig. 4.9 shows the plots of the function, $f(N_{sp})$ vs $(area/N_{sp})$, which can be considered to be a straight line. A least square method was used to fit this straight line with the equation

$$f(N_{sp}) = .01(area/N_{sp})^{\frac{3}{4}} \tag{4.27}$$

and the desired relationship for the anisotropic correlation length is then seen to be:

$$\frac{L_x}{L_y} = (\frac{\beta}{\alpha})^{.01(area/N_{sp})^{\frac{3}{4}}} \tag{4.27}$$

The correlation length in an anisotropic field can be related to the correlation length in isotropic field by the formula:

$$L_c = \sqrt{L_x L_y} \tag{4.28}$$

By using Eq. 4.24, the N_{sp} can be computed as:

$$N_{sp} = 4.0(\frac{area}{L_x L_y}) \tag{4.29}$$

In order to obtain the desired anisotropic field, the values L_x and L_y are used as input and the N_{sp} is computed from Eq. 4.29. The ratio β/α can then be computed from Eq. 4.27. Fig. 4.10 shows the permeability surfaces for both isotropic and anisotropic fields. In the anisotropic field, the correlation length in the x direction is input as 25 feet, whereas in the y direction it is 15 feet. As seen in Fig. 4.10(b) the anisotropy has produced layering in the generated field. Fig. 4.11 shows the variograms in the two directions. The desired correlation lengths in both directions are clear from the figures. In previous analysis of anisotropy, the angle of anisotropy was assumed to be 90 degrees. A desired angle of anisotropy can be obtained simply by rotating the coordinate system.

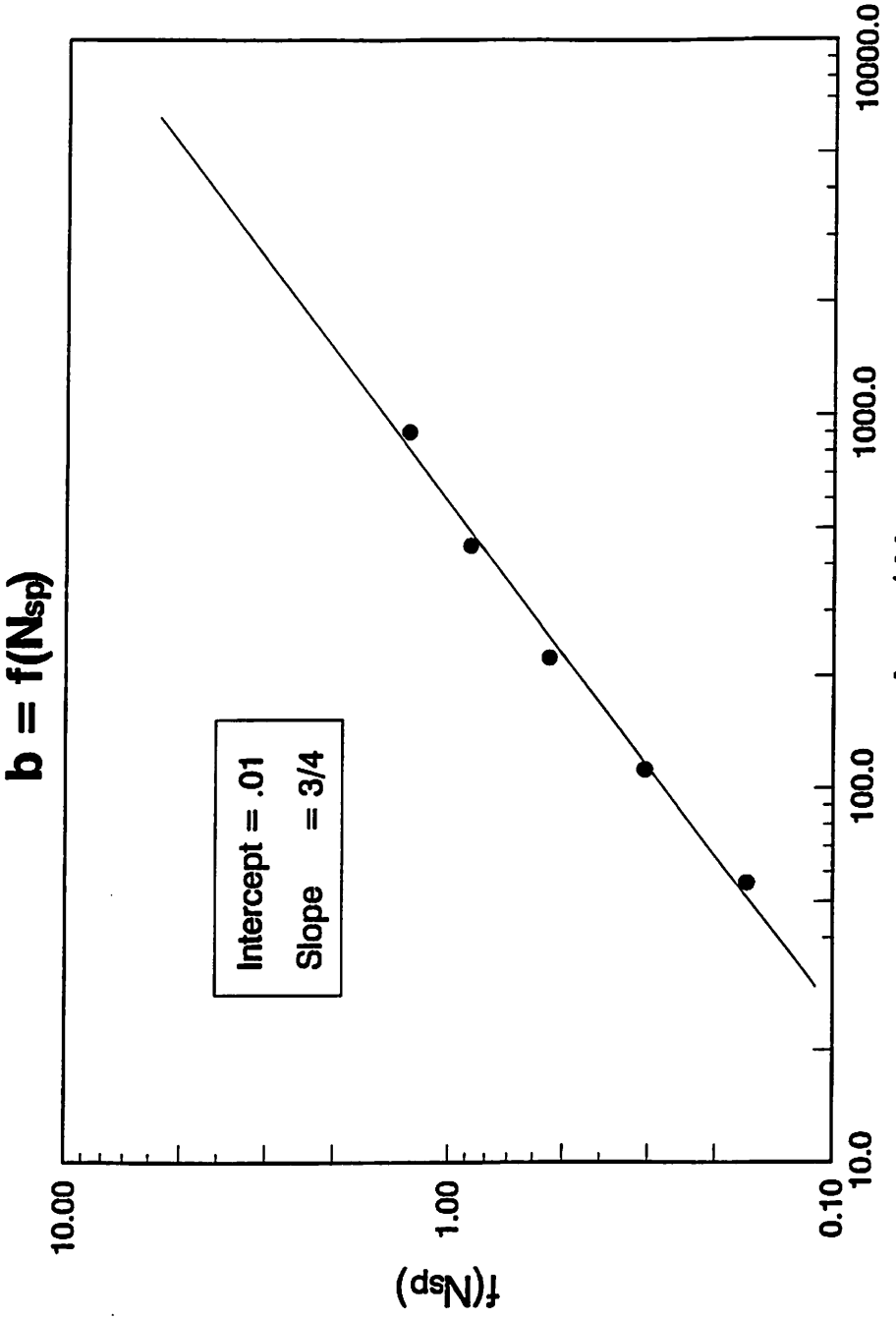

Fig. 4.9 Plot of the Slopes ($f(N_{sp})$) vs the Quantity $area/N_{sp}$.

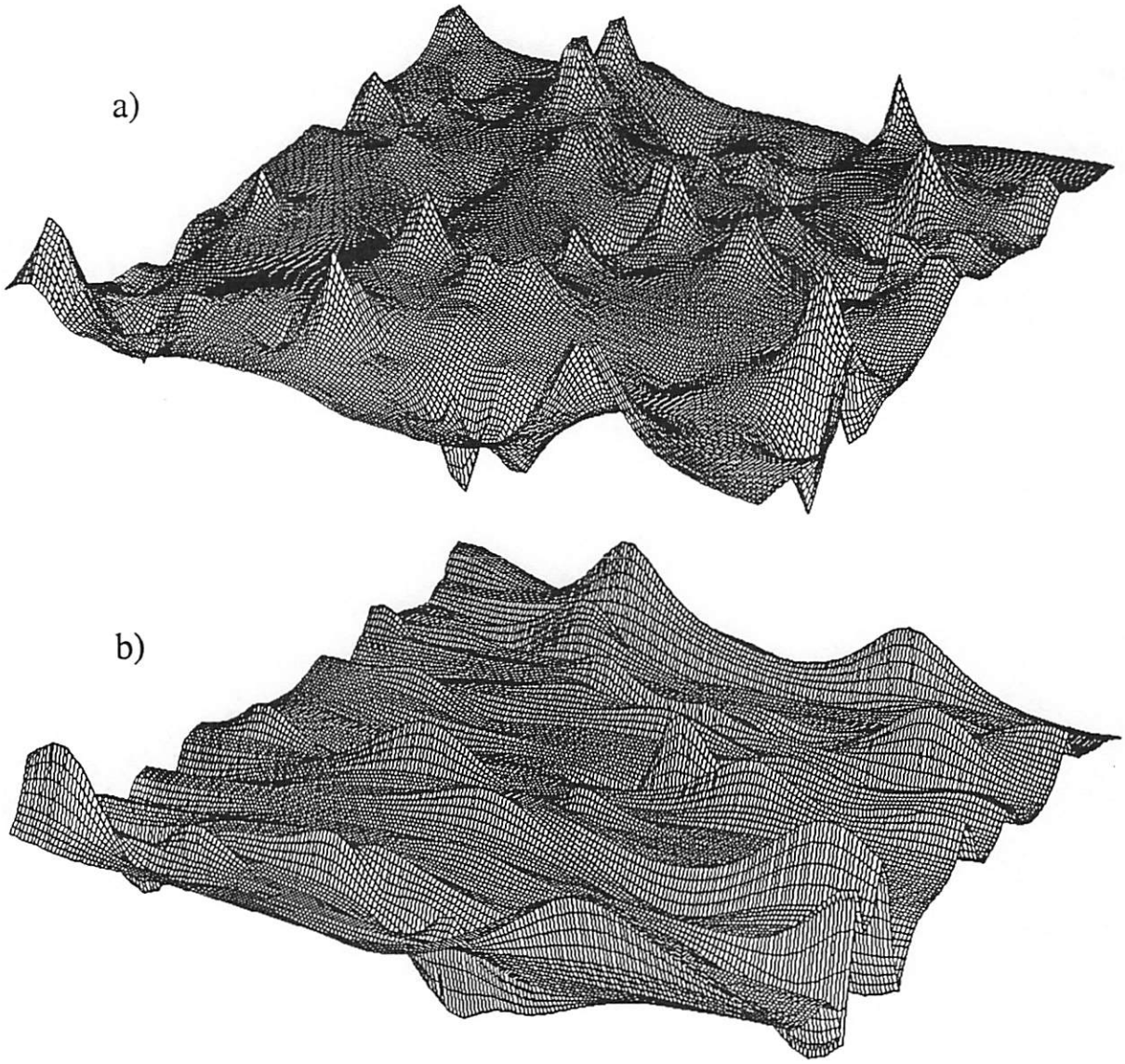

Fig. 4.10 Log Permeability Surfaces
a) Isotropic Field, $L_c = 20ft$; b)
Anisotropic Field, $L_x = 25ft$, $L_y = 15ft$.

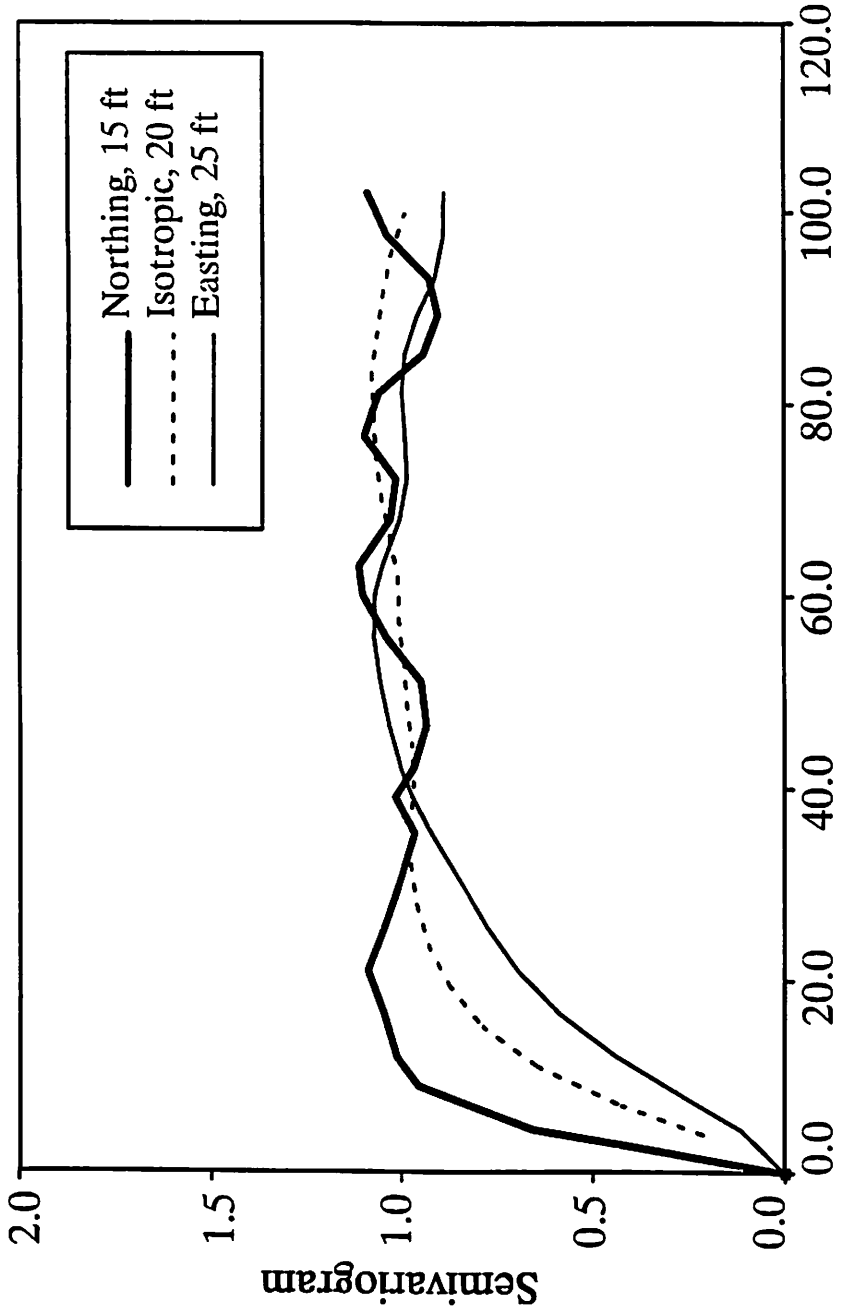

Fig. 4.11 Semivariogram vs Lag Distance for Both Isotropic and Anisotropic Fields.

4.6 Summary and Conclusions

In this chapter, a geostatistical method of generating random permeability fields with specified correlation structure is presented. The chapter first explained those elements of the theories of probability and geostatistics that are required for the presented subject. The theory is further extended to the 'theory of regionalized variables' of Matheron. The necessary assumptions for the random generator are also stated. In the generation of random field, Heller's source point method (SPM) is modified. We see that the correlation length in the SPM can be prespecified. Finally the SPM is modified to include the effect of anisotropy in the generated field. As a result of the work presented in this chapter, the following conclusions can be drawn:

1. Source point method is one of the most efficient method of generating random fields with regard to computer time and storage.
2. The desired correlation length can be prespecified by an empirical formula which is proportional to the quantity, $area/N_{sp}$.
3. A modified form of the SPM is derived that can take into account the desire anisotropy in the generated field.
4. A formula for a two dimensional anisotropic field is derived to prespecify the desire correlation length in any direction. For a three dimensional field a similar formula can be evaluated by using the theory of conditional covariance.

5 Numerical Simulation of the Flow of Miscible Tracer Slug

5.1 Introduction

It has been recognized that heterogeneity of the reservoir is one of the most important characteristics that influence oil recovery. This is especially so in enhanced oil recovery projects (EOR) where displacement patterns are more critical (Lasseter, et al., 1986; Weber, 1986). The most important aspect of reservoir heterogeneity may be the spatial permeability variations. It is impossible to quantify this by single values, but the spatial distribution can be described by probabilistic theory (Journel and Huijbregts, 1978; Matheron, 1973; Marsily, 1984). Unfortunately, not enough actual field permeability data is available to define the spatial permeability variation statistically. In general, to characterize the heterogeneity of a reservoir, one needs to know not only the parameters of the distribution (the mean and variance) but also the parameters describing the auto-correlation of nonuniformities in the field. The correlation structure, in fact, has been observed at different scales from pore level to interwell distance (Bahralolom and Heller, 1989; Goggin, et al., 1989).

Radioactive or chemical tracers have long been used in reservoir floods to give information about reservoir and flow characteristics (Wagner, 1977; Carpenter, et al., 1954; Strum and Johnson, 1951). Operating engineers use output concentration at the production well to predict the behavior of the reservoir qualitatively (Wagner, 1977) but these tests do not reveal quantitative information about the permeability heterogeneity.

This chapter imparts a better understanding of the effect of permeability heterogeneity on the displacement of a miscible tracer in flooding patterns such as the five-spot, the staggered line drive, and the direct line drive. A single component, single phase, miscible tracer with unit mobility ratio for numerical computations is considered. The formation is assumed to have only a single layer. The results are produced in several sections of this chapter. In the first of these sections, the results are presented for the flow of tracer movements in porous media. In this section, numerical results are compared with the known analytical solutions. Second,

with the availability of a synthesized permeability field that was generated by the Source Point Method (SPM), tracer output curves are produced. These curves are used to see the effect of two parameters (variance and correlation length) and of the dispersivity of the rock. The output curves are also affected by the seed value of the random generator of a computer. Therefore, the effect of realizations on the output curves is discussed in the last section.

5.2 Tracer Movements in Porous Media

For the presentation of results, an arbitrary five-spot pattern is considered. Only one quarter of the pattern is considered for numerical computations (see section 3.2). The dimensions and the reservoir data are close to a real field situation. Following is the data used in the analysis.

Pattern Area	= 2.1 Acres
Distance between producers, a	= 300 ft
Distance between injector and producers, a	= 300 ft
Volume of tracer	= 10 bbls
Net pay thickness	= 12 ft.
Average permeability	= 1500 md
Average porosity	= .26
Average saturation of the mobile phase that carries tracer	= .55
Molecular diffusion coefficient, D_m	= .0022 ft^2/day
Formation resistivity factor	= 38.0
Average constant flow rate	= 600.0 bpd

The simulation follows the injection of ten barrels of an aqueous tracer into the injection well. Successive locations of the tracer slug are computed using the numerical technique presented in chapter 3. It was assumed that the only mobile fluid is water, and the tracer slug is followed by the water injection again. The concentration profile is assigned to each streamline. Near the injection well, high flow velocity is encountered, therefore, convection is dominant. In addition, geometric effects are such that the flow velocity is decreasing away from the injection well. As a result the spacing of the isoconcentration points on a concentration profile

decreases during this initial period. As the front of the tracer slug proceeds away from the injection well, dispersion finally becomes dominant, and this in turn makes the concentration profile broader and the peak concentration decreases.

5.2.1 Tracer Band Widths

The narrowing of the concentration profile can also be explained from the tracer band width or transition zone calculations. The tracer band width is different along each streamline. Although the length of the transition zone is generally easy to measure in a linear unidirectional flow, it is more convenient to measure the band width of the concentration profile separately for each streamline in a flow regime where flow direction changes from point to. Tracer band width is measured along a streamline as the distance between the fifty percent isoconcentration points on each ramp of the concentration profile. Fig. 5.1 shows the plot of tracer band width against distance along a single stream line. In this figure the initial decline of tracer band width shows that convection is more dominant near the injection well. The subsequent increase in the bandwidth , further from the injector, shows the dominance of dispersion effects in most of the flow region.

The displacement of fluid in a five spot pattern can be divided into two flow regimes. In the first flow regime, the flow velocity decreases along a streamline as the fluid moves away from the injection well. In the second flow regime which starts from the mid distance along a single stream line, the flow velocity increases toward the production well. We call the first flow regime the diverging flow regime and the second flow regime the converging flow regime. In the converging flow regime, effects of both the convection and dispersion on the tracer band width are in the same direction and consequently tracer band width increases more rapidly in this region (Fig. 5.1).

5.2.2 Effect on Tracer Peaks

Tracer peak concentration decreases most rapidly in the early stage of the displacement, while the change in the later stage is insignificant. Fig. 5.2 shows the plot of peak concentration against distance along a single streamline. Geometric and dispersion effects cause the peak concentration to decrease more rapidly near the

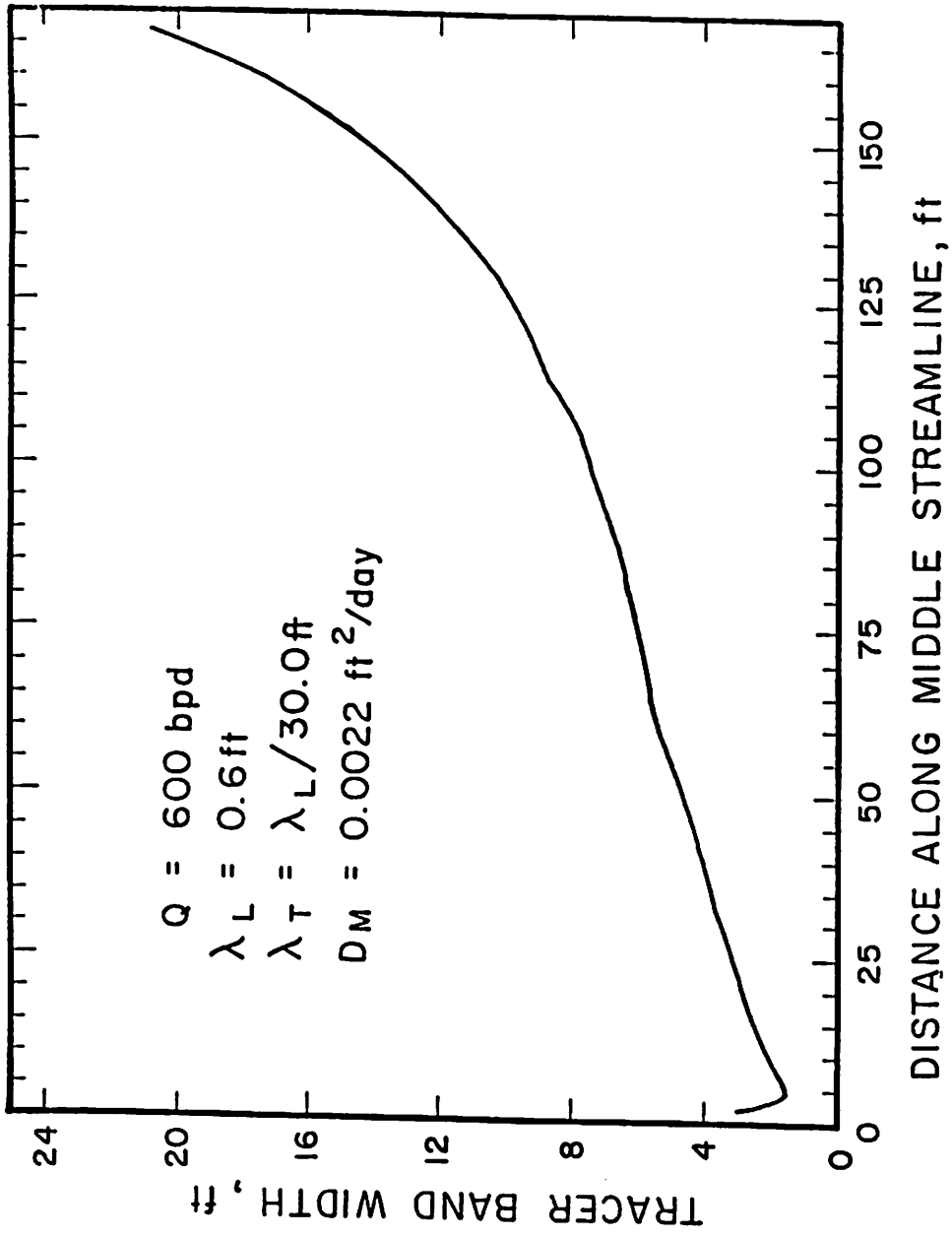

Fig. 5.1 Behavior of Tracer Bandwidth on a Single Streamline, $a/\lambda_L = 500$.

injection well. In the diverging flow regime, away from the injection well, velocity is decreasing and peak concentration decreases slowly. Even though it is not evident on the plot (Fig. 5.2), the tracer peak concentration decreases more slowly near the production well for a converging flow situation.

5.2.3 Output Concentration

The Equation of Motion can give the output concentration profiles as a function of time along all of the streamlines entering the production well. At any particular time, the overall effluent tracer concentration, $\bar{C}(t)$, from the system would then be given by the integral:

$$\bar{C}(t) = \frac{\int_0^{\pi/2} q(\Psi) C(\Psi, t)\, d\Psi}{q_t/4} \tag{5.1}$$

where $\bar{C}(\Psi, t)$ is the concentration that enters the production well from a streamline at a time t, and $q(\Psi)$ is the flow rate on that streamline.

In order to check the validity of the simulator, numerical results were compared with the known analytical solution of a homogeneous formation. Fig. 5.3 shows the comparison of the numerical results with the known approximate analytical solution (Abbaszadeh, 1983) for different values of the Peclet number (Peclet number is here defined as the ratio between the distance of like wells in the pattern, to the dispersivity distance). According to our knowledge, this is the first time that such a good comparison could be obtained especially for a Peclet number greater than 800 (Saad et. al 1990).

5.2.4 Effect of Geometry on Output Concentration

At the production well, the output concentration is the integration, over the sum of the arrival time, of the concentration levels on different streamlines. Fig. 5.4 shows the resulting integrated output concentration profile in the absence of mixing. It is obvious from this figure that the peak concentration is much lower than the input peak concentration. This dilution is due to the geometry of the five-spot pattern. The geometric effects introduce variations in the flow velocity at every point. These variations in the velocity introduce variation in the arrival time of the tracer on different streamlines. To preserve material balance, the area under the

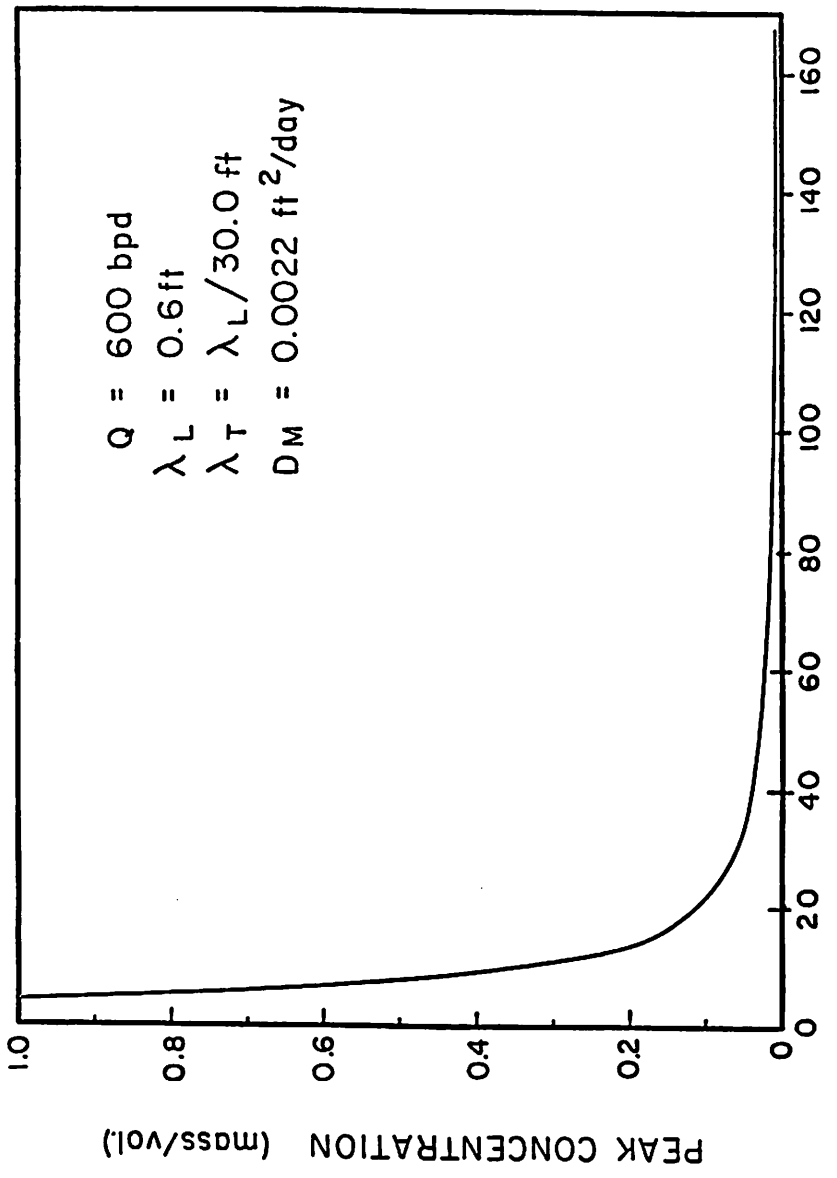

Fig. 5.2 Behavior of Tracer Peak Concentration on a Single Streamline, $a/\lambda_L = 500$.

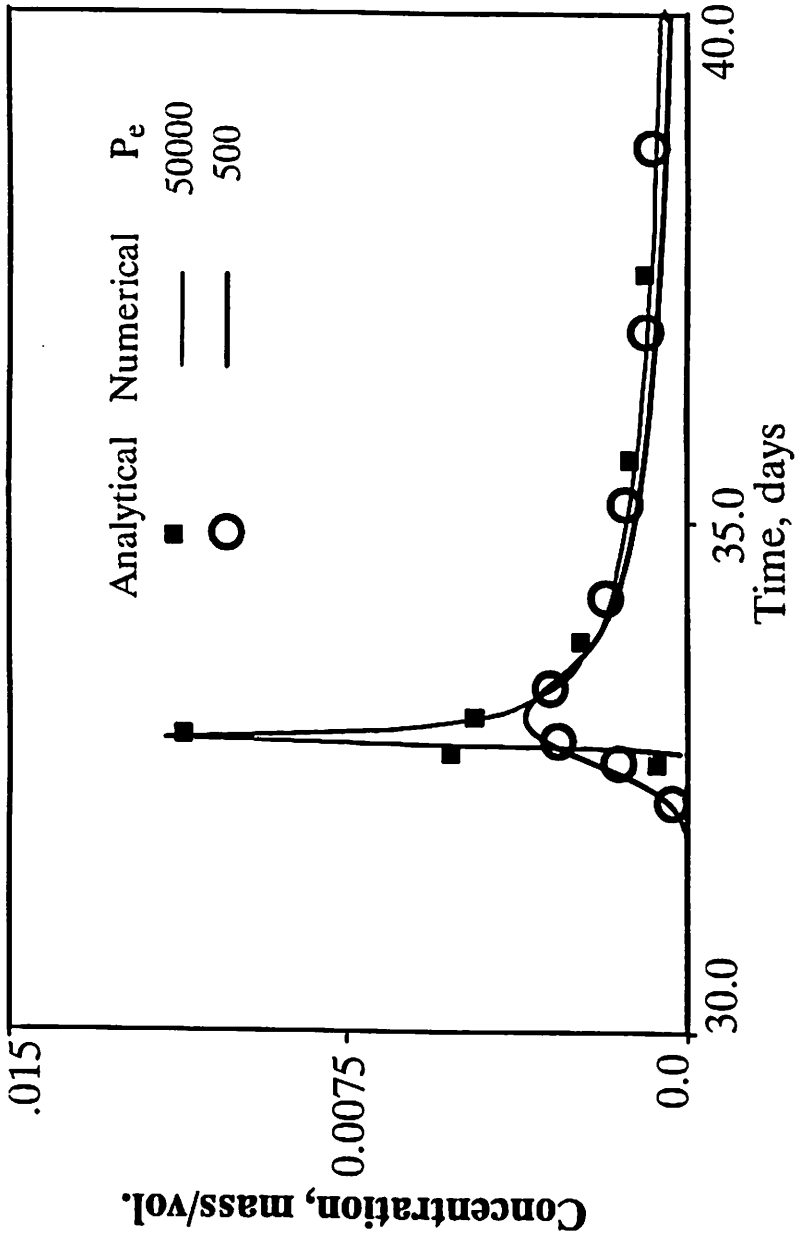

Fig. 5.3 Comparison of Numerical Solutions with the Known Analytical Solutions (Abbaszadeh and Brigham, 1983) for Homogeneous Five-spot Pattern.

input and the output concentration profile remains the same.

5.2.5 Effect of Dispersion on Output Concentration

Dispersion is important in understanding reservoir performance during enhanced oil recovery projects. Dispersion phenomenon is the result of the non-steady irreversible mixing of two miscible fluids displacing in a porous media. On a microscopic level, dispersion is due to both diffusion and microscopic variations in flow velocity. Its measurements are based on laboratory studies of miscible displacements of fluids in small columns. In this study, it is assumed that the dispersivity values are known based on laboratory studies. These dispersivity values are used as input into the simulator.

Dispersivity affects the sweep efficiency of the displacing front and the spreading of the tracer slug as it moves through the reservoir. For a formation with high dispersivity, a larger amount of the displacing fluid is required. Dispersivity values as low as 0.005 ft. for a Berea sandstone to 2.0 ft. for field cores are reported in the literature. In the present study, we have considered three values of dispersivity distance (0.06 ft., 0.6 ft., and 6.0 ft.) to cover all possible ranges of dispersivity in the field. It has been found that more streamlines are required to define the output concentration curve as the dispersivity distance used in the calculation is decreased. This was observed in the simulation of the homogeneous formation. In that case, the number of streamlines was increased until a smooth output concentration was obtained. Fig. 5.5 shows the output tracer concentration from a homogeneous formation for different values of dispersivity. Notice that in the tracer output concentration curve from a single-layered homogeneous formation, only a single real peak occurs. It is apparent that the increase in the dispersivity smoothes the profile by introducing more dilution.

5.2.6 Effect of Transverse Dispersion

As, mentioned early in the literature survey, the effect of transverse dispersion is much smaller than the effect of longitudinal dispersion. An attempt was made to quantify these effects. The computer program was run twice. In the first run, both longitudinal and transverse dispersion were included, with ($\lambda_T = \lambda_L/30$). and in

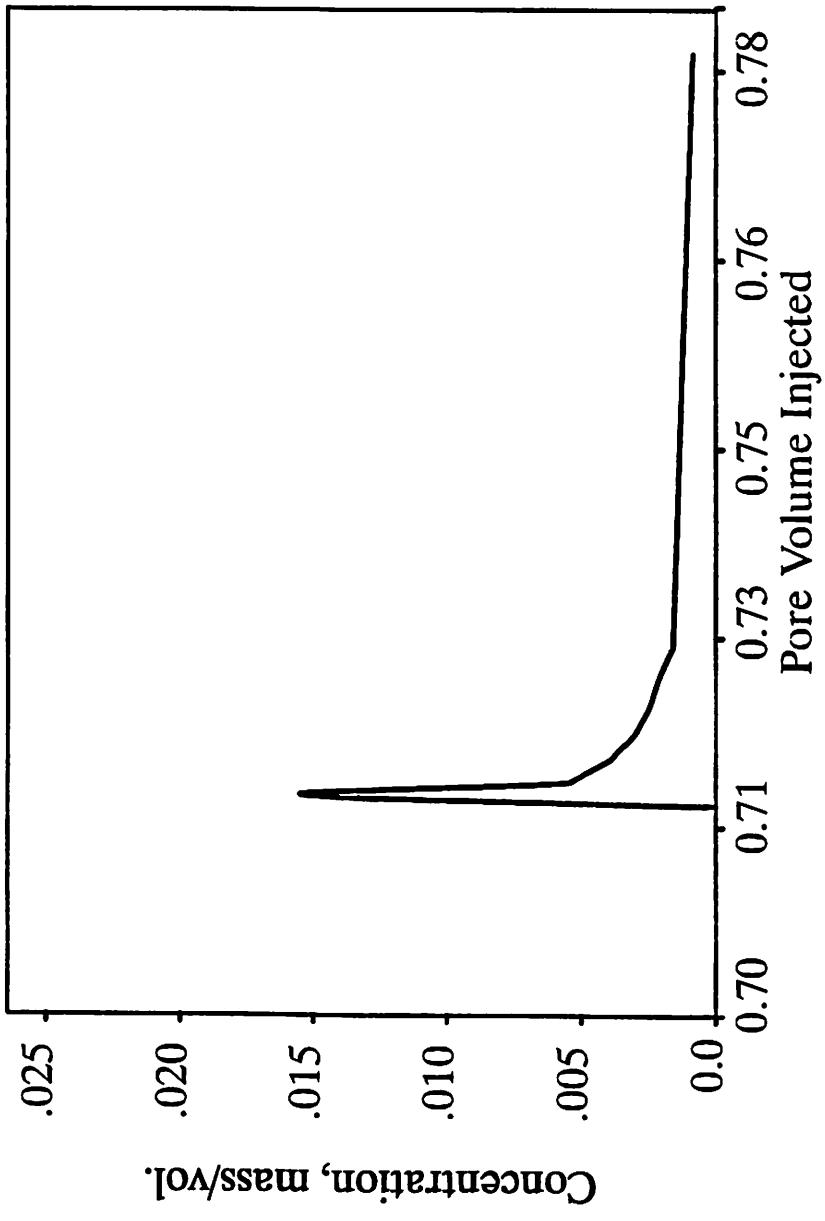

Fig. 5.4 Plot of Tracer Output Concentration, no Dispersion.

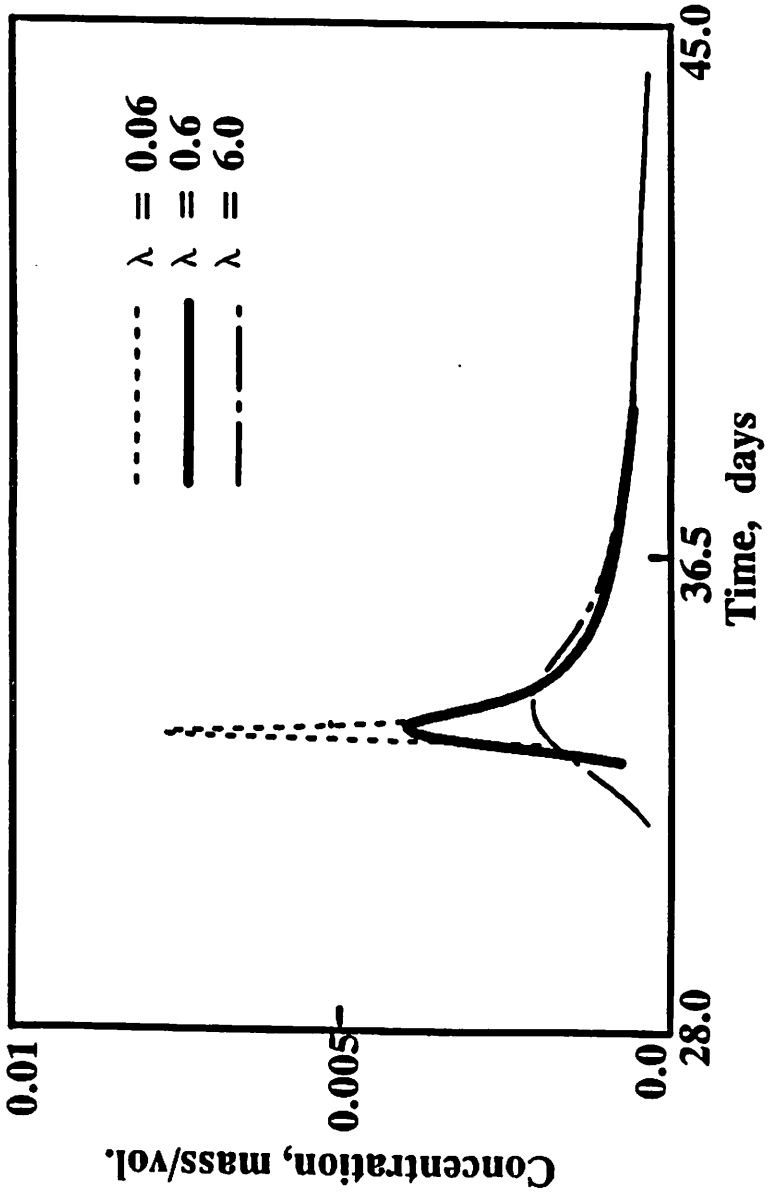

Fig. 5.5 Effect of Dispersivity Distance on the Tracer Output Concentration for a Homogeneous Five-spot Pattern.

the second run transverse dispersion was set equal to zero. The integrated output tracer concentrations for both cases were then plotted against pore volume injected as shown in Fig. 5.6. Lower peak values of tracer concentration were obtained for the case where $\lambda_T = 0$ than for $\lambda_T \neq 0$. This was expected because the effect of transverse dispersion is to homogenize the concentration of the tracer slug.

5.3 Effect of Permeability Heterogeneity on Tracer Output Concentration

The two parameters, σ and N_{sp}, of the SPM determine the degree of heterogeneity. The N_{sp} determines the correlation length; the greater the number of source points, the smaller is the correlation length, and vice versa. A large correlation implies that the displacement pattern in this reservoir will show a highly channeled structure, whereas a small correlation length means a less channeled flow pattern. The value of σ, which determines the width of the permeability distribution, also contributes towards channeling in the displacement pattern. A large value of σ shows more channeling. Fig. 5.7(a) through 5.7(d) show front locations of the 50% isoconcentration lines at different values of the pore volume injected for a five-spot pattern. Fig. 5.7(a) and 5.7(b) show the front locations for $N_{sp} = 250$ ($\lambda_D \simeq 0.13$) and σ as 0.3 and 2.0, respectively. It can again be noted that an increase in the σ value corresponds to more channeling. Similar conclusions can be drawn from Fig. 5.7(c) and 5.7(d). Comparison of Fig. 5.7(b) and 5.7(d) show that for $\lambda_D = 0.13$ ($N_{sp} = 250$) less channeling is observed, whereas for $N_{sp} = 50$ ($\lambda_D \simeq 0.3$), more channeling is evident.

The time history of the tracer concentration at the production well shows the combined effect of the geometry of the flow pattern, the degree of heterogeneity, and the dispersivity of the formation. The effect of the geometry is due to the great variation of the arrival times at the production well of the tracer that has moved along different streamlines. Because of the geometric effect alone, the peak of the output concentration profile is considerably less than 100% even in the absence of heterogeneity and dispersive mixing. The degree of heterogeneity and dispersive mixing induce further dilution in the tracer concentration at production well.

Heterogeneity of the reservoir, as described by the values of λ_D and σ^2, results in an

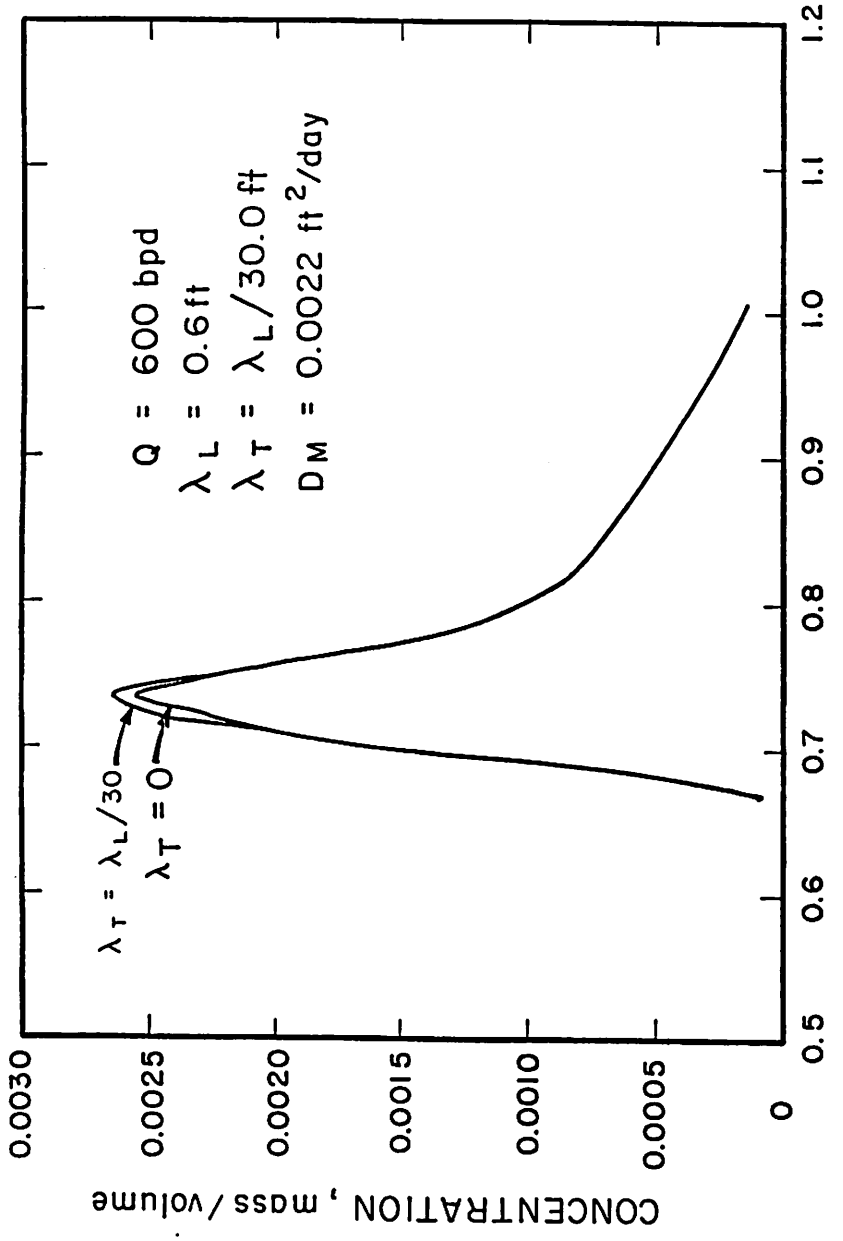

Fig. 5.6 Plot of Integrated Output Concentration vs Pore Volume Injected to Show the Effect of Transverse Dispersion, $a/\lambda_L = 500$.

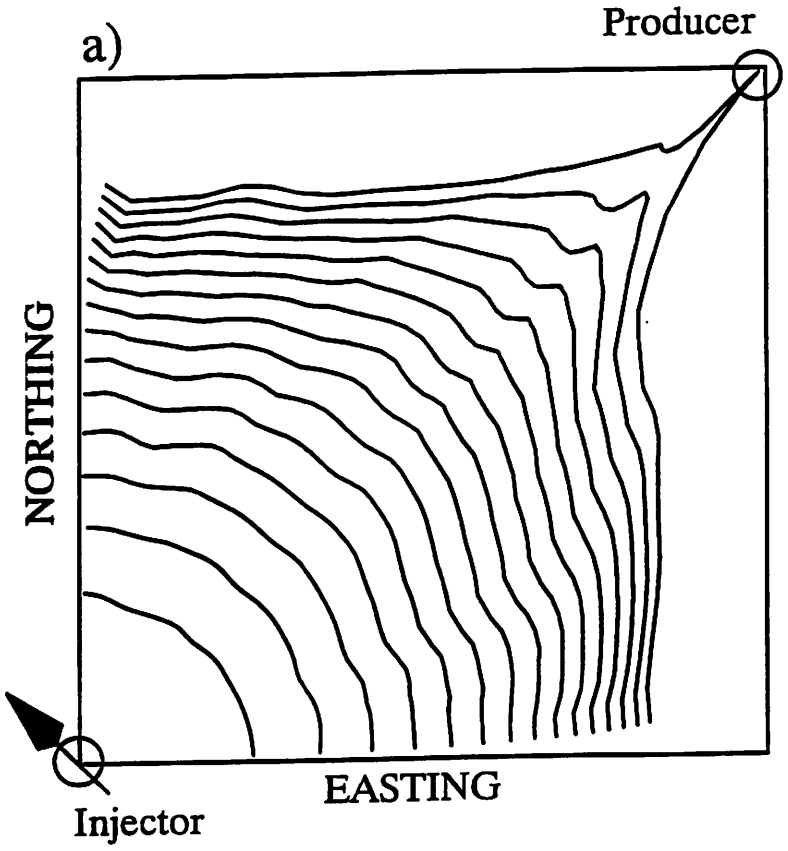

Fig. 5.7a Front Locations of 50% Isoconcentration Lines for a Five-spot Pattern, $\lambda_D = 0.13$, $\sigma^2 = 0.09$.

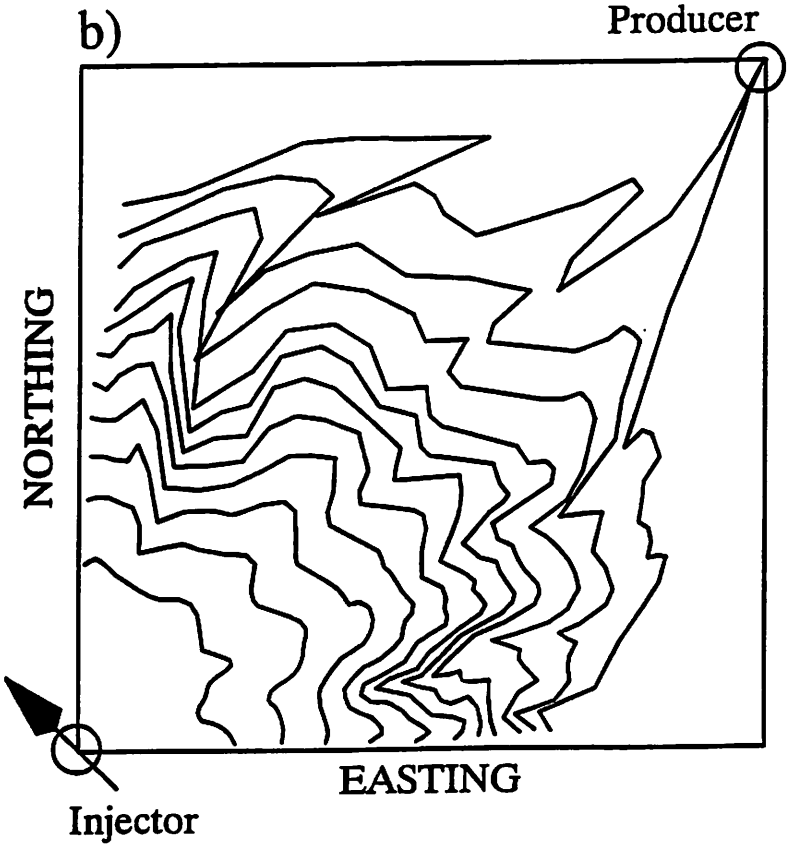

Fig. 5.7b Front Locations of 50% Isoconcentration Lines for a Five-spot Pattern, $\lambda_D = 0.13$, $\sigma^2 = 4.0$.

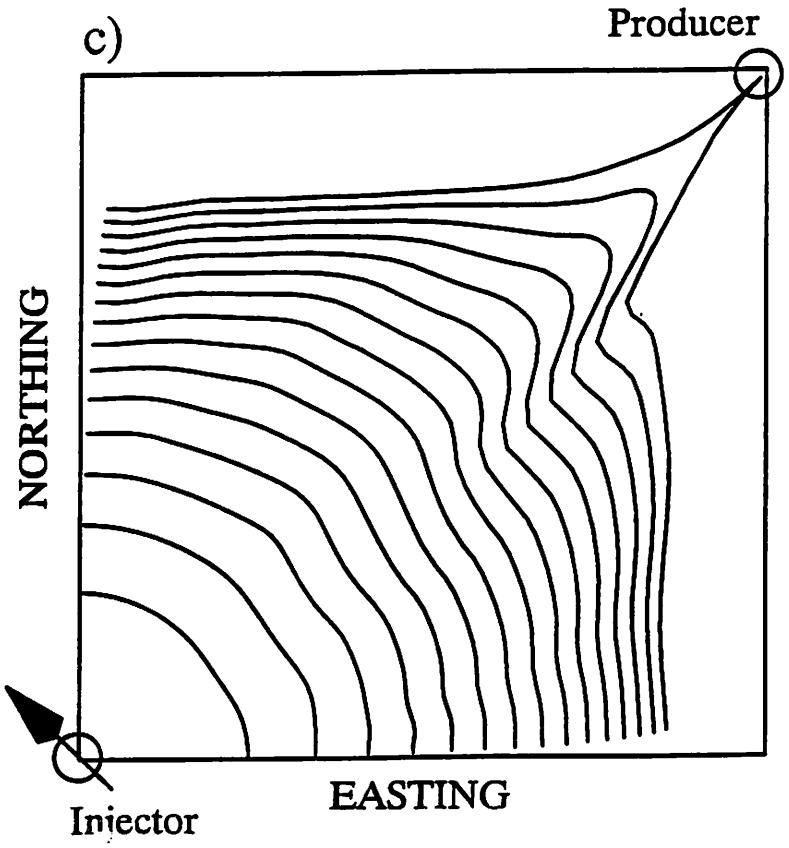

Fig. 5.7c Front Locations of 50% Isoconcentration Lines for a Five-spot Pattern, $\lambda_D = 0.3$, $\sigma^2 = 0.09$.

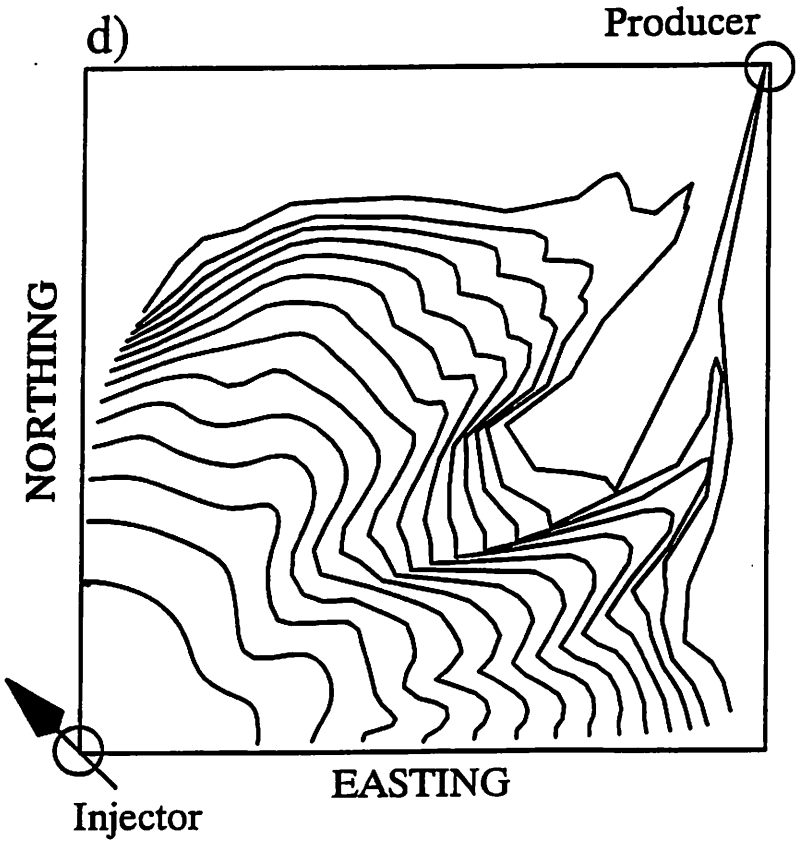

Fig. 5.7d Front Locations of 50% Isoconcentration Lines for a Five-spot Pattern, $\lambda_D = 0.3$, $\sigma^2 = 4.0$.

output concentration profile quite different than that observed from a homogeneous formation. For a small λ_D and small σ^2 value, tracer concentration is comparable with that of a homogeneous formation [Fig. 5.6]. The increase in the channeling effect produces output concentration profiles with multiple peaks [Figs. 5.8(a) through 5.8(d)]. It has not been reported previously that a single layered reservoir can produce such results, as if the formation has multiple layers. The existence of peaks and valleys is because of the areal variation of the permeability. We already noticed that in the tracer output concentration curve from a single-layered homogeneous formation, only a single real peak occurs. Whereas, if the formation is heterogeneous, several peaks appear in the output curve.

5.3.1 Other Flooding Patterns

Some results have also been obtained for other flooding patterns; for example, a staggered line drive and a direct line drive. The flooding area considered in both the patterns is the same as that of the five-spot pattern. The staggered line drive is similar to a five-spot pattern, except the boundaries are not square. Front locations of the $50\sigma^2 = 4.0$, is shown in Fig. 5.9(a). It has been observed that for a heterogeneous formation, earlier breakthrough of the tracer occurs than in the homogeneous case (Fig. 5.9(b)). The shape of the output tracer concentration curve for the heterogeneous formation is not very different from the homogeneous case. Similarly, the direct line drive is similar to a five spot-pattern, except the wells are at the center of the sides of the boundary. The front locations and the output concentration are given in Fig. 5.10(a) and 5.10(b). Here, the output concentration profile has more peaks and valleys, which are apparently associated with the distortion in the flood front [Fig. 10(a)].

In order to quantify the permeability heterogeneity, the results obtained from the simulator can be compared with the field tracer tests. There are three parameters involved: the correlation length (defined by the N_{sp}), the value of σ^2, and the dispersivity distance. One approach is to use an optimization technique that can minimize the error between the observed values and simulated values. It is more desirable to evaluate the geostatistical parameters of permeability by the quantita-

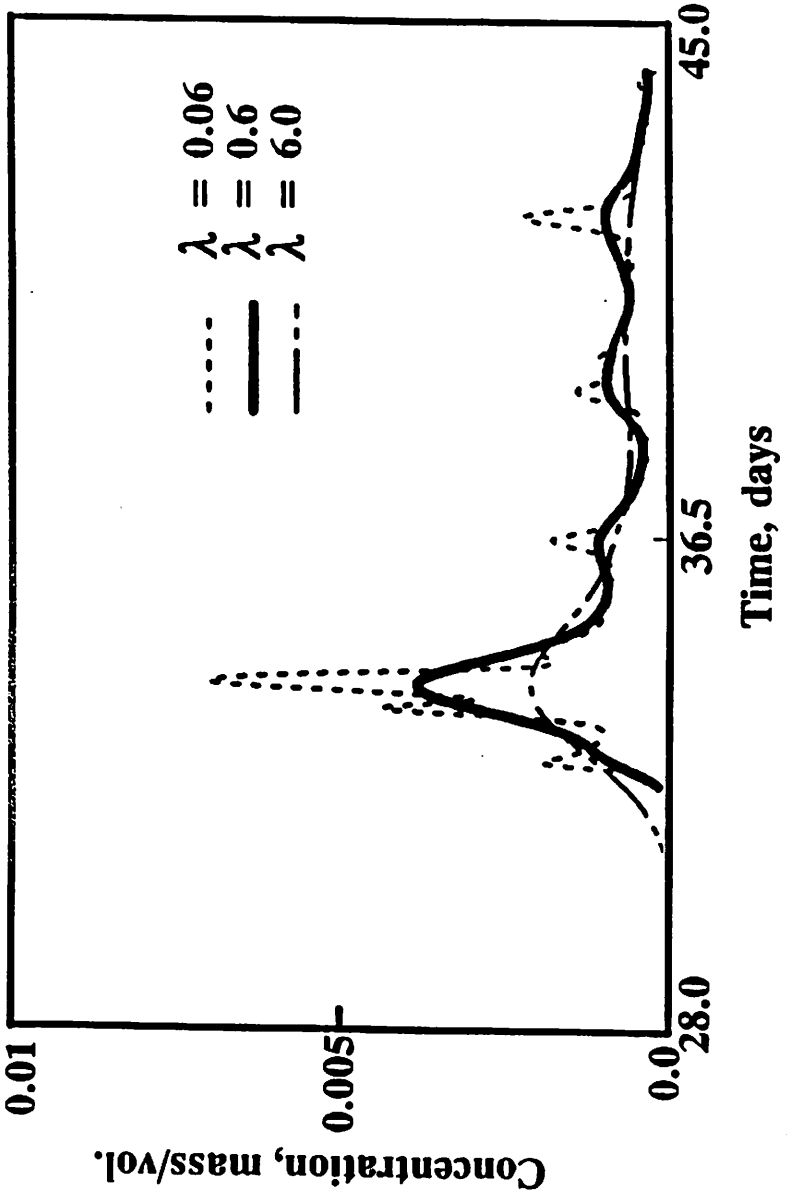

Fig. 5.8a Integrated Tracer Output Concentration for a Five-spot Pattern, $\lambda_D = 0.13$, $\sigma^2 = 0.09$.

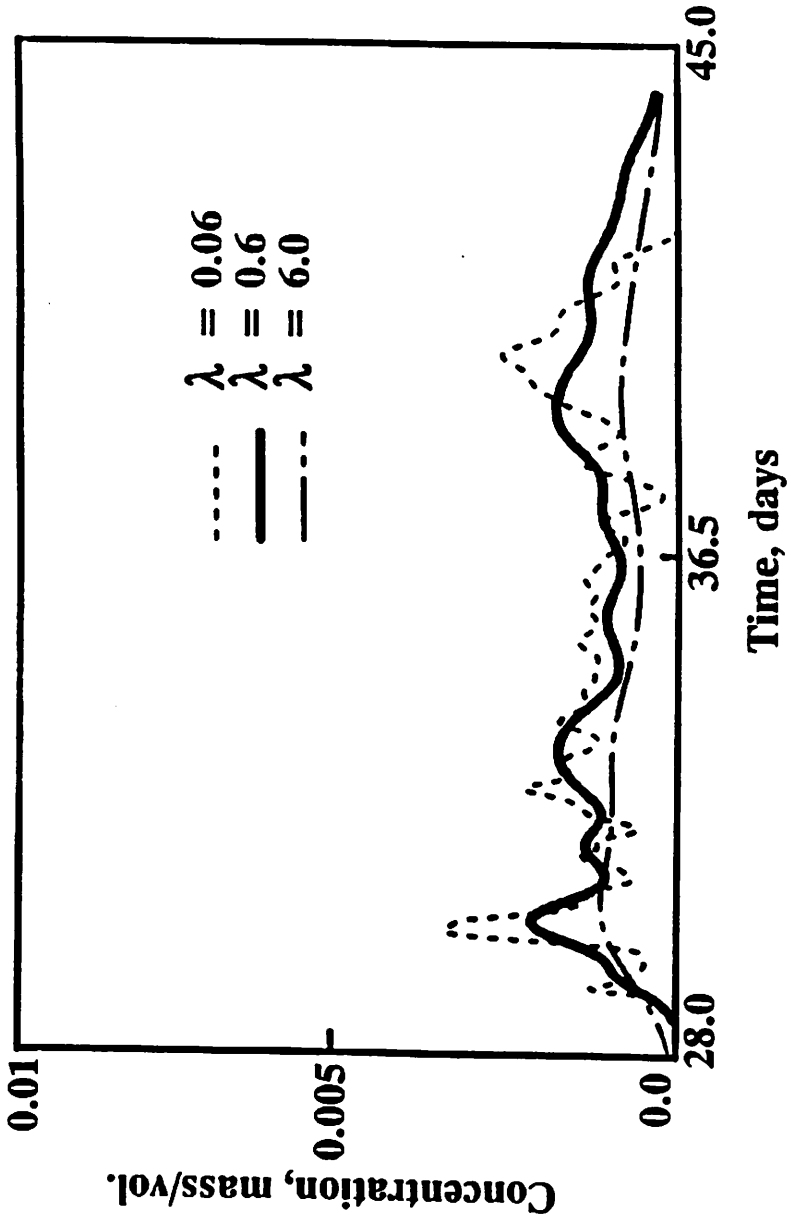

Fig. 5.8b Integrated Tracer Output Concentration for a Five-spot Pattern, $\lambda_D = 0.13$, $\sigma^2 = 4.0$.

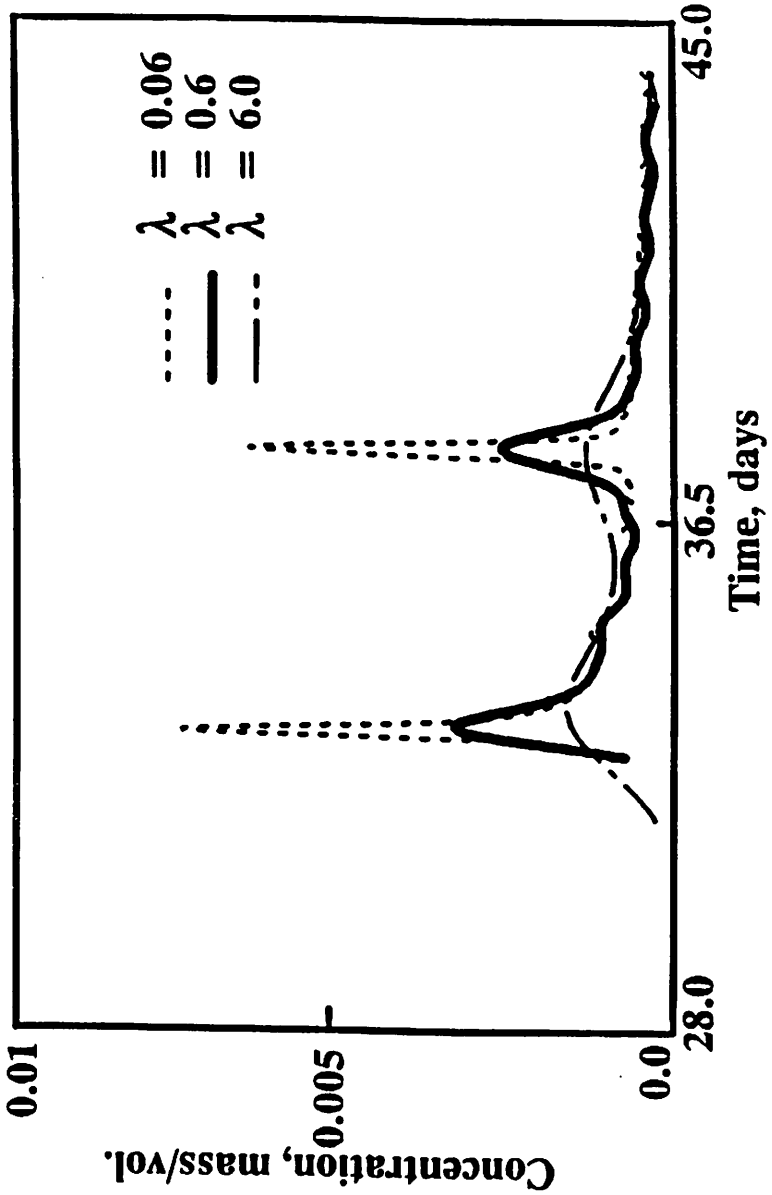

Fig. 5.8c Integrated Tracer Output Concentration for a Five-spot Pattern, $\lambda_D = 0.3$, $\sigma^2 = 0.09$.

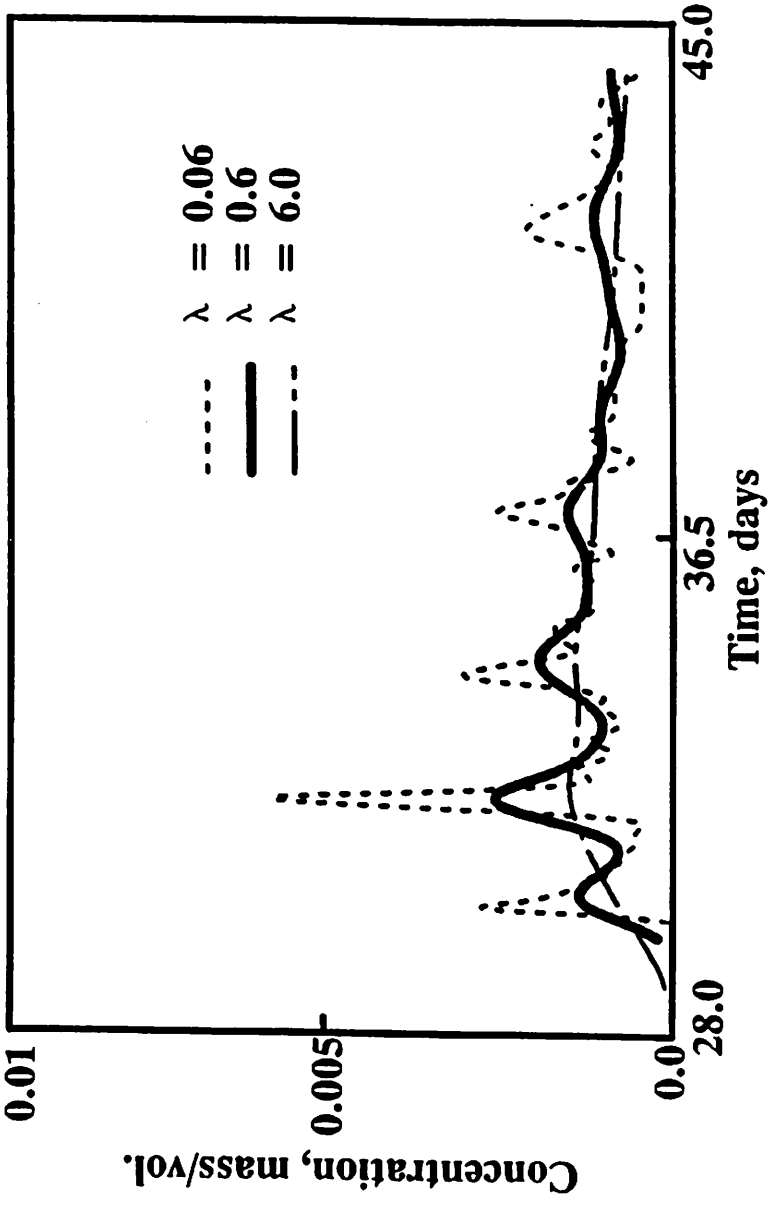

Fig. 5.8d Integrated Tracer Output Concentration for a Five-spot Pattern, $\lambda_D = 0.3$, $\sigma^2 = 4.0$.

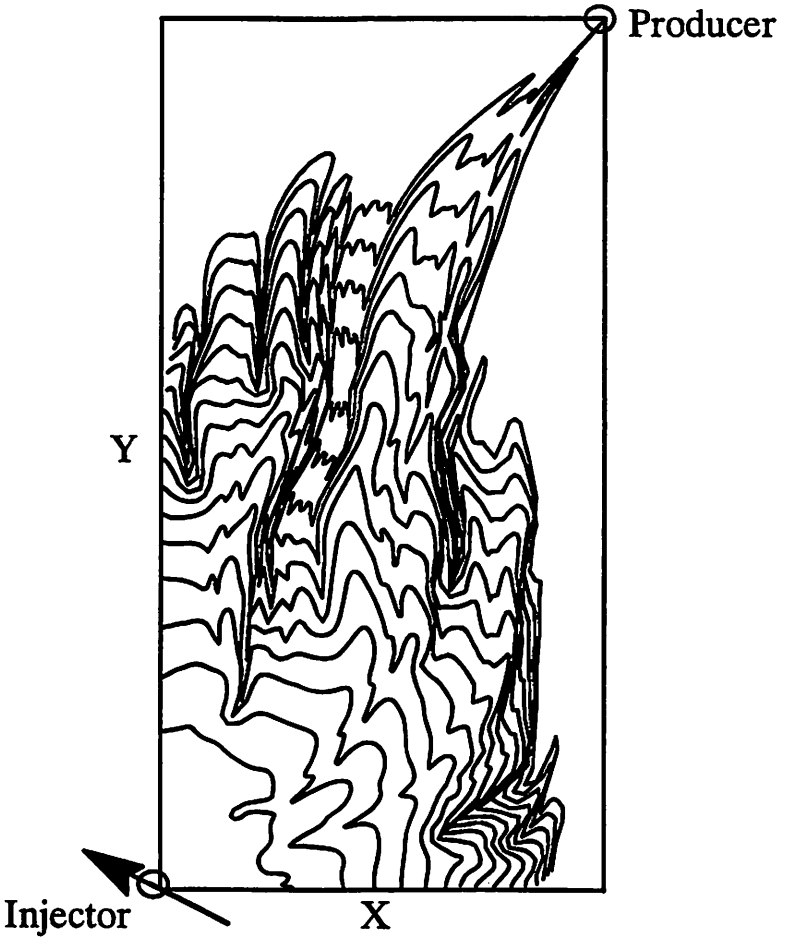

Fig. 5.9a Front Locations of 50% Isoconcentration Lines for a Staggered Line Drive, $\lambda_D = 0.13$, $\sigma^2 = 4.0$.

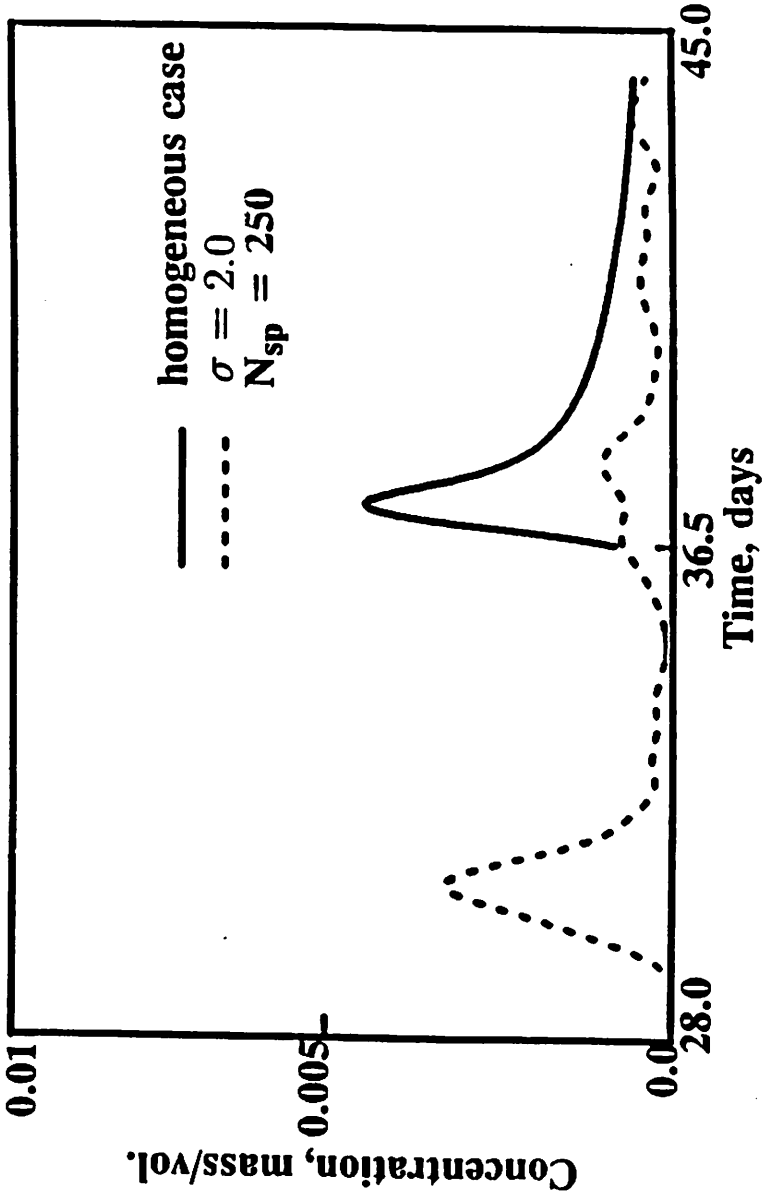

Fig. 5.9b Integrated Tracer Output Concentration for a Staggered Line Drive, $\lambda_D = 0.13$, $\sigma^2 = 4.0$.

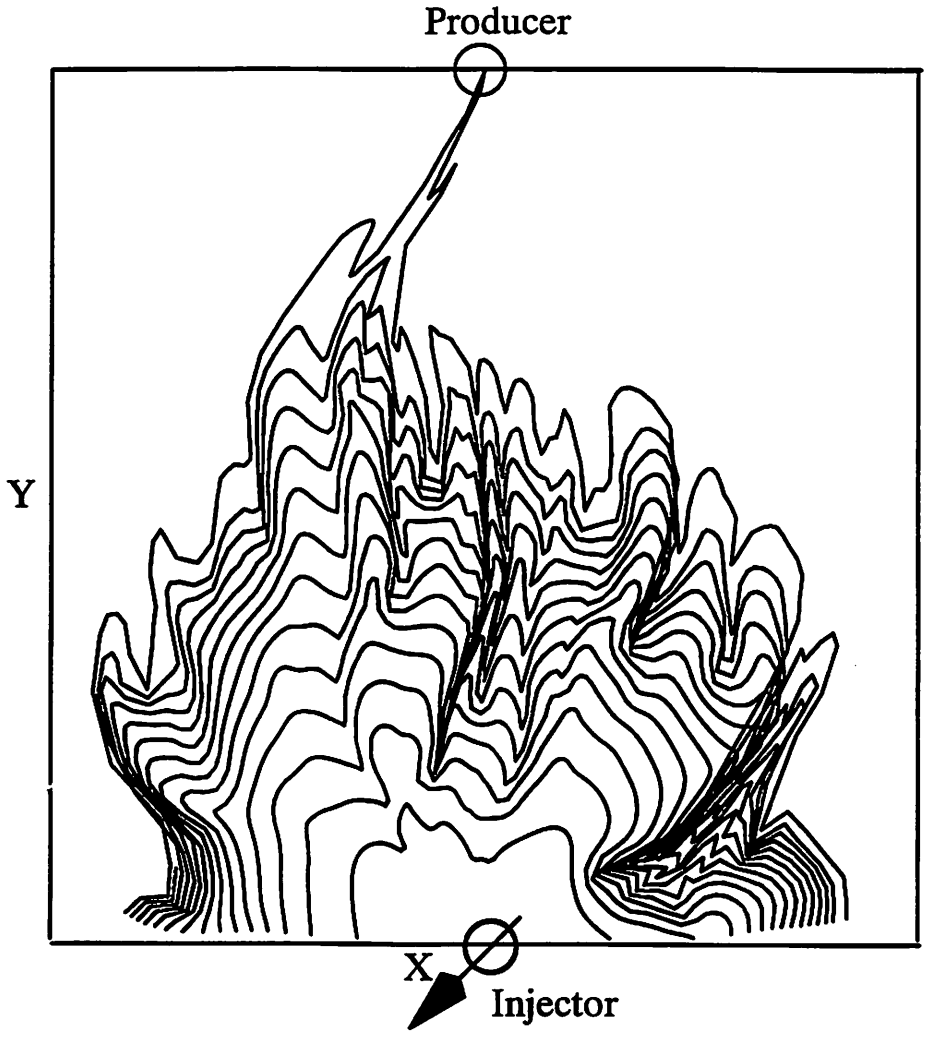

Fig. 5.10a Front Locations of 50% Isoconcentration Lines for a Direct Line Drive, $\lambda_D = 0.13$, $\sigma^2 = 4.0$.

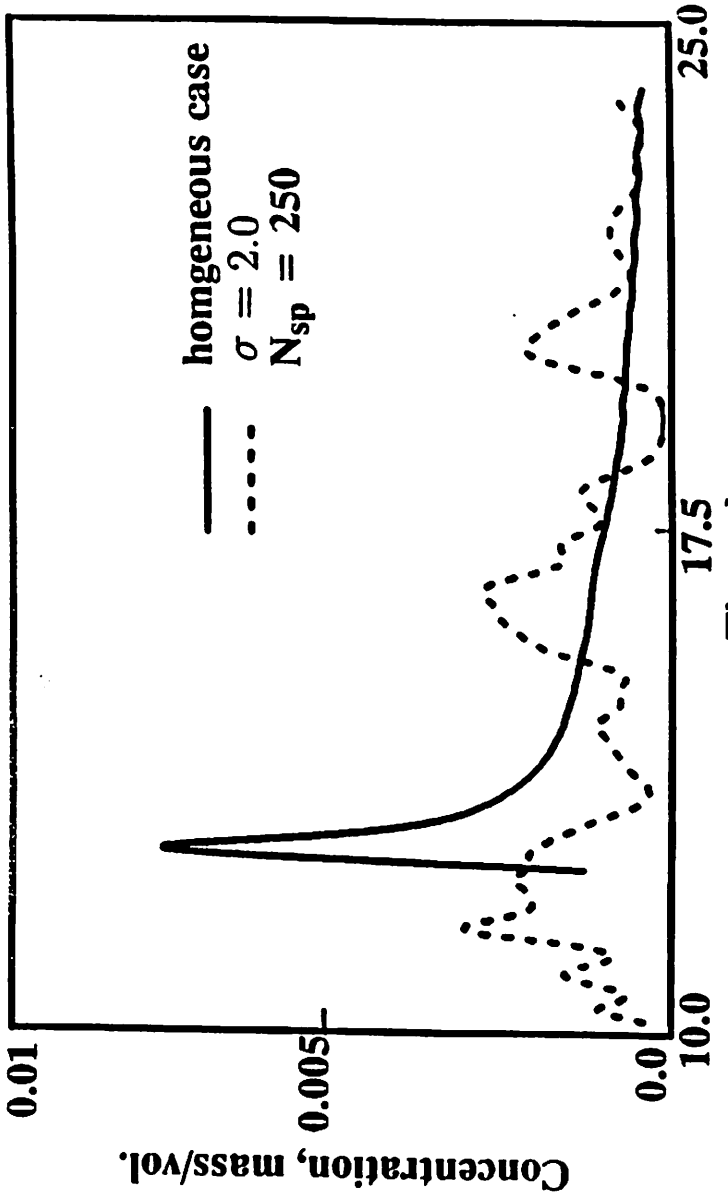

Fig. 5.10b Integrated Tracer Output Concentration for a Direct Line Drive, $\lambda_D = 0.13$, $\sigma^2 = 4.0$.

tive analysis of the tracer output concentration. This is an *inverse problem*, which becomes more complicated due to the effect of computer generated realizations of permeability of specific correlation length and variance. An attempt has been made to quantify the effect of realizations of the permeability field on the tracer output concentration curves.

5.4 Effect of Realizations of the Synthetic Permeability Field

Results have also shown that the details of the multiple peaks are unique for a particular realization of the permeability field. The number and position of the multiple peaks depend upon the correlation lengths with respect to the total flow dimension. For small correlation lengths, the multiple peaks are very similar for different realizations.

It is clear that, for a constant correlation length with an increase of the variance, σ^2, the number of peaks increases, the time between the occurrence of peaks decreases, and the overall time span of the occurrence of tracer increases. The effect of correlation length for a constant variance can not be judged simply by examining the plots of tracer output concentration curves. This is because different realizations (seed values) used in the generation of the synthetic permeability field produce different output curves. Results not presented here have shown that the effect of using different realizations, on tracer output curves, increases with the increase of correlation length and the overall variance of the permeability field. An attempt has been made to quantify the effect of different realizations on the tracer output concentration curves.

It may appear that with different realizations of the permeability field, the tracer output concentration appears to differ randomly. To test this, a catalogue of tracer output concentrations for different realizations, and for each set of permeability distributions (correlation length and variance), was constructed. Fig. 5.11 shows a curve (solid line) of the tracer output concentration ($\lambda_D = 0.4$, $\sigma^2 = 0.09$) that was averaged over fifty realizations. The figure also shows the curves of data with one standard deviation added and subtracted from the averaged curve. It is clear that more variation occurs near the peak of the tracer output concentration curves.

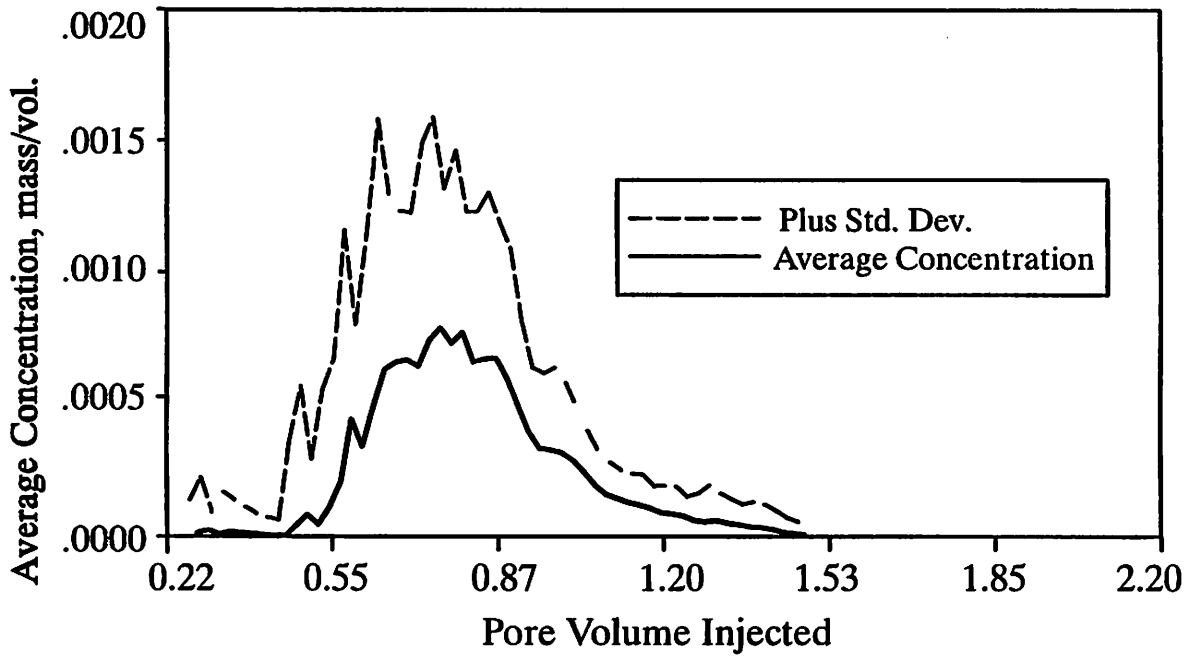

Fig. 5.11 Tracer Output Concentration, Averaged Over 50 Different Realizations of Permeability, $\lambda_D = 0.4$, $\sigma^2 = 0.09$.

Similar types of averaged concentration profiles were constructed to search for any change of the property. Unfortunately, the results did not show any particular trend. In another attempt, a time span between the occurrence of the highest peak to the following valley is computed and averaged over different realizations. Fig. 5.12 shows the plot of this time span vs. the dimensionless correlation length, λ_D, for two variances, $\sigma^2 = 0.09$ and 0.6. The time span is also plotted against the quantity, $N_{sp} = 4/\lambda_D{}^2$, which shows two straight curves. This shows that it is possible to produce such types of curves that can relate the correlation length and the variance to the tracer output curves which requires more tracer flow simulation runs.

5.5 Summary and Conclusions

The tracer production curve reflects the effect of the flow process in underground reservoirs. Therefore, tracer production history can be used as a diagnostic tool in the determination of the permeability heterogeneity. The following conclusions have been drawn from the results of this work:

1. The new numerical method was used to follow the progress of a miscible fluid displacement process by computing the successive positions of the floodfront in a reservoir with arbitrary permeability distribution.
2. The numerical method allows the value of the dispersion coefficient to be varied independently so that its effect may also be studied.
3. The source point method (SPM) was used for the generation of the random permeability field.
4. The numerical method has been applied to the study of the effect of permeability heterogeneity on several production patterns in well-to-well tracer studies for single-layer reservoirs. These studies included the five-spot, the staggered line drive, and the direct line drive. Results show marked differences among them.
5. Heterogeneity generally causes an increase of the time interval, over which tracer emerges from the production well.
6. The tracer output concentration at the production well is affected by the ge-

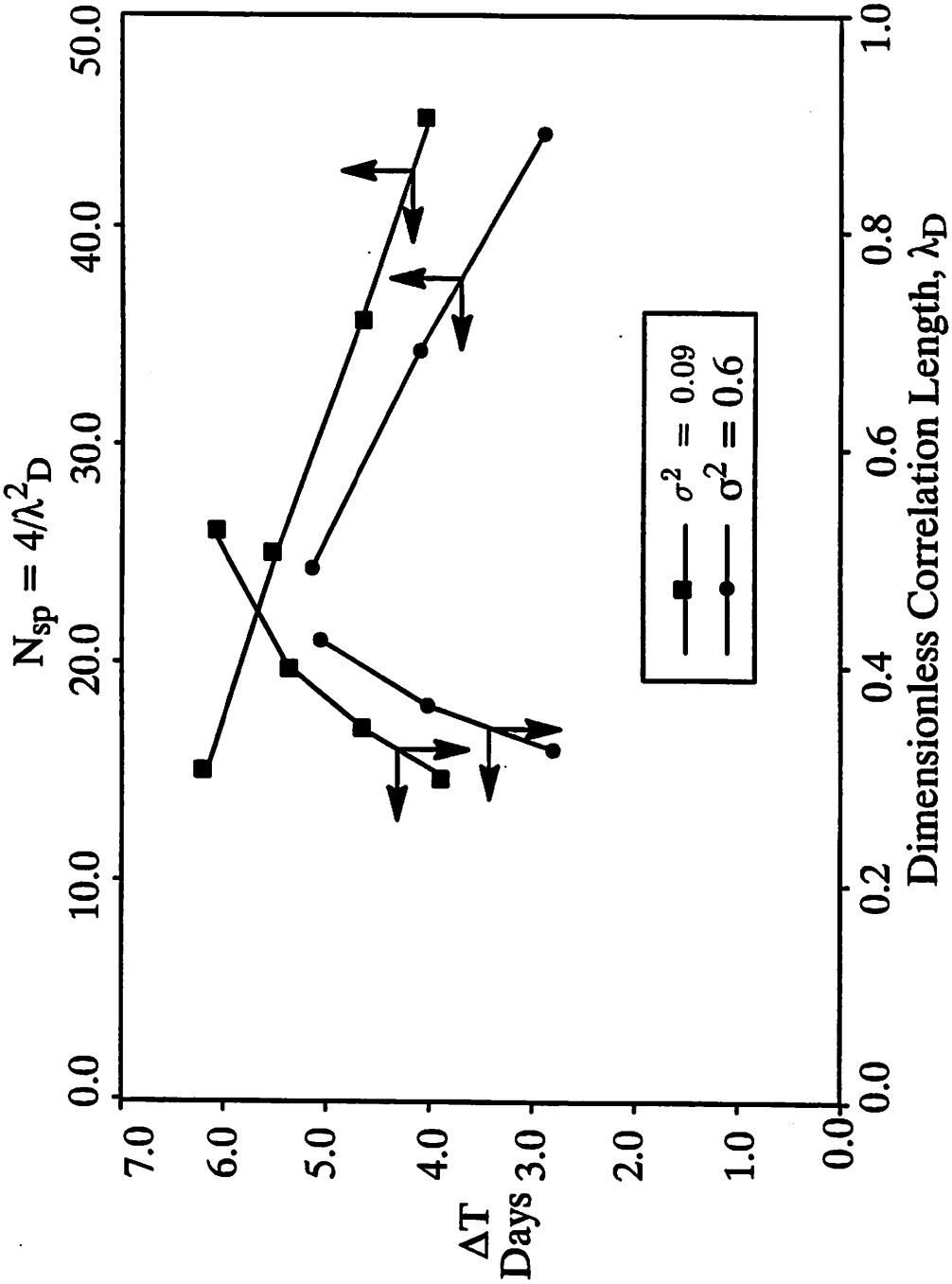

Fig. 5.12 Relationship of the Time Span, ΔT, Between the Occurrence of the Peak and the Next Valley, for Two Cases of Permeability Variances.

ometry of the well pattern, and the channeling resulted from the permeability heterogeneity as modified by the dispersive mixing.

7. The geometric effect produces a nonuniform velocity field which, in turn, induces variability in the arrival time of a tracer on different streamlines. Because of this effect, the tracer output concentration is diluted with the geometric effect alone.
8. The channeling, as a result of the permeability heterogeneity, also causes variation in the arrival time of a tracer at the production well. Therefore, the integrated output profile, even for a single layered reservoir, shows peaks and valleys and more mixing.
9. Unless dispersivity is unusually large, the tracer production pattern is characterized by a number of peaks and valleys, apparently caused by the variability of streamline paths in the heterogeneous formation. These peaks and their distribution can be used to evaluate the heterogeneities. Channeling increases with the increase of the correlation length and variance of the permeability field. It is evident from the results that correlation of permeabilities in even a small fraction of the flow domain produces noticeable channeling.
10. It is possible to infer the geostatistical parameters of the permeability field by measuring the average time span between the occurrence of the prominent peak to the next appearing valley. More research is required in this area. It is suggested that another property should be quantified from the tracer output curves to make the analysis complete.

6 Laboratory Experiment

6.1 Introduction

It is a well recognized fact that permeability is the most important parameter of reservoir heterogeneity. The other parameters, such as porosity, cation exchange capacity, and the amount of clay minerals present are of secondary importance (Lake et al 1989). Permeability has a direct impact on fluid flow and varies much more than the other properties. Therefore, variations in permeability are dominant over the changes in other properties. Results from present numerical studies show that tracer output concentration curves can be well characterized by the statistical variation of permeability. For a particular realization these curves were found to be the function of two geostatistical parameters (variance and correlation length) and the macroscopic dispersivity distance. These theoretical results require experimental verification.

The optimum verification of the numerical results would be obtained with real data from the field. This has always been a problem due to two main reasons. First, the only permeability data available are at the well bore locations, which are not sufficient for the grid system of the computer model. Secondly, the geostatistical techniques of kriging and conditional simulation do not provide permeability data with enough accuracy for our purpose. The reasons are summarized as follows. The basic requirement of the kriging technique is the availability of an accurate variogram. Lack of data makes it very difficult to fit a theoretical variogram to the actual one. Kriging, though an exact interpolator, shows unacceptable smoothing between the data values. The variance estimation increases in locations where fewer data are available. These errors are then transferred to the conditional simulations, since this technique requires that kriging be a dependent tool. Further more, the conditional simulation fields use the unconditional fields which are strongly dependent upon the realization of the synthetic random permeability field.

In view of these considerations, a laboratory experiment is designed and constructed. A locally available sandstone was used for tracer experiment analysis. This chapter is divided into four sections. In the first section, criteria for the selection of the

rock sample is presented. The design and construction of an air minipermeameter is presented in the second section. This device is used to measure the areal permeability values and geostatistical properties of the permeability. In the third section, the procedure for the tracer flood experiment is presented. Finally, the numerical and experimental results are compared in the last section.

6.2 Selection of Reservoir Rock Sample

Numerical results presented in the last chapter show that tracer output concentration curves yield multiple peaks for a variable permeability field. These multiple peaks can be characterized by the two geostatistical parameters of the permeability field, the overall variance and the correlation length. The effect of the dispersivity is of secondary importance. Lake et al (1989) stated that reservoir rock showing more randomness in the permeability field tends to behave like a homogeneous formation. In this case, the permeability at one point is independent of the permeability at neighboring points. For example, if a high permeability value occurs at one point, the next point may have a low value, and the point next to the second may again have a high permeability value, and so on. This implies that channeling, introduced at one location due to high or low permeability, will be canceled out at the next point. Of course, this analysis depends upon the scale at which the permeability is measured.

The use of different scales in reservoir description has been discussed extensively in the literature (Hewett and Behrens, 1988). These scales can be divided into four major classes: 1) microscopic scale, at the level of a few pore sizes; 2) macroscopic scale, the scale of core plugs; 3) megascopic scale, grid block size for an oil reservoir; and 4) gigascopic scale, the scale of a reservoir. During flow through porous media, a fluid can encounter all these scales depending upon the average distance traveled. If variance of heterogeneity at the microscopic scale is comparable to the macroscopic scale, then the fronts will have the same effect on both scales. This comparison can be made by computing the variogram at both scales. This type of reservoir can be well described by the fractal distribution of permeability, which has the tendency of representing a property distribution at any scale. A similar type of analysis can

be made on megascopic and gigascopic scales.

The rock samples used in this work should reflect the effect of both microscopic and macroscopic scaling. The effect of macroscopic scaling is more important. This is because the channeling introduced by permeability heterogeneity at this scale will produce an output concentration profile with multiple peaks. To find a sample which exhibits this quality, preliminary measurements of permeabilities on three rock samples are made, and variograms are constructed. Two out of the three rocks yield correlation lengths equal to the spacing between the grid points. This shows that the permeability on the scale of grid block size (.25 in $\sim$ .635 cm) is independent and random. The output concentration profile from this system would be comparable to the profile from a totally homogeneous medium (Lake et al., 1989). The third sample shows a proper correlation structure, and therefore, is selected for the tracer experiment.

6.3 Permeability Measurements on Rock Sample

Minipermeameters have been widely used in the laboratory and field, to measure permeability over short distances. The permeability measured by this device is nondestructive, and is more accurate than the conventional methods. Perhaps the first form of the minipermeameter was used by Dykstra and Parson in 1950. Later, Morineu et al. (1965), Eijpe and Weber (1971), Goggin (1988) and Davis (1990) used minipermeameters for laboratory and field measurements of permeability. The minipermeameter designed in this study is based on the measurements of the air flow rate at some applied constant pressure.

This study is mainly concerned with the flow of miscible tracer through a five-spot pattern. Therefore, each rock sample is carefully cut into a square (5.63 $\times$ 5.63 in $\sim$ 14.3 $\times$ 14.3 cm) with constant thickness (1.5 in $\sim$ 3.81 cm) as shown in Fig. 6.1. The rock samples are commercially available sandstone. Using the permeability results, one rock sample is selected based on the criteria mentioned above.

To obtain accurate measurements of permeability by the newly designed minipermeameter, an analysis of fluid dynamics is required. One of the most important goals

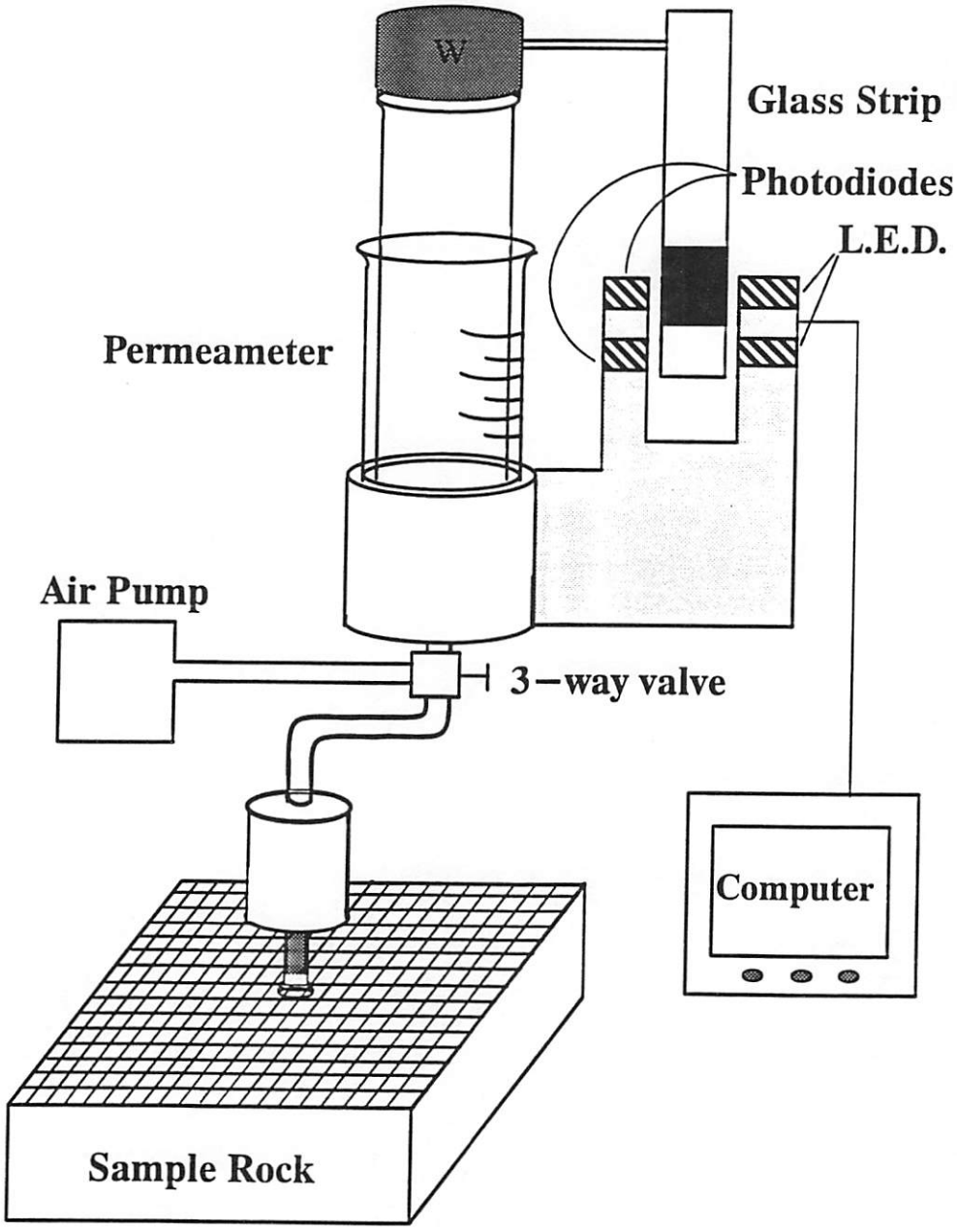

Fig. 6.1 Schematic Diagram of the Minipermeameter Device.

is the achievement of a steady state condition for the flow of gas/air in the porous rock. The steady state condition can be affected by the non-steady, vertical movement of the plunger with low frictional forces between the syringe and the plunger. The leakage that may occur between the interface of the syringe and plunger, and between the rubber tip-seal and the rock surface can void an assumption that air flows only through the rock. Therefore, the time required for the air flow to reach its steady state condition needs to be determined. In this section, we will perform a quantitative analysis of the fluid dynamics of the air minipermeameter as described by Heller (1991).

It is almost impossible to avoid any leakage from the minipermeameter. Hence, the total flow rate can be divided into two parts, 1) Darcy flow rate in porous rock within the hemispherical region below the rubber tip-seal, 2) flow rate due to the leakage in the system. The Darcy flow rate can be written as

$$q_d = \frac{kp}{\mu} G_g(b_D, R) \tag{6.1}$$

where, $G_g(b_D, R)$ is a geometrical factor (Goggin, 1988), and is a function of the ratio of the outer to inner radii (b_D) of the rubber tip-seal and the outer boundary radius, R, of the reservoir rock. The second flow rate due to leakage is also proportional to the pressure and can be written as

$$q_l = \frac{A_p \Delta x}{t_l} = pC_l \tag{6.2}$$

where,

A_p = cross-sectional area of the plunger, L^2

t_l = time interval in which the syringe plunger will come down the distance in the absence of flow through the rock, i.e., with a glass plate substituted for rock

C_l = A leakage constant

The total flow rate can then be written as

$$A_p \dot{x} = p(C_l + \frac{kG_g}{\mu}) \tag{6.3}$$

where $\dot{x}$ represents the derivative of the distance x with respect to time.

$$p = \frac{A_p \dot{x}}{(C_l + \frac{kG_g}{\mu})} \tag{6.4}$$

This is the pressure inside the syringe during the experiment. It is proportional to the total air flow rate if p is small in comparison to atmospheric pressure. This pressure is due to the weight of the plunger and the applied weight. The balance of the upward forces can be written as

$$-M\ddot{x} = pA_p - Mg + (f_v\dot{x} - f_s)a_s \tag{6.5}$$

where,

M = mass of the plunger and applied weight, M

g = acceleration due to gravity, L/T^2

f_v = friction due to viscous forces, M/L^2T

f_s = friction forces between syringe and plunger, M/LT^2

a_s = surface area of the syringe, $2\pi r_s(h + x), L^2$

In Eq. 6.5, the x is measured downward from an arbitrary zero. Over dots represent differentiation with respect to time. Substituting Eq. 6.4 into Eq. 6.5 for pressure, dividing by M through out and rearranging, we get

$$\ddot{x} + [\frac{A_p^2}{M(C_l + \frac{kG_g}{\mu})} + \frac{f_v a_s}{\mu}]\dot{x} = g + \frac{f_s a_s}{M} \tag{6.6}$$

Eq. 6.6 is a second-order non-linear partial differential equation. The non-linearity arises because a_s contains the variable x, $(a_s = 2\pi r_s(h + x))$. This implies that the velocity of the plunger will never be constant. This equation can be made linear by comparing and neglecting the terms containing x with the ones they are associated with,

$$f_v a_s \ll \frac{A_p^2}{(C_l + \frac{kG_g}{\mu})}$$

and,

$$\frac{f_s a_s}{M} \ll g \tag{6.7}$$

Equation 6.7 can be applied by the following justification. The friction due to viscous forces is already small because the air has little viscosity. The first part of Eq. 6.7 is possible if coefficient of leakage C_l is kept small. The second part is true if the mass of the applied weight and the plunger is large enough. In this case Eq. 6.6 can be reduced to a simple linear differential equation

$$\dot{z}_t + Bz_t = C_g \tag{6.8}$$

where,

$$z_t = \dot{x}$$
$$C_g = \mathrm{g}$$
$$B = \frac{A_p^2}{M(C_l + \frac{kG_a}{\mu})}$$

The solution of Eq. 6.8 with the boundary condition, that is at t = 0 $z_t = 0$, is

$$z_t = \frac{C_g}{B}(1 - e^{-Bt}) \tag{6.9}$$

or

$$\dot{x} = \frac{Mg(C_l + \frac{kG_a}{\mu})}{A_p^2}(1 - e^{\frac{-A_p^2}{M(C_l + \frac{kG_a}{\mu})}t}) \tag{6.10}$$

It is obvious from Eq. 6.10, that the velocity of the plunger is a function of time. Applying boundary conditions,

$$\dot{x} = 0 \; at \; t = 0$$

and,

$$\dot{x} = \frac{Mg(C_l + \frac{kG_a}{\mu})}{A_p^2} \qquad at \; t = \infty$$

The required condition of constant velocity can be attained at infinity, which can be obtained by equating the term $e^{-Bt} = .01$, i.e. if $Bt > 4.6$ then we can define a critical time after the plunger is released

$$t_c > \frac{4.6}{B} \simeq \frac{4.6M(C_l + \frac{kG_a}{\mu})}{A_p^2} \tag{6.11}$$

This is the minimum time after which the velocity of the plunger becomes reasonably constant. Similarly, the minimum distance the plunger moves from the point of release can be computed by integrating Eq. 6.10 and using Eq. 6.11

$$x = x_1 = \frac{4.6M^2g(C_l + \frac{KG_g}{\mu})^2}{A_p^4} + ge^{-4.6} \tag{6.12}$$

The point x_1 is the starting location for the air volume measurements. The volume of air expelled during the time the plunger moves from x_1 to x_2 is

$$(x_2 - x_1)A_p = \Delta x A_p \tag{6.13}$$

Let Δt be the time for the plunger to move the distance increment Δx. The total flow rate is therefore,

$$q_t = \frac{kp}{\mu}G_g + pC_l$$

Using $p = \frac{Mg}{A_p}$, and $C_l = \frac{A_p^2\Delta x}{Mgt_l}$ we can write,

$$\frac{A_p\Delta x}{\Delta t} = \frac{kMgG_g}{A_p\mu} + \frac{A_p\Delta x}{t_l}$$

or

$$k = \frac{\mu}{G_g}\frac{A_p^2\Delta x}{Mg}(\frac{1}{\Delta t} - \frac{1}{t_l}) \tag{6.14}$$

Here, t_l is the time of leakage along the side of the plunger and is determined in a separate test by using a glass plate substituted for the rock. G_g is a constant that depends upon the inner and outer radius of the tip-seal and the dimension of the rock as described by Goggin (1988). The other variables in Eq. 6.14 are described in the Nomenclature. Note that Eq. 6.14 does not have a squared pressure term, as is generally the case in the flow of compressible fluids. This is because the difference between the atmospheric pressure and applied air pressure on the rock is not large. Eq. 6.14 is the formula for computing permeability values from the minipermeameter designed in this study.

6.3.2 Experimental Apparatus

The minipermeameter device used in this study was similar to that described by Bahralolom (1991). It is a simple device (Fig. 6.1) consisting of a glass syringe and plunger. The syringe and plunger are kept very clean to avoid any friction caused by dust. A constant pressure/force is applied by placing a weight on top of the plunger. The lower part of the syringe is attached to a small air pump and a probe through a three-way valve. The pump injects air into the syringe and lifts the plunger to the desired height. The three-way valve is then turned to isolate the pump from the syringe, allowing the air to flow from the syringe through the probe. The probe consists of a hollow metallic pin, a tip-seal, and a solid metallic cylinder. The purpose of the metallic cylinder is to apply pressure on the tip-seal. The tip-seal is made of silicone rubber with a hole bored through the center. The ratio of the outer radius of the tip-seal to the radius of the inner hole determines the geometry of the flow. In order to measure the time during which a fixed volume of air enters and flows through the rock, two light- emitting diodes, and associated detectors (LED), are fixed at the side of the syringe (Fig. 6.1) with a mask attached to the plunger. As air passes through the tip and through the rock, the plunger moves downward and the mask obscures first one of the LEDs and then the second. These two signals pass through an electronic device to a personal computer that computes the time span of the movement of the plunger through the fixed distance by counting the number of ticks (on the built-in computer clock) between the two signals. The elapsed time, corrected for leak trend, is inversely proportional to the permeability of the rock which is computed by Eq. 6.14.

6.3.3 Experimental Procedure

After the selection of a proper rock, a grid system with 21×21 nodal points is drawn on the rock with pencil. The grid size is .715 cm in both the x and y directions. The rock is marked for east-west direction and is placed on a firm, horizontal cross feed table (also called $x - y$ positioning table, generally used in lathe or milling machines). The purpose of this table is to be able to move the rock in both east-west and north-south directions.

Before measuring the permeability of the rock sample, the minipermeameter device is calibrated. To do this, a smooth glass plate is set on the rock, and the tip-seal is gently set over the glass plate. Air is injected in the glass syringe by an air pump through a three-way valve. The air lifts the plunger in the syringe up to a certain height above the LED's marked as x_1 on the syringe. The three-way valve is then turned so that only the syringe and the tip-seal are communicating. As the glass plate is impermeable, the plunger should not come down. However, there is always some leakage, particularly at the syringe, and at the contact of the tip-seal and the glass plate. The time for the plunger to move from point x_1 to x_2 is recorded in the computer. This gives the leakage time, t_l, to be used in Eq. 6.14.

To proceed with the permeability measurement, the glass plate is removed and the tip-seal is placed on the first grid of the rock. The same procedure is followed as for calibration. In this way, the permeability is measured in each grid square on both the top and bottom surfaces of the rock. Tables a-1 and a-2 in appendix A show the permeability values measured on the top and bottom surfaces of the rock, respectively. The permeability values in these tables are corrected for the geometry of the tip-seal and the rock sample, using the correction factor described in Goggin (1988).

6.4 Tracer Experiment

Tracers are one of the most popular diagnostic tools to study the production, injection and processing of oil field fluids. A tracer is defined as a substance, when traced through a biological, chemical, or physical system, study the system. Three types of tracers are most common in the petroleum industry; radioactive, chemical (both organic and inorganic), and optical tracers (dyes and fluorescents). When selecting a tracer for a specific application, the following conditions should be taken into account (Taylor and Bandy, 1989): a) naturally occurring concentrations of the tracer species, b) adsorption onto tubulars or formation during transport, c) molecular diffusion, fluid dispersion, and dilution, d) chemical and biological degradation, e) radioactivity decay (half life), and f) interference of other matters with detection technique.

The most commonly used aqueous tracers in the oil fields are halides, thiocyanates, nitrates, water soluble alcohols and radioactive chemicals. The tracers are generally analyzed for anions by chromatographic methods. Spot plate techniques are used for the detection of thiocyanates, formaldehyde, dichromate and nitrate. Ultraviolet lamps can be used to detect fluorescent chemicals. In the detection of alcohols such as methanol and ethanol, gas chromatography is used. Radioactive tritium is detected using scintillation counters, which measure the number of radioactive isotope disintegrations per minute (Hutchins and Dovan, 1991).

In this study, a simple tracer experiment is presented. The rock is fully saturated with 1000 *ppm* brine which is also used as the displacing fluid. A 50,000 *ppm* brine is used as a tracer. This tracer can be easily detected by measuring the conductivity of the fluid at the production well.

6.4.1 Experimental Apparatus

The rock sample is sealed to ensure no flow boundaries. The sealing of the rock is done in two steps. First, a mixture of Armstrong $c-7$ and w epoxy with a volume ratio of 2:3 is prepared. The viscosity of this mixture is approximately 25,000 *centipoise*. The epoxy is mixed thoroughly and is put in a sonic bath to draw off entrained air bubbles. A thin layer of this epoxy mixture is applied to the surface of the rock sample. The highly viscous epoxy mixture will make a seal around the rock without entering the pores of the rock. In the second step, a tray of plexiglass with dimensions $22 \times 23 \times 10$ *cm* is built to encase the rock. The tray is open at the top. A mixture of Armstrong $c-4$ and v epoxy with a volume ratio of 2:3 is prepared. The viscosity of the epoxy mixture is approximately 6 *centipoise*. Four 2.54 *cm* long and 1.4 *cm* thick plastic sticks are placed and glued at the four inner corners of the plexiglass tray making a stand on which the rock can rest on. Before pouring into the plexiglass tray, the low viscosity epoxy mixture is put in a sonic bath to draw off entrained air bubbles. The tray is filled with this epoxy mixture to cover the plastic sticks. The rock is then placed on the plastic sticks and the tray is filled completely with the remaining epoxy. The epoxy is allowed to set for 48 hours. After the epoxy is sufficiently dry, the tray is removed and the epoxy

is smoothed with a cutter on a milling machine.

Two wells are fabricated at opposite corners of the rock sample to represent injection and production wells. The injection well has a diameter of $\frac{1}{4}$ *inches* (0.635 *cm*), whereas the production well has a diameter of 1 *inch* (2.54 *cm*). The holes are drilled at the very edge of the corners so that a minimal amount of rock is cut. The injection well is attached to a constant flow rate pump through $\frac{1}{8}$ *inch* (0.317 *cm*) plastic tubing. The tracer concentration must be measured along the entire depth of the formation. To accomplish this, the acrylic probe described below is constructed. The acrylic probe is a 5×1 *inch* (12.7×2.54 *cm*) cylinder with a notch 2 *inches* (5.1 *cm*) long and $\frac{1}{8}$ *inch* wide (Fig. 6.2) in the side. The fluid from the production well will pass through the notch. Sixteen electrodes are incorporated in the probe by threading them through small holes in the notch of the probe, allowing them to come in contact with the production fluid. The two electrodes at the top and bottom are the current electrodes. The rest are voltage electrodes. The spacing of the array of voltage electrodes is such that fourteen would cover the entire depth of the rock sample at the production well, although only three pairs near the top surface of the rock and three pairs at the lower surface were used. A rubber padding is glued at the outer edge of the notch. Another notch is made in the probe to pass the wires to a multiplexer. A multiplexer is a device which consists of arrays of electronic switches. It selects 1 out of N input data sources, and transmits the selected data to a single information channel. The multiplexer used in this work is described in detail by Heller and Taber (1981). The probe is placed in the 1 *inch* (2.54 *cm*) hole at the production end of the rock, with the notch facing the naked face of the rock. Fig. 6.2 shows the schematic diagram of the tracer experiment performed on the slab of rock.

One important point of care is temperature control. According to calculations from the Arps' approximation quoted on the Schlumberger Resistivity Monograph Chart Gen-9, a ± 0.05 degree Fahrenheit change in temperature is enough to make a change of about one part per thousand in the measured voltage. This is why it is useful to construct a temperature controlled airbath for the experiment.

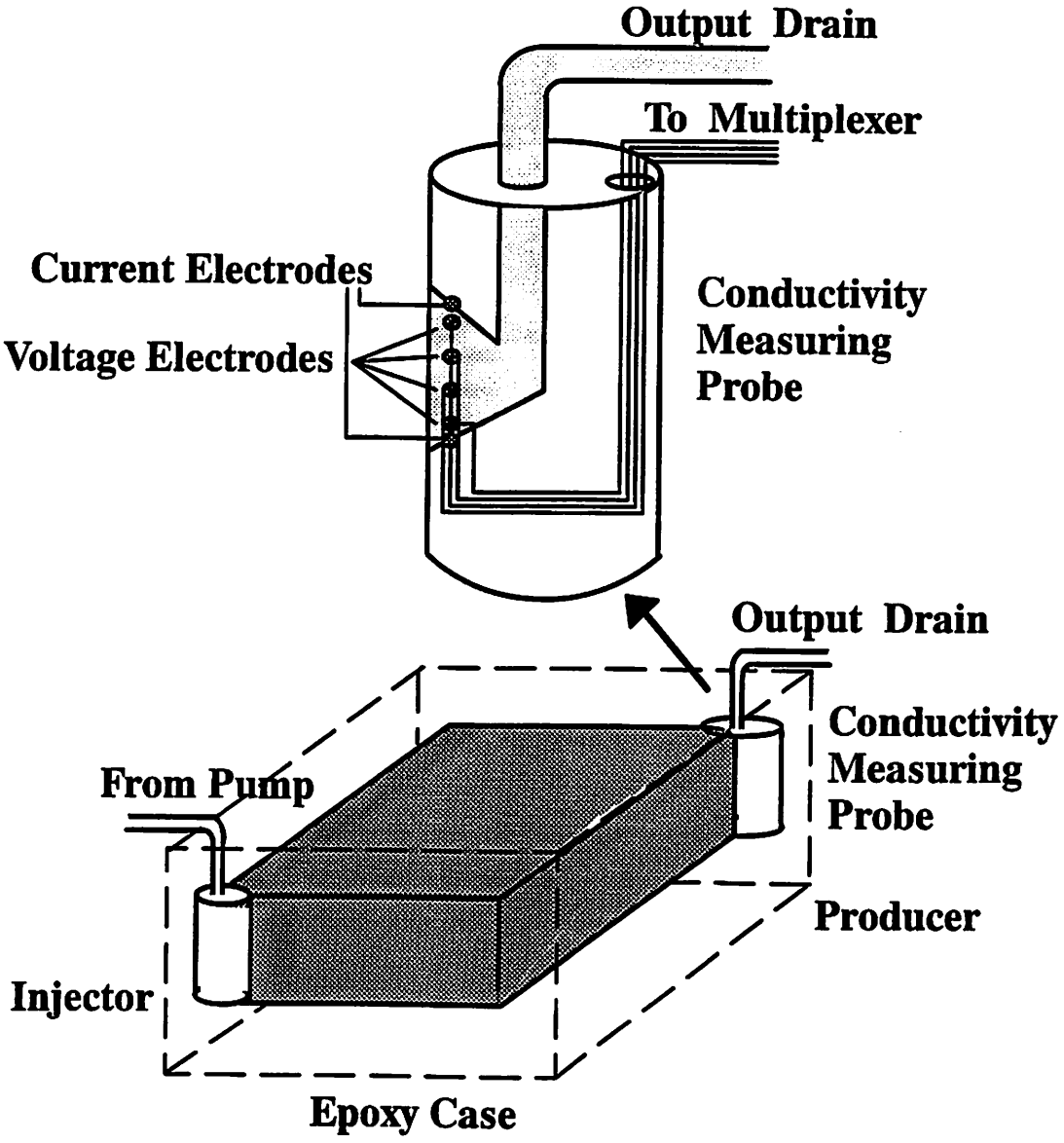

Fig. 6.2 Schematic Diagram of the Tracer Flow Laboratory Experiment on a Five-spot Pattern.

Automatic data acquisition is achieved by the use of a microcomputer that operates under the Turbo Pascal software system. A 12-bit analog-to-digital converter card with several additional digital input/output circuits is installed in the computer to enable recognition of electrical signals and transmission of control signals with the experimental apparatus. The micro-computer controls the measuring current flow and calculates conductivity from the voltages measured across adjoining pairs of electrodes. During the passage of the current, the ohmic potential drop between a particular pair of adjacent voltage electrodes along the production face of the rock sample is measured using a high-input impedance instrumentation amplifier whose output is sent to the computer. The voltage drop is also measured across a standard resistor in series with the current path along the output wellface of the rock. The current is then reversed and the measurements are made again. A conductivity ratio is calculated from

$$C_r = \frac{(s_p - s_m)}{(v_p - v_m)} \tag{6.15}$$

where s_p and s_m are the voltages measured across the standard resistor during the two current directions, and v_p and v_m are the voltages across the particular electrode pair. The average conductivity of the fluid in the space between the two electrodes is then

$$C_a = \frac{L_v}{A_v} \frac{C_r}{R_{std}} \tag{6.16}$$

where L_v is the distance between the pair of voltage electrodes, A_v is the effective cross-sectional area of the current channel, and R_{std} is the value of the standard resistance in ohms. If L_v and A_v are expressed in meters and square meters, the fluid conductivity will be in siemens/meter. The ratio $\frac{L_v}{A_v}$ is determined in a calibration run. Concentration is computed from the analytical form of the standard curves.

6.4.2 Experimental Procedure

The rock sample was first saturated with a 1000-ppm brine. After a .5 *cc* square slug of 50,000 *ppm* brine was injected at the injection well, the recording program was started. Following are the steps in the tracer injection procedure:

1) Measure the flow rate before the tracer injection.

2) Shut off the pump and drain 1000 *ppm* brine through a valve attached at the lower end of the injection well.
3) Turn the three way valve and drain approximately 5 *cc* of tracer through the bottom valve. Make sure that flow lines from the three way valve to the bottom of the injection well contain 50,000 *ppm* brine.
4) Turn the three way valve and turn on the pump long enough only to inject the desired amount of tracer (.5 *cc*).
5) After the desired amount of tracer has been injected, shut off the pump immediately. Open the bottom valve and drain the rest of the tracer from the bottom flow lines.
6) After sufficient draining, close the bottom valve and start the pump to displace the tracer with 1000 *ppm* brine.
7) Start the computer software that measures the conductivity and collects data after the tracer injection.

Several tracer runs were performed. Each run was followed by the injection of 3 to 4 pore volumes of low salinity brine to clean tracer from the rock.

6.5 Experimental Results

Numerical studies showed that the tracer output concentrations produce multiple peaks because of permeability variations. Therefore, the experimental work is performed in two steps; first the areal permeability is measured on both the top and bottom surfaces of the rock, and secondly a tracer flow experiment is performed. Fig. 6.3 shows the semivariograms of permeabilities for the top and bottom surfaces of the rock sample. The figure also shows the fitted variograms. The fitted geostatistical parameters for the top surface are $\lambda_D = 0.18$, $\sigma^2 = 0.18$; and for the bottom surface, $\lambda_D = 0.24$, $\sigma^2 = 0.45$. Analysis of the permeability surface maps showed that both the top and bottom surfaces of the rock have high permeability zones along the northeast and southwest directions. The high permeability zones in both surfaces are responsible for the early breakthrough and poor sweep efficiency, as shown in Fig. 6.4a and Fig. 6.4b. These figures show the front locations of the 50% isoconcentration lines at different values of the pore volume injected (until

breakthrough). The high and low permeability zones are responsible for multiple peaks in the tracer output concentration curves. Fig. 6.5 shows the tracer output concentration curves that were obtained by measuring the conductivity of the brine between pairs of voltage electrodes located at the output face of the formation. Electrode pairs 1 to 3 are for the top portion of the rock, whereas electrode pairs 4 to 6 are for the bottom surface of the rock. It is evident from this figure that six different kinds of tracer concentration curves are obtained. This confirms that the downhole sampling of the tracer would be important in obtaining more information about reservoir rock.

To compare the numerical results with experimental tracer curves, the actual permeability values were used in the simulator to simulate the tracer flow and to compute tracer output concentration curves. Fig. 6.6 shows the comparison of the numerical curve with the experimental curve for electrode pair 3. The numerical tracer curve was adjusted for the dispersivity distance ($\lambda_L = .008cm$) and breakthrough time. Both numerical and experimental curves show similarity in the occurrence of the peaks. The reason that pair 3 yields a better comparison could be due to the following reasons: 1) the distance between the electrode pair is small (0.2 cm) and there is a possibility that electrode pair 3 did indeed measure the conductivity of the tracer from the top layer, 2) the conductivity measuring probe is a little offset, or 3) the minipermeameter gives an average value of the permeability of the zone, whose dimension depends upon the outer diameter of the tip-seal, and the location of electrode pair 3 is right for that portion of the rock.

Similarly, Fig. 6.7 shows the comparison of the numerical tracer curve with the experimental curve that was measured at electrode pair 6. The numerical curve was produced with a longitudinal dispersivity of 0.02 cm. Again a similar trend of high and low concentration was obtained at early times. The experimental curve from bottom surface of the rock produces tracer for a long period of time. The experimental results, in general, show that the tracer output concentration is affected by the permeability variation. Even a single layer can produce multiple peaks in the output concentration. The dispersivity of the rock also changes from one layer to

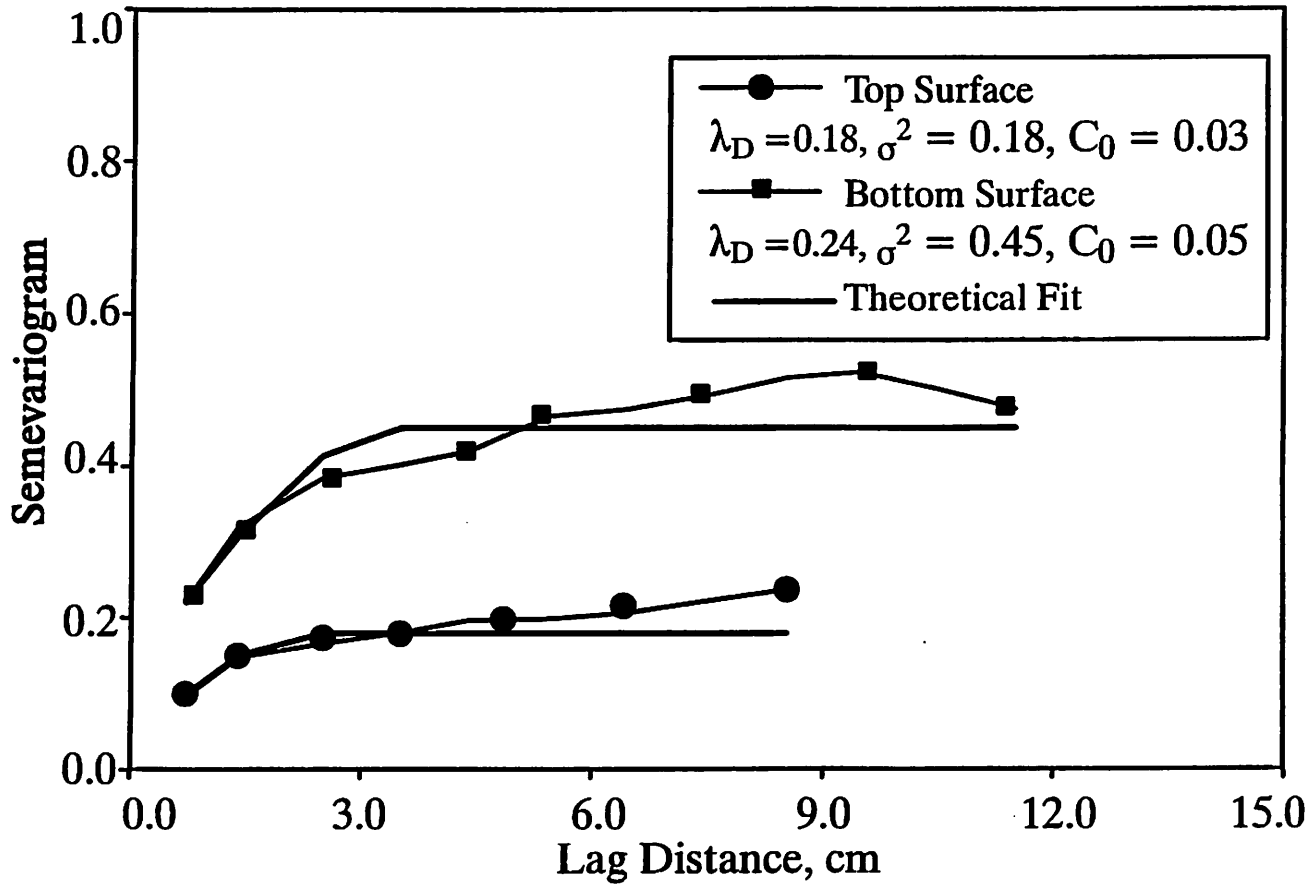

Fig. 6.3 Semivariograms of the Permeability Data and Their Theoretical Fit for Both the Top and Bottom Surfaces of the Rock.

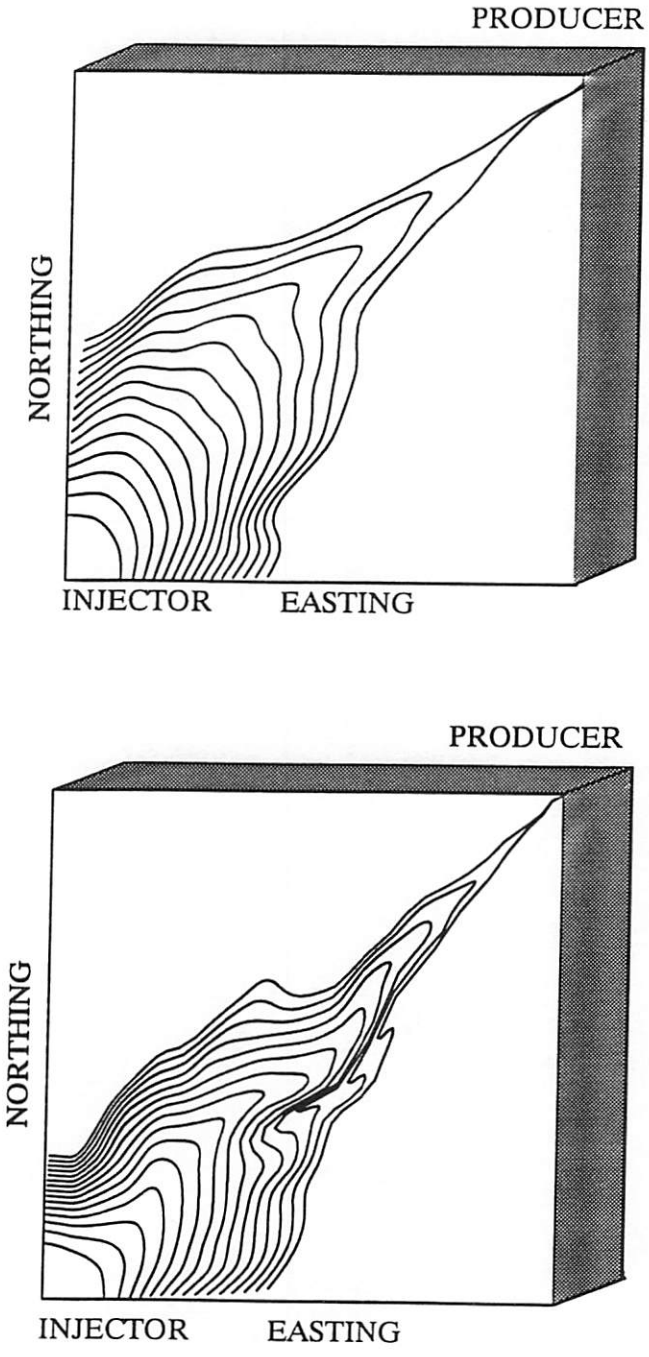

Fig. 6.4 Front Locations of the 50% Isoconcentration Lines for the Rock Sample at the a) Top Surface and b) Bottom Surface.

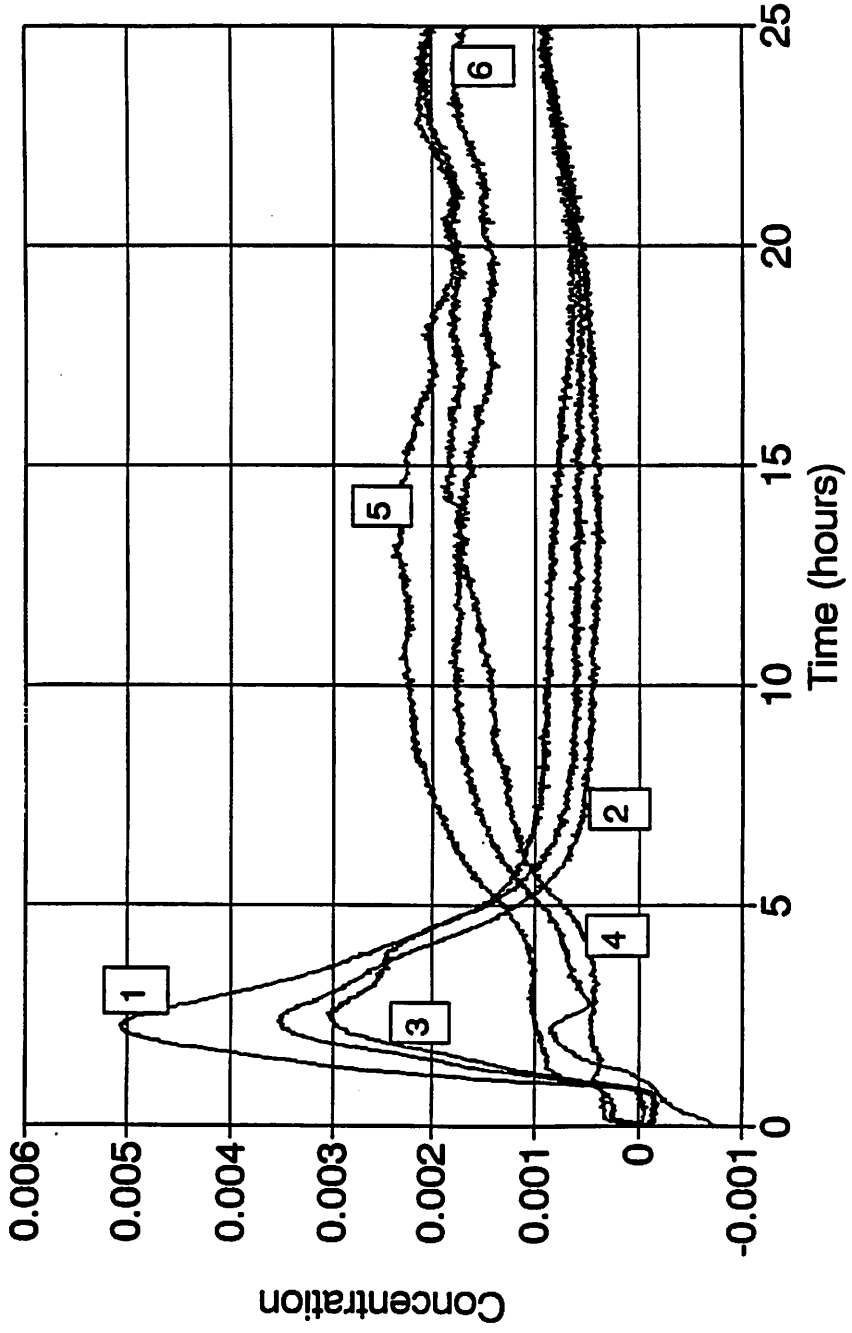

Fig. 6.5 Tracer Indicated Output Concentration for Electrode Pair 1 through 6.

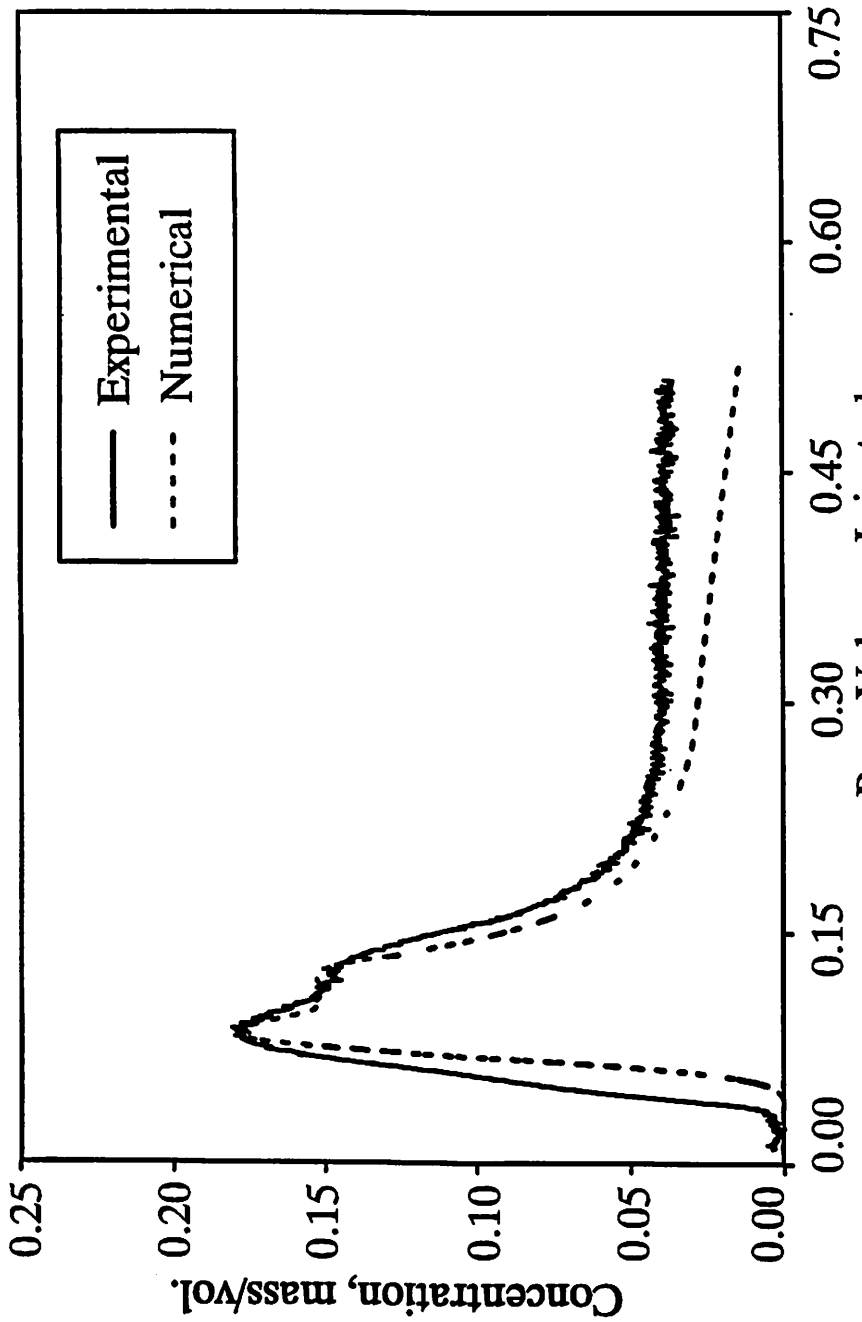

Fig. 6.6 Comparison of the Experimental Tracer Curve for the Top Surface of the Rock, with the Numerical Solution.

another. These results indicate that downhole sampling of the tracer is essential for thorough assessment of the reservoir.

6.6 Summary and Conclusions

This study presents the importance of well-to-well tracer tests to determine the geostatistical parameters of permeability. In the experimental work, permeabilities were measured on both the top and bottom surfaces of a rock sample. This rock sample can represent a quarter of a five-spot pattern. A tracer experiment was performed to produce tracer output concentration at the production well. The following conclusions can be drawn from the presented work:

1. Comparison of the numerical and experimental tracer curves indicates that the tracer output curves are affected mainly by the permeability variation.
2. In the tracer experiment, six different types of the tracer output curves were obtained at the six measuring locations.
3. The geostatistical parameters (variance and correlation length) of the permeability changes from layer to layer.
4. The dispersivity of the rock sample also changes from one layer to the other.
5. Downhole sampling of the tracer concentration at each known layer would be very useful in achieving further valuable information about the reservoir.

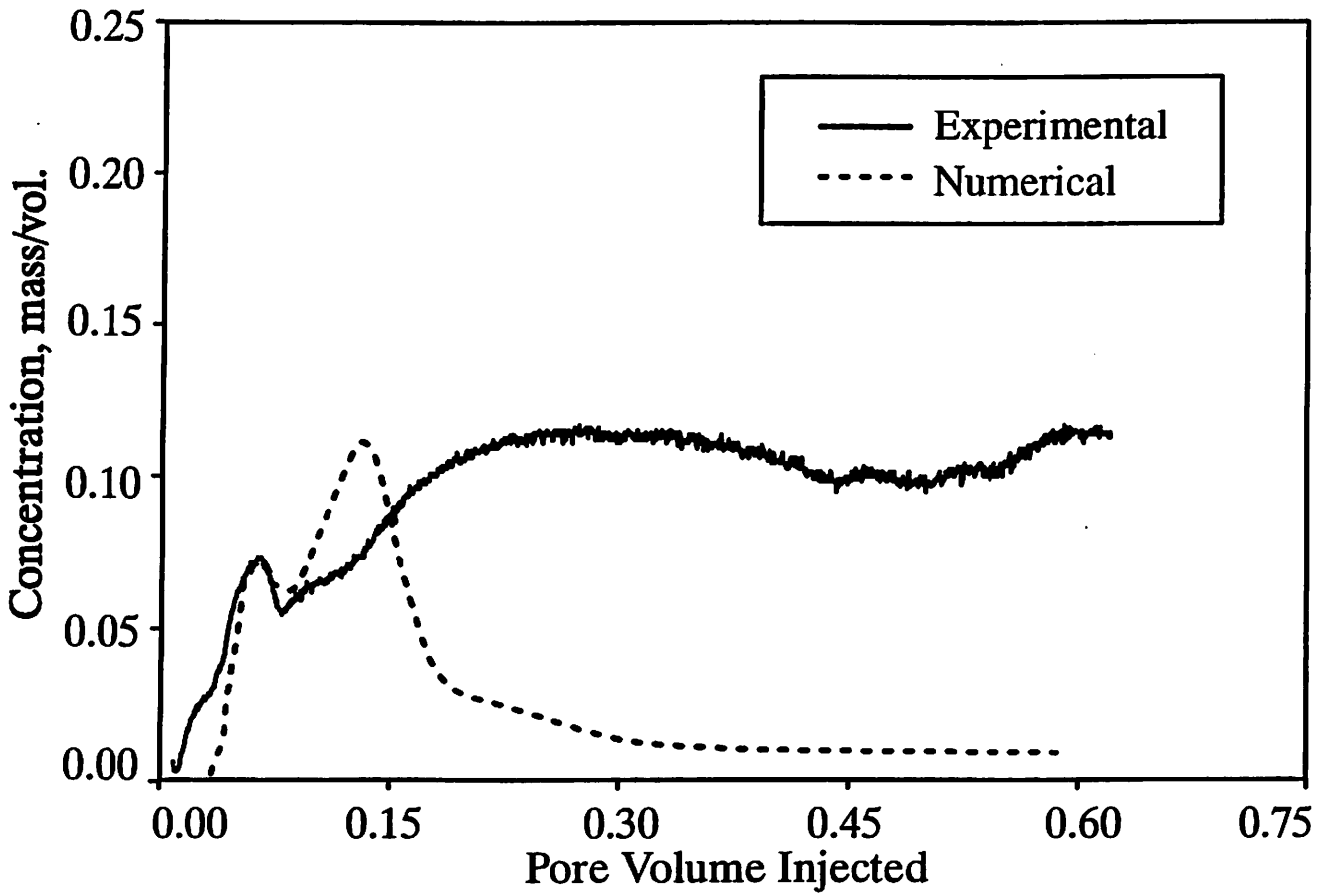

Fig. 6.7 Comparison of the Experimental Tracer Curve for the Bottom Surface of the Rock, with the Numerical Solution.

7 Conditional Simulation with a New Estimation Method

7.1 Introduction

Reliable estimates of field permeability from known data at well locations is necessary for accurate numerical flow modeling of underground reservoirs. The performance predictions that can be made from these reservoir simulations require not merely the data obtained at well locations, but the values of the rock properties at all specified grid points. Several interpolation and simulation techniques are available in the literature; for example, a quadratic projection method, kriging, conditional simulation, etc. (Journel and Huijbregts, 1978; Chopra et al., 1990). In this chapter, conditional simulation with a new estimation method is presented. The new estimation method is based on a modified form of the source point method. The chapter is divided into three main sections. The first section describes the conventional conditional simulation (CS) method. In this section, a brief review of the kriging technique is presented. Conditional simulation with the new estimation technique is presented in the second section. The similarity between kriging and the new estimation technique is also discussed in this section. Finally, in the last section, the conventional simulation and new methods are compared using laboratory data.

7.2 Conventional Conditional Simulation Method

Knowledge of the permeability distribution of underground reservoirs is very important in the simulation of oil displacement. For example, a simulator can predict the performance of water and chemical flooding more accurately if the permeability and its variations are known at every specified grid block. Since the size of the grid block is much smaller than the scale at which the data is available (interwell distance), special techniques are required to interpolate/simulate the permeability using known data. A good technique should satisfy the following four objectives:

1. It should be exact at the known location.
2. It should keep the same statistics as the original data.
3. It should provide an estimation of uncertainty for each estimated value.
4. It should keep the same amount of variability as the true data in nature.

The first of these objectives can be achieved by the use of several conventional techniques, for example; triangulation, piecewise linear least square, or quadratic projection methods (Chopra et al., 1990). One limitation of these techniques is that the computed values do not preserve the correlation structure, and an estimate of uncertainty can not be provided. Kriging, however, includes the desired correlation structure, and can yield the uncertainty in the estimated value. Although kriging is an exact interpolator, it is an estimation technique and results in smoothing in the computed field. The conditional simulation method in fact can satisfy all the four objectives mentioned above. The following sections describe the methodology of conditional simulation.

7.2.1 Kriging

In mining geostatistics finding the best estimate of the mean value of a variable has generally been a problem. The variable is assumed to be a regionalized variable over a limited domain. The value of the random variable, R.V., is presumed to be homogeneous at the scale of measurement. If the scale of measurement is small compared to the scale at which the properties are stationary, then estimation is called local. Otherwise it is referred to as global estimation. In order to develop a good model with a variogram that characterizes the spatial variability at the scale of measurement in the zone of interest, local estimation requires a sufficient number of known data. Given these data, local estimation method which provides the best linear unbiased estimation (BLUE) is called kriging.

Mathematics of Kriging

Kriging is the best linear unbiased estimator (BLUE). It is 'linear' because it estimates an unknown z_o^* at any location by the linear relationship

$$z_o^* = \sum_{i=1}^{n} \lambda_o^i z_i \tag{7.1}$$

where $\lambda's$ are the weights at n known locations and z_i's are the values of the process at these locations. It is 'unbiased' because

$$E[z_o^*] = E[\sum_{i=1}^{n} \lambda_o^i z_i] = E[z_o] = m \tag{7.2}$$

That is, under the hypothesis of stationarity, the expectation is constant and equal to the mean of the known data. A non-bias condition can only be achieved if

$$\sum_{i=1}^{n} \lambda_o^i = 1 \tag{7.3}$$

Eq. 7.3 implies that the expected value of the estimate is equal to the true expected value, m. Kriging is referred to as the 'best' estimator because the error of estimation, $E[z_o^* - z_o]^2$, is minimized. The error of estimation, or kriging variance, can be estimated as

$$\sigma_{ok}{}^2 = -\sum_{i=1}^{n}\sum_{j=1}^{n} \lambda_o^i \lambda_o^j \gamma(x_j - x_i) + 2\sum_{i=1}^{n} \lambda_o^i \gamma(x_i - x_o) \tag{7.4}$$

where $\gamma's$ are the semi-variograms. Eq. 7.4 is minimized, and the resulting system of kriging equations is solved for the $\lambda's$ to be used in Eq. 7.1.

7.2.2 Unconditional Field

One of the requirements of reservoir characterization is the generation of synthetic random fields. The need for such fields is based on the fact that the field permeability/porosity data available from well logging, well testing, core analysis etc., are generally not sufficient to describe these properties completely in whole domain. Furthermore, prediction of the property distribution of a reservoir, for example, by the conditional simulation method, requires the generation of a synthetic random field. Early investigators did not consider the spatial correlation structure (Warren and Price, 1961; Freeze, 1975). In later studies, investigators (Marsily, 1984) showed that reservoir properties exhibit a correlation structure; i.e., that the permeability values are not totally random but are dependent on the values at neighboring points. An unconditional synthetic random field may have the same correlation structure and variation as the real field generally, but it does not honor the known data. Several techniques of generating unconditional fields are available in the literature; for example, the source point method (SPM) (Heller, 1972), the fast fourier transform

method (FFTM) (Gutjahr, 1989), the turning band method (TBM) (Mantoglou et al., 1982), and the simulated annealing method (SAM) (Ouenes et al., 1991). In this work the FFTM given in Gutjahr (1989), and the SPM given by Heller (1972) are used.

Source Point Method

The SPM uses the inverse square law assumption to compute the natural log of permeability values at the specified grid points as

$$S_g(N,M) = \frac{\sum_{j=1}^{N_{sp}} \frac{s(j)}{\alpha^2(x(j)-x_g(N))^2 + \beta^2(y(j)-y_g(M))^2}}{\sum_{j=1}^{N_{sp}} \frac{1}{\alpha^2(x(j)-x_g(N))^2 + \beta^2(y(j)-y_g(M))^2}} \tag{7.5}$$

where α and β are the coefficients of anisotropy (Ghori et al., 1991); for an isotropic medium $\alpha = \beta$. The permeability values at each grid point are then calculated as

$$k(N,M) = k_o e^{\sigma S_g(N,M)} \tag{7.6}$$

where k_o is the base permeability and σ is the parameter defining the width of the isotropic permeability distribution. With the SPM, a random permeability field with some correlation structure can be generated. As shown in chapter 4, the correlation length for an isotropic medium can be computed from the number of source points

$$L_c = 2.0\sqrt{\frac{area}{N_{sp}}} \tag{7.7}$$

The SPM is one of the most efficient methods with regard to computer time and storage. It produces an unconditional field with the desired correlation length and variance. Recently, it was shown (Ghori et al., 1991, and Chapter 4) that the SPM can also generate an anisotropic field.

Fast Fourier Transform Method

One method of generating spatially correlated realizations which have some spatially prescribed covariance behavior is the FFTM (Gutjahr, 1989). The generated field

from FFTM follows the hypothesis of a second order stationary process. A brief outline of the method is discussed below

1. Let $X(\underline{t})$ be a second order stationary process with some covariance behavior $c(\underline{x})$. The covariance function $c(\underline{x})$ can be described alternatively via the spectral density of $X(\underline{t})$

$$f(\underline{\lambda}) = \frac{1}{(2\pi)^{\frac{1}{2}}} \int_{-\infty}^{+\infty} c(\underline{x}) e^{i\underline{\lambda}^{\circ}\underline{x}} d\underline{x} \tag{7.8}$$

$c(\underline{x})$ can be obtained with the inverse fourier transform of $f(\underline{\lambda})$ as

$$c(\underline{x}) = \int_{-\infty}^{+\infty} f(\underline{\lambda}) e^{-i\underline{\lambda}^{\circ}\underline{x}} d\underline{\lambda} \tag{7.9}$$

2. Using the spectral representation theorem, which implies that for a stochastic process, $X(\underline{t})$, there exists a unique real spectral distribution function, $F(\underline{\lambda})$, such that $c(\underline{x})$ is the Fourier-Stieltjes transform of $f(\underline{\lambda})$ as

$$c(\underline{x}) = \int_{-\infty}^{+\infty} e^{i\underline{\lambda}^{\circ}\underline{x}} dF(\underline{\lambda}) \tag{7.10}$$

Applying the same rule to $X(\underline{t})$

$$X(\underline{t}) = \int_{-\infty}^{+\infty} e^{i\underline{\lambda}^{\circ}\underline{t}} dZ(\underline{\lambda}) \tag{7.11}$$

The Z process and $F(\underline{\lambda})$ are related as

$$E[dZ(\underline{\lambda})] = 0$$

and,

$$E[dZ(\underline{\lambda}).dZ^{*}(\underline{u})] = \begin{cases} dF(\underline{\lambda}) & \text{if } \underline{\lambda} = \underline{u} \\ 0 & \text{if } \underline{\lambda} \neq \underline{u} \end{cases} \tag{7.12}$$

The dZ^{*} in Eq. (7.12) is the complex conjugate of dZ. The Fourier Stieltjes transform of the complex process is then expanded in a series and evaluated using a fast fourier transform algorithm.For a detailed discussion of this method, refer to Gutjahr (1989) or Mckay (1988).

7.2.3 Theory of Conditional Simulation

A regionalized variable $z(x)$ is interpreted as one realization of a certain random function RF. Although, there is an infinite number of possible realizations of a RF, its statistical properties can be characterized by a distribution function and a covariance or variogram function. The purpose of conditional simulation is that it chooses a particular realization of the RF that characterizes the variability of the experimental data and agrees with the experimental data values at actual data locations, i.e.,

$$z_{cs}(x_\alpha, y_\alpha) = z_0(x_\alpha, y_\alpha) \tag{7.13}$$

where $z_{cs}(x_\alpha, y_\alpha)$ is the two dimensional simulated conditional value at the actual data location and $z_0(x_\alpha, y_\alpha)$ is the experimental value at the same location. The means by which the conditional field is generated is now considered. Consider a kriged value, $z^*_{0k}(x, y)$, which is an estimate of the true value, $z_0(x, y)$. The values of the two can differ due to an unknown error,

$$z^*_0(x, y) = z^*_k(x, y) + [z_0(x, y) - z^*_k(x, y)] \tag{7.14}$$

It is impossible to find the exact value of the unknown error $[z_0(x, y) - z^*_k(x, y)]$. Instead, we can replace this error by an isomorphic and independent kriging error $[z_u(x, y) - z^*_{uk}(x, y)]$, where $z_u(x, y)$ is the generated unconditional field. This field is isomorphic to the original field, i.e. it has the same amount of variability and correlation structure. The kriged unconditional field at the known data location is $z_{uk}(x, y)$. The generated field is known as 'unconditioned' because it need not agree with the known data and is independent of the kriged field $z^*_k(x, y)$. The required conditioned field can then be defined (Journel and Huijbregts, 1978) as

$$z^*_{cs}(x, y) = z^*_k(x, y) + [z_u(x, y) - z^*_{uk}(x, y)] \tag{7.15}$$

where

$z^*_{cs}(x, y)$ = conditioned field in two dimensions,

$z_k^*(x,y)$ = kriged field of known samples in two dimensions,

$z_u(x,y)$ = unconditioned field in two dimensions, and

$z_{uk}^*(x,y)$ = unconditioned kriged field in two dimensions.

The concept of conditional simulation is illustrated in Fig. 7.1.

Properties of Conditional Simulations

Conditional simulation produces random fields that have the same amount of variability as the original data, and honor the known locations. Following are the properties of the conditional simulation method (Journel and Huijbregts, 1978)

1) The conditioned field provides both simulated and kriged values at every point, (x,y), in the domain.
2) The kriging weights are the same for both $z_k^*(x,y)$ and $z_{uk}^*(x,y)$.
3) As with the case of the kriging estimate, the conditioned field, $z_{cs}^*(x,y)$, has the same expected value as $z_0(x,y)$.
4) Since the isomorphic error, $[z_u(x,y) - z_{uk}^*(x,y)]$, is zero at the known location, the simulated realization honors the known experimental data.

7.3 Conditional Simulation with New Estimation Method

We have noticed that the conventional conditional simulation method requires an unconditioned field and two kriged fields, i.e., one for the experimental data and the other for the unconditioned data. The kriged field requires values of the weights at every grid point of the domain. These weights are obtained by the solution of a system of equations. For a large system, for example, greater than 30×30, direct solution methods are difficult to use on average size computers. Instead, iterative methods are employed to solve the matrices. For a three dimensional field the problem of solving a system of equations is more cumbersome. In this section conditional simulation with a new estimation method is proposed. This new method is called the *conditioned source point method* (CSPM). The new estimation method is based on a modified form of the source point method. The new method has several advantages over the conventional simulation method. The following is a description of the CSPM.

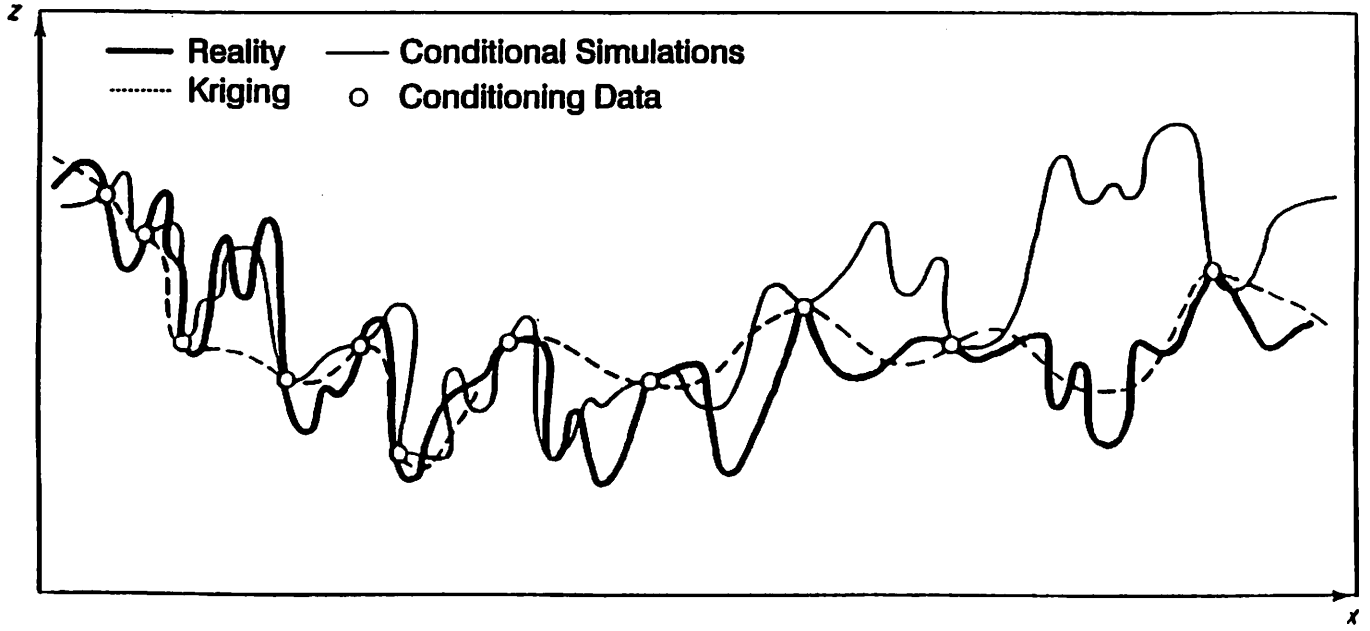

Fig. 7.1 Concept of Conditional Simulation Illustrated in One Dimension. (Journel and Huijbregts, 1978)

From Eq. 7.7 it is evident that the correlation length of the field generated by the SPM is inversely proportional to the square root of the number of source points. The source points, in fact, represent the permeability extrema, or minima. In the proposed method, the permeability values of the source points and their locations are assigned by the known data. It turns out that for a second order stationary process, CSPM is a very efficient method. Where a trend is present, it should be removed before using CSPM; for example, one can subtract the mean values from the blocks and the mean removed data can then be used in CSPM. The simulated field, like any other conditional simulation method, characterizes the variability of the true data and honors the data values at known locations. A pseudo code for the CSPM can be summarized as follows

1) Use Eq. (7.7) to compute the number of source points, N_{sp}, required for the desired correlation length.
2) Use the known data values and their coordinates as the source point values and their coordinates in Eq. (7.5).
    a) If the N_{sp} required is greater than the number of known data available then, obtain the rest of the source point locations, (x_i, y_i), randomly from a uniform distribution, and the permeability minima or maxima, s_o^i from a normal distribution with the same mean and variance of log permeabilities as is possessed by the known points.
3) Use Eq. (7.5) to obtain an estimated field that honors the known data.

In cases, where the N_{sp} required is less than the number of known data available some experience is required. One can, for example, ignore the points that are relatively close and have comparable values in a cluster of known locations, to meet the desired number of source points, and variogram. An outlier can also be neglected in comparing the variograms. The known points which have not been used can be estimated and compared.

7.3.1 Properties of CSPM

The inverse square law can be written as

$$S_g^*(x,y) = \sum_{i=1}^{N_{sp}} s_o^i w^i(N, M, \widehat{x}\widehat{y}) \tag{7.16}$$

where,

$$w^i = \frac{\dfrac{1}{(x(i) - x_g(N))^2 + (y(i) - y_g(M))^2}}{\sum_{k=1}^{N_{sp}} \dfrac{1}{(x(k) - x_g(N))^2 + (y(k) - y_g(M))^2}} \qquad i = 1, ..N_{sp}$$

and,

$$\sum_{i=1}^{N_{sp}} w^i = 1 \qquad \sum_{i=1}^{N_{sp}} (w^i)^2 \neq 1 \tag{7.17}$$

The weights, w^i's are conditioned over the source points locations (other than known locations), that are generated randomly. It is to be noticed that determination of weights in the CSPM does not involve the solution of a system of equations as in the case of kriging. For an illconditioned matrix the solution is very difficult. This is one of the main advantages of the CSPM over kriging.

Linear Estimator: CSPM is a linear estimator

$$S_g{}^* = \sum_{i=1}^{N_{sp}} s_o^i w^i$$

Non-bias Condition: It is an unbiased estimator, which requires a zero error $[S_g^* - s_o]$ in expectation. This condition is easily met since

$$\sum_{i=1}^{N_{sp}} w^i = 1$$

and,

$$E[S_g^*] = E[\sum_{i=1}^{N_{sp}} w^i s_o^i] = E[s_o] = m$$

Exact Estimator: Since the known data retain their original values, It is an exact estimator.

Error in Estimation: The new method can also provide conditional *mean square error* (MSE) as

$$MSE = E[S_g^* - s_o]^2 = var[S_g^* - s_o]$$

$$= var[S_g^*] - 2cov[S_g^*, s_o] + var[s_o] \tag{7.18}$$

The variance of the property is

$$var[s_o] = cov[s_o, s_o] = c(0) \tag{7.19}$$

and the variance of the estimated value can be written as

$$var[S_g^*] = var[\sum_{i=1}^{N_{sp}} w^i s_o^i]$$

$$= \sum_{i=1}^{N_{sp}} \sum_{j=1}^{N_{sp}} w^i w^j cov(s^i, s^j) = \sum_{i=1}^{N_{sp}} \sum_{j=1}^{N_{sp}} w^i w^j cov(x_i - x_j) \tag{7.20}$$

Also, the covariance between the estimated and the known data can be computed as

$$cov[S_g^*, s_o] = cov[\sum_{i=1}^{N_{sp}} w^i s_o^i, s_o]$$

$$= \sum_{i=1}^{N_{sp}} w^i cov[s_o^i, s_o] = \sum_{i=1}^{N_{sp}} w^i c[s_o^i - s_o] \tag{7.21}$$

Substituting Eq. (7.19) thru Eq. (7.21) into Eq. (7.18) we get the MSE as

$$MSE = {\sigma_{oc}}^2 = c(0) - 2\sum_{i=1}^{N_{sp}} w^i c(x_i - x_o) + \sum_{i=1}^{N_{sp}} \sum_{j=1}^{N_{sp}} w^i w^j c(x_j - x_i) \tag{7.22}$$

For an intrinsic random field, we can simply replace $c(x_i - x_o)$ with $-\gamma(x_i - x_o)$

$${\sigma_{oc}}^2 = -\sum_{i=1}^{N_{sp}} \sum_{j=1}^{N_{sp}} w^i w^j \gamma(x_j - x_i) + 2\sum_{i=1}^{N_{sp}} w^i \gamma(x_i - x_o) \tag{7.23}$$

This type of analysis is analogous to the method of kriging.

Simulation of Variability: In order to simulate the variability Eq. 7.15 can be written as:

$$z_{cs}^*(x, y) = z_e^*(x, y) + [z_u(x, y) - z_{ue}^*(x, y)] \tag{7.24}$$

where

$z_{cs}^*(x, y)$ = conditioned field in two dimensions,

$z_e^*(x, y)$ = estimated field of known samples in two dimensions,

$z_u(x,y)$ = unconditioned field in two dimensions, and

$z^*_{ue}(x,y)$ = unconditioned estimated field in two dimensions.

Eq. 7.24 can be used to produce a simulated field using the new estimation method. One of the requirements for the conditioned field is that the error, $[z_u(x,y) - z^*_{uk}(x,y)]$, (Eq. 7.15) be isomorphic to the error, $[z_0(x,y) - z^*_{0k}(x,y)]$, (Eq. 7.14) and is independent of the kriged value, $z_k{}^*$. For the simulated field by CSPM, the error, $[z_u(x,y) - z^*_{ue}(x,y)]$, is automatically independent of the data. Theoretically, it is not possible to prove that this error is isomorphic to the estimated experimental field, $z^*_e(x,y)$. Hence, it is not possible to prove that the variogram produced by the simulated field in the CSPM is exactly the same as that of the experimental one. In the next section, by using permeability data, it is shown that the simulated field that uses an estimated field by the CSPM, does however approximately reproduce the variogram.

7.4 Comparison of CSPM with Kriging and Conventional CS

In order to verify the validity of the CSPM, it was applied to a set of experimental data obtained by the permeability measurements on rock samples by a minipermeameter device. The results are compared with those of kriging and and conventional conditional CS.

In the data set it is assumed that at some locations, permeabilities are known. Based on this knowledge, the CSPM and conventional CS methods are applied to predict the rest of the known data. The methods are compared for computer efficiency, relative error between predicted and experimental values, variograms, and spatial distribution of the highs and lows of the permeability distribution.

7.4.1 Laboratory Example

The set of data includes the permeability measurements on a sandstone slab ($14.3 \times 14.3\ cm^2$). A total of 441 (or 21×21) samples were measured on a regular grid system. Fig. 7.2 shows the greyscale map of the experimental data. The figure uses four colors, white being the highest permeability value. It is assumed that the permeability is known at 25 locations. Fig. 7.3 shows the locations (that were picked randomly from a uniform distribution) of known permeability. Fig. 7.4 shows the

histogram of the permeability (Lnk) data. Although the histogram shown is somewhat skewed, it can be approximated by a normal distribution. A semivariogram of the entire data is constructed as shown in Fig. 7.5. The experimental variogram does not appear to approach a sill, indicating non-stationarity in the field as shown in Fig. 7.5.

At first this non-stationary behavior is neglected and a theoretical variogram is fit to the experimental one (Fig. 7.5). The parameters thus obtained are variance, $\sigma^2 = .18$, nugget, $C_o = 0.3$, and correlation length, $L_c = 2.5\ cm$. These parameters are then used in kriging and in the new CSPM. Fig. 7.6 shows semivariograms of the two methods along with the experimental one. The semivariograms of the estimated fields from kriging and CSPM show less variability than the experimental semivariogram. The smoothing behavior in kriging is due to the kriging weights that are computed by minimizing the error of estimation. The weights in the CSPM are the inverse square distances normalized over the summation of these inverse square distances. To simulate the variability of the original data, the conditional simulation method is used to see the effect of both kriging and CSPM on the simulated fields. Fig. 7.7 shows the semivariograms of these simulated fields. The semivariograms indicate that the variability in both methods have increased considerably. The semivariograms of the simulated fields from both methods are identical, and are close to the experimental semivariogram. Fig. 7.8a and 7.8b show the greyscale map of the estimated fields by kriging and CSPM respectively. Comparison of Fig. 7.2 with Fig. 7.8a and 7.8b confirms that both estimation methods produce fields that are smoother than the real data. In the case of the conditional simulations, the produced field's variability is comparable to that of the experimental data (Fig. 7.8c and Fig. 7.8d). The highs and lows of the permeability values are comparable in both methods.

Effect of Stationarity

As mentioned earlier, the permeability data show a trend or drift, which makes it a non-stationary process, i.e. the mean of the experimental data is not constant. In order to handle this type of data, we chose a simple approach which involves the

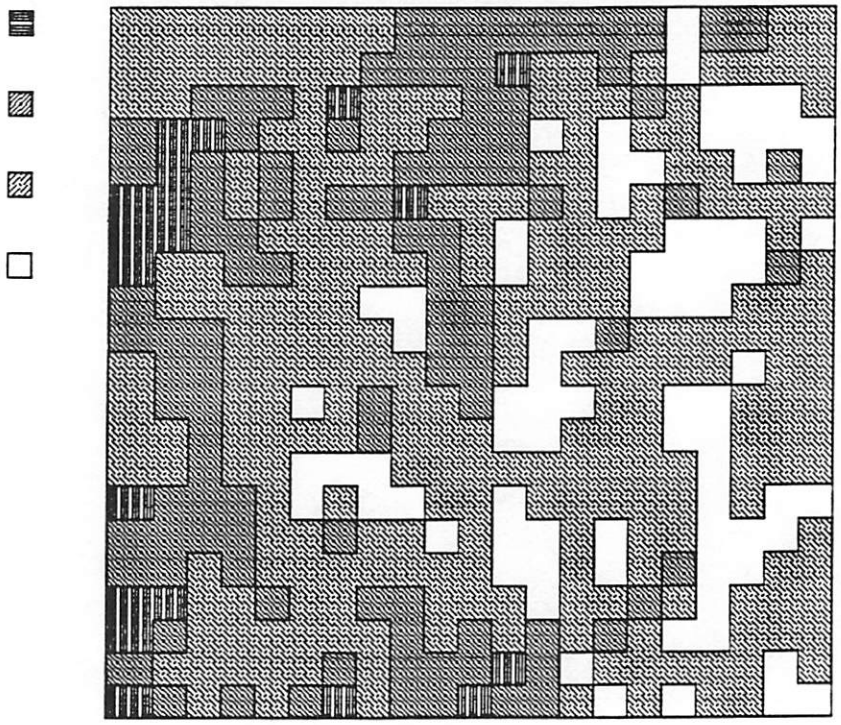

Fig. 7.2 Greyscale map of the measured permeability with minipermeameter.

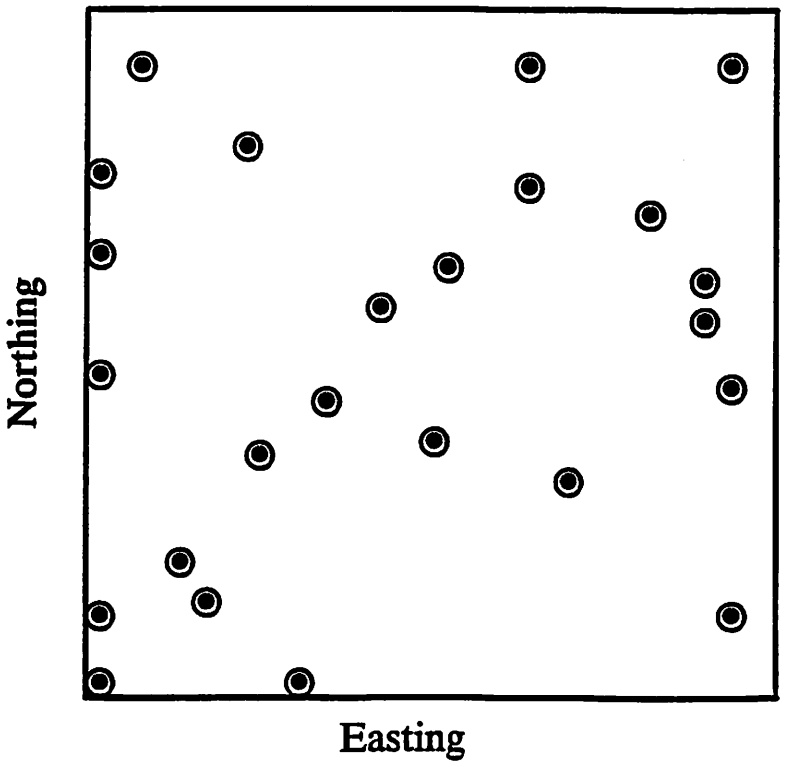

Fig. 7.3 Locations of the assumed known permeability.

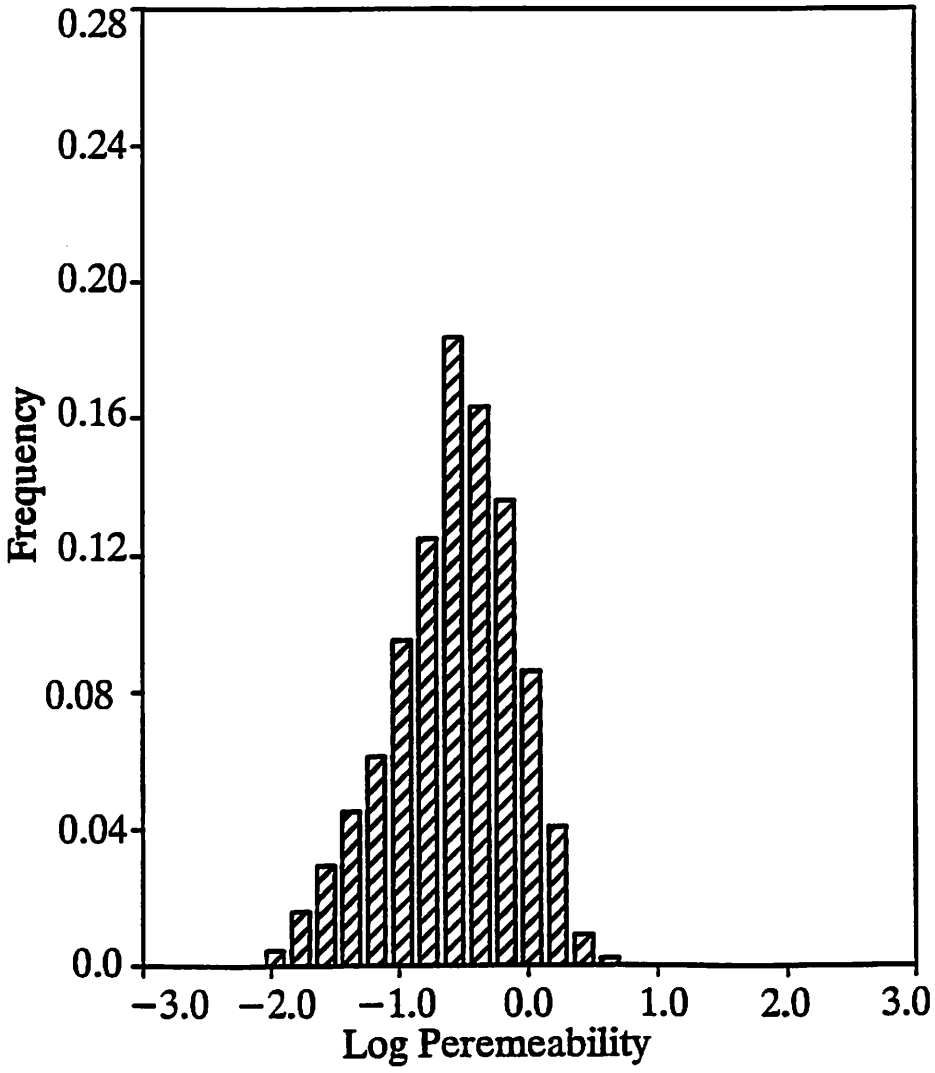

Fig. 7.4 Histogram of the measured natural logarithm of permeability.

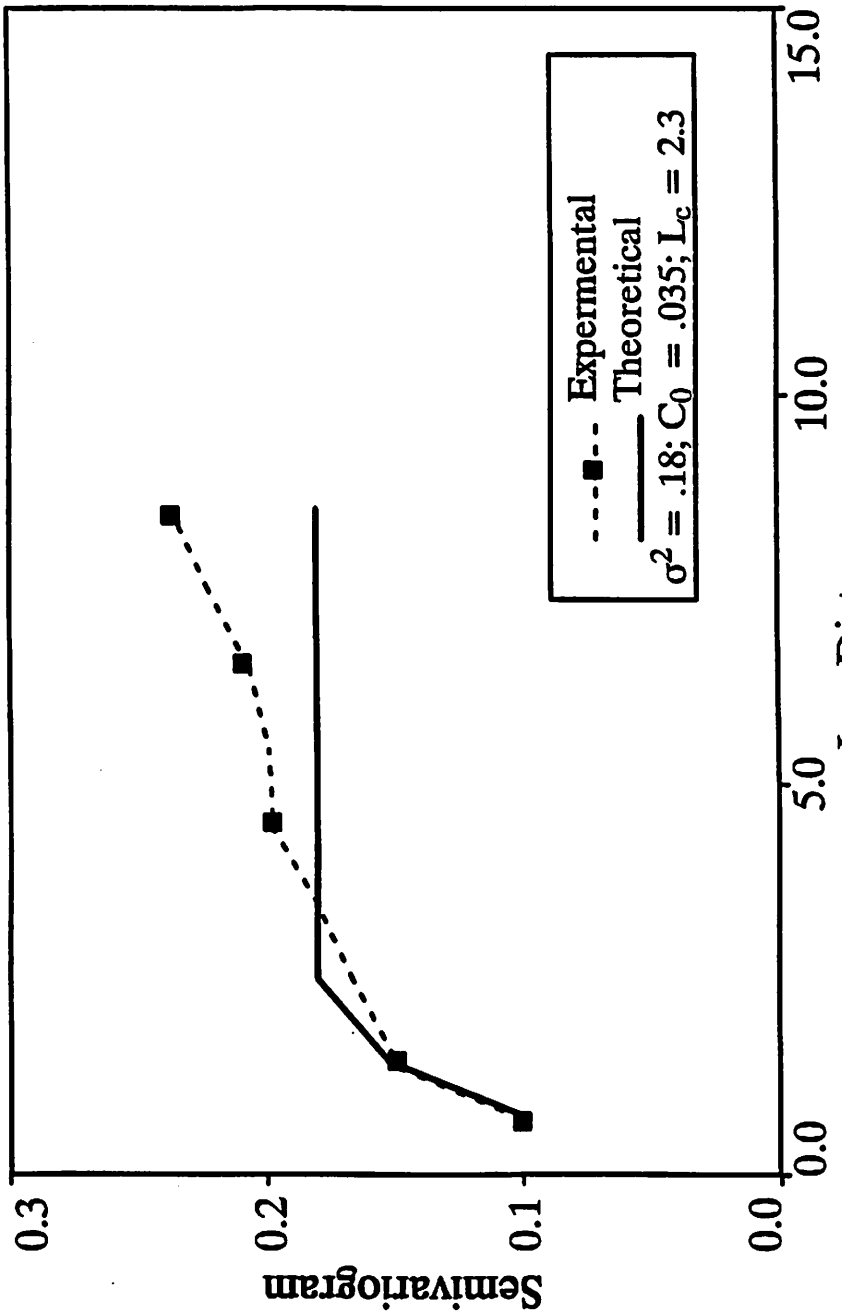

Fig. 7.5 Plot of Experimental and Fitted Theoretical Semivariograms (non-stationary case).

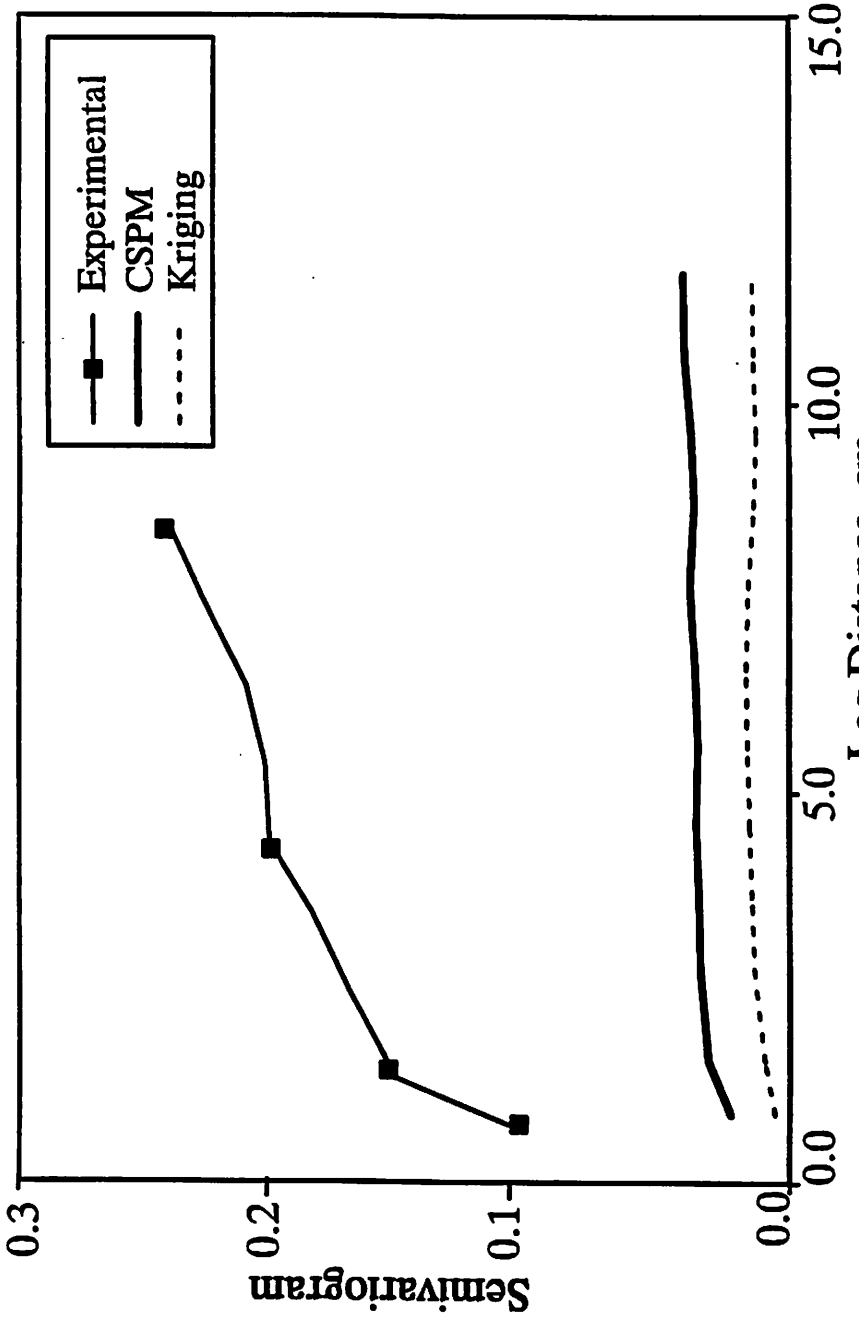

Fig. 7.6 Plot of Semivariograms of the Estimated Kriged and CSPM Fields (Non-stationary Case).

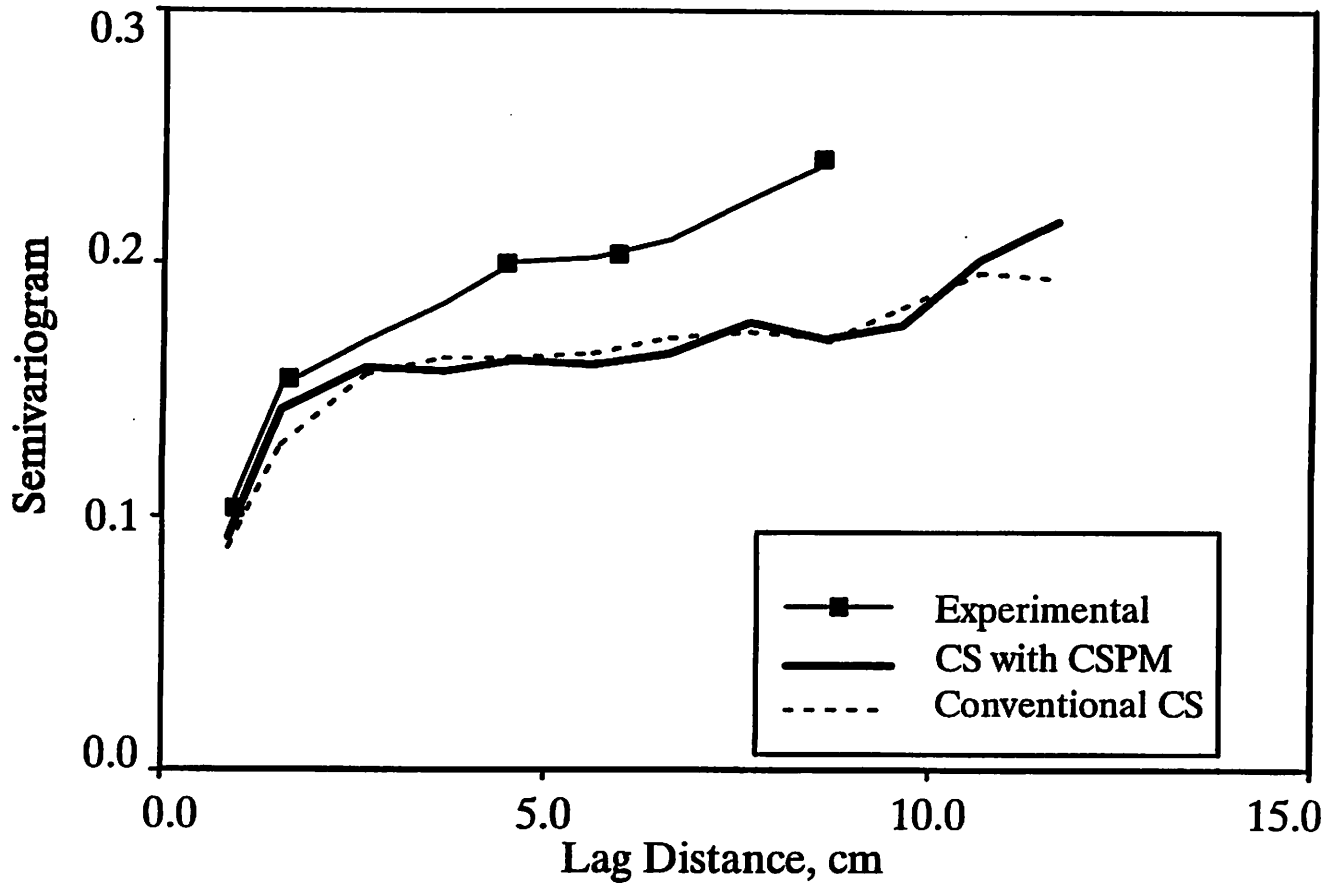

Fig. 7.7 Plot of Semivariograms of the Simulated Kriged and CSPM Fields (Non-stationary Case).

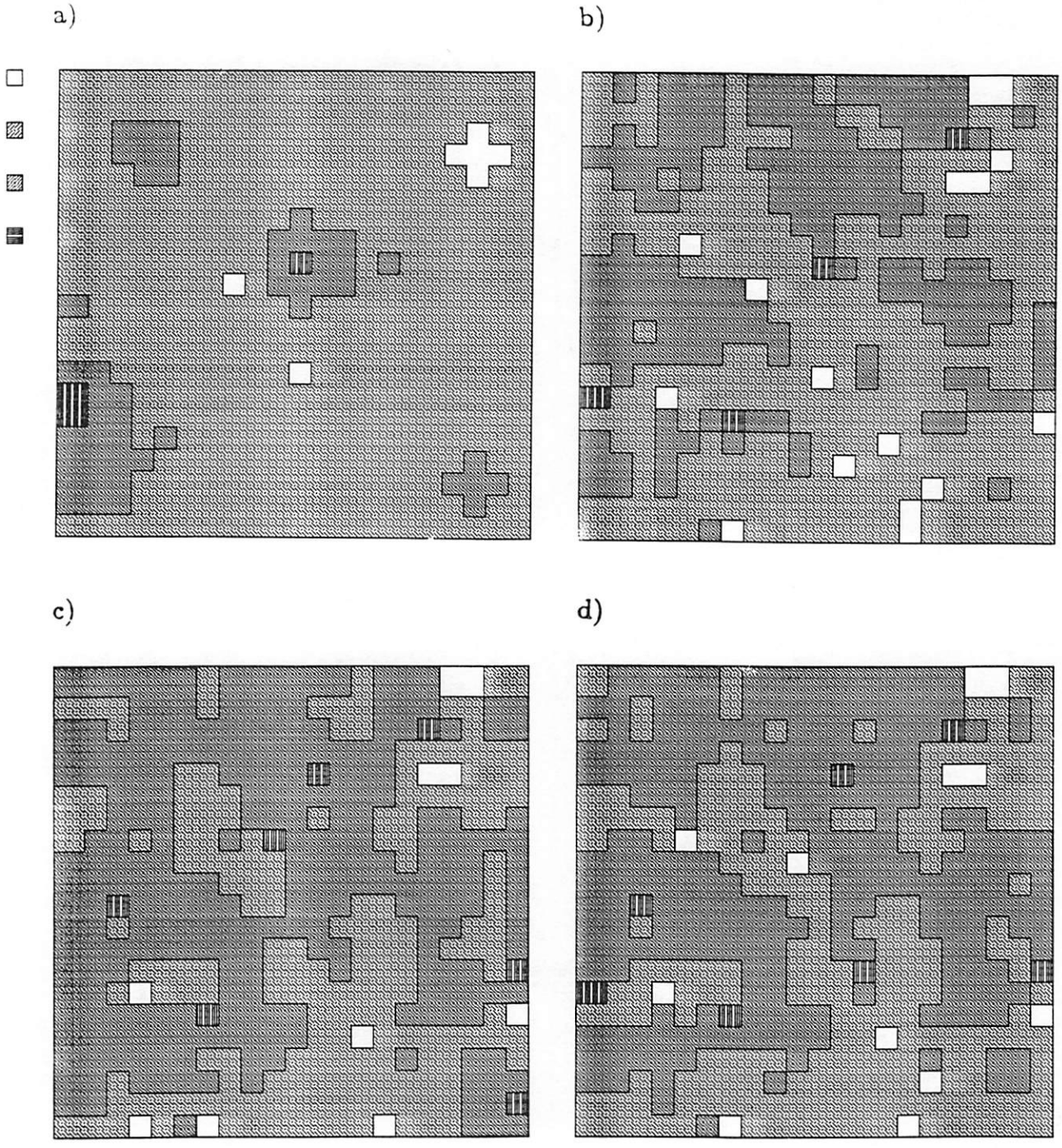

Fig. 7.8 Greyscale maps (non-stationary case)
of a)estimated kriged field, b) estimated CSPM
filed, c)simulated kriged field, d)simulated CSPM field.

removal of the mean from blocks. The experimental data is divided into 7×7 blocks. Each block contains a total of 9 sample points. The mean of each block is estimated and then subtracted from the block. Fig. 7.9 shows the experimental variogram of the mean removed data. Again a theoretical variogram is fitted to the experimental curve (Fig. 7.9), and the parameters of the variogram obtained are variance, $\sigma^2 = .111$; nugget, $C_o = .056$; correlation length, $L_c = 1.5$. The parameters of the mean removed data are then used in kriging, CSPM and conditional simulation method. The mean of the blocks is added back to the mean removed estimated/simulated fields.

Fig. 7.10 shows the variograms produced by CSPM and kriging. These semivariograms now have the same type of trend as the experimental variogram. However, both still show smoothing behavior. For the generation of the simulated field, the conditional simulation method is again generated using both CSPM and kriging. Fig. 7.11 shows the semivariograms of the simulated fields along with the experimental one. The variograms from the simulated fields are not only similar to the experimental one, but they also follow the same trend. Fig. 7.12a and 7.12b show the greyscale map of the generated estimated field by CSPM and kriging. The maps show a better representation of the trend that exists in the data. Fig. 7.12c and 7.12d show the greyscale maps of the experimental data and the simulated fields from the two methods. The highs and lows of the permeability values in both methods are quite similar. Both methods show a better behavior with the stationary (mean removed) field. This confirms that stationarity of the data is a requirement for both the CSPM and for the simple kriging method.

A relative error is defined as the ratio of the difference of predicted and experimental values to the experimental data, $(z_p - z_{exp})/z_{exp}$. Fig. 7.13 shows the relative error in the predicted field by the CSPM and the conventional CS method. The two methods are comparable to each other.

Table 7.1a through 7.1c summarizes the comparison of the two methods used in the simulation of mean removed data. Table 7.1a compares the computer CPU time of kriging and CSPM for both the estimated and simulated fields. As can be

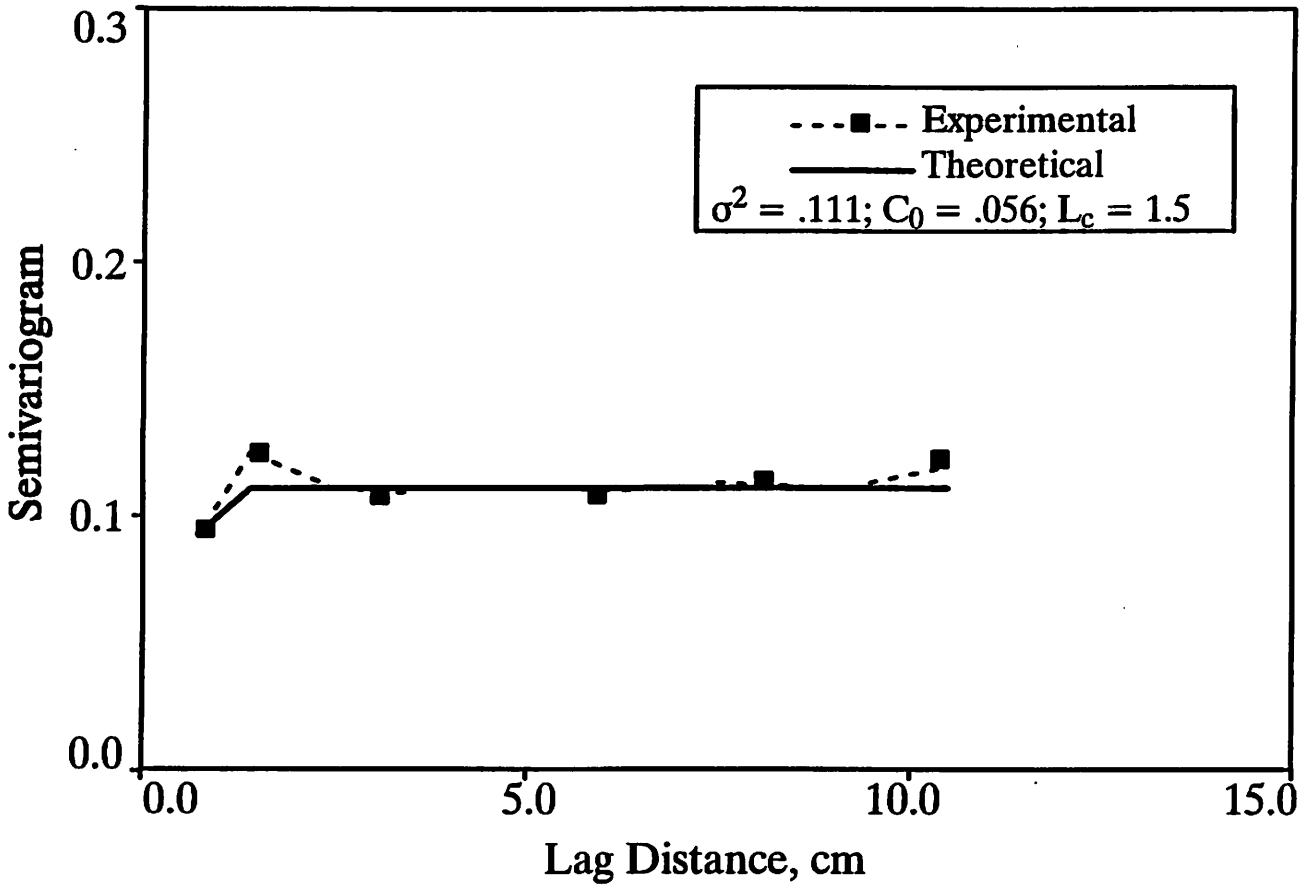

Fig. 7.9 Plot of (mean removed) Experimental and Fitted Theoretical Semivariograms (Stationary Case).

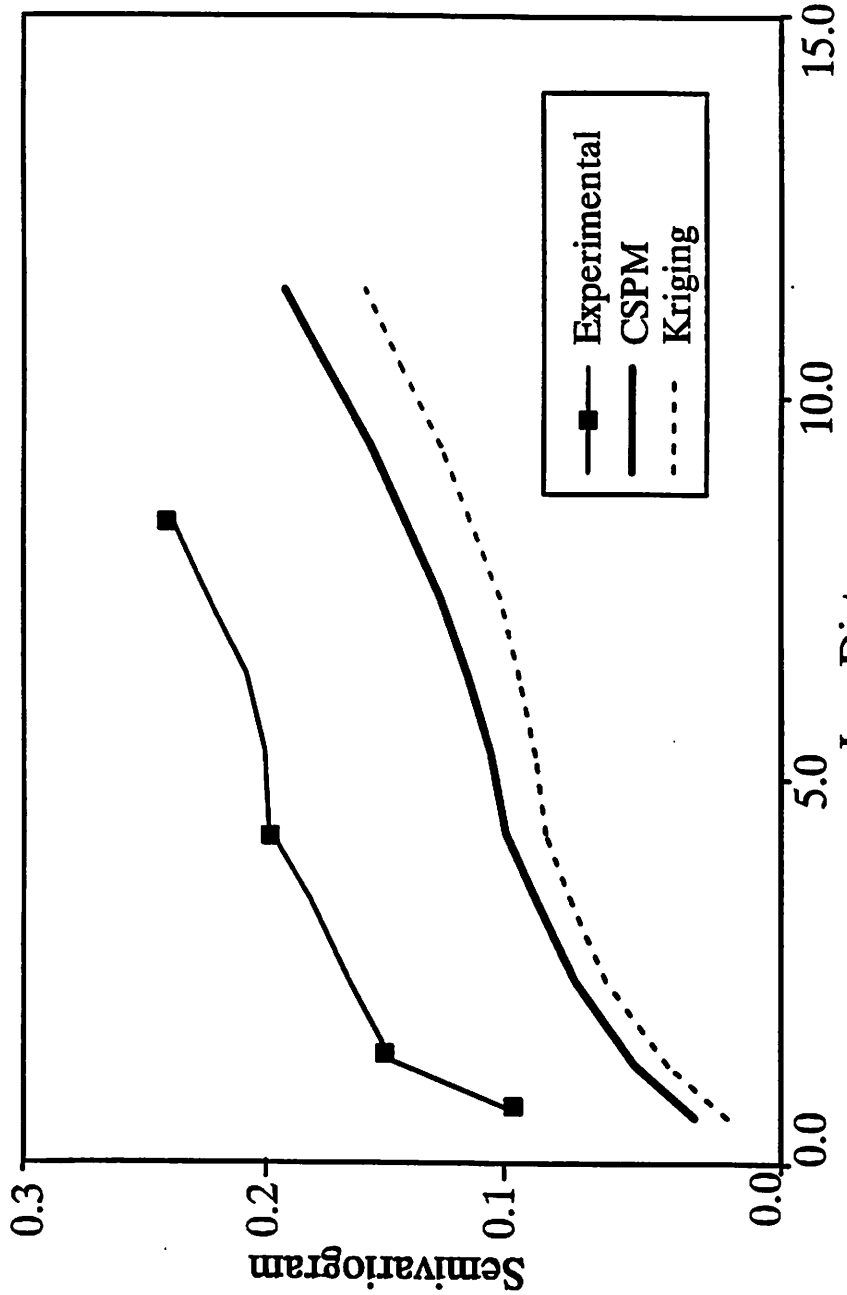

Fig. 7.10 Plot of Semivariograms of the Estimated Kriged and CSPM Fields (Stationary Case).

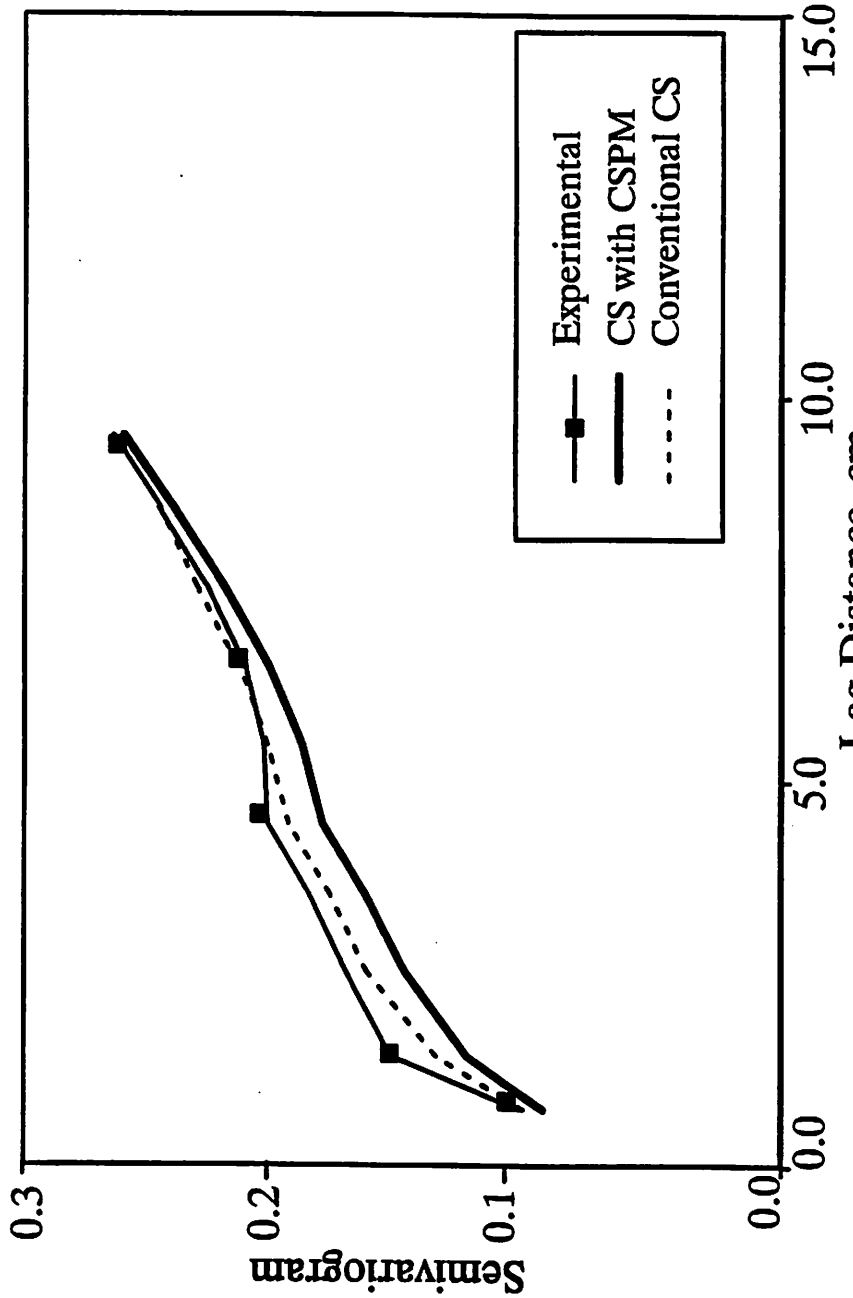

Fig. 7.11 Plot of Semivariograms of the Simulated Kriged and CSPM Fields (Stationary Case).

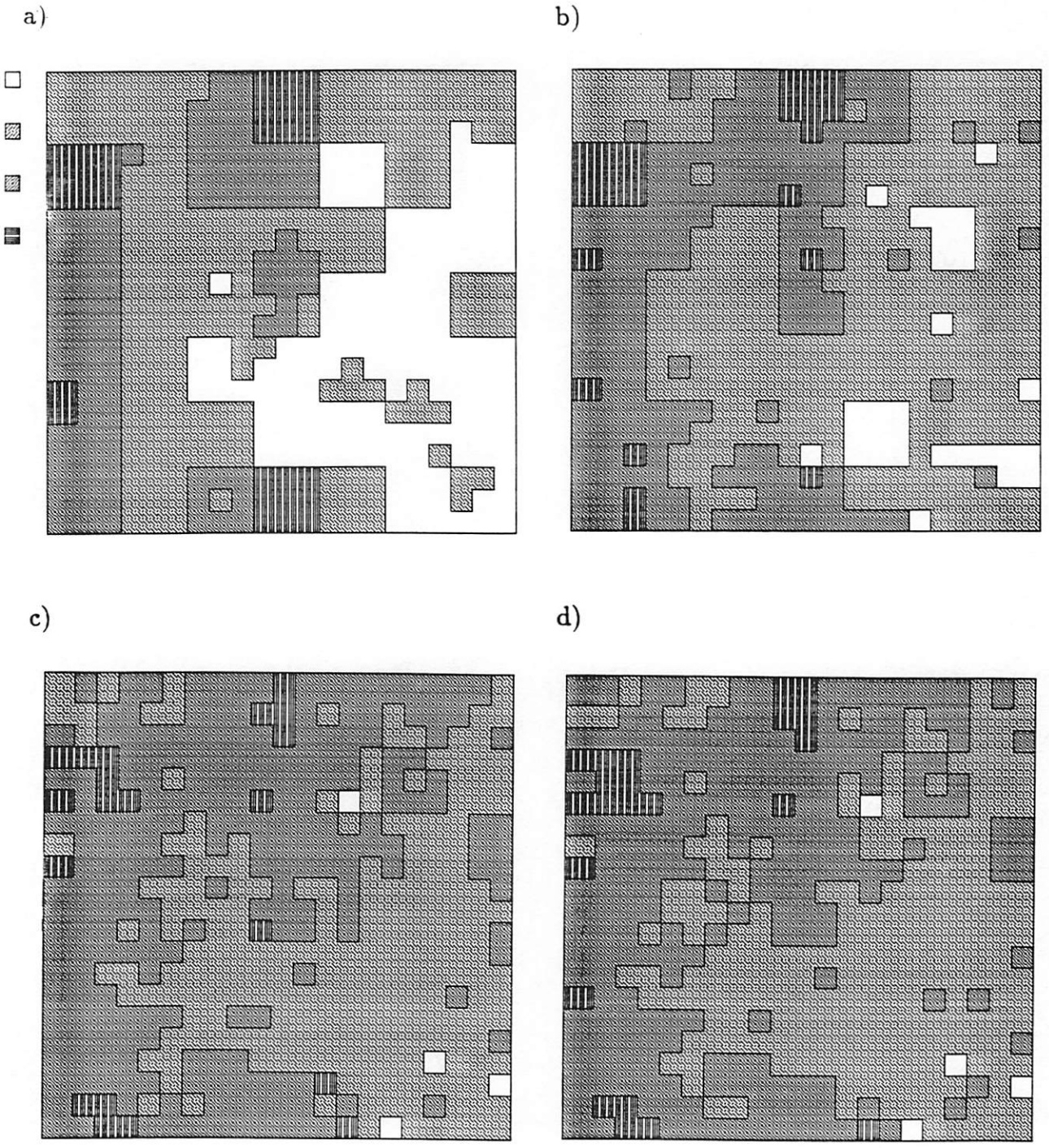

Fig. 7.12 Greyscale maps (non-stationary case)
of a)estimated kriged field, b) estimated CSPM
filed, c)simulated kriged field, d)simulated CSPM field.

noticed that improvement of CPU time in CSPM is around 300%. The improvement in the CPU time is expected to increase more for a three dimensional system. Table 7.1b shows the comparison of the global error variance for both kriging and CSPM. A global error variance is defined as the sum of square of the differences between experimental and predicted values, $\sum (z_{exp} - z_p)^2$. Both kriging and CSPM techniques are comparable to each other. Table 7.1c shows the error divided by the estimation standard deviation, $\sum \frac{(z_{exp} - z_p)}{\sigma_{ok/oc}}$, for both the methods. As can be seen, the CSPM shows a much smaller absolute error, which is due to the smaller values of the estimation variance. It is to be noted that CSPM does not include the nugget effect in estimation.

The example presented in this section shows that conditional simulation with CSPM gives results comparable to the conventional CS method and that less computer time is required in its attainment.

7.5 Summary and Conclusions

In this chapter, a new linear and unbiased estimation method is presented. The new method is based on the conditioning of the source points in the *source point method* and is called the *conditioned source point method* (CSPM). The new method is compared with the kriging method by using two sets of permeability data that were measured with a minipermeameter device. The CSPM is compared for computer efficiency, incorporation of anisotropy in the estimated field, relative error, variograms and spatial distribution of high and low permeability values. Following conclusions are made:

1. The CSPM is an unbiased linear estimator. It is very simple and suitable for large three dimensional field problems.
2. Like kriging, the CSPM can be used in the conditional simulation method (CS), in the sense that the desired variograms are reproduced in the simulated fields.
3. There is an improvement in *CPU* time of more than 300% over the conventional CS method. The improvement is expected to increase further in the simulation of three dimensional fields.

a)

CPU Time		
	Kriging	CSPM
Estimated Field	3.6 sec	1.0 sec
Simulated Field	9.4 sec	2.5 sec

b)

Global Error Variance		
	Kriging	CSPM
Estimated Field	48.65	56.85
Simulated Field	96.30	87.361

c)

Error/Estimation Variance		
	Kriging	CSPM
Estimated Field	-42.00	-34.08
Simulated Field	60.36	-31.36

Table 7.1 Comparison of CSPM with kriging (stationary case), a) CPU time b) global error variance, c) $\frac{error}{\sigma_{ok/oc}}$.

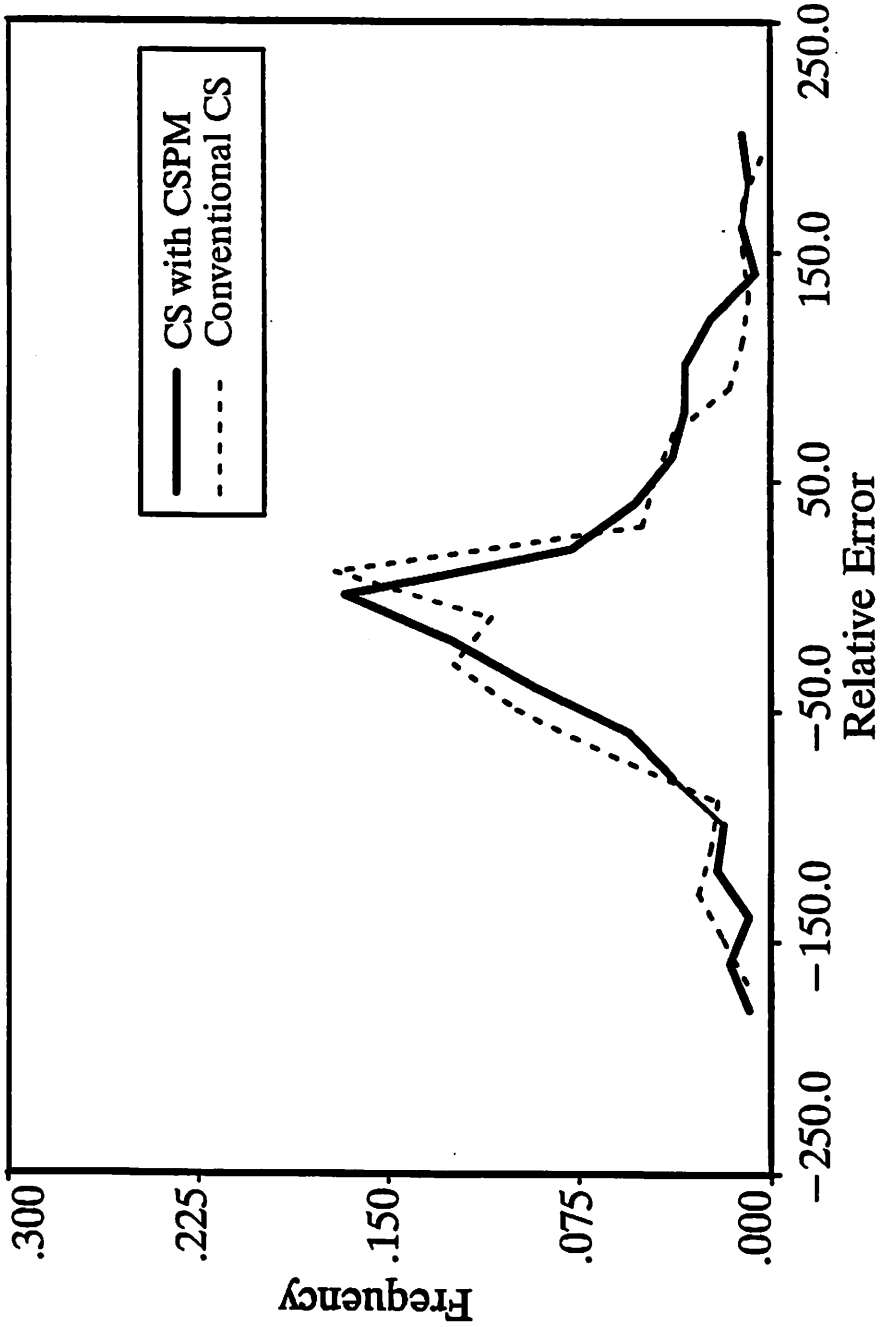

Fig. 7.13 Plot of the Relative Error of the Simulated Kriged and CSPM Fields (Stationary Case).

4. The simulated fields from CSPM produce variograms that are close to experimental variograms.
5. There is an improvement in the relative error of the simulated field by CSPM over those obtained with the conventional CS method.
6. The spatial distribution of the highs and lows are comparable in both the two methods.
7. The method can easily produce anisotropic fields and is a good substitute for methods like kriging.

The applications of this method is important in petroleum, environmental, geology, hydrology and mining industry. In hydrology and petroleum industry, this method can be used to estimate/simulate the permeability or porosity fields. In mining, the method is useful in estimation of ore concentrations in the mines. Geologists can use this method to simulate the deposition and variability of sediments. Environmentalists can use this method to evaluate contaminant concentrations in the environments.

8 Summary and Conclusion

This study is mainly concerned with the assessment of the two geostatistical parameters (variance and the correlation length) of the permeability field. Both numerical and experimental work is performed. In addition, some geostatistical methods for the characterization of the reservoir rock is also presented.

Numerical Work

In this study, a new numerical method of solving (C-D) equation, for the displacement of miscible tracers in oil field flooding patterns, is presented. The numerical technique considers both convection and physical dispersion during flow of the tracer and approaches the solution differently then do conventional finite difference methods. An equation of motion, which contains both Darcy and dispersive terms, allows tracking of isoconcentration lines. Numerical results have shown that the tracer production curve reflects the effect of the flow process in underground reservoirs. Therefore, tracer production history can be used as a diagnostic tool in the determination of the permeability heterogeneity. The following conclusions have been drawn from the results of this work:

1. The proposed numerical method is stable and does not show any numerical dispersion.
2. The method can take into account the effect of both longitudinal and transverse dispersion along with their components of molecular diffusion at low flow velocity.
3. The method can be easily extended to three dimensional field problem.
4. The new numerical method was used to follow the progress of a miscible fluid displacement process by computing the successive positions of the floodfront in a reservoir with arbitrary permeability distribution.
5. The numerical method allows the value of the dispersion coefficient to be varied independently so that its effect may also be studied.
6. The source point method (SPM) was used for the generation of the random permeability field.
7. The numerical method has been applied to the study of the effect of per-

meability heterogeneity on several production patterns in well-to-well tracer studies for single-layer reservoirs. These studies included the five-spot, the staggered line drive, and the direct line drive. Results show marked differences among them.

8. Heterogeneity generally causes an increase of the time interval, over which tracer emerges from the production well.
9. The tracer output concentration at the production well is affected by the geometry of the well pattern, and the channeling resulted from the permeability heterogeneity as modified by the dispersive mixing.
10. The geometric effect produces a nonuniform velocity field which, in turn, induces variability in the arrival time of a tracer on different streamlines. Because of this effect, the tracer output concentration is diluted with the geometric effect alone.
11. The channeling, as a result of the permeability heterogeneity, also causes variation in the arrival time of a tracer at the production well. Therefore, the integrated output profile, even for a single layered reservoir, shows peaks and valleys and more mixing.
12. Unless dispersivity is unusually large, the tracer production pattern is characterized by a number of peaks and valleys, apparently caused by the variability of streamline paths in the heterogeneous formation. These peaks and their distribution can be used to evaluate the heterogeneities. Channeling increases with the increase of the correlation length and variance of the permeability field. It is evident from the results that correlation of permeabilities in even a small fraction of the flow domain produces noticeable channeling.
13. It is possible to infer the geostatistical parameters of the permeability field by measuring the average time span between the occurrence of the prominent peak to the next appearing valley.

Experimental Work

This study presents the importance of well-to-well tracer tests to determine the geostatistical parameters of permeability. In the experimental work, permeabilities

were measured on both the top and bottom surfaces of a rock sample. This rock sample can represent a quarter of a five-spot pattern. A tracer experiment was performed to produce tracer output concentration at the production well. The following conclusions can be drawn from the presented work:

1. Comparison of the numerical and experimental tracer curves indicates that the tracer output curves are affected mainly by the permeability variation.
2. In the tracer experiment, six different types of the tracer output curves were obtained at the six measuring locations along the producing wellface.
3. The geostatistical parameters (variance and correlation length) of the permeability changes from layer to layer.
4. The dispersivity of the rock sample also changes from one layer to the other.
5. Downhole sampling of the produced tracer concentration at each known layer would be very useful in achieving further valuable information about real reservoirs.

Geostatistical Methods

Generation of Random Fields

In this study, a geostatistical method of generating random permeability fields with specified correlation structure is presented. In this method, Heller's source point method (SPM) is modified, so that the correlation length in the SPM can be prespecified. Finally the SPM is modified to include the effect of anisotropy in the generated field. As a result of the work presented in this study, the following conclusions can be drawn:

1. The source point method is one of the most efficient method of generating random fields with regard to computer time and storage.
2. The desired correlation length can be prespecified by an empirical formula which is proportional to the quantity, $area/N_{sp}$.
3. A modified form of the SPM is derived that can take into account the desired anisotropy in the generated field.
4. A formula for a two dimensional anisotropic field is derived to prespecify the desire correlation length in any direction. For a three dimensional field a

similar formula can be evaluated by using the theory of conditional covariance.

A New Estimation Method

In this study, a new linear and unbiased estimation method is presented. The new method is based on the conditioning of the source points in the *source point method* and is called the *conditioned source point method* (CSPM). The new method is compared with the kriging method by using two sets of permeability data that were measured with a minipermeameter device. The CSPM is compared for computer efficiency, incorporation of anisotropy in the estimated field, relative error, variograms and spatial distribution of high and low permeability values. The following conclusions hold:

1. The CSPM is an unbiased linear estimator. It is very simple and suitable for large three dimensional field problems.
2. Like kriging, the CSPM can be used in the conditional simulation method (CS), in the sense that the desired variograms are reproduced in the simulated fields.
3. There is an improvement in CPU time of more than 300% over the conventional CS method. The improvement is expected to increase further in the simulation of three dimensional fields.
4. The simulated fields from CSPM produce variograms that are close to experimental variograms.
5. There is an improvement in the relative error of the simulated field by CSPM over those obtained with the conventional CS method.
6. The spatial distribution of the highs and lows are comparable in both the two methods.
7. The method can easily produce anisotropic fields and is a good substitute for methods like kriging.

9 Recommendation for Future Work

In the presented work, the new numerical technique is applied to solve a two-dimensional, areal flow problem. The method can be easily exended to a three-dimensional flow system. A three-dimensional analysis might be helpful for a system in which the layers have communication.

The results produced have shown that by investigating the time-span between the occurances of the peak and the valley, the correlation length and the variance of permeability of a five-spot pattern can be estimated. This work can be extended to other flooding patterns, e.g. staggered line drive, direct line drive, etc. This will require more simulation runs for a wide variety of variances and correlation lengths of permeability.

Experimental work performed in this study has shown that each layer can produce a different type of tracer output concentration. This behavior is due to the different areal variations of the permeability distribution and dispersion of the rock in each layer. Therefore, it is recommended that a down hole tracer sampling tool be designed and constructed. The tool should be cheap and easily operated by a small wireline machine, so that it will not be economically prohibitive to leave it downhole for extended periods of time, in order to gather sufficient data after tracer injection.

Nomenclature

A = Area of the pattern, L^2.

A_d = differential operator

ALP = a constant, depends on current and previous values of the volume correction factor, dimensionless.

A_p = crosssectional area of the plunger, L^2.

A_q = flowrate per unit thickness, L^2/T.

a = distance between like wells, L.

$C(\Psi)$ = tracer concentration in a stream tube, M/V.

C = concentration of the displacing fluid, M/V.

$\bar{C}(t)$ = overall effluent tracer concentration , M/V.

C_0 = nugget value in the variograms.

d = distance between unlike wells, L.

D_L = longitudinal dispersion coefficient, L^2/T.

D_m = molecular diffusion coefficient, L^2/T.

D_T = transverse dispersion coefficient, L^2/T.

e_i = natural base vectors.

e^i = dual or reciprocal base vector.

F = formation resistivity factor, dimensionless.

G = gravitational constant vector.

F_g = "fudge" factor, dimensionless.

g^{ij}, g_{ij} = covariant and contravariant components of the symmetric metric tensor

h_f = thickness of the formation, L.

h^i, h_i = scale factors in coordinate transformation.

K = effective permeability, md.

L_c = correlation length of the permeability field, L.

L_x , L_y = correlation length n x and y directions, L.

NIS = total number of isoconcentration points in a concentration profile.

p = pressure, psi.

P = position vector.

$q(\Psi)$ = volumetric flow rate into a stream tube, L^3/T.

Q = volumetric flow rate, L^3/T.

r = radial distance, L.

r_1 = radius of the back of the slug, L.

r_2 = radius of the front of the slug, L.

r_e = radius of the radial element, L.

r_w = radius of the well bore, L.

S = distance along streamlines, L.

S_w = water saturations, fraction of pore volume.

S_{cen} = distance from the center of the well to the center of the concentration profile, L.

$S_g(N, M)$ = log of permeability values at $(N, M)^{th}$ grid point.

s(j) = maxima, or minima, of the source points.

t = time, T.

t_b = breakthrough time of the particle on a streamline, T.

t_p = arrival time of the peak concentration at the production well, T.

T_{init} = initial time value, calculated as the fill up time to the center of the tracer slug, T.

u = Darcy velocity, L/T.

u_x = component of Darcy velocity in x-direction, L/T

u_y = component of Darcy velocity in y-direction, L/T

V = average volume of all the streamtube under consideration, L^3.

VC = volume correction factor.

V_{TR} = volume of tracer solution, L^3.

V_{in} = volume input at the injection well, L^3.

$V_{pD,bt}$ = breakthrough pore volume or breakthrough areal sweep efficiency of the pattern, dimensionless.

v = frontal velocity, or velocity of the isoconcentration lines, L/T.

v_Φ = component of frontal velocity in Φ-direction, L/T

v_Ψ = component of frontal velocity in Ψ-direction, L/T

$w(\Psi)$ = width of the streamtube, L.

x, y = coordinates of a cartesian system.

z = complex variable.

α, β, γ = coefficients of anisotropy in the source point method.

ϵ = amount of curvature on the concentration profile, L.

$\mathcal{L}$ = difference operator

ζ = pseudo stream function, L^2/T^2.

η = a constant for a particular streamline, $\tan^2 \Psi$.

λ_D = dimensionless correlation length.

λ_L = longitudinal dispersion constant, L.

λ_T = transverse dispersion constant, L.

μ = viscosity, cp.

ν = strength of the source, M/LT^2.

ξ = pseudo potential, L^2/T^2.

ρ = density, M/V.

ρ_D = dimensionless distance.

σ^2 = variance of permeability distribution.

Φ = potential, M/LT^2.

ϕ = porosity.

Ψ = stream function, M/LT^2.

$\Omega(z)$ = complex potential, M/LT^2.

θ = azimuthal axis of cylinderical coordinate system, dimensionless.

References

1. Abbaszadeh, D.M., and Brigham, W.E.: "Analysis of Unit Mobility Ratio Well-to-Well Tracer Flow to Determine Reservoir Heterogeneity," DOE/SF/11564-1 (1983).
2. Allison, S.B., Pope, G.A., and Sepehrnoori, K.: " Analysis of Field Tracers for Reservoir Description," Journal of Petroleum Sciences and Engineeing, 5 (1991) 173–186.
3. Aronofsky, J. S., and Heller, J. P: "A Diffusion model to Explain Mixing of flowing Miscible Fluids in Porous Media," *Trans.*, AIME (1957), **210**, 345–349.
4. Aziz, K. and Settari, A.: "Petroleum Reservoir Simulation," Applied Science Publishers Ltd., London (1979).
5. Bahralolom, I., and Heller, J.P.:" Core Sample Heterogeneity from Laboratory Flow Experiments," Proc. 2nd Int'l. Res. Char. Tech. Conf., Dallas (1989).
6. Bahralolom, I.: PhD Thesis, New Mexico Institute of Mining and Technology, Socorro, NM, to be published (1991).
7. Bakr, A. A., Gelhar, L. W., Gutjahr, A. L., and MacMillan J. R.: " Stochastic Analysis of Spatial Variability in Subsurface Flows, 1. Comparison of One- and Three-Dimensional Flows", *Water Resour. Resear.*, (1978), 14(2), 263–271.
8. Baldwin, D. E., Jr.: "Prediction of Tracer Performance in a Five Spot Pattern," *J. Pet. Tech.* (April 1966) 513–517.
9. Barton, C.C., Schutter, T.A., and Samuel, J.K., *Trans. Amer. Geophys. Union*, **68**, (1987).
10. Bear, J.: "On the Tensor Form of Dispersion in Porous Media," J. of Geophys. Res. (1961) vol. 66, no. 4, 1185-1198.
11. Bear, J.: *Dynamics of Fluids in Porous Media,* Elsevier, New York (1972).
12. Bentsen, R. G., and Nielsen, R. F.: "A Study of Plane, Radial Miscible Displacement in a Consolidated Porous Medium," *Soc. Pet. Eng. J.* (March 1965), 1–5.
13. Bird, R. B., Stewart, W. E., Lightfoot, E. N.: "Transport Phenomena," 715-742, John Wiley & Sons, NY 1960.
14. Blackwell, R. J.: "Laboratory Studies of Microscopic Dispersion Phenomena," *Soc. Pet. Eng. J.* (March 1962), 1–8.

15. Brigham, W. E., Reed, P. W., and Dew, J. N.: "Experiments on Mixing During Miscible Displacements in Porous Media," *Soc. Pet. Eng. J.* (March 1961), 1–8.

16. Brigham, W. E., and Smith, D. H.: "Prediction of Tracer Behavior in Five Spots," Paper SPE 1130, presented at the 40th Annual Fall Meeting of SPE–AIME, Denver, Colorado, (Oct 1965).

17. Brigham, W. E.: "Mixing Equations in Short Laboratory Cores," *Soc. Pet. Eng. J.* (Feb 1974), 91–99.

18. Brigham, W. E.: "Mixing Equations in Various Geometries," SPE Paper 4585, or SPE Res. Eng. (1986), 203–208.

19. Carpenter, P. G., Morgan, T. D., and Parsons, E. D.: "Use of Boron Compounds as Water Flood Tracers," *Prod. Monthly* (1952), 16, No. 12, 12–19.

20. Chaudhari, N. M.: "An Improved Numerical Technique for Solving Multidimensional Miscible Displacement Equations", *Soc. Pet. Eng. J.* (Sept. 1971), 277–284.

21. Chen Chia-Shyun: "Analytical and Approximate Solutions to Radial Dispersion From an Injection Well to a Geological Unit with Simultaneous Diffusion into Adjacent Strata," *Water Res. Research*, Vol 21, No. 8 (Aug 1985), 1069–1076.

22. Chopra, A.K., Severson, C.D., and Carhart, S.R.: "Evaluation of Geostatistical Techniques for Reservoir Characterization," SPE 20734 (1990).

23. David, M.: "Geostatistical Ore Reserve Estimation," Elsevier Scientific Publishing Company, NY (1977).

24. Davis, J.M.: An Approach for the Characterization of Spatial Variability of Permeability In Sierra Ladrones Formation, Albuquerque Basin, Central New Mexico. M.S. ,Thesis. New Mexico Institute of Mining and Technology, Socorro, New Mexico (1990).

25. Deans, H. A.: "A Mathematical Model for Dispersion in the Direction of Flow in Porous Media," *Trans.*, AIME (1963), **228**, 49–52.

26. Douglas, J. Jr., et. al: "A Method for Calculating Multi-Dimensional Immiscible Displacement," *Trans* AIME Vol. 216 (1959) 297–308

27. Dykstra, H. and Parsons, R. L.: "The Prediction of Oil Recovery by Water Flood", **API**, The Lord Baltimore Press (1950).

28. Eijpe, R. and Weber, K.J.: "Mini-Permeameter for Consolidated Rock and Unconsolidated Sand," The American Association of Petroleum Geologists Bulletin, **55, 2** (1971) pp. 307-309.

29. Emanuel, G.K., Behrens, R.A., and Hewett, T.A.: "Reservoir Performance Prediction Methods Based on Fractal Geostatistics", SPE 16971, pp. 405-417, (1987).

30. Fanchi, J. R.: "Multidimensional Numerical Dispersion", *Soc. Pet. Eng. J.* (Feb. 1983), 143–151.

31. Fanchi, J.R. and Christiansen, R.L.: " Applicability of Fractals to the Description of Viscous Fingering", SPE 19782, (1989).

32. Fogg, G.E., Lucia, F.J.: Report of Investigations No. 190. Bureau of Economic Geology, The University of Texas at Austin , (1990).

33. Freeze, R. A.: "A Stochastic-Conceptual Analysis of 1-D Ground Water Flow in Non-Uniform Homogeneous Media", *Water Resour. Resear.*, (1975), 11(5), 725–741.

34. Garder, A.O., Peaceman, D.W. and Pozzi, A.L.: " Numerical calculation of multidimensional miscible displacement by the method of characteristics," Soc. Pet. J. (1964) pp. 26-36.

35. Gelhar, L. W.: "Effects of Hydraulic Conductivity Variations on Ground Water Flows",

36. Gelhar, L. W., and Collins, M. A.: "General Analysis of Longitudinal Dispersion in Nonuniform Flow," *Water Res. Research* (Dec. 1971), **7**, no. 6, 5111–1521.

37. Gelhar, L. W., Axness, C. L.: " Three-Dimensional Stochastic Analysis of Macrodispersion in Aquifers", *Water Resour. Resear.*, (1983), 19(1), 161–180.

38. Genuchten, M. T. Van and Parker, J. C.: "Boundary Conditions for Displacement Experiments through Short Laboratory Soil Columns," *Soil Sci. Soc. Am. J.*, Vol 48, (1984) 703–208.

39. Gershon, N. D. and Nir, A.: "Effects of Boundary Conditions of Models on Tracer Distributions in Flow through Porous Mediums," *Water Res. Research* (Aug 1969) 830–838.

40. Ghori, S.G.: Numerical Simulation of Miscible Displacement of a Tracer Slug in

Homogeneous Five-Spot Patterns, Master's Thesis, NMIMT, Socorro, NM (1988) 37-47.

41. Ghori, S.G., and Heller, J.P.: "Computed Effect of Heterogeneity on Well-to-Well Tracer Results," Proceedings Fifth Canadian/American Conference on Hydrology, Parameter Identification and Estimation for Aquifer and Reservoir Characterization (Sept. 1990).
42. Ghori, S.G., Heller, J.P., and Singh, A.K.: "An Efficient Method of Generating Random Fields," Proceedings International Conference on Finite Fields, Coding Theory, and Advances in Communications and Computing, UNLV, Las Vegas, NV (Aug. 10, 1991).
43. Goggin, D.J.: "Geologically-Sensible Modeling of the Spatially Distribution of Permeability In Eolian Deposits: Page Sandstone (jurassic), Northern Arizona", Ph.D. Dissertation, University of Texas, Austin, Texas (1988).
44. Goggin, D. J., Chandler, M.A., Kocurek G., and Lake, L.W.: " Permeability Transits in Eolian Sands in Their Use in Generating Random Permeability Fields," 64th Annual Tech. Conf. SPE 19586 (1989) pp. 149-163.
45. Gutjahr, A. L., Gelhar, L. W., Bakr, A. A., and MacMillan J. R.: " Stochastic Analysis of Spatial Variability in Subsurface Flows, 2. Evaluation Application", *Water Resour. Resear.*, (1978), 14(5), 953–959.
46. Gutjahr, A.L.: Fast Fourier Transforms for Random Field Generation, New Mexico Institute of Mining and Technology, Project Report, LANL Contract 4-R58-2690R (1989).
47. Gutjahr, A.L.: Personal Communications (1990).
48. Harleman, R. F., and Rumer, R. R.: "Longitudinal and Lateral Dispersion in an Isotropic Porous Medium," *J. Fluid Mech.* (193), **3**, No. 16, 385–394.
49. Heller, J.P.: "Observations of Mixing and Diffusion in Porous Media," Proc. Second Symposium, Fundamentals of Transport Phenomena in Porous Media IAHR-1SSS, Ontario, (1972) 1-26.
50. Heller, J.P., and Taber J.J.: "Development of Mobility Control Methods to Improve Oil Recovery by CO_2," DOE/MC/10689-11 (Dec 1981) 20-22.

51. Heller, J. P.: "Mobility Control For CO_2 Injection," DOE/MC/16426-19, (Aug 1986), 111-136.

52. Heller, J. P.: "Dynamic Analysis of syringe (Mini)Permeameter," PRRC Report No. 91-27, (1991).

53. Heravi, N.E.: Five-Spot Displacement at Unit Mobility Ratio in a Reservoir with Heterogeneous Permeability. Master thesis, New Mexico Tech. Socorro, NM (1988).

54. Hewett, T.A., Behrens, R.A.: " Conditional Simulation of Reservoir Heterogeneity with Fractals", SPE 18326, pp. 645-660, (1988).

55. Hoopes, J. A. and Harleman, D. R. F.: "Dispersion in Radial Flow from a Recharge Well," *J. Geo. Research* (Jul 1967), 3595–3607.

56. Hutchins, R. D. and Dovan, H. T.: "Aqueous Tracers for Oilfield Applications", *SPE 21049* (Feb. 1991), 491–498.

57. de Jong, de Josselin, G.: "Longitudinal and Transverse Diffusion in Granule Deposits," Trans. Am. Geophys. Union (1958) vol. 39, 67-74.

58. Journel, A.G., and Huijbregts, C.J.: Mining Geostatistics, Academic Press, London (1978).

59. Kazemi, H and Shinta, A.A.: " Determination Orientation and Conductivity of High Permeability Channels in Naturally Fractured Reservoirs," Paper presented at the Third International Reservoir Characterization Technical Conference (1991).

60. Kelkar, B. G. and Gupta, S. P.: "The Effects of Small Scale Heterogeneities on the Effective Dispersivity of Porous Medium", SPE/DOE 17339, (1988), 215–226.

61. Koch, H. A., Jr., and Slobod, R. L.: "Miscible Slug Process," *Trans.* AIME (1957), **210**, 40.

62. Lake, L.W., and Jensen, J.L.: "A Review of Heterogeneity Measures Used in Reservoir Characterization," NMT Centennial Symposium (SPE) (1989) 223-234.

63. Lantz, R. B.: "Quantitative Evaluation of Numerical Diffusion (Truncation Error)", *Soc. Pet. Eng. J.* (Sept. 1971), 315–320.

64. Larson, R.G.: "Controlling numerical dispersion by variably timed flux updating in one dimension," Soc. Pet. J. (1982) pp. 399-408.

65. Lasseter, T.J., Waggoner, J.R. and Lake L.W. Resevoir heterogeneities and their

influence on ultimate recovery. Reservoir Characterization, Academic Press, NY. (1986) pp. 545-559.

66. Lau, L. K., Kaufman, W. J., and Todd, D. K.: "Dispersion of a Water Tracer in Radial Laminar Flow Through Homogeneous Porous Media," Progress Report No. 5, Sanitary Engineering Research Lab., U. of California at Berkeley, (1959).
67. Laumbach, D.D.: "A high-accuracy finite-difference technique for treating the convection-diffusion equation," Soc. Pet. J. (1975) pp. 517-531.
68. Law, J.: "Statistical Approach to the Interstitial Heterogeneity of Sand Reservoirs", *Trans.* AIME (1944), **155**, 202.
69. Lichtenberger, G.J.: "Field Applications of Interwell Tracers for Reservoir Characterization of Enhanced Oil Recovery Pilot Areas," Paper SPE 21652, presented at the Production Operations Symposium, Oklahoma City, OK, (April 7-9, 1991) pp 209–225.
70. Malvern, L. E. : *Introduction to the Mechanics of a Continous Medium*, Prentice-Hall, NJ (1969) 569–640.
71. Marsily, G.: Spatial Variability of Properties in Porous Media: A Stochastic Approach. Transport Phenomena In Porous Media (1984) 721-769.
72. Matheron, G.: " The Theory of Regionalized Variables, and its Application", Cahier n° 5, Centre de Morphologie Mathematiques, Ecole des Mines, Fontainebleau, pp 250, 1971.
73. Matheron, G.: "The Intrinsic Random Functions and Their Applications," Advan. Appl. Prob. (1973) 439-468.
74. McKay, D.H.: A Fast Fourier Transform method for Generation of Random Fields, M.S. Thesis, New Mexico Institue of Mining and Technology, Socorro, NM (1988).
75. Middleman, S.: "The Flow of High Polymers, " Interscience Publishers, (1968), Appendix A, 200-209.
76. Mantoglou, A., and Wilson,J.L.: "The Turning Bands Method for Simulation of Random Fields Using Line Generation by a Spectral Method," Water Res. Research vol. 18, No. 5 (1982).
77. Muskat, M.: "Effect of Permeability Stratification in Cycling Operations ", *Trans.*

AIME (1948), **179**, 313.

78. Ogata, A.: "Dispersion in Porous Media," Ph.D. Thesis, Northwestern Univ., Evanston, Ill. (1958).
79. Ogata, A., and Banks, R. B.: "A Solution of the Differential Equation of Longitudinal Dispersion in Porous Media," *U.S. Geol. Serv. Prof. Pap.* (1961), 411–A.
80. Ouenes, A., Bahralolom, I., Ghori, S.G., Gutjahr, A., Lee, B., and Siarry, P.: "Simulated Annealing Method (SAM): A New Approach for Reservoir Characterization," PRRC Report No. 91-40, New Mexico Petroleum Recovery Research Center, Socorro, New Mexico (Aug. 1991).
81. Peaceman, D.W., and Rachford, H.H.: "Numerical Calculation of Multidimensional Miscible Displacement," Soc. Pet. J. (1962) 327-339.
82. Peaceman, D. W.: "Fundamentals of Numerical Reservoir Simulation", Elsevier Scientific Publishing Co., New York City (1977).
83. Perkins T. K. and Johnson O. C.: "A Review of Diffusion and Dispersion in Porous Media", *Soc. Pet. Eng. J.* (Sept 1962).
84. Raimondi, P., Garder, G. H. F., and Petrick, C. B.: "Effect of Pore Structure and Molecular Diffusion on the Mixing of Miscible Liquids Flowing in Porous Media", Paper 43, A.I.Ch.E.-SPE joint Symposium, National AIChE Meeting, San Francisco, Dec. 6–9, 1959.
85. von Rosenberg, D. U.: "Mechanics of Steady-State Single-Phase Fluid Displacement from Porous Media", *AIChE Jour.* (March 1956), **2**, No. 1, 55.
86. Saad, N., Pope, G.A. and Sepehrnoori, K.: "Application of Higher-Order Methods in Compositional Simulation," SPE Reservoir Engineering, (Nov 1990) 623-630.
87. Schafer-Perini A.L.: Numerical Study of the Influence of Permeability Heterogeneity in Non-uniform Steady-State Flow Systems. Phd thesis, New Mexico Tech. Socorro, NM (1990).
88. Scheidegger, A. E.: "Statistical Hydrodynamics in Porous Media", *J. App. Physics* Vol. 25 No. 8 (Aug 1954) 994–1001.
89. Scheidegger, A. E.: "General Theory of Dispersion in Porous Media", *J. Geo. Res.* (Oct 1961) 3273–3277.

90. Schwartz, F. W.: " Macroscopic Dispersion in Porous Media: The Controlling Factors", *Water Resour. Resear.*, (Aug., 1977), 13(4), 743–752.

91. Settari, A. and Aziz K.: "Use of Irregular Grid in Reservoir Simulation", *Soc. Pet. Eng. J.* (April 1972), 103–114.

92. Smith, D. H. and Brigham, W. E.: "Field Evaluation of Waterflood Tracers in a Five-Spot", *Prod. Monthly* (Aug. 1965), 8–12.

93. Smith, L. and Freeze, R. A.: "Stochastic Analysis of Steady State GroundWater Flow in a Bounded Domain, 1. One-Dimensional Simulations", *Water Resour. Resear.*, (Jun., 1979), 15(3), 521–528.

94. Smith, L. and Freeze, R. A.: "Stochastic Analysis of Steady State GroundWater Flow in a Bounded Domain, 2. Two-Dimensional Simulations", *Water Resour. Resear.*, (Dec., 1979), 15(6), 1543–1559.

95. Smith, L. and Schwartz, F. W.: " Mass Transport, 1. A Stochastic Analysis of Macroscopic Dispersion", *Water Resour. Resear.*, (Apr., 1980), 16(2), 303–313.

96. Smith, L. and Schwartz, F. W.: " Mass Transport, 2. Analysis of Uncertainty in Prediction", *Water Resour. Resear.*, (Apr., 1981), 17(2), 351–369.

97. Spain, B.: *Tensor Calculus* Oliver and Boyd Ltd., London (1955).

98. Stiles, W. E.: "Use of Permeability Distribution in Water Flood Calculations", *Trans.* AIME (1949), **186**, 9.

99. Stone H. L. and Brian P. L. T.: "Numerical Solution of Convective Transport Problems", *A.I.Ch.E.J.* Vol. 9, No. 5 (Sept 1963) 681–688.

100. Strum, P. W., and Johnson, W. E.: "Field Experiments with Chemical Tracers in Flood Waters", *Prod. Monthly* (1951), **15**, No.2, 11–18.

101. Sultan, A.J.: Geostatistical Characterization of Heterogeneity and its Application, Phd thesis, New Mexico Tech. Socorro, NM, (1992).

102. Tang, D. H. and Babu D. K.: "Analytical Solution of a Velocity Dependent Dispersion Problem", *Water Res. Research*, Vol. 15, No. 6 (Dec 1979), 1471–1478.

103. Taylor, J. L. and Bandy, T. R.: "Tracer Technology Finds Expanding Applications", *Petroleum Eng. Int.* (June 1989), 31–36.

104. Wagner, O. R.: "The Use of Tracers in Diagnosing Interwell Reservoir Hetero-

geneities Field Results", *J. Pet. Tech.* (Nov. 1977), 1410–1416.

105. Warren, J. E. and Price, H. S.: "Flow in Heterogeneous Porous Media", *Soc. Pet. Eng. J.* (Sept., 1961), 153–169.

106. Warren, J. E., Skiba, F. F. and Price, H. S.: "An Evaluation of the Significance of Permeability Measurements", *J. Pet. Tech.* (Aug., 1961), 739.

107. Warren, J. E., Skiba, F. F.: "Macroscopic Dispersion", *Soc. Pet. Eng. J.* (Sept., 1964), 215–230.

108. Weber, K.J.: "How heterogeneity affects oil recovery," Reservoir Characterization, Academic Press, NY. (1986) pp. 487-544.

Appendix A
Equation of Motion of Isoconcentration Lines in Φ and Ψ Coordinate System

A.1 Introduction

In most multidimensional miscible displacements, for example flow in a developed flooding pattern, such as five-spot, staggered line drive, or direct line drive, the flow vectors are not simply oriented with respect to the coordinate axis. Although most of the reservoir problems can be simulated on rectangular grids, there are many instances in which the geometry of the reservoir is suitable to a curvilinear coordinate system. For example, an areal flow in a flooding pattern can be described by the grid, produced by the family of streamlines, Ψ = constant, and isopotential lines, Φ = constant. These are shown in Fig. 3.8 for a homogeneous five-spot pattern.

The chapter is divided into three main sections. The first section presents a brief introduction to the general theory of curvilinear coordinates. The second section derives the equation of motion (EOM) in a general curvilinear coordinate system. Finally, in the last section, the equation of motion is derived in an orthogonal (Φ, Ψ) coordinate system.

A.2 General Theory Curvilinear Coordinates

The location of a point in space can be specified either by three Cartesian coordinates, x^1, x^2, x^3, or by three curvilinear coordinates, y^1, y^2, y^3. In the Cartesian coordinate system, the base vectors $\mathbf{i}$, $\mathbf{j}$ and $\mathbf{k}$ are mutually orthogonal vectors having unit magnitude. Because their orientation is always along the positive direction of the coordinate axes, these base vectors remain independent of the spatial location (or coordinates x^i) of any point. On the other hand, consider a general curvilinear coordinate system (which may be non-orthogonal) in which two types of base vectors may be defined by geometrical construction (see Fig. A.1). The first type of base vectors, referred to as a *natural* basis, is denoted by $\mathbf{e}_i$, with free index i appearing as a subscript. Given a position vector $\mathbf{P}$, (where $\mathbf{P} = x^1\mathbf{i} + x^2\mathbf{j} + x^3\mathbf{k}$), these natural base vectors represent tangent vectors to the three coordinate curves,

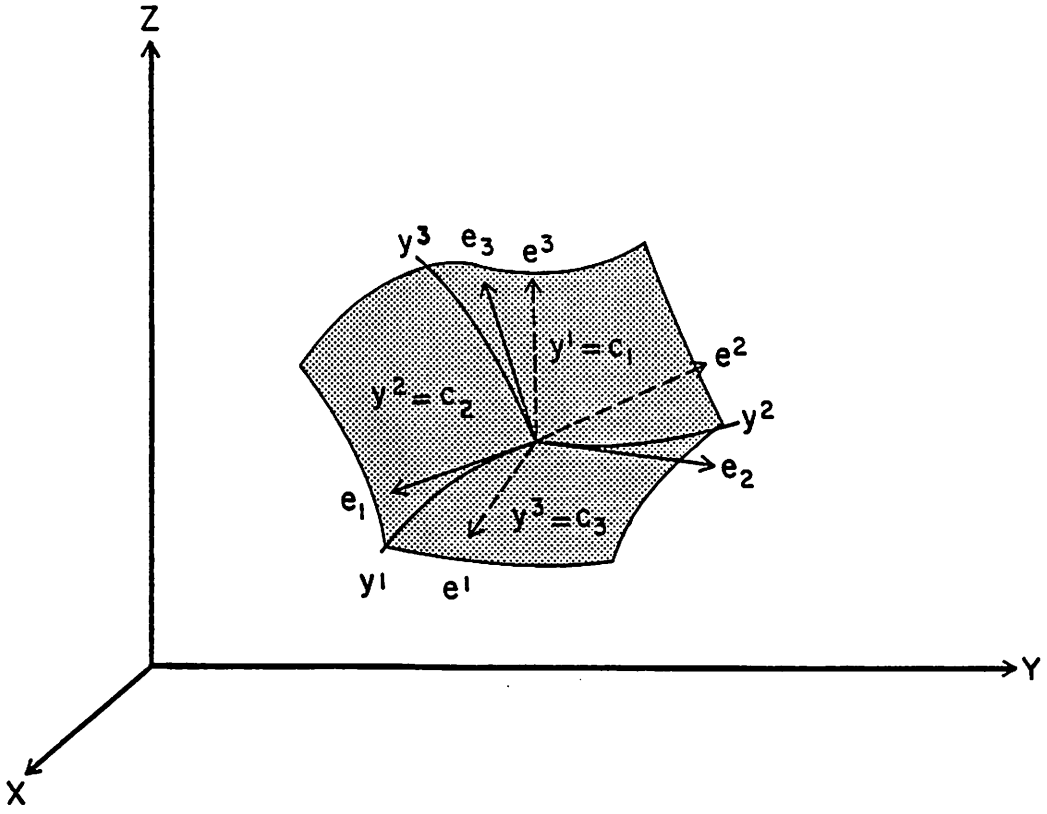

Fig. A.1 Curvilinear Coordinates Defined
by Three Intersecting curves, y^1, y^2, y^3.

taken in the direction of increasing y^i, i.e., $\mathbf{e}_i = \dfrac{\partial \mathbf{P}}{\partial y^i}$ for $i = 1$, 2 and 3 (Spiegel, 1959). In general, the natural base vectors are neither orthogonal nor of unit length. The second type of base vectors is called a *reciprocal* (or *dual*) basis, $\mathbf{e}^i$, for which the free index i is written as a superscript. Geometrically, these represent vectors normal to each of the coordinate surfaces, $y^i =$ constant; i.e., $\mathbf{e}^i = \nabla y^i$.

At every point in space, a unique relationship exists between the dual base vectors and natural base vectors, given by

$$\mathbf{e}^i \cdot \mathbf{e}_j = \delta^i{}_j \tag{A.1}$$

where the Kronecker delta symbol is defined by

$$\delta^i{}_j = \begin{cases} 0, & \text{if } i \neq j; \\ 1, & \text{if } i = j. \end{cases} \tag{A.2}$$

The geometrical implications of Eq. (A.1) allows one to express the dual basis in terms of the natural basis, and vice versa. For example, the dual base vectors for a given set of $\mathbf{e}_i$, $i = 1, 2, 3$ may be defined as

$$\mathbf{e}^1 = \frac{\mathbf{e}_2 \times \mathbf{e}_3}{\mathbf{e}_1 \cdot (\mathbf{e}_2 \times \mathbf{e}_3)}, \quad \mathbf{e}^2 = \frac{\mathbf{e}_3 \times \mathbf{e}_1}{\mathbf{e}_1 \cdot (\mathbf{e}_2 \times \mathbf{e}_3)}, \quad \mathbf{e}^3 = \frac{\mathbf{e}_1 \times \mathbf{e}_2}{\mathbf{e}_1 \cdot (\mathbf{e}_2 \times \mathbf{e}_3)} \qquad (A.3)$$

where the scalar triple product in the denominator numerically repesents the volume of a parallelepiped formed by the natural base vectors (Fig. A.1).

In general, dot products between natural base vectors or between dual base vectors do not result in values of 0 or 1. By definition (Bird et.al., 1977),

$$\mathbf{e}_i \cdot \mathbf{e}_j = g_{ij} \quad \text{and} \quad \mathbf{e}^i \cdot \mathbf{e}^j = g^{ij} \qquad (A.4)$$

denote the covariant and contravariant components, respectively, of the symmetric metric tensor $\mathbf{g}$. Its mixed components are given by the Kronecker delta $\delta^i{}_j$

The components of a vector or a tensor with respect to the natural basis are defined to be *contravariant* components; whereas, the components with respect to the dual basis are defined to be *covariant* components. By convention, free indices are shown as superscripts in writing contravariant components; they appear as subscripts in expressing covariant components. In an orthogonal curvilinear coordinate system, the corresponding natural base vectors and dual base vectors coincide in directions but not necessarily in magnitude. A set of unit vectors can be defined with respect to the natural basis as

$$\hat{\mathbf{e}}_i = \frac{\mathbf{e}_i}{|\mathbf{e}_i|} = \frac{\dfrac{\partial \mathbf{P}}{\partial y^i}}{\left|\dfrac{\partial \mathbf{P}}{\partial y^i}\right|} \qquad (A.5a)$$

Similarly, another set of unit vectors can be defined with respect to the dual basis as

$$\hat{\mathbf{e}}^i = \frac{\mathbf{e}^i}{|\mathbf{e}^i|} = \frac{\nabla y^i}{|\nabla y^i|} \qquad (A.5b)$$

Note that $\left|\dfrac{\partial \mathbf{P}}{\partial y^i}\right| = h_i$ and $|\nabla y^i| = h^i$ are called *scale factors.* In a general curvilinear system, the base vectors $\mathbf{e}_i$ and $\mathbf{e}^i$ are functions of spatial position; therefore, their magnitudes given by h_i and h^i respectively, are also dependent on the coordinates

y^i. Of course, the unit vectors $\hat{\mathbf{e}}_i$ (or $\hat{\mathbf{e}}^i$) change directions from point to point just as the base vectors do.

For an orthogonal curvilinear system, defined by $\hat{\mathbf{e}}_i \cdot \hat{\mathbf{e}}_j = \delta_{ij}$ at every point in space, the unit vectors $\hat{\mathbf{e}}_i$ and $\hat{\mathbf{e}}^i$ become identical. Additionally, the following results apply:

$$\begin{aligned} g_{ii} &= (h_i)^2 \quad ; \quad g_{ij} = 0 \text{ for } i \neq j \\ g^{ii} &= (h^i)^2 \quad ; \quad g^{ij} = 0 \text{ for } i \neq j \\ \text{and} \quad h^i &= \tfrac{1}{h_i} \end{aligned} \tag{A.6}$$

In the case of a Cartesian coordinate system, a further simplification arises because all scale factors equal unity. Thus, $\mathbf{e}_i = \hat{\mathbf{e}}_i = \mathbf{e}^i$, and it becomes obvious that the base vectors $\mathbf{e}_1 = \mathbf{i}$, $\mathbf{e}_2 = \mathbf{j}$, $\mathbf{e}_3 = \mathbf{k}$ form an orthonormal set. Therefore given an orthonormal basis, $\hat{\mathbf{e}}_i$, we can define the physical components of a vector as

$$\mathbf{a} = \sum_i a_{<i>} \hat{\mathbf{e}}_i \tag{A.7}$$

and a tensor as

$$\mathbf{A} = \sum_i \sum_j A_{<ij>} \hat{\mathbf{e}}_i \hat{\mathbf{e}}_j \tag{A.8}$$

The orthonormal basis vectors are unit and orthogonal. The physical components of a vector or a tensor have the same units of dimension as the physical quantity itself. Also, the metric tensor components, g_{ij} and g^{ij}, coincide with the Kronecker delta δ_{ij}.

If ds is the infinitesimal distance between two neighboring points with coordinates x^i and $x^i + dx^i$ in the Cartesian system or y^i and $y^i + dy^i$ in the general curvilinear system, then

$$\begin{aligned} (ds)^2 &= \sum_i \sum_j \delta_{ij}\, dx^i\, dx^j = \sum_m dx^m dx^m \\ (ds)^2 &= d\mathbf{P} \cdot d\mathbf{P} = \sum_i \sum_j g_{ij}\, dy^i\, dy^j \end{aligned} \tag{A.9}$$

It follows that the covariant metric tensor components are given by

$$g_{ij} = \sum_m \left(\frac{\partial x^m}{\partial y^i}\right)\left(\frac{\partial x^m}{\partial y^j}\right) \tag{A.10}$$

A.3 EOM in General Curvilinear Coordinates

In the following discussion, the physical component form of the equation

$$\mathbf{v}\cdot\nabla C=\left(\frac{1}{\phi S_w}\right)\mathbf{u}\cdot\nabla C-\nabla\cdot(D\cdot\nabla C) \qquad (A.11)$$

is derived in orthogonal curvilinear coordinates. First, each term of Eq. (A.11) is described in a general curvilinear coordinate system. Then the results are written for an orthogonal curvilinear coordinate system. Finally, the equation is expressed in a simplified form in which one family of coordinate curves is chosen to be the family of streamlines, Ψ = constant.

A.3.1 The General Form of Dispersion

The dispersion tensor in any curvilinear coordinate system may be represented as:

$$\mathbf{D}=\sum_i\sum_j D^{ij}\mathbf{e}_i\mathbf{e}_j \qquad (A.12a)$$

where D^{ij} are the contravariant components of dispersion tensor with respect to the natural basis. In an orthogonal coordinate system, these natural base vectors can be expressed in terms of scale factors and unit base vectors as

$$\mathbf{D}=\sum_i\sum_j D^{ij}h_ih_j\hat{\mathbf{e}}_i\hat{\mathbf{e}}_j \qquad (A.12b)$$

The physical components of $\mathbf{D}$ with respect to the orthonormal basis $\hat{\mathbf{e}}_i$ are thus given by

$$D_{<ij>}=D^{ij}h_ih_j \qquad (A.12c)$$

A.3.2 The Scalar $\bar{s}=\mathbf{u}\cdot\,\mathrm{grad}\,C$

The scalar $\bar{s}$ in Cartesian coordinates x^i has the form

$$\bar{s}=\sum_i u_i\frac{\partial C}{\partial x^i} \qquad (A.13a)$$

It is conventional to give a covariant component representation of the gradient of a scalar point function in a general curvilinear system (Ref: Middleman 1978, or Malvern, 1979). Therefore, in any curvilinear coordinate system y^i, scalar $\bar{s}$ takes on the form

$$\bar{s}=\sum_i u_i\mathbf{e}^i\cdot\sum_j\mathbf{e}^j\frac{\partial C}{\partial y^j}=\sum_i\sum_j u_i\frac{\partial C}{\partial y^j}g^{ij} \qquad (A.13b)$$

where g^{ij} are the contravariant components of the metric tensor. The matrix $[g^{ij}]$ is called the conjugate or reciprocal of the covariant matrix $[g_{ij}]$ and its elements can be found from

$$g^{ij} = \frac{(\text{cofactor of } g_{ij})}{g}, \qquad (\text{for } g \neq 0) \tag{A.14a}$$

where g is the determinant of the matrix $[g_{ij}]$. In an orthogonal curvilinear coordinate system

$$\left[g^{ij}\right] = \begin{bmatrix} g^{11} & 0 & 0 \\ 0 & g^{22} & 0 \\ 0 & 0 & g^{33} \end{bmatrix} = \begin{bmatrix} (h^1)^2 & 0 & 0 \\ 0 & (h^2)^2 & 0 \\ 0 & 0 & (h^3)^2 \end{bmatrix} \tag{A.14b}$$

Note that $g^{ij} = 0$ for $i \neq j$ and

$$g^{ij} = \sum_m \left(\frac{\partial y^i}{\partial x^m}\right)\left(\frac{\partial y^j}{\partial x^m}\right) = h^i h^j \tag{A.14c}$$

for $i = j$. Then, in orthogonal curvilinear coordinates Eq. (A.13b) becomes

$$\bar{s} = \sum_i u_i \frac{\partial C}{\partial y^i}(h^i)^2 = \sum_i \frac{u_i}{h_i^2}\frac{\partial C}{\partial y^i} \tag{A.15a}$$

The physical components of the scalar $\bar{s}$ can then be written as

$$\bar{s} = \sum_i \frac{u_{<i>}}{h_i}\frac{\partial C}{\partial y^i} \tag{A.15b}$$

Similarly, we can write the displacement velocity in a general coordinate system as

$$\mathbf{v} \cdot \nabla C = \sum_i \sum_j v_i \frac{\partial C}{\partial y^j} g^{ij} \tag{A.16a}$$

and in an orthogonal coordinate system as

$$\mathbf{v} \cdot \nabla C = \sum_i \frac{v_i}{h_i^2}\frac{\partial C}{\partial y^i} g^{ij} \tag{A.16b}$$

In physical component form

$$\mathbf{v} \cdot \nabla C = \sum_i \frac{v_{<i>}}{h_i}\frac{\partial C}{\partial y^i} \tag{A.16c}$$

A.3.3 The Vector $\mathbf{T} = \mathbf{D} \cdot \text{grad}\,\mathbf{C}$

The vector $\mathbf{T}$, which in Cartesian coordinates x^i has the components

$$T_i = \sum_j D_{ij} \frac{\partial C}{\partial x^j} \tag{A.17a}$$

is an inner product of the 2nd order tensor $\mathbf{D}$ and the vector grad C. Therefore, in any curvilinear coordinate system y^i, it takes on the form

$$\begin{aligned} \mathbf{T} &= \sum_i \sum_j \sum_k D_{ij} \mathbf{e}^i \mathbf{e}^j \cdot \mathbf{e}^k \frac{\partial C}{\partial y^k} \\ &= \sum_i \sum_j \sum_k D_{ij} g^{jk} \frac{\partial C}{\partial y^k} \mathbf{e}^i \end{aligned} \tag{A.17b}$$

The i^{th} component of $\mathbf{T}$ is $T_i = \sum_j \sum_k D_{ij} g^{jk} \frac{\partial C}{\partial y^k}$. Hence, in an orthogonal curvilinear coordinate system

$$T_i = \sum_j D_{ij} \frac{1}{h_j^2} \frac{\partial C}{\partial y^j} \tag{A.17c}$$

In physical components form

$$T_{<i>} = \sum_j D_{<ij>} \frac{h_i}{h_j} \frac{\partial C}{\partial y^j} \tag{A.17d}$$

A.3.4 Divergence of T

In Cartesian coordinates, $\text{div}\,(D\ \text{grad}\,C)$ is given by

$$\nabla \cdot \mathbf{T} = \sum_i \frac{\partial T_i}{\partial x^i} \tag{A.18a}$$

In a general curvilinear coordinate system (Spain, 1956, p.33)

$$\text{div}\,T = \sum_i \sum_k \frac{1}{\sqrt{g}} \frac{\partial}{\partial y^i} (\sqrt{g} g^{ik} T_k) \tag{A.18b}$$

Hence, by combining (A.18b) and (A.17b), we get

$$\text{div}\,T = \sum_i \sum_k \sum_l \sum_m \frac{1}{\sqrt{g}} \frac{\partial}{\partial y^i} \left(\sqrt{g} g^{ik} D_{kl} g^{lm} \frac{\partial C}{\partial y^m} \right) \tag{A.18c}$$

In an orthogonal curvilinear coordinate system, $\sqrt{g} = h_1 h_2 h_3$, therefore

$$\text{div}\,T = \sum_i \sum_j \frac{1}{h_1 h_2 h_3} \frac{\partial}{\partial y^i} \left(h_1 h_2 h_3 \frac{1}{h_i^2} D_{ij} \frac{1}{h_j^2} \frac{\partial C}{\partial y^j} \right) \tag{A.18d}$$

In a physical component form,

$$\text{div}\,T = \sum_i \sum_j \frac{1}{h_1 h_2 h_3} \frac{\partial}{\partial y^i} \left(h_1 h_2 h_3 \frac{1}{h_i} D_{<ij>} \frac{1}{h_j} \frac{\partial C}{\partial y^j} \right) \tag{A.18e}$$

A.3.5 The General Equation of Motion of Isoconcentration Surfaces

By combining Eq. (A.13b) Eq. (A.16a) and Eq. (A.18c), the general equation of motion of isoconcentration surfaces in a general curvilinear coordinate system for a homogeneous porous medium is

$$\sum_i \sum_j g^{ij} v_i \frac{\partial C}{\partial y_j} = \sum_i \sum_j g^{ij} u_i \frac{\partial C}{\partial y^j} - \sum_i \sum_k \sum_l \sum_m \frac{1}{\sqrt{g}} \frac{\partial}{\partial y^i} \left(\sqrt{g} g^{ik} D_{kl} g^{lm} \frac{\partial C}{\partial y^m} \right) \tag{A.19a}$$

In an orthogonal system

$$\sum_i \frac{v_i}{h_i^2} \frac{\partial C}{\partial y^i} = \sum_i \frac{u_i}{h_i^2} \frac{\partial C}{\partial y^i} - \sum_i \sum_j \frac{1}{h_1 h_2 h_3} \frac{\partial}{\partial y^i} \left(h_1 h_2 h_3 \frac{1}{h_i^2} \frac{1}{h_j^2} D_{ij} \frac{\partial C}{\partial y^j} \right) \tag{A.19b}$$

In physical components form

$$\sum_i \frac{v_{<i>}}{h_i} \frac{\partial C}{\partial y^i} = \sum_i \frac{u_{<i>}}{h_i} \frac{\partial C}{\partial y^i} - \sum_i \sum_j \frac{1}{h_1 h_2 h_3} \frac{\partial}{\partial y^i} \left(h_1 h_2 h_3 \frac{1}{h_i} D_{<ij>} \frac{1}{h_j} \frac{\partial C}{\partial y^j} \right) \tag{A.19c}$$

if the flow is such that $u_{<1>} = u \neq 0$, $u_{<2>} = u_{<3>} = 0$ and $v_{<1>} \neq 0$, $v_{<2>} \neq 0, v_{<3>} \neq 0$. Moreover, if the porous medium is isotropic, in which the principal axis of dispersion at each point lies along the coordinate curves, then

$$D_{<ij>} \begin{cases} \neq 0, & \text{if } i = j; \\ = 0, & \text{if } i \neq j. \end{cases}$$

and Eq. (A.19c) becomes

$$\frac{v_1}{h_1} \frac{\partial C}{\partial y^1} + \frac{v_2}{h_2} \frac{\partial C}{\partial y^2} + \frac{v_3}{h_3} \frac{\partial C}{\partial y^3} = \frac{u}{h_1} \frac{\partial C}{\partial y^1} - \frac{1}{h_1 h_2 h_3} \left\{ \frac{\partial}{\partial y^1} \left(\frac{h_2 h_3}{h_1} D_{<11>} \frac{\partial C}{\partial y^1} \right) + \frac{\partial}{\partial y^2} \left(\frac{h_1 h_3}{h_2} D_{<22>} \frac{\partial C}{\partial y^2} \right) + \frac{\partial}{\partial y^3} \left(\frac{h_1 h_2}{h_3} D_{<33>} \frac{\partial C}{\partial y^3} \right) \right\} \tag{A.20}$$

This is the equation of motion of the isoconcentration surfaces in a three-dimensional orthogonal curvilinear coordinate system.

A.4 Equation of Motion of Isoconcentration Surfaces in $\Phi - \Psi$ Coordinates

A system composed of the family of streamlines, Ψ = constant, and the family of equipotential lines, Φ = constant, is sufficient to describe a two dimensional flow. From (A.5)

$$h_i^{-1} = |\operatorname{grad} y^i| = \left| \sum_j \frac{\partial y^i}{\partial x^j} \right|$$

Hence,

$$\begin{aligned} h_1 = h_\Phi &= \left[\left(\frac{\partial x}{\partial \Phi}\right)^2 + \left(\frac{\partial y}{\partial \Phi}\right)^2\right]^{1/2} \\ &= \left[\left(\frac{\partial \Phi}{\partial x}\right)^2 + \left(\frac{\partial \Phi}{\partial y}\right)^2\right]^{-1/2} \\ h_2 = h_\Psi &= \left[\left(\frac{\partial x}{\partial \Psi}\right)^2 + \left(\frac{\partial y}{\partial \Psi}\right)^2\right]^{1/2} \\ &= \left[\left(\frac{\partial \Psi}{\partial x}\right)^2 + \left(\frac{\partial \Psi}{\partial y}\right)^2\right]^{-1/2} \end{aligned} \qquad (A.21a)$$

Since $\frac{\partial \Phi}{\partial x} = \frac{\partial \Psi}{\partial y}$ and $\frac{\partial \Phi}{\partial y} = -\frac{\partial \Psi}{\partial x}$, we can write

$$h_\Phi = h_\Psi = h \qquad (A.21b)$$

Using $D_L = D_{<11>}$, $D_T = D_{<22>}$ and substituting Eq. (A.21a), Eq. (A.21b) in Eq. (A.20), we get

$$v_\Phi \frac{\partial C}{\partial \Phi} + v_\Psi \frac{\partial C}{\partial \Psi} = \frac{u}{\phi}\frac{\partial C}{\partial \Phi} - \frac{1}{h}\left[\frac{\partial}{\partial \Phi}\left(D_L \frac{\partial C}{\partial \Phi}\right) + \frac{\partial}{\partial \Psi}\left(D_T \frac{\partial C}{\partial \Psi}\right)\right] \qquad (A.22)$$

This is the equation of motion of isoconcentration surfaces in a two dimensional $(\Phi - \Psi)$ coordinate system.

This analytic expression is used directly in the two-dimensional miscible displacement of a five-spot pattern. The method involves injecting a tracer slug of a "*ramp up ramp down*" shape with concentration distribution values assigned to these *ramps* ranging from 0 to 1. This concentration profile is divided into seventeen iso-concentration lines or points. Each iso-concentration line is subjected to the influence of convection and dispersion, and outward, or front, velocity on a streamline of a flooding pattern is calculated.

Appendix B
Permeability Data Measured at the Top Surface of the Rock

X	Y	Log K	X	Y	Log K
0.000	0.000	-0.3998	0.715	0.000	-0.2316
0.000	0.715	-0.5606	0.715	0.715	-0.7019
0.000	1.430	-0.4369	0.715	1.430	-0.5432
0.000	2.145	-1.3237	0.715	2.145	-1.6582
0.000	2.860	-1.3237	0.715	2.860	-2.1118
0.000	3.575	-1.9372	0.715	3.575	-1.7438
0.000	4.290	-1.5804	0.715	4.290	-1.6354
0.000	5.005	-1.7244	0.715	5.005	-0.6783
0.000	5.720	-0.8917	0.715	5.720	-0.2220
0.000	6.435	-0.9919	0.715	6.435	-0.9573
0.000	7.150	-0.6170	0.715	7.150	-0.7432
0.000	7.865	-0.6294	0.715	7.865	-0.8244
0.000	8.580	-0.4373	0.715	8.580	-0.4536
0.000	9.295	-0.5797	0.715	9.295	-0.4956
0.000	10.010	-1.4444	0.715	10.010	-1.3043
0.000	10.725	-1.1549	0.715	10.725	-0.9515
0.000	11.440	-1.2348	0.715	11.440	-0.9164
0.000	12.155	-1.8078	0.715	12.155	-1.4249
0.000	12.870	-1.4518	0.715	12.870	-0.8060
0.000	13.585	-1.2190	0.715	13.585	-0.2053
0.000	14.300	-1.5561	0.715	14.300	-0.8587

X	Y	Log K	X	Y	Log K
1.430	0.000	-0.1139	2.145	0.000	-0.3072
1.430	0.715	-0.6792	2.145	0.715	-0.6769
1.430	1.430	-1.3334	2.145	1.430	-0.8563
1.430	2.145	-1.6759	2.145	2.145	-0.8238
1.430	2.860	-1.2203	2.145	2.860	-0.5511
1.430	3.575	-0.7562	2.145	3.575	-0.6412
1.430	4.290	-0.9965	2.145	4.290	-0.8708
1.430	5.005	-0.6760	2.145	5.005	-0.9930
1.430	5.720	-0.5788	2.145	5.720	-0.6115
1.430	6.435	-1.0327	2.145	6.435	-0.3928
1.430	7.150	-1.3844	2.145	7.150	-0.5256
1.430	7.865	-1.0768	2.145	7.865	-0.7186
1.430	8.580	-1.3511	2.145	8.580	-0.5967
1.430	9.295	-1.1245	2.145	9.295	-0.6883
1.430	10.010	-1.3190	2.145	10.010	-0.8119
1.430	10.725	-0.9764	2.145	10.725	-1.3563
1.430	11.440	-0.4745	2.145	11.440	-0.8423
1.430	12.155	-0.7287	2.145	12.155	-0.6111
1.430	12.870	-0.6633	2.145	12.870	-0.2501
1.430	13.585	-0.2859	2.145	13.585	-0.4494
1.430	14.300	-0.5282	2.145	14.300	-0.9209

Table B.1 Permeability Data Measured at the top Surface of the Rock Sample.

X	Y	Log K	X	Y	Log K
2.860	0.000	-0.5080	3.575	0.000	-0.2581
2.860	0.715	-0.4553	3.575	0.715	-0.2123
2.860	1.430	-1.0809	3.575	1.430	-0.5797
2.860	2.145	-0.3881	3.575	2.145	-0.6184
2.860	2.860	-1.1569	3.575	2.860	-0.0905
2.860	3.575	-1.0769	3.575	3.575	-0.6196
2.860	4.290	-0.7147	3.575	4.290	-0.4475
2.860	5.005	-0.8062	3.575	5.005	-0.3128
2.860	5.720	-0.2487	3.575	5.720	-0.1436
2.860	6.435	-0.1583	3.575	6.435	-0.3328
2.860	7.150	-0.3702	3.575	7.150	-0.0509
2.860	7.865	-0.2061	3.575	7.865	-0.0296
2.860	8.580	-0.2253	3.575	8.580	-0.2662
2.860	9.295	-0.2513	3.575	9.295	-0.0327
2.860	10.010	-0.4410	3.575	10.010	-0.0195
2.860	10.725	-0.5108	3.575	10.725	-0.3534
2.860	11.440	-0.6283	3.575	11.440	-0.5553
2.860	12.155	-0.9291	3.575	12.155	-0.4953
2.860	12.870	-0.2889	3.575	12.870	-0.4307
2.860	13.585	-0.4700	3.575	13.585	-0.4465
2.860	14.300	-0.7032	3.575	14.300	-1.2559

Table B.1 (Continued) Permeability Data

Measured at the Top Surface of the Rock Sample.

X	Y	Log K	X	Y	Log K
4.290	0.000	-0.3162	5.005	0.000	-0.4791
4.290	0.715	-0.7185	5.005	0.715	-1.0653
4.290	1.430	-1.5255	5.005	1.430	-0.6978
4.290	2.145	-0.9696	5.005	2.145	-0.3002
4.290	2.860	-0.4888	5.005	2.860	-0.3237
4.290	3.575	-0.7578	5.005	3.575	-0.8810
4.290	4.290	-0.6888	5.005	4.290	-0.2822
4.290	5.005	-0.7147	5.005	5.005	-0.2605
4.290	5.720	-0.0609	5.005	5.720	0.0682
4.290	6.435	-0.2855	5.005	6.435	-0.1441
4.290	7.150	-0.7200	5.005	7.150	-0.3692
4.290	7.865	-0.4762	5.005	7.865	-0.8977
4.290	8.580	-0.5776	5.005	8.580	-1.0562
4.290	9.295	0.0614	5.005	9.295	-0.0411
4.290	10.010	-0.3211	5.005	10.010	0.2241
4.290	10.725	-0.9091	5.005	10.725	-0.2368
4.290	11.440	-0.5838	5.005	11.440	-0.5726
4.290	12.155	-0.6769	5.005	12.155	-1.0604
4.290	12.870	-0.5788	5.005	12.870	-0.0577
4.290	13.585	-0.9157	5.005	13.585	-0.3721
4.290	14.300	-1.5497	5.005	14.300	-0.7010

Table B.1 (Continued) Permeability Data
Measured at the Top Surface of the Rock Sample.

X	Y	Log K	X	Y	Log K
5.720	0.000	-1.2310	6.435	0.000	-0.8023
5.720	0.715	-1.0511	6.435	0.715	-1.4092
5.720	1.430	-0.7347	6.435	1.430	-0.6881
5.720	2.145	-0.4684	6.435	2.145	-0.9809
5.720	2.860	-1.0824	6.435	2.860	-0.9504
5.720	3.575	-1.4408	6.435	3.575	-0.4945
5.720	4.290	-1.1174	6.435	4.290	-0.9073
5.720	5.005	-0.5365	6.435	5.005	-1.3375
5.720	5.720	-0.0105	6.435	5.720	-0.7782
5.720	6.435	-0.0452	6.435	6.435	-0.8966
5.720	7.150	-0.4687	6.435	7.150	-0.7690
5.720	7.865	-0.1592	6.435	7.865	-0.4749
5.720	8.580	-0.2074	6.435	8.580	-0.3603
5.720	9.295	-0.5560	6.435	9.295	-0.5079
5.720	10.010	0.1508	6.435	10.010	-0.1934
5.720	10.725	-0.1675	6.435	10.725	0.1728
5.720	11.440	-0.2954	6.435	11.440	-0.5873
5.720	12.155	-1.0408	6.435	12.155	-0.5996
5.720	12.870	-1.1293	6.435	12.870	-0.7303
5.720	13.585	-1.2697	6.435	13.585	-1.1755
5.720	14.300	-0.7731	6.435	14.300	-1.4048

Table B.1 (Continued) Permeability Data
Measured at the Top Surface of the Rock Sample.

X	Y	Log K	X	Y	Log K
7.150	0.000	-1.0437	7.865	0.000	-1.1406
7.150	0.715	-1.3268	7.865	0.715	-1.5887
7.150	1.430	-0.9736	7.865	1.430	-1.3374
7.150	2.145	-0.9417	7.865	2.145	-0.9693
7.150	2.860	-1.2084	7.865	2.860	-0.9626
7.150	3.575	-0.2830	7.865	3.575	-0.1560
7.150	4.290	-0.3001	7.865	4.290	0.1487
7.150	5.005	-0.5001	7.865	5.005	0.1390
7.150	5.720	-1.1580	7.865	5.720	-0.5561
7.150	6.435	-0.7444	7.865	6.435	-0.7162
7.150	7.150	-1.4219	7.865	7.150	-0.2305
7.150	7.865	-1.1420	7.865	7.865	0.0485
7.150	8.580	-0.2357	7.865	8.580	0.1203
7.150	9.295	-0.0724	7.865	9.295	-0.1737
7.150	10.010	-0.1101	7.865	10.010	0.1031
7.150	10.725	-0.1857	7.865	10.725	0.0757
7.150	11.440	-0.3688	7.865	11.440	0.1939
7.150	12.155	-0.0765	7.865	12.155	-0.4158
7.150	12.870	-1.2850	7.865	12.870	-0.5347
7.150	13.585	-1.3139	7.865	13.585	-1.4391
7.150	14.300	-1.4656	7.865	14.300	-0.9060

Table B.1 (Continued) Permeability Data

Measured at the Top Surface of the Rock Sample.

X	Y	Log K	X	Y	Log K
8.580	0.000	-0.8010	9.295	0.000	-0.9621
8.580	0.715	-0.1407	9.295	0.715	-0.1797
8.580	1.430	-0.2203	9.295	1.430	-0.3855
8.580	2.145	0.2336	9.295	2.145	-0.4220
8.580	2.860	-0.1733	9.295	2.860	-0.4021
8.580	3.575	-0.7417	9.295	3.575	-0.5055
8.580	4.290	-0.1699	9.295	4.290	-0.1604
8.580	5.005	-0.5209	9.295	5.005	-0.4220
8.580	5.720	-0.1288	9.295	5.720	-0.0749
8.580	6.435	0.0119	9.295	6.435	0.0688
8.580	7.150	0.0583	9.295	7.150	-0.0785
8.580	7.865	0.0631	9.295	7.865	0.0069
8.580	8.580	-0.0296	9.295	8.580	-0.0618
8.580	9.295	-0.3416	9.295	9.295	-0.0959
8.580	10.010	-0.5083	9.295	10.010	-0.3121
8.580	10.725	0.0279	9.295	10.725	-0.0665
8.580	11.440	0.0700	9.295	11.440	-0.1066
8.580	12.155	0.0046	9.295	12.155	-0.0645
8.580	12.870	-0.8040	9.295	12.870	-0.2665
8.580	13.585	-1.0378	9.295	13.585	-0.0059
8.580	14.300	-0.8299	9.295	14.300	-0.5105

Table B.1 (Continued) Permeability Data

Measured at the Top Surface of the Rock Sample.

X	Y	Log K	X	Y	Log K
10.010	0.000	-1.1645	10.725	0.000	-0.9201
10.010	0.715	-0.8981	10.725	0.715	-0.3626
10.010	1.430	-0.5672	10.725	1.430	-1.1918
10.010	2.145	0.0332	10.725	2.145	-0.3231
10.010	2.860	0.2751	10.725	2.860	0.0795
10.010	3.575	0.1517	10.725	3.575	-0.2294
10.010	4.290	-0.3257	10.725	4.290	-0.1717
10.010	5.005	-0.3892	10.725	5.005	0.3969
10.010	5.720	-0.5978	10.725	5.720	0.1486
10.010	6.435	-0.8698	10.725	6.435	-0.2850
10.010	7.150	-0.4206	10.725	7.150	-0.5322
10.010	7.865	-0.3644	10.725	7.865	-0.4169
10.010	8.580	-0.5217	10.725	8.580	-0.4022
10.010	9.295	-0.3990	10.725	9.295	-0.4251
10.010	10.010	-0.1039	10.725	10.010	-0.3972
10.010	10.725	0.0506	10.725	10.725	-0.0541
10.010	11.440	0.3694	10.725	11.440	-0.2424
10.010	12.155	-0.2358	10.725	12.155	-0.9134
10.010	12.870	-1.0360	10.725	12.870	-0.4181
10.010	13.585	-0.3853	10.725	13.585	-0.2169
10.010	14.300	0.0050	10.725	14.300	-0.1378

Table B.1 (Continued) Permeability Data
Measured at the Top Surface of the Rock Sample.

X	Y	Log K	X	Y	Log K
11.440	0.000	0.0384	12.155	0.000	-0.8230
11.440	0.715	0.2118	12.155	0.715	-0.2048
11.440	1.430	-0.2222	12.155	1.430	0.0846
11.440	2.145	-0.5194	12.155	2.145	0.1008
11.440	2.860	-0.3192	12.155	2.860	-0.6466
11.440	3.575	-0.7440	12.155	3.575	-0.5443
11.440	4.290	0.1763	12.155	4.290	0.2528
11.440	5.005	0.1343	12.155	5.005	0.2500
11.440	5.720	0.1310	12.155	5.720	0.0705
11.440	6.435	-0.0974	12.155	6.435	-0.1136
11.440	7.150	-0.2886	12.155	7.150	-0.0597
11.440	7.865	-0.0322	12.155	7.865	0.1497
11.440	8.580	0.0996	12.155	8.580	0.4620
11.440	9.295	-0.6289	12.155	9.295	0.4100
11.440	10.010	-0.5629	12.155	10.010	0.3939
11.440	10.725	-0.5239	12.155	10.725	0.3446
11.440	11.440	-0.7927	12.155	11.440	0.2497
11.440	12.155	-0.2606	12.155	12.155	0.0433
11.440	12.870	0.2414	12.155	12.870	0.4292
11.440	13.585	-0.2704	12.155	13.585	-0.6736
11.440	14.300	0.4378	12.155	14.300	-0.6730

Table B.1 (Continued) Permeability Data

Measured at the Top Surface of the Rock Sample.

X	Y	Log K	X	Y	Log K
12.870	0.000	-0.7500	13.585	0.000	-0.3938
12.870	0.715	-0.6666	13.585	0.715	-0.4793
12.870	1.430	-0.0427	13.585	1.430	-0.0114
12.870	2.145	0.2703	13.585	2.145	-0.0124
12.870	2.860	0.2115	13.585	2.860	-0.8923
12.870	3.575	-0.4817	13.585	3.575	-0.1177
12.870	4.290	0.1825	13.585	4.290	-0.3755
12.870	5.005	0.0371	13.585	5.005	-0.7891
12.870	5.720	-0.2398	13.585	5.720	-0.4721
12.870	6.435	-0.2398	13.585	6.435	-0.2504
12.870	7.150	0.0402	13.585	7.150	-0.2772
12.870	7.865	-0.3120	13.585	7.865	-0.5785
12.870	8.580	-0.2469	13.585	8.580	-0.2522
12.870	9.295	-0.2450	13.585	9.295	-0.7194
12.870	10.010	-0.3491	13.585	10.010	0.0180
12.870	10.725	0.4226	13.585	10.725	0.4094
12.870	11.440	0.1707	13.585	11.440	-0.3784
12.870	12.155	-0.0847	13.585	12.155	-0.5272
12.870	12.870	-0.7058	13.585	12.870	-0.1388
12.870	13.585	-0.4109	13.585	13.585	0.3264
12.870	14.300	-0.6333	13.585	14.300	0.2818

Table B.1 (Continued) Permeability Data

Measured at the Top Surface of the Rock Sample.

X	Y	Log K
14.300	0.000	-0.0773
14.300	0.715	-0.1729
14.300	1.430	-0.1578
14.300	2.145	0.4315
14.300	2.860	0.2031
14.300	3.575	-0.1466
14.300	4.290	0.2544
14.300	5.005	-0.3692
14.300	5.720	-0.4708
14.300	6.435	-0.7321
14.300	7.150	-0.6548
14.300	7.865	-0.4039
14.300	8.580	-0.4668
14.300	9.295	-0.3953
14.300	10.010	0.6366
14.300	10.725	-0.5017
14.300	11.440	-0.3110
14.300	12.155	-0.3188
14.300	12.870	-0.4281
14.300	13.585	-0.2332
14.300	14.300	0.5506

Table B.1 (Continued) Permeability Data Measured at the Top Surface of the Rock Sample.

Appendix C
Permeability Data Measured at the Bottom Surface of the Rock

X	Y	Log K	X	Y	Log K
0.000	0.000	0.1745	0.715	0.000	0.1382
0.000	0.715	0.1759	0.715	0.715	0.2023
0.000	1.430	0.2190	0.715	1.430	0.2642
0.000	2.145	0.2242	0.715	2.145	0.1911
0.000	2.860	0.1773	0.715	2.860	0.1406
0.000	3.575	0.1475	0.715	3.575	0.1732
0.000	4.290	0.1835	0.715	4.290	0.3397
0.000	5.005	0.1695	0.715	5.005	0.2483
0.000	5.720	0.1689	0.715	5.720	0.3787
0.000	6.435	0.1619	0.715	6.435	0.2472
0.000	7.150	0.2281	0.715	7.150	0.2568
0.000	7.865	0.3647	0.715	7.865	0.4660
0.000	8.580	0.3645	0.715	8.580	0.4197
0.000	9.295	0.2734	0.715	9.295	0.4375
0.000	10.010	0.3906	0.715	10.010	0.3561
0.000	10.725	0.4073	0.715	10.725	0.7472
0.000	11.440	0.3636	0.715	11.440	0.4270
0.000	12.155	0.3336	0.715	12.155	1.1136
0.000	12.870	0.3249	0.715	12.870	0.7465
0.000	13.585	0.1513	0.715	13.585	0.1829
0.000	14.300	0.0852	0.715	14.300	0.1292

X	Y	Log K	X	Y	Log K
1.430	0.000	0.2168	2.145	0.000	0.1567
1.430	0.715	0.2878	2.145	0.715	0.3383
1.430	1.430	0.1997	2.145	1.430	0.1362
1.430	2.145	0.1383	2.145	2.145	0.1139
1.430	2.860	0.2186	2.145	2.860	0.1400
1.430	3.575	0.1787	2.145	3.575	0.1161
1.430	4.290	0.2262	2.145	4.290	0.2057
1.430	5.005	0.3895	2.145	5.005	0.5850
1.430	5.720	0.3366	2.145	5.720	0.2056
1.430	6.435	0.2938	2.145	6.435	0.2343
1.430	7.150	0.5817	2.145	7.150	0.8165
1.430	7.865	0.4152	2.145	7.865	0.3793
1.430	8.580	0.3783	2.145	8.580	0.4019
1.430	9.295	0.3412	2.145	9.295	0.1859
1.430	10.010	0.3599	2.145	10.010	0.4160
1.430	10.725	0.4300	2.145	10.725	0.6690
1.430	11.440	1.6036	2.145	11.440	1.2840
1.430	12.155	1.3687	2.145	12.155	1.8850
1.430	12.870	0.6382	2.145	12.870	1.0415
1.430	13.585	0.3715	2.145	13.585	0.2586
1.430	14.300	0.1775	2.145	14.300	0.2529

Table C.1 Permeability Data Measured at the Bottom Surface of the Rock Sample.

X	Y	Log K	X	Y	Log K
2.860	0.000	0.1892	3.575	0.000	0.1469
2.860	0.715	0.0814	3.575	0.715	0.1295
2.860	1.430	0.0923	3.575	1.430	0.0740
2.860	2.145	0.1001	3.575	2.145	0.2714
2.860	2.860	0.1914	3.575	2.860	0.2491
2.860	3.575	0.1816	3.575	3.575	0.3785
2.860	4.290	0.2101	3.575	4.290	0.2449
2.860	5.005	0.2390	3.575	5.005	0.2845
2.860	5.720	0.2572	3.575	5.720	0.2582
2.860	6.435	0.3028	3.575	6.435	0.3952
2.860	7.150	0.4705	3.575	7.150	1.3378
2.860	7.865	0.5882	3.575	7.865	0.8886
2.860	8.580	0.3542	3.575	8.580	1.0766
2.860	9.295	0.3458	3.575	9.295	0.4414
2.860	10.010	0.1937	3.575	10.010	0.2283
2.860	10.725	0.4744	3.575	10.725	0.3446
2.860	11.440	3.4213	3.575	11.440	1.2890
2.860	12.155	0.3738	3.575	12.155	0.6089
2.860	12.870	0.4010	3.575	12.870	0.1221
2.860	13.585	0.2157	3.575	13.585	0.1173
2.860	14.300	0.1773	3.575	14.300	0.1078

Table C.1 (Continued) Permeability Data

Measured at the Bottom Surface of the Rock Sample.

X	Y	Log K	X	Y	Log K
4.290	0.000	0.1114	5.005	0.000	0.1054
4.290	0.715	0.1192	5.005	0.715	0.0939
4.290	1.430	0.1168	5.005	1.430	0.1189
4.290	2.145	0.1981	5.005	2.145	0.2016
4.290	2.860	0.1754	5.005	2.860	0.2424
4.290	3.575	0.3140	5.005	3.575	0.3741
4.290	4.290	0.3020	5.005	4.290	0.4740
4.290	5.005	0.3155	5.005	5.005	0.5778
4.290	5.720	0.2012	5.005	5.720	0.2127
4.290	6.435	0.2731	5.005	6.435	0.3160
4.290	7.150	18.2439	5.005	7.150	0.4999
4.290	7.865	0.2362	5.005	7.865	0.2216
4.290	8.580	0.1892	5.005	8.580	0.2084
4.290	9.295	0.2865	5.005	9.295	3.6654
4.290	10.010	1.2140	5.005	10.010	0.1194
4.290	10.725	0.4012	5.005	10.725	0.3132
4.290	11.440	0.2006	5.005	11.440	0.3439
4.290	12.155	0.2374	5.005	12.155	0.5475
4.290	12.870	0.2089	5.005	12.870	0.3033
4.290	13.585	0.0558	5.005	13.585	0.1086
4.290	14.300	0.0858	5.005	14.300	0.0815

Table C.1 (Continued) Permeability Data

Measured at the Bottom Surface of the Rock Sample.

X	Y	Log K	X	Y	Log K
5.720	0.000	0.1244	6.435	0.000	0.0985
5.720	0.715	0.3258	6.435	0.715	0.0727
5.720	1.430	0.2113	6.435	1.430	0.1323
5.720	2.145	0.1634	6.435	2.145	0.1318
5.720	2.860	0.1838	6.435	2.860	0.1497
5.720	3.575	0.3694	6.435	3.575	0.1143
5.720	4.290	0.8081	6.435	4.290	0.3595
5.720	5.005	0.6508	6.435	5.005	0.4461
5.720	5.720	1.4540	6.435	5.720	0.3356
5.720	6.435	0.9231	6.435	6.435	0.4262
5.720	7.150	2.1071	6.435	7.150	0.2755
5.720	7.865	0.6221	6.435	7.865	0.4509
5.720	8.580	1.7323	6.435	8.580	0.0927
5.720	9.295	0.3656	6.435	9.295	0.2598
5.720	10.010	1.5525	6.435	10.010	0.4286
5.720	10.725	0.4739	6.435	10.725	0.5142
5.720	11.440	0.7579	6.435	11.440	0.4748
5.720	12.155	0.5092	6.435	12.155	0.2489
5.720	12.870	0.3390	6.435	12.870	0.1818
5.720	13.585	0.3046	6.435	13.585	0.2976
5.720	14.300	0.4712	6.435	14.300	0.1357

Table C.1 (Continued) Permeability Data

Measured at the Bottom Surface of the Rock Sample.

X	Y	Log K	X	Y	Log K
7.150	0.000	0.1709	7.865	0.000	0.1835
7.150	0.715	0.1507	7.865	0.715	0.2310
7.150	1.430	0.2361	7.865	1.430	0.3262
7.150	2.145	0.1909	7.865	2.145	0.2296
7.150	2.860	0.3093	7.865	2.860	0.2883
7.150	3.575	0.2159	7.865	3.575	0.2172
7.150	4.290	0.3347	7.865	4.290	0.5848
7.150	5.005	0.5036	7.865	5.005	0.4523
7.150	5.720	0.6592	7.865	5.720	0.2291
7.150	6.435	0.5126	7.865	6.435	0.0804
7.150	7.150	0.2702	7.865	7.150	0.1437
7.150	7.865	0.2931	7.865	7.865	0.1117
7.150	8.580	0.3651	7.865	8.580	0.3973
7.150	9.295	0.6679	7.865	9.295	0.3529
7.150	10.010	0.6427	7.865	10.010	0.2479
7.150	10.725	0.1866	7.865	10.725	0.1038
7.150	11.440	0.2347	7.865	11.440	0.2179
7.150	12.155	0.1076	7.865	12.155	0.1816
7.150	12.870	0.1560	7.865	12.870	0.3727
7.150	13.585	0.1661	7.865	13.585	0.6759
7.150	14.300	0.1749	7.865	14.300	0.2255

Table C.1 (Continued) Permeability Data

Measured at the Bottom Surface of the Rock Sample.

X	Y	Log K	X	Y	Log K
8.580	0.000	0.0676	9.295	0.000	0.1815
8.580	0.715	0.0680	9.295	0.715	0.1649
8.580	1.430	0.1141	9.295	1.430	0.1457
8.580	2.145	0.2072	9.295	2.145	0.2683
8.580	2.860	0.2526	9.295	2.860	0.3746
8.580	3.575	0.1716	9.295	3.575	0.3337
8.580	4.290	0.1847	9.295	4.290	0.4998
8.580	5.005	0.3467	9.295	5.005	0.6220
8.580	5.720	0.3401	9.295	5.720	0.5469
8.580	6.435	0.0837	9.295	6.435	0.1448
8.580	7.150	0.0807	9.295	7.150	0.0755
8.580	7.865	0.1041	9.295	7.865	0.1181
8.580	8.580	0.1622	9.295	8.580	0.1944
8.580	9.295	0.2328	9.295	9.295	0.1050
8.580	10.010	0.3789	9.295	10.010	0.2473
8.580	10.725	0.2724	9.295	10.725	0.1400
8.580	11.440	0.5729	9.295	11.440	0.1994
8.580	12.155	0.8264	9.295	12.155	0.2082
8.580	12.870	0.4353	9.295	12.870	0.1714
8.580	13.585	0.3575	9.295	13.585	0.2257
8.580	14.300	0.6600	9.295	14.300	0.1357

Table C.1 (Continued) Permeability Data

Measured at the Bottom Surface of the Rock Sample.

X	Y	Log K	X	Y	Log K
10.010	0.000	0.1092	10.725	0.000	0.1293
10.010	0.715	0.2197	10.725	0.715	0.1103
10.010	1.430	0.2192	10.725	1.430	0.1725
10.010	2.145	0.2198	10.725	2.145	0.0852
10.010	2.860	0.2254	10.725	2.860	0.1071
10.010	3.575	0.3001	10.725	3.575	0.0863
10.010	4.290	0.4531	10.725	4.290	0.1328
10.010	5.005	0.4522	10.725	5.005	0.1194
10.010	5.720	0.3649	10.725	5.720	0.1519
10.010	6.435	0.2254	10.725	6.435	0.3067
10.010	7.150	0.2365	10.725	7.150	0.3638
10.010	7.865	0.5098	10.725	7.865	0.4757
10.010	8.580	0.4049	10.725	8.580	0.3618
10.010	9.295	0.1574	10.725	9.295	0.0839
10.010	10.010	0.0941	10.725	10.010	0.0939
10.010	10.725	0.2068	10.725	10.725	0.0648
10.010	11.440	0.3101	10.725	11.440	0.0664
10.010	12.155	0.1800	10.725	12.155	0.1081
10.010	12.870	0.1346	10.725	12.870	0.0686
10.010	13.585	0.1599	10.725	13.585	0.0790
10.010	14.300	0.1080	10.725	14.300	0.0595

Table C.1 (Continued) Permeability Data

Measured at the Bottom Surface of the Rock Sample.

X	Y	Log K	X	Y	Log K
11.440	0.000	0.2189	12.155	0.000	0.1924
11.440	0.715	0.3913	12.155	0.715	0.2428
11.440	1.430	0.3203	12.155	1.430	0.3422
11.440	2.145	0.4515	12.155	2.145	0.3330
11.440	2.860	0.2598	12.155	2.860	0.1433
11.440	3.575	0.1285	12.155	3.575	0.1092
11.440	4.290	0.1807	12.155	4.290	0.1433
11.440	5.005	0.2078	12.155	5.005	0.1533
11.440	5.720	0.2549	12.155	5.720	0.2255
11.440	6.435	0.3162	12.155	6.435	0.1279
11.440	7.150	0.4032	12.155	7.150	0.1094
11.440	7.865	0.3369	12.155	7.865	0.1994
11.440	8.580	0.2600	12.155	8.580	0.1895
11.440	9.295	0.1605	12.155	9.295	0.1445
11.440	10.010	0.1897	12.155	10.010	0.1807
11.440	10.725	0.2143	12.155	10.725	0.2212
11.440	11.440	0.1424	12.155	11.440	0.2069
11.440	12.155	0.1122	12.155	12.155	0.1657
11.440	12.870	0.1364	12.155	12.870	0.1200
11.440	13.585	0.1281	12.155	13.585	0.1581
11.440	14.300	0.2576	12.155	14.300	0.4627

Table C.1 (Continued) Permeability Data

Measured at the Bottom Surface of the Rock Sample.

X	Y	Log K	X	Y	Log K
12.870	0.000	0.4561	13.585	0.000	0.2446
12.870	0.715	0.2085	13.585	0.715	0.1773
12.870	1.430	0.2002	13.585	1.430	0.3339
12.870	2.145	0.1414	13.585	2.145	0.1426
12.870	2.860	0.1401	13.585	2.860	0.5264
12.870	3.575	0.2223	13.585	3.575	0.4660
12.870	4.290	0.2415	13.585	4.290	0.2341
12.870	5.005	0.2145	13.585	5.005	0.2526
12.870	5.720	0.1985	13.585	5.720	0.2545
12.870	6.435	0.1595	13.585	6.435	0.1612
12.870	7.150	0.1448	13.585	7.150	0.2967
12.870	7.865	0.2184	13.585	7.865	0.2856
12.870	8.580	0.3034	13.585	8.580	0.2865
12.870	9.295	0.2236	13.585	9.295	0.2743
12.870	10.010	0.1864	13.585	10.010	0.1157
12.870	10.725	0.1682	13.585	10.725	0.1422
12.870	11.440	0.0861	13.585	11.440	0.1476
12.870	12.155	0.0330	13.585	12.155	0.2037
12.870	12.870	0.1064	13.585	12.870	0.1997
12.870	13.585	0.1907	13.585	13.585	0.2807
12.870	14.300	0.1201	13.585	14.300	0.1847

Table C.1 (Continued) Permeability Data

Measured at the Bottom Surface of the Rock Sample.

X	Y	Log K
14.300	0.000	0.3248
14.300	0.715	0.2923
14.300	1.430	0.3851
14.300	2.145	0.4004
14.300	2.860	0.2443
14.300	3.575	0.3764
14.300	4.290	0.2697
14.300	5.005	0.1572
14.300	5.720	0.1952
14.300	6.435	0.2884
14.300	7.150	0.2801
14.300	7.865	0.1965
14.300	8.580	0.2113
14.300	9.295	0.2277
14.300	10.010	0.1340
14.300	10.725	0.1396
14.300	11.440	0.1668
14.300	12.155	0.1233
14.300	12.870	0.0810
14.300	13.585	0.0774
14.300	14.300	0.1260

Table C.1 (Continued) Permeability Data
Measured at the Bottom Surface of the Rock Sample.

Appendix D

```
C     ****************************************************************
C     *                                                              *
C     * THIS PROGRAM COMPUTES TRACER CONCENTRATION DISTRIBUTION OF   *
C     * OF A HOMOGENEOUS\HETEROGENEOUS PATTERN WITH TWO WELL SYSTEM. *
C     * THE PROGRAM CAN HANDLE LONGITUDINAL DISPERSION, TRANSVERSE   *
C     * DISPERSION AND NO DISPERSION.                                *
C     *                                                              *
C     ****************************************************************
C
C                          PREPARED BY
C
C                       SALEEM GHOUS KHAN GHORI
C               NEW MEXICO INSTITUTE OF MINING AND TECHNOLOGY
C                          MAY 1992
C
C
C_____________________________________________________________________
C
C     NOMENCLATURE :
C
C     C       _ CONCENTRAION
C     S       _ DISTANCE ALONG STREAMLINES
C     VR      _ MAGNITUDE OF THE DARCY VELOCITY
C     VD      _ DISPLACEMENT VELOCITY
C     LAML    _ LONGITUDINAL DISPERSIVITY CONSTANT
C     LAMT    _ TRANSVERSE DISPERSIVITY CONSTANT
C     DL      _ LONGITUDINAL DISPERSION COEFFICIENT
C     DT      _ TRANSVERSE DISPERSION COEFFICIENT
C     DDL     _ DERIVATIVE OF LONGITUDINAL DISPERSION COFFICIENT
C     DDT     _ DERIVATIVE OF TRANSVERSE DISPERSION COFFICIENT
C     PDCX    _ FIRST DERIVATIVE OF CONCENTRATION IN X-DIRECTION
C     PDCY    _ FIRST DERIVATIVE OF CONCENTRATION IN Y-DIRECTION
C     PDDCX   _ SECOND DERIVATIVE OF CONCENTRATION IN X-DIRECTION
C     PDDCY   _ SECOND DERIVATIVE OF CONCENTRATION IN Y-DIRECTION
C     Q       _ FLOW RATE
C     H       _ THICKNESS OF THE FORMATION
C     PERM    _ PERMEABILITY
C     MU      _ VISCOSITY
C     SW      _ INITIAL WATER SATURATION IN THE RESERVOIR
C     FF      _ FORMATION RESISTIVITY FACTOR
C     DFC     _ MOLECULAR DIFFUSION COEFFICIENT
C     PHI     _ POROSITY OF THE FORMATION
C     AP      _ DISTANCE BETWEEN PRODUCTION/INJECTION WELLS
C     DI      _ DISTANCE BETWEEN INJECTOR AND PRODUCER
C     AREA    _ AREA OF THE PATTERN
C     T       _ TIME
C     VC      _ VOLUME CORRECTION FACTOR
C     VOLR    _ VOLUME OF TRACER IN A STREAMTUBE
C     TVOL    _ TOTAL VOLUME OF TRACER
C     BW      _ TRACER BAND WIDTH
C     CPK     _ PEAK CONCENTRATION
C     WST     _ WIDTH OF THE STREAMTUBE
C     TBT     _ BREAKTHROUGH TIME OF A STREAMLINE
C     VPDBT   _ BREAKTHROUGH PORE VOLUME
C     HINV    _ SCALE FACTOR IN COORDINATE TRANSFORMATIONS
```

```
      PROGRAM NUMURKLP


      INTEGER NST,NISO(100),JL(100),JR(100),NH,ICNS(100)
      COMMON /COMNST/NST,NISO,JL,JR,NH,ICNS
      INTEGER GONE(100)
      COMMON /PTGONE/GONE
      REAL C(100,17),S(100,17)
      COMMON /COMCS/C,S
      REAL SCEN(100),VRCEN(100),POTCEN(100)
      COMMON /CENTRE/SCEN,VRCEN,POTCEN
      REAL VMAX,PMAX,DMAX,HMAX,SMAX
      COMMON /MAXIMUM/ VMAX,PMAX,DMAX,HMAX,SMAX
      INTEGER ICONE(100),ICJR1(100),ICJR2(100),ICJL(100),ICJR(100),
     &        ICTRE(100),ICEN(100)
      COMMON /CONDITION/ ICONE,ICJR1,ICJR2,ICJL,ICJR,ICTRE,ICEN
      REAL BLR(100),BW(100)
      COMMON /BAND/BLR,BW
      INTEGER QU,RNUM
      COMMON /ITER/RNUM,ITL
      REAL AVOLR,AVOLIN,VOL(100),VOLIN(100),TVOL
      COMMON /VOLUME/AVOLR,AVOLIN,VOL,VOLIN,TVOL
      REAL CPK(100)
      COMMON /PEAK/CPK
      COMMON /DTIME/DTA,DTB
      COMMON /STABLE/NTIM,IMAX,JMAX
      COMMON/NUMG/NX,NY
      REAL LAML,LAMT
      LOGICAL BREAKT,COMPLT
      COMMON /COMLOG/BREAKT,COMPLT
      CHARACTER *16 PRES,PERM,VEL,ORIGHT,OLEFT


      NX = 151
      NY = 151
      IMAX = 1


      OPEN (UNIT=7,FILE='INPUTF')
      IRUN = 1

1     IF (IRUN .LE. 1) THEN
      OPEN (UNIT=7,FILE='INPUTF',ACCESS='SEQUENTIAL')

      COMPLT = .FALSE.

      READ(7,*)PRES
      READ(7,*)PERM
      READ(7,*)VEL
      READ(7,*)ORIGHT
      READ(7,*)OLEFT
      READ(7,*)LAML

      OPEN (UNIT=3,FILE=PRES)
      OPEN (UNIT=4,FILE=PERM)
      OPEN (UNIT=10,FILE=VEL)
      OPEN (UNIT=12,FILE=ORIGHT)
```

```
      OPEN (UNIT=8,FILE=OLEFT)

C     OPEN (UNIT=7,FILE='ST501.DAT')
C     OPEN (UNIT=8,FILE='FRONT501.DAT')
C     OPEN (UNIT=11,FILE='F501.DAT')


      BREAKT = .FALSE.
      RFAR = 10000.0
      NTIM = 1

      CALL INIT(LAML,LAMT,CR,NMID,G,WVCOF,PHI,T,QU,NIS,ALP,
     &          VC)

      KK = 1

      CALL VARBLE(T,NIS)
      CALL CENTER
      CALL DERIVP(KK,LAML,CR,G)
      CALL TPEAK(NIS)

      ITL = 1

      CALL STWITH
      CALL VOLUME(WVCOF)



10    IF (COMPLT .EQ. .FALSE.) THEN
      CALL FLUSH
          RTAR = S(1,1)+.5
          ITL = 1
          K1 = 0
          CALL DELTIM (DLT,1,PHI)

20        IF (S(1,1) .LT. RTAR .AND. COMPLT .EQ. .FALSE.) THEN
              K1 = K1+1
              ITL = ITL+1


              IF (K1 .EQ. KK) THEN
                  K1 = 0
                  CALL DELTIM (DLT,1,PHI)
              ENDIF

               CALL VARBLE(T,NIS)
               IF(COMPLT) GO TO 50
               CALL CENTER
               CALL DERIVP(KK,LAML,CR,G)
C              CALL DERSIH(NMID,G,LAMT)

               CALL MOVE (DLT,CR,NMID,T,QU,NIS)
               CALL TPEAK(NIS)

              IF (MOD(ITL,10) .EQ. 0) THEN
                  CALL STWITH
                  CALL VOLUME(WVCOF)
```

```
                IF ( ICONE(NMID) .EQ. 0 ) THEN
                IF (MOD(ITL,20) .EQ. 0) THEN
                    CALL CRECTV(ALP,VC)
                END IF
                END IF

                ENDIF

50      CONTINUE
                    GOTO 20
            ENDIF

              IF(COMPLT) GO TO 75

              IF ( MOD(RNUM,20) .EQ. 0 ) CALL FRONT(T)

                    CALL STWITH
                    CALL VOLUME(WVCOF)
                    CALL TPEAK(NIS)

            WRITE(6,*)'                                ITL = ',ITL
            WRITE(6,*)' Total Volume of Tracer =  ',TVOL
            WRITE(6,500)RNUM, GONE(1), CPK(1), BW(1)
            WRITE(6,*)IMAX,'  ',JMAX,' SMAX=',SMAX,' VMAX=',VMAX
            WRITE(6,200)DLT, SCEN(45), T, VOL(1)

            RNUM = RNUM+1
75      CONTINUE

            GOTO 10
        ENDIF


        IRUN = IRUN+1
        GO TO 1

        END IF
        STOP

100     FORMAT (1X,'SCEN= ',F10.5)
200     FORMAT (1X,' DLT= ',F10.6,' SCEN= ',F12.6,', T= ',F12.6,
     1  ' V= ',F7.4)
300     FORMAT (1X,' ITL = ',I5,'CPK = ',F12.7,', BW = ',F14.7,
     1  ', ALP= ',F12.6)
500     FORMAT (1X,'RNUM = ',I3,'     GONE= ',I3,', CPK= ',F14.7
     1  ,', BW= ',F14.7)
600     FORMAT(1X,I3,3X,F10.6,3X,F10.6,3X,F10.6,3X,F10.6,3X,I3)
        END


C-----------------------------------------------------------------------
C
C       SUBROUTINE INIT :
C       READ INPUT DATA FROM THE TERMINAL
C       CALCULATES INITIAL CONCENTRATION DISTRIBUTION AS A " RAMP UP AND
C       RAMP DOWN ".
C-----------------------------------------------------------------------
C
```

```
      SUBROUTINE INIT (LAML,LAMT,CR,NMID,G,WVCOF,PHI,T,QU,NIS,
     &                 ALP,VC)

      INTEGER NST,NISO(100),JL(100),JR(100),NH,ICNS(100)
      COMMON /COMNST/NST,NISO,JL,JR,NH,ICNS
      INTEGER GONE(100),INK
      COMMON /PTGONE/GONE
      REAL C(100,17),S(100,17)
      COMMON /COMCS/C,S
      INTEGER ICONE(100),ICJR1(100),ICJR2(100),ICJL(100),ICJR(100),
     &        ICTRE(100),ICEN(100)
      COMMON /CONDITION/ ICONE,ICJR1,ICJR2,ICJL,ICJR,ICTRE,ICEN
      REAL VMAX,PMAX,DMAX,HMAX,SMAX
      COMMON /MAXIMUM/ VMAX,PMAX,DMAX,HMAX,SMAX
      REAL SCEN(100),VRCEN(100),POTCEN(100)
      COMMON /CENTRE/SCEN,VRCEN,POTCEN
      COMMON /SATWITH/SW,H
      REAL TIN(100),TFIN(100),TPK(100),TP(100,17)
      COMMON /FINAL/TIN,TFIN,TPK,TP
      REAL CPK(100)
      COMMON /PEAK/CPK
      REAL BLR(100),BW(100)
      COMMON /BAND/BLR,BW
      COMMON /REMAIN/NSTR,INK

      REAL LAML,LAMT
      INTEGER QU

      PI = 3.141592654
      CFPB = 5.615
      DIN = .4
      CR = 1.414
      NIS = 17

      WRITE(6,100)
      READ(5,*) Q

      WRITE(6,200)
      READ(5,*) H

      WRITE(6,300)
      READ(5,*) PHI

      PHI = .26

      WRITE(6,400)
      READ(5,*) SW

      SW = .55

      WRITE(6,500)
      READ(5,*) FF

      FF = 38.0

      WRITE(6,6000)
      READ(5,*) DFC
```

```
      WRITE(6,700)
      READ(5,*) LAML

      PK = 1500.
      AMU = 20.0
      WT = PI*H*PHI*SW/(Q*CFPB)


      BB = DFC/(PHI*FF)
      WVCOF = (H*PHI*SW)/CFPB

      AD = 150.0
      AP = 300.

      AREA = AP*AP
      TD = .016667
      NSTR = 89
      NST = 89
      NMID = (NST/2)+1
      G = .35
      QU = 4

      NH = 2*QU
      BR = .1
      NISO(1) = 4*QU+1
      GONE(1) = 0
      JL(1) = NH+1
      JR(1) = NH+1

      DO 2 I = 1,NST
       NISO(I) = NISO(1)
       JL(I) = JL(1)
       JR(I) = JR(1)
       GONE(I) = GONE(1)
       BLR(I) = BR
       TPK(I) = 0.0
       TIN(I) = 0.0
       TFIN(I) = 0.0
       ICONE(I) = 0
       ICJR1(I) = 0
       ICJR2(I) = 0
       ICJL(I) = 0
       ICJR(I) = 0
       ICTRE(I) = 0
       ICEN(I) = 0
       ICNS(I) = 0
2     CONTINUE

C  WHILE GONE IS ZERO

      VC = 1.0E-8
      ALP = 1.0
      VMAX = 1290.0
      PMAX = 5.0
      HMAX = .000043
      DMAX = 103.0
```

```
      VPD = (Q*TD)/(AREA*H*PHI*SW)
      WT = (2.*PI*H*PHI*SW)/(Q*CFPB)

      RFT = SQRT(TD/WT)
      RF = SQRT(TD/WT+DIN*(1.5+0.25*DIN)+1.0) - 1.5*DIN - 1.15
      RH = 1.5+DIN+RF/2.0

C  DIN IS RADIAL THICKNESS OF FRONT AND BACK RAMPS ON CONCENTRATION
C  DISTRIBUTION.  RF IS RADIAL THICKNESS OF FLAT TOP PORTION.

      DR = DIN/(NH+1)
      FC = 1.0/(NH+1)

      DO 10, J = 1,NH
          S(1,J) = 1.5+J*DR
          C(1,J) = J*FC
      WRITE(6,*)S(1,J),C(1,J)
10    CONTINUE

      S(1,NH+1) = RH
      C(1,NH+1) = 1.0
      WRITE(6,*)S(1,NH+1),C(1,NH+1)

      DO 20, J = NH+2, NIS
          S(1,J) = 1.5+DIN+RF+(J-NH-1)*DR
          C(1,J) = 1.0-(J-NH-1)*FC
      WRITE(6,*)S(1,J),C(1,J)
20    CONTINUE
      SCEN(1) = (S(1,NH)+S(1,NH+2))/2.0
      S(1,NH+1) = SCEN(1)
      T = 2.0*WT*SCEN(1)**2

C  THIS T IS STARTING VALUE NOT 0, BUT TO CENTER OF INITIAL TRACER SLUG


      DO 101 I = 1,NST
       DO 50 J = 1,NIS
        IF ( J .LE. JL(I) .OR.  J .GE. JR(I)) THEN
         S(I,J) = S(1,J)
         C(I,J) = C(1,J)
         TP(I,J) = 0.0
        END IF
50     CONTINUE
       SCEN(I) = SCEN(1)
       C(I,NH+1) = 1.0
       CPK(I) = 1.0
101   CONTINUE
      PARAME = 1./(AMU*PHI*SW)

      CALL DVEL(AD,AP,Q,BB,LAML,LAMT,NST,PARAME,PHI,PK)

      RETURN
100   FORMAT(1X,'ENTER FLOW RATE IN STRATUM (BPD) ')
200   FORMAT(1X,'ENTER THICKNESS OF STRATUM (FEET) ')
300   FORMAT(1X,'ENTER POROSITY OF STRATUM ')
400   FORMAT(1X,'ENTER CONATE WATER SATURATION ')
500   FORMAT(1X,'ENTER FORMATION RESISTIVITY FACTOR ')
600   FORMAT(1X,'ENTER MOLECULAR DIFFUSION COEF. (SQ FT/DAY) ')
```

```
700     FORMAT(1X,'ENTER CHAR. LENGTH FOR DISPERSIVITY (FEET) ')
800     FORMAT(1X,'ENTER LARGEST RADIUS FOR COMPUTATIONS (FEET) ')
900     FORMAT(1X,'ENTER AREA OF THE PATTERN ')
1000    FORMAT(1X,'WANT CONC. DISTRIBUTION LISTED IN WRITPROF (Y/N)? ')

        END
```

```
C-----------------------------------------------------------------------
C
C       SUBROUTINE DERIVP :
C       COMPUTES 1ST AND 2ND DERIVATIVES OF CONCENTRATION WITH RESPECT
C       TO X WHILE  THE FLAT TOP EXISTS. AFTER THE FLAT TOP DISAPPEARS
C       CALLS SUBROUTINE DERPHI.
C-----------------------------------------------------------------------

        SUBROUTINE DERIVP(KK,LAML,CR,G)

        INTEGER NST,NISO(100),JL(100),JR(100),NH,ICNS(100)
        COMMON /COMNST/NST,NISO,JL,JR,NH,ICNS
        INTEGER GONE(100)
        COMMON /PTGONE/GONE
        REAL C(100,17),S(100,17)
        COMMON /COMCS/C,S
        REAL PDCX(100,17),PDDCX(100,17),DDL(100,17)
        COMMON /DERIVX/PDCX,PDDCX,DDL
        REAL P(100,17),VR(100,17)
        COMMON /PRESS/P,VR
        REAL SCEN(100),VRCEN(100),POTCEN(100)
        COMMON /CENTRE/SCEN,VRCEN,POTCEN
        INTEGER ICONE(100),ICJR1(100),ICJR2(100),ICJL(100),ICJR(100),
     &          ICTRE(100),ICEN(100)
        COMMON /CONDITION/ ICONE,ICJR1,ICJR2,ICJL,ICJR,ICTRE,ICEN
        REAL LAML


        PD1MX = 0.0

        DO 20 I = 1,NST
          IF (ICNS(I) .NE. 0 ) GO TO 20
        IC = I
        IF (GONE(I) .EQ. 0) THEN
            DO 10, J = 2, NISO(I)-1
                RDL = P(I,J)-P(I,J-1)
                RDR = P(I,J+1)-P(I,J)
                IF (J .EQ. NH) RDR = CR*RDL
                IF (J .EQ. NH+2) RDL = CR*RDR
                DLD = (C(I,J)-C(I,J-1))/RDL
                DR = (C(I,J+1)-C(I,J))/RDR
                PDCX(I,J) = (DLD+DR)/2.0
                VDL = VR(I,J)-VR(I,J-1)
                VDR = VR(I,J+1)-VR(I,J)
                PDL = P(I,J)-P(I,J-1)
                PDR = P(I,J+1)-P(I,J)
                DXL = VDL/PDL
                DXR = VDR/PDR
                DVRX = (DXL+DXR)/2.0
                DDL(I,J) = LAML*DVRX

                IF (J .EQ. NH+1) THEN
                    PDCX(I,J) = 0.0
                    PDDCX(I,J) = 0.0
                    DDL(I,J) = 0.0
                ENDIF
```

```
                IF (ABS(PDCX(I,J)) .GT. PD1MX) PD1MX = ABS(PDCX(I,J))

                PDDCX(I,J) = 2.0*(DR-DLD)/(RDL+RDR)

                IF (J .EQ. 2) THEN
                    PDCX(I,1) = DLD/2.
                    PDDCX(I,1) = DLD*G/RDL
                    DDL(I,1) = LAML*DXL
                ENDIF

                IF (J .EQ. NISO(I)-1) THEN
                    PDCX(I,NISO(I)) = DR/2.0
                    PDDCX(I,NISO(I)) = -DR*G/RDR
                    DDL(I,NISO(I)) = LAML*DXR
                ENDIF

10          CONTINUE
            ELSE
               IF (ICTRE(I) .EQ. 0 ) THEN
                CALL  DERPHI(IC,KK,LAML,G,CR)
               END IF
            ENDIF
20          CONTINUE
            IF (PD1MX .LT. 1.0) KK = 10

            RETURN

            END
```

```
C
C-----------------------------------------------------------------------
C       SUBROUTINE DERPHI :
C               THIS SUBROUTINE COMPUTES THE FIRST AND SECOND DERIVATIVES
C       OF CONCENTRATION IN THE LONGITUDINAL DIRECTION.
C-----------------------------------------------------------------------
C
        SUBROUTINE DERPHI(I,KK,LAML,G,CR)

        INTEGER NST,NISO(100),JL(100),JR(100),NH,ICNS(100)
        COMMON /COMNST/NST,NISO,JL,JR,NH,ICNS
        REAL C(100,17),S(100,17)
        COMMON /COMCS/C,S
        INTEGER ICONE(100),ICJR1(100),ICJR2(100),ICJL(100),ICJR(100),
     &          ICTRE(100),ICEN(100)
        COMMON /CONDITION/ ICONE,ICJR1,ICJR2,ICJL,ICJR,ICTRE,ICEN
        REAL PDCX(100,17),PDDCX(100,17),DDL(100,17)
        COMMON /DERIVX/PDCX,PDDCX,DDL
        REAL P(100,17),VR(100,17)
        COMMON /PRESS/P,VR
        REAL SCEN(100),VRCEN(100),POTCEN(100)
        COMMON /CENTRE/SCEN,VRCEN,POTCEN
        REAL LAML,LDY

        PD1MX = 0.0

         DO 100 J = 2,NISO(I)-1

          IF (J .LT. JL(I) .OR. J .GT. JR(I)) THEN
                VDL = VR(I,J)-VR(I,J-1)
                VDR = VR(I,J+1)-VR(I,J)
                PDL = P(I,J)-P(I,J-1)
                PDR = P(I,J+1)-P(I,J)
                DXL = VDL/PDL
                DXR = VDR/PDR
                DVRX = (DXL+DXR)/2.0
                DDL(I,J) = LAML*DVRX
                CDL = C(I,J)-C(I,J-1)
                CDR = C(I,J+1)-C(I,J)
            DLU = CDL/PDL
            DRU = CDR/PDR
            PDCX(I,J) = (DLU+DRU)/2.0
            PDDCX(I,J) = 2.0*(DRU-DLU)/(PDL+PDR)

            IF ( ABS(PDCX(I,J)) .GT. PD1MX ) PD1MX = ABS(PDCX(I,J))

                IF (J .EQ. 2) THEN
                    PDCX(I,1) = DLU/2.0
                    PDDCX(I,1) = G*DLU/PDL
                    DDL(I,1) = LAML*DXL
                ENDIF

                IF (J .EQ. NISO(I)-1) THEN
                    PDCX(I,NISO(I)) = DRU/2.0
                    PDDCX(I,NISO(I)) = -G*DRU/PDR
                    DDL(I,NISO(I)) = LAML*DXR
                ENDIF
```

```
          END IF

100       CONTINUE

          IF (ICJR(I) .EQ. 1 ) RETURN

          IF ( ICJR1(I) .EQ. 0 ) THEN
           USX =  P(I,JR(I))-P(I,JL(I))
           UBX = P(I,JR(I)+1)-P(I,JL(I)-1)
           RDY = - C(I,JR(I)+1)+C(I,JR(I))
           LDY =  C(I,JL(I))-C(I,JL(I)-1)
           UCZ = 4.0/(UBX*UBX-USX*USX)
           PDCX(I,JL(I)) = LDY*UCZ*USX
           PDCX(I,JR(I)) = -RDY*UCZ*USX
           PDDCX(I,JL(I)) = -2.0*LDY*UCZ
           PDDCX(I,JR(I)) = -2.0*RDY*UCZ
           VDL = VR(I,JL(I))-VR(I,JL(I)-1)
           VDR = VRCEN(I)-VR(I,JL(I))
           PDL = P(I,JL(I))-P(I,JL(I)-1)
           PDR = POTCEN(I)-P(I,JL(I))
                 DXL = VDL/PDL
                 DXR = VDR/PDR
                 DVRX = (DXL+DXR)/2.0
                 DDL(I,JL(I)) = LAML*DVRX
           VDL = VR(I,JR(I))-VRCEN(I)
           VDR = VR(I,JR(I)+1)-VR(I,JR(I))
           PDL = P(I,JR(I))-POTCEN(I)
           PDR = P(I,JR(I)+1)-P(I,JR(I))
                 DXL = VDL/PDL
                 DXR = VDR/PDR
                 DVRX = (DXL+DXR)/2.0
                 DDL(I,JR(I)) = LAML*DVRX

          ELSE
           DEN = (POTCEN(I)-P(I,JL(I)-1))**2-(POTCEN(I)-
     &     P(I,JL(I)))**2
           PDCX(I,JL(I)) = (2.*(C(I,JL(I))-C(I,JL(I)-1))/DEN)*
     &     (POTCEN(I)-P(I,JL(I)))
           PDDCX(I,JL(I))= -2.*(C(I,JL(I))-C(I,JL(I)-1))/DEN
           PDCX(I,JR(I)) = -PDCX(I,JL(I))
           PDDCX(I,JR(I)) = -PDDCX(I,JL(I))
          END IF

          IF (ICJR2(I) .EQ. 1 ) THEN
           DIFE =  P(I,JR(I)+1)-P(I,JR(I))
           PDCX(I,JR(I)+1) = (C(I,JR(I)+1)-C(I,JR(I)))/DIFE
           PDDCX(I,JR(I)+1) = G*PDCX(I,JR(I)+1)/DIFE
          END IF

          IF (PD1MX .LT. 1.0) KK = 10

          RETURN

          END
```

```
C-----------------------------------------------------------------------
C       SUBROUTINE DERSIH :
C               THIS SUBROUTINE CALCULATES THE CONCENTRATION GRADIENT IN
C       THE TRANSVERSE DIRECTION.
C-----------------------------------------------------------------------
C
        SUBROUTINE DERSIH(NMID,G,LAMT)

        INTEGER NST,NISO(100),JL(100),JR(100),NH,ICNS(100)
        COMMON /COMNST/NST,NISO,JL,JR,NH,ICNS
        REAL C(100,17),S(100,17)
        COMMON /COMCS/C,S
        REAL PDCY(100,17),PDDCY(100,17),DDT(100,17)
        COMMON /DERIVY/PDCY,PDDCY,DDT
        REAL P(100,17),VR(100,17)
        COMMON /PRESS/P,VR
        REAL SIGH(0:100)
        COMMON /ANGLES/SIGH
        REAL LAMT


        IF ( S(NMID,1) .LE. 3.0 ) THEN
          DO 20 I = 1,NST
            DO 10 J = 1,NISO(I)
              IF ( J .LE. JL(I) .OR. J .GE. JR(I) ) THEN
               PDCY(I,J) = 0.0
               PDDCY(I,J) = 0.0
               DDT(I,J) = 0.0
              END IF
10          CONTINUE
20        CONTINUE
          RETURN
        END IF

        DO 40 I = 2,NST-1
          IF (ICNS(I) .NE. 0 ) GOTO 40
            I1 = I
            DZ = SIGH(I)-SIGH(I-1)

            DO 30, J = 1, NISO(I)
              IF ( J .LE. JL(I) .OR. J .GE. JR(I) ) THEN
                I2 = J

                CALL WAVGC (I1,I2,C1,C2,VR1,VR2)

                PDCY(I,J) = (C2-C1)/(2.*DZ)
                PDDCY(I,J) = (C2-2.*C(I,J)+C1)/(DZ**2)
                DDT(I,J) = LAMT*ABS((VR2-VR1)/(2.*DZ))

                IF (I .EQ. 2) THEN
                    PDCY(1,J) =(C2-C(1,J))/DZ
                    PDDCY(1,J) =PDCY(1,J)*G/DZ
                    DDT(1,J) = LAMT*ABS((VR2-VR(1,J))/DZ)
                ENDIF

                IF (I .EQ. NST-1) THEN
```

```
                PDCY(NST,J) = (C(NST,J)-C1)/DZ
                PDDCY(NST,J) = PDCY(NST,J)*G/DZ
                DDT(NST,J) = LAMT*(VR(NST,J)-VR1)/DZ
              ENDIF
            END IF
30        CONTINUE
40      CONTINUE

        RETURN

        END
```

```
C
C-----------------------------------------------------------------------
C       SUBROUTINE WAVGC :
C               THIS SUBROUTINE IS CALLED FROM SUBROUTINE DERSIH. ROUTINE
C       CALCULATES THE VLUES OF THE WEIGHTED AVERAGE CONCENTRATION ON THE
C       ADJACENT STREAMLINES.
C-----------------------------------------------------------------------
C
        SUBROUTINE WAVGC (IN,JN,C1,C2,VR1,VR2)

        INTEGER NST,NISO(100),JL(100),JR(100),NH,ICNS(100)
        COMMON /COMNST/NST,NISO,JL,JR,NH,ICNS
        REAL C(100,17),S(100,17)
        COMMON /COMCS/C,S
        REAL PDCY(100,17),PDDCY(100,17),DDT(100,17)
        COMMON /DERIVY/PDCY,PDDCY,DDT
        REAL P(100,17),VR(100,17)
        COMMON /PRESS/P,VR
        REAL CPK(100)
        COMMON /PEAK/CPK
        REAL SCEN(100),VRCEN(100),POTCEN(100)
        COMMON /CENTRE/SCEN,VRCEN,POTCEN


        DP = P(IN,JN)


        I1 = IN-1
        IF ( DP .GT. P(I1,NISO(I1)) .OR. DP .LT. P(I1,1) ) THEN
           C1 = 0.0
           VR1 = 0.0
           GO TO 101
        END IF

           IK = 1
           IF (IK .GE. NISO(I1)) IK = 1
           IF (DP .LT. P(I1,IK)) GO TO 22
           IF (DP .LE. P(I1,IK+1)) GO TO 26
22         IK = 1
           JK = NISO(I1)+1
24         KC = (IK+JK)/2
           IF (DP .LT. P(I1,KC)) JK = KC
           IF (DP .GE. P(I1,KC)) IK = KC
           IF ( JK .GT. IK+1) GO TO 24
26         P1 = P(I1,IK)
           P2 = P(I1,IK+1)

           VA = VR(I1,IK)
           VB = VR(I1,IK+1)
           CA = C(I1,IK)
           CB = C(I1,IK+1)

           IF ( IK .EQ. JL(I1) ) THEN
            CB = CPK(I1)
            VB = VRCEN(I1)
```

```
          P2 = POTCEN(I1)
         ELSE IF ( IK .EQ. JL(I1) .AND. DP .GE. POTCEN(I1) ) THEN
          CA = CPK(I1)
          VA = VRCEN(I1)
          P1 = POTCEN(I1)
         END IF

         PA = ABS(DP-P1)
         PB = ABS(DP-P2)

         IF (PA .LT. PB) THEN
           C1 = (PB*CA+PA*CB)/(PA+PB)
           VR1 = (PB*VA+PA*VB)/(PA+PB)
         ELSE
           C1 = (PA*CA+PB*CB)/(PA+PB)
           VR1 = (PA*VA+PB*VB)/(PA+PB)
         END IF

101      I2 = IN+1

       IF ( DP .GT. P(I2,NISO(I2)) .OR. DP .LT. P(I2,1) ) THEN
         C2 = 0.0
         VR2 = 0.0
         RETURN
       END IF

         IK = 1
         IF (IK .GE. NISO(I2)) IK = 1
         IF (DP .LT. P(I2,IK)) GO TO 28
         IF (DP .LE. P(I2,IK+1)) GO TO 32
28       IK = 1
         JK = NISO(I2)+1
30       KC = (IK+JK)/2
         IF (DP .LT. P(I2,KC)) JK = KC
         IF (DP .GE. P(I2,KC)) IK = KC
         IF ( JK .GT. IK+1) GO TO 30

32       P1 = P(I2,IK)
         P2 = P(I2,IK+1)

         VA = VR(I2,IK)
         VB = VR(I2,IK+1)
         CA = C(I2,IK)
         CB = C(I2,IK+1)

         IF ( IK .EQ. JL(I2) ) THEN
          CB = CPK(I2)
          VB = VRCEN(I2)
          P2 = POTCEN(I2)
         ELSE IF ( IK .EQ. JL(I2) .AND. DP .GE. POTCEN(I2) ) THEN
          CA = CPK(I2)
          VA = VRCEN(I2)
          P1 = POTCEN(I2)
         END IF

         PA = ABS(DP-P1)
         PB = ABS(DP-P2)
```

```
  IF (PA .LT. PB) THEN
    C2 = (PB*CA+PA*CB)/(PA+PB)
    VR2 = (PB*VA+PA*VB)/(PA+PB)
  ELSE
    C2 = (PA*CA+PB*CB)/(PA+PB)
    VR2 = (PA*VA+PB*VB)/(PA+PB)
  END IF

RETURN
END
```

```
C-----------------------------------------------------------------------
C       SUBROUTINE DELTIM :
C              THIS SUBROUTINE DETERMINES THE TIME STABILITY CRITERIA
C       FOR THE NEXT POSITION OF THE ISOCONCENTRAION LINES.
C-----------------------------------------------------------------------
C
        SUBROUTINE DELTIM (DLT,NMID,PHI)

        INTEGER NST,NISO(100),JL(100),JR(100),NH,ICNS(100)
        COMMON /COMNST/NST,NISO,JL,JR,NH,ICNS
        REAL C(100,17),S(100,17)
        COMMON /COMCS/C,S
        REAL VMAX,PMAX,DMAX,HMAX,SMAX
        COMMON /MAXIMUM/ VMAX,PMAX,DMAX,HMAX,SMAX
        REAL SLAST(100),PLAST(100)
        COMMON /LASTV/SLAST,PLAST
        REAL SCEN(100),VRCEN(100),POTCEN(100)
        COMMON /CENTRE/SCEN,VRCEN,POTCEN
        INTEGER ICONE(100),ICJR1(100),ICJR2(100),ICJL(100),ICJR(100),
     &          ICTRE(100),ICEN(100)
        COMMON /CONDITION/ ICONE,ICJR1,ICJR2,ICJL,ICJR,ICTRE,ICEN
        COMMON /DTIME/DTA,DTB
        COMMON /STABLE/NTIM,IMAX,JMAX
        INTEGER RNUM,ITL
        COMMON /ITER/RNUM,ITL


C  CRITERION A TO KEEP QUADRATIC TAYLOR TERM SMALL

         IF (S(IMAX,1) .LE. SLAST(IMAX)/2. ) THEN
          DTA = .003*S(IMAX,1)/VMAX
         ELSE
          DTA = .004*(SLAST(IMAX)-S(IMAX,NISO(IMAX)))/VMAX
         END IF

C  CRITERION B IS TO MAINTAIN ARITHMETIC STABILITY

          DISPL = HMAX*DMAX/PMAX
          DTB = .001*PHI/DISPL

C  CRITERION C SETS MAX TIME INCREMENT TO BE PERMITTED

           DTC = .03


        IF ((DTA .LT. DTB) .AND. (DTA .LT. DTC)) THEN
            DLT = DTA
        ELSE
            IF (DTB .LT. DTC) THEN
                DLT = DTB
            ELSE
                DLT = DTC

            ENDIF
```

```
ENDIF


  IF( ICONE(NTIM) .EQ. 1 ) THEN
   DLT = .0055
  END IF

RETURN
END
```

```
C-----------------------------------------------------------------------
C       SUBROUTINE MOVE :
C              THIS SUBROUTINE COMUTES THE VELOCITY OF THE ISOCONCENTRATION
C       LINES AND ALSO DETERMINES THE CRITERIA FOR GIVING INCREMENT
C       TO THE VARIABLE INTEGER ' GONE '. A SUBROUTINE REDO IS CALLED IF
C       THE VALUE OF GONE EXCEEDS QU.
C-----------------------------------------------------------------------
C
        SUBROUTINE MOVE (DLT,CR,NMID,T,QU,NIS)

        INTEGER NST,NISO(100),JL(100),JR(100),NH,ICNS(100)
        COMMON /COMNST/NST,NISO,JL,JR,NH,ICNS
        INTEGER GONE(100)
        COMMON /PTGONE/GONE
        INTEGER QU,RNUM
        COMMON /ITER/RNUM,ITL
        REAL C(100,17),S(100,17)
        COMMON /COMCS/C,S
        INTEGER ICONE(100),ICJR1(100),ICJR2(100),ICJL(100),ICJR(100),
     &          ICTRE(100),ICEN(100)
        COMMON /CONDITION/ ICONE,ICJR1,ICJR2,ICJL,ICJR,ICTRE,ICEN
        REAL VMAX,PMAX,DMAX,HMAX,SMAX
        COMMON /MAXIMUM/ VMAX,PMAX,DMAX,HMAX,SMAX
        REAL PDCX(100,17),PDDCX(100,17),DDL(100,17)
        COMMON /DERIVX/PDCX,PDDCX,DDL
        REAL SLAST(100),PLAST(100)
        COMMON /LASTV/SLAST,PLAST
        REAL PDCY(100,17),PDDCY(100,17),DDT(100,17)
        COMMON /DERIVY/PDCY,PDDCY,DDT
        REAL DL(100,17),DT(100,17),HINV(100,17)
        COMMON /DISP/DL,DT,HINV
        REAL P(100,17),VR(100,17)
        COMMON /PRESS/P,VR
        REAL SCEN(100),VRCEN(100),POTCEN(100)
        COMMON /CENTRE/SCEN,VRCEN,POTCEN
        REAL BLR(100),BW(100)
        COMMON /BAND/BLR,BW
        COMMON /STABLE/NTIM,IMAX,JMAX
        REAL CPK(100)
        COMMON /PEAK/CPK

        REAL DISP(100,17),VD(100,17)

C       OPEN(UNIT=21,FILE='DERPHI.DAT')
C       OPEN(UNIT=22,FILE='DERSIH.DAT')
C       OPEN(UNIT=23,FILE='MOVE.DAT')
C       WRITE(21,1000)
C       WRITE(22,2000)
C       WRITE(23,2500)

        VMAX = 0.0

        DO 200 I = 1,NST

          IF (ICNS(I) .NE. 0 ) GOTO 200
```

```
C       WRITE(21,*)' I = ',I
C       WRITE(22,*)' I = ',I
C       WRITE(23,*)' I = ',I
        DO 100 J = 1,NISO(I)

         IF (J .LE. JL(I) .OR. J .GE. JR(I) )THEN

            DELC = SQRT(PDCX(I,J)**2+PDCY(I,J)**2)
            THETA = DELC/PDCX(I,J)

           IF ( J .EQ. NH+1) THEN
             DISP(I,J) = 0.0
           ELSE
             DISP(I,J) = HINV(I,J)*(DL(I,J)*PDDCX(I,J))/PDCX(I,J)
           END IF

             CONVEC = VR(I,J)
             VD(I,J) = CONVEC-DISP(I,J)
             DELS = VD(I,J)*DLT
             S(I,J) = S(I,J)+DELS

           IF ( VR(I,J) .GT. VMAX )THEN
             VMAX = VR(I,J)
             PMAX = (P(I,2)-P(I,1))**2
             HMAX = HINV(I,J)**2
             DMAX = DL(I,J)

            IF(J .EQ. NISO(I) .AND. NISO(I) .NE. 1 .OR.
     &         J .EQ. JL(I)) THEN
             SMAX = S(I,J)-S(I,J-1)
            ELSE
             SMAX = S(I,J+1)-S(I,J)
            ENDIF

             IMAX = I
             JMAX = J
           END IF

C            WRITE(21,1100)J,PDCX(I,J),PDDCX(I,J),DL(I,J),C(I,J),
C     &                    DELC
C            WRITE(22,1100)J,PDCY(I,J),PDDCY(I,J),DT(I,J),DDT(I,J),
C     &                    HINV(I,J)
C             WRITE(23,1100)J,S(I,J),P(I,J),CONVEC,DISP(I,J),VD(I,J)

         END IF

100      CONTINUE
200     CONTINUE
        T = T+DLT

        DO 300 I = 1,NST
         IF (ICNS(I) .NE. 0 ) GOTO 300
        ICOND = 0
        IJK = I
        SL = (S(I,JL(I))+S(I,JR(I)))/2.0
        SDM = S(I,JR(I))-S(I,JL(I))
        SDH = (S(I,JR(I)+1)-S(I,JR(I))+S(I,JL(I))-
     &  S(I,JL(I)-1))/4.0
```

```
          DIFER = S(I,JR(I))-S(I,JL(I))

         IF(GONE(I) .EQ. 0 ) THEN
           CALL FLADJ(IJK,CR)
         ELSE
           IF ( ICJR1(I) .EQ. 0 ) THEN
             FC = C(I,JL(I))-C(I,JL(I)-1)
             RCG1 = SQRT(.015*FC/BLR(I))
             RCG = SQRT(.05*FC/BLR(I))
             IF(DIFER .LE. RCG) ICOND = 3

             IF ( ICOND .EQ. 3 ) THEN
               IF (NISO(I) .EQ. JR(I)+1) ICJR1(I) = 1


               S(I,JL(I)) = SL
               S(I,JR(I)) = SL
               C(I,JL(I)) =-C(I,JL(I))
               C(I,JR(I)) =-C(I,JR(I))
               GONE(I) = GONE(I)+1
               JL(I) = NH-GONE(I)+1
               JR(I) = NH+GONE(I)+1

               IF ( ICONE(I) .EQ. 0 ) THEN
                IF (GONE(I).GT.QU.AND.SDM.LT.SDH)
     &              CALL REDO(IJK,T,CR,QU,NIS)
               ENDIF

             ENDIF

           END IF

         END IF

         SCEN(I) = (S(I,JL(I))+S(I,JR(I)))/2.0

          IF (ICJR(I) .EQ. 1 .AND. ICEN(I) .EQ. 0)THEN
            SCEN(I) = VRCEN(I)*DLT+SCEN(I)
          END IF

          IF ( ICEN(I) .EQ. 0)THEN

           IF ( POTCEN(I) .GE. PLAST(I))THEN
C            WRITE(6,*)' ### Center Point is Gone I = ',I
             ICEN(I) = 1
             POTCEN(I) = 0.0
           END IF

          END IF

300      CONTINUE

C        CLOSE(UNIT=21)
C        CLOSE(UNIT=22)
C        CLOSE(UNIT=23)


1000     FORMAT(2X,' J ',4X,' PDCX ',4X,' PDDCX ',4X,' DL ',9X,' CONC ',
```

```
     &        4X,' DELC ',/)
2000    FORMAT(2X,' J ',4X,' PDCY ',4X,' PDDCY ',4X,' DT ',9X,' DDT ',
     &        4X,' HINV ',/)
3000    FORMAT(2X,' J ',4X,' DIST ',4X,' VR ',4X,' CONVEC ',7X,'DISP',
     &        4X,' VD ',/)
1100    FORMAT(1X,I3,5(1X,F10.4))


        RETURN
        END
```

```
C
C-----------------------------------------------------------------
C
C       SUBROUTINE FLADJUST :
C       COMPARES SPACING OF POINTS AROUND PEAK, TO DETERMINE WHETHER GONE
C       SHOULD BE SET FROM 0 TO 1.ALSO, WHILE GONE IS 0 I.E. WHILE TRACER
C       BAND IS STILL FLAT EVALUATES RLT AND RRT FOR AREA AND VOLUME CALCS
C-----------------------------------------------------------------
C
        SUBROUTINE FLADJ(I,CR)

        INTEGER NST,NISO(100),JL(100),JR(100),NH,ICNS(100)
        COMMON /COMNST/NST,NISO,JL,JR,NH,ICNS
        INTEGER GONE(100)
        COMMON /PTGONE/GONE
        REAL C(100,17),S(100,17)
        COMMON /COMCS/C,S
        REAL SCEN(100),VRCEN(100),POTCEN(100)
        COMMON /CENTRE/SCEN,VRCEN,POTCEN

        RR2 = S(I,NH+3)
        RR1 = S(I,NH+2)
        RPK = S(I,NH+1)
        RL1 = S(I,NH)
        RL2 = S(I,NH-1)
        RLT = RL1+CR*(RL1-RL2)
        RRT = RR1-CR*(RR2-RR1)
        RL = (RL1+RR1)/2.0
        S(I,NH+1) = RL

        IF (ABS(RRT-RLT) .LE. .1) THEN
            GONE(I) = 1
            JL(I) = NH
            JR(I) = NH+2
            S(I,NH+1) = (RL1+RR1)/2.0
            C(I,NH+1) = -1.0
        ENDIF

        RETURN

100     FORMAT (1X,' ** ONE GONE **  ST. LINE NUMBER  ',I3)
200     FORMAT (1X,' RLT=',F14.7,' RPK=',F14.7,' RRT=',F14.7)

        END
```

```
C-----------------------------------------------------------------------
C       SUBROUTINE VARBLE :
C              THIS SUBROUTINE INTERPOLATES AND GIVE VALUES OF DARCY
C       VELOCITY, X & Y COORDINATES, POTENTIAL VALUES, LONGITUDINAL AND
C       TRANSVERSE DISPERSION, SCALE FACTOR, AT CORRESPONDING ISOCONCENTR_
C       ATION POINTS. ROUTINE ALSO KEEPS TRACK THE DISAPPEARENCE OF THE
C       ISOCONCENTRATION POINTS ON A PIRTICULAR STREAMLINE AT THE PRODUCTION
C       WELL. A SUBROUTINE OUTPUT IS THEN CALLED AFTER THE LAST STREAM
C       LINE HAS BROKENTHROUGH.
C-----------------------------------------------------------------------

        SUBROUTINE VARBLE(T,NIS)

        INTEGER NST,NISO(100),JL(100),JR(100),NH,ICNS(100)
        COMMON /COMNST/NST,NISO,JL,JR,NH,ICNS
        INTEGER GONE(100)
        COMMON /PTGONE/GONE
        REAL C(100,17),S(100,17)
        COMMON /COMCS/C,S
        REAL VXVAL(100,2500),VYVAL(100,2500),VVAL(100,2500)
        COMMON /COMVXY/VXVAL,VYVAL,VVAL
        INTEGER ICONE(100),ICJR1(100),ICJR2(100),ICJL(100),ICJR(100),
     &          ICTRE(100),ICEN(100)
        COMMON /CONDITION/ ICONE,ICJR1,ICJR2,ICJL,ICJR,ICTRE,ICEN
        REAL XVAL(100,2500),YVAL(100,2500)
        COMMON /XYCOORD/XVAL,YVAL
        REAL DLVAL(100,2500),DTVAL(100,2500),HVAL(100,2500)
        COMMON /DLDTHV/DLVAL,DTVAL,HVAL
        REAL DL(100,17),DT(100,17),HINV(100,17)
        COMMON /DISP/DL,DT,HINV
        REAL P(100,17),VR(100,17)
        COMMON /PRESS/P,VR
        INTEGER NS(100)
        COMMON /NPOINTS/NS
        REAL SVAL(100,2500),PVAL(100,2500)
        COMMON /DISPRES/SVAL,PVAL
        REAL SCEN(100),VRCEN(100),POTCEN(100)
        COMMON /CENTRE/SCEN,VRCEN,POTCEN
        REAL SLAST(100),PLAST(100)
        COMMON /LASTV/SLAST,PLAST
        REAL TIN(100),TFIN(100),TPK(100),TP(100,17)
        COMMON /FINAL/TIN,TFIN,TPK,TP
        REAL CPK(100)
        COMMON /PEAK/CPK
        INTEGER INK,IJK
        COMMON /REMAIN/NSTR,INK
        COMMON /STABLE/NTIM,IMAX,JMAX
        REAL X(100,17),Y(100,17),VX(100,17),VY(100,17)
        REAL DIF(100)
        LOGICAL BREAKT,COMPLT
        COMMON /COMLOG/BREAKT,COMPLT

        DO 275 I = 1,NST
          IJK = I
          IF (ICNS(I) .NE. 0 ) GOTO 275
         DO 250 J = 1,NISO(I)
```

```
      IF (J .LE. JL(I) .OR. J .GE. JR(I) )THEN
       IK = 1
       IF (IK .GE. NS(I)) IK = 1
       IF (S(I,J) .LT. SVAL(I,IK)) GO TO 16
       IF (S(I,J) .LE. SVAL(I,IK+1)) GO TO 20
16     IK = 1
       JK = NS(I)+1
18     KC = (IK+JK)/2
       IF (S(I,J) .LT. SVAL(I,KC)) JK = KC
       IF (S(I,J) .GE. SVAL(I,KC)) IK = KC
       IF ( JK .GT. IK+1) GO TO 18
20     DELX = (S(I,J)-SVAL(I,IK))/(SVAL(I,IK+1)-SVAL(I,IK))

       X(I,J) =DELX*(XVAL(I,IK+1)-XVAL(I,IK))+XVAL(I,IK)
       Y(I,J) =DELX*(YVAL(I,IK+1)-YVAL(I,IK))+YVAL(I,IK)
       VX(I,J) =DELX*(VXVAL(I,IK+1)-VXVAL(I,IK))+VXVAL(I,IK)
       VY(I,J) =DELX*(VYVAL(I,IK+1)-VYVAL(I,IK))+VYVAL(I,IK)
       DL(I,J) =DELX*(DLVAL(I,IK+1)-DLVAL(I,IK))+DLVAL(I,IK)
       DT(I,J) =DELX*(DTVAL(I,IK+1)-DTVAL(I,IK))+DTVAL(I,IK)
       VR(I,J) = SQRT(VX(I,J)**2+VY(I,J)**2)
       P(I,J) = DELX*(PVAL(I,IK+1)-PVAL(I,IK))+PVAL(I,IK)
       HINV(I,J) = DELX*(HVAL(I,IK+1)-HVAL(I,IK))+HVAL(I,IK)

       IF(P(I,J) .GE. PLAST(I) )THEN
         IF(BREAKT .EQ. .FALSE.) THEN
           BREAKT = .TRUE.
           INK = IJK
         END IF
         TP(I,J) = T
         IF(ICONE(I) .EQ. 0 ) THEN
           TFIN(I) = T
         END IF
         IF ( NSTR .EQ. NST ) NTIM = I
         IF(NISO(I) .EQ. NIS ) THEN
          TIN(I) = T
         END IF
         ICONE(I) = 1
        IF(NISO(I) .EQ. JR(I)+1 ) ICJR1(I) = 1
        IF(NISO(I) .EQ. JL(I) ) THEN
         ICJL(I) = 1
         TPK(I) = (TP(I,JL(I))+TP(I,JR(I)))/2.0
        END IF

        IF(NISO(I) .EQ. JR(I) ) ICJR(I) = 1
        IF(NISO(I) .EQ. 3 ) ICTRE(I) = 1

101     IF( J .EQ. JR(I))THEN
         NISO(I) = J-2*GONE(I)
        ELSE
         NISO(I) = J-1
        END IF

        WRITE(6,*)'**Point Gone on St. Line ',I,' NISO = ',NISO(I)
       END IF
      END IF
250   CONTINUE

      IF (NISO(I) .EQ. 0) THEN
```

```
            IF(IJK .LE. INK) THEN
               WRITE(12,*)I,2*JL(I)+1,JL(I),JR(I)
            ELSE
               WRITE(8,*)I,2*JL(I)+1,JL(I),JR(I)
            END IF
               DO 333 J = NIS,1,-1

                IF (J .LE. JL(I) .OR. J .GE. JR(I) )THEN
            IF(I .LE. INK) THEN
                 WRITE(12,*)TP(I,J),'  ',C(I,J)
            ELSE
                 WRITE(8,*)TP(I,J),'  ',C(I,J)
            END IF
                END IF

                IF ( J .EQ. JR(I) ) THEN
            IF(I .LE. INK) THEN
                 WRITE(12,*)TPK(I),'  ',CPK(I)
            ELSE
                 WRITE(8,*)TPK(I),'  ',CPK(I)
            END IF
                END IF

333            CONTINUE
             DIF(I) = 0.0
             ICNS(I) = 1
             NSTR = NSTR-1
             WRITE(6,*)'** One Streamline Gone **   NSTR = ',NSTR
           END IF

           IF ( NSTR .EQ. 6) THEN
                WRITE(6,*)' *** Last Streamline Gone *** '
                CLOSE(UNIT=11)
                CLOSE(UNIT=12)
                CLOSE(UNIT=8)
                CLOSE(UNIT=26)
                CLOSE(UNIT=14)
                CLOSE(UNIT=15)



            WRITE(6,*)'******   Done   ******  '
            COMPLT = .TRUE.
            STOP
           ENDIF
275     CONTINUE


        RETURN
        END
```

```
C
C-----------------------------------------------------------------------
C
C       SUBROUTINE REDO :
C       CALLED FROM SUBROUTINE MOVE. REDOUBLES THE NUMBER OF S AND C
C       POINTS, AFTER GONE HAS REACHED QU+1
C-----------------------------------------------------------------------
C
        SUBROUTINE REDO(I,T,CR,QU,NIS)

        INTEGER NST,NISO(100),JL(100),JR(100),NH,ICNS(100)
        COMMON /COMNST/NST,NISO,JL,JR,NH,ICNS
        INTEGER GONE(100)
        COMMON /PTGONE/GONE
        REAL C(100,17),S(100,17)
        COMMON /COMCS/C,S
        REAL SCEN(100),VRCEN(100),POTCEN(100)
        COMMON /CENTRE/SCEN,VRCEN,POTCEN
        INTEGER QU
        REAL RT(1:8), CT(1:8)

        WRITE(6,100)

        DO 10, KC = 1, QU
            RT(KC) = S(I,KC)
            CT(KC) = C(I,KC)
10      CONTINUE

        DO 20, KC = QU+1, NH
            LK = NISO(I)-2*QU+KC
            RT(KC) = S(I,LK)
            CT(KC) = C(I,LK)
20      CONTINUE

        DO 30, LK  = QU, 1, -1
            KP = 2*LK
            KC = KP-1
            IF (LK .GT. 1) THEN
                S(I,KP) = RT(LK)
                S(I,KC) = (RT(LK)+RT(LK-1))/2.0
                C(I,KP) = CT(LK)
                C(I,KC) = (CT(LK)+CT(LK-1))/2.0
            ELSE
                S(I,2) = RT(1)
                S(I,1) = RT(1)-CR*(S(I,3)-S(I,2))
                C(I,2) = CT(1)
                C(I,1) = CT(1)/2.0
            ENDIF
30      CONTINUE

        DO 40, LK = QU+1, NH
            KP = 2*LK
            KC = KP+1
            IF (LK .LT. NH) THEN
                S(I,KP) = RT(LK)
```

```
                S(I,KC) = (RT(LK)+RT(LK+1))/2.0
                C(I,KP) = CT(LK)
                C(I,KC) = (CT(LK)+CT(LK+1))/2.0
              ELSE
               S(I,NISO(I)-1) = RT(NH)
               S(I,NISO(I)) = RT(NH)+CR*(S(I,NISO(I)-1)-
     &         S(I,NISO(I)-2))
               C(I,NISO(I)-1) = CT(NH)
               C(I,NISO(I)) = CT(NH)/2.0
              ENDIF
40        CONTINUE

          GONE(I) = 1
          JL(I) = NH
          JR(I) = NH+2
          WRITE(6,200)
          SCEN(I) = (S(I,JL(I))+S(I,JR(I)))/2.0

          CALL VARBLE(T,NIS)
          CALL CENTER

          RETURN

100       FORMAT (1X,' ...ENTERING SUBROUTINE REDO ... ')
200       FORMAT (1X,'REDONE')

          END
```

```
C-----------------------------------------------------------------------
C       SUBROUTINE TPEAK :
C                  TO CALCULATE MAXIMUM CONCENTRATION (CPK) OF THE
C       TRACER SLUG ON EACH STREAMLINE AND CALLS SUBROUTINE BWIDTH TO
C       CALCULATE TRACER BANDWIDTHS (BW)
C-----------------------------------------------------------------------
C
        SUBROUTINE TPEAK(NIS)

        INTEGER NST,NISO(100),JL(100),JR(100),NH,ICNS(100)
        COMMON /COMNST/NST,NISO,JL,JR,NH,ICNS
        INTEGER GONE(100)
        COMMON /PTGONE/GONE
        REAL C(100,17),S(100,17)
        COMMON /COMCS/C,S
        INTEGER ICONE(100),ICJR1(100),ICJR2(100),ICJL(100),ICJR(100),
     &          ICTRE(100),ICEN(100)
        COMMON /CONDITION/ ICONE,ICJR1,ICJR2,ICJL,ICJR,ICTRE,ICEN
        REAL CPK(100)
        COMMON /PEAK/CPK
        REAL BLR(100),BW(100)
        COMMON /BAND/BLR,BW
        REAL SCEN(100),VRCEN(100),POTCEN(100)
        COMMON /CENTRE/SCEN,VRCEN,POTCEN
        COMMON /STABLE/NTIM,IMAX,JMAX
        REAL SLAST(100),PLAST(100)
        COMMON /LASTV/SLAST,PLAST

        DO 100 I = 1,NST
         IJK = I
         IF (GONE(I) .EQ. 0) THEN
            CPK(I) = 1.0
            CHALF = CPK(I)/2.0
            CALL BWIDTH(IJK,CHALF)
         ELSE
            RC = (S(I,JR(I))+S(I,JL(I)))/2.0
            RR1 = S(I,JR(I))
            CR1 = C(I,JR(I))
            RR2 = S(I,JR(I)+1)
            CR2 = C(I,JR(I)+1)
            RL1 = S(I,JL(I))
            CL1 = C(I,JL(I))
            RL2 = S(I,JL(I)-1)
            CL2 = C(I,JL(I)-1)
            BR = (CR1-CR2)/(((RC-RR2)**2)-((RC-RR1)**2))
            BL = (CL1-CL2)/(((RC-RL2)**2)-((RC-RL1)**2))
            BLR(I) = (BL+BR)/2.0
            CPK(I) = (CL1+BL*((RC-RL1)**2)+CR1+BR*((RC-RR1)**2))/2.0

           CHALF = CPK(I)/2.0

            IF (ICONE(I) .EQ. 0 ) THEN
             CALL BWIDTH(IJK,CHALF)
```

```
            END IF

          ENDIF
100       CONTINUE

          RETURN

          END
```

```
C
C-----------------------------------------------------------------------
C       SUBROUTINE BWIDTH :
C               COMPUTES TRACER BAND WIDTHS ON EACH STREAMLINE
C-----------------------------------------------------------------------
C
        SUBROUTINE BWIDTH(I,CHALF)

        INTEGER NST,NISO(100),JL(100),JR(100),NH,ICNS(100)
        COMMON /COMNST/NST,NISO,JL,JR,NH,ICNS
        REAL C(100,17),S(100,17)
        COMMON /COMCS/C,S
        REAL BLR(100),BW(100)
        COMMON /BAND/BLR,BW

        KF = 0
        CK = C(I,1)

10      IF(CK .LE. CHALF)THEN
        KF = KF+1
        CK = C(I,KF)
        GO TO 10
        END IF

        RLH = S(I,KF-1)+(CHALF-C(I,KF-1))*(S(I,KF)-S(I,KF-1))/
     &  (C(I,KF)-C(I,KF-1))
        KF = NISO(I)+1

20      KF = KF-1
        CK = C(I,KF)
        IF (.NOT.(CK .GT. CHALF)) GOTO 20

        RRH = S(I,KF+1)-(CHALF-C(I,KF+1))*(S(I,KF+1)-S(I,KF))/
     &  (C(I,KF)-C(I,KF+1))
        BW(I) = RRH-RLH

        IF (BW(I) .LT. 0.0 ) THEN
         WRITE(6,*)'I = ',I,' Negative Band Width '
        END IF

        RETURN

        END
```

```
C-----------------------------------------------------------------------
C
C       SUBROUTINE CRECTV :
C       TO KEEP ROUNDOFF AND OTHER ERRORS FROM CHANGING INITIAL VALUE OF
C       TRACER BAND VOLUME TOO FAR.  ACTS BY ADJUSTING VALUES OF S
C-----------------------------------------------------------------------
C
        SUBROUTINE CRECTV(ALP,VC)

        INTEGER NST,NISO(100),JL(100),JR(100),NH,ICNS(100)
        COMMON /COMNST/NST,NISO,JL,JR,NH,ICNS
        REAL C(100,17),S(100,17)
        COMMON /COMCS/C,S
        REAL AVOLR,AVOLIN,VOL(100),VOLIN(100),TVOL
        COMMON /VOLUME/AVOLR,AVOLIN,VOL,VOLIN,TVOL
        REAL VCP,VC,ALP
        INTEGER ICONE(100),ICJR1(100),ICJR2(100),ICJL(100),ICJR(100),
     &          ICTRE(100),ICEN(100)
        COMMON /CONDITION/ ICONE,ICJR1,ICJR2,ICJL,ICJR,ICTRE,ICEN

        VCP = VC
        VC = 1.-AVOLR/AVOLIN

        DO 20 I = 1,NST
         IF(ICONE(I) .EQ. 1) GO TO 20
         RM = (S(I,JR(I))+S(I,JL(I)))/2.0
         DO 10, J = 1, NISO(I)
            IF ((J .LE. JL(I)) .OR. (J .GE. JR(I))) THEN
             S(I,J) = S(I,J)+ALP*VC*(S(I,J)-RM)
            ENDIF

10      CONTINUE
20      CONTINUE

         IF ((VC*VCP .LT. 0.) .AND. (ALP .GT. 0.05)) THEN
                ALP = ALP*0.5
         ELSE
                IF (ABS(VC) .GT. 0.0005) THEN
                           ALP = ALP*1.25
                ENDIF
         ENDIF

        RETURN

        END
```

```
C-----------------------------------------------------------------------
C       SUBROUTINE STWITH :
C              THIS SUBROUTINE COMPUTES THE WIDTH OF THE STREAMTUBE AT
C       THE ISOCONCENTRATION LINES. THE WIDTH OF THE STREAMTUBE IS NEEDED
C       IN COMPUTING VOLUME OF THE TRACER SLUG
C-----------------------------------------------------------------------

        SUBROUTINE STWITH

        INTEGER NST,NISO(100),JL(100),JR(100),NH,ICNS(100)
        COMMON /COMNST/NST,NISO,JL,JR,NH,ICNS
        REAL P(100,17),VR(100,17)
        COMMON /PRESS/P,VR
        INTEGER QINT(100)
        COMMON /FLOWST/QINT
        COMMON /SATWITH/SW,H
        REAL WSTCEN(100),WST(100,17)
        COMMON /CENWIT/WSTCEN,WST
        REAL SCEN(100),VRCEN(100),POTCEN(100)
        COMMON /CENTRE/SCEN,VRCEN,POTCEN


        DO 100 I = 1,NST

          IF (ICNS(I) .NE. 0 ) GOTO 100
         DO 50 J = 1,NISO(I)

           IF ( J .LE. JL(I) .OR. J .GE. JR(I) ) THEN
             WST(I,J) = QINT(I)/(VR(I,J)*H*SW)
           END IF

50        CONTINUE

           WSTCEN(I) = QINT(I)/(VRCEN(I)*H*SW)
100     CONTINUE


        RETURN
        END
```

```
C-----------------------------------------------------------------------
C       SUBROUTINE VOLUME :
C              THIS SUBROUTINE COMPUTES THE VOLUME OF THE TRACER SLUG
C       IN A STREAMTUBE. THE TOTAL VOLUME CONFINED IN 1/8 OF A FIVE SPOT
C       PATTERN IS THE ADDITION OF THE VOLUME IN EACH STREAMTUBE.
C-----------------------------------------------------------------------

        SUBROUTINE VOLUME(WVCOF)

        INTEGER NST,NISO(100),JL(100),JR(100),NH,ICNS(100)
        COMMON /COMNST/NST,NISO,JL,JR,NH,ICNS
        INTEGER GONE(100)
        COMMON /PTGONE/GONE
        REAL C(100,17),S(100,17)
        COMMON /COMCS/C,S
        REAL SCEN(100),VRCEN(100),POTCEN(100)
        COMMON /CENTRE/SCEN,VRCEN,POTCEN
        REAL AVOLR,AVOLIN,VOL(100),VOLIN(100),TVOL
        COMMON /VOLUME/AVOLR,AVOLIN,VOL,VOLIN,TVOL
        REAL CPK(100)
        COMMON /PEAK/CPK
        REAL WSTCEN(100),WST(100,17)
        COMMON /CENWIT/WSTCEN,WST
        INTEGER RNUM
        COMMON /ITER/RNUM,ITL

        REAL FUNWC(0:17),SDUM(0:17),COB(0:17),COC(0:17),COD(0:17)

        DO 25 I = 1,NST
25        VOL(I) = 0.0

        TVOL = 0.0
        DO 100 I = 1,NST

          IF (ICNS(I) .NE. 0 ) GOTO 100

            NP = 0

            DO 50 J = 1,NISO(I)

              IF ( J .LE. JL(I) .OR. J .GE. JR(I) ) THEN
                NP = NP+1
                FUNWC(NP-1) = WST(I,J)*C(I,J)
                SDUM(NP-1) = S(I,J)

                IF ( J .EQ. JL(I) .AND. GONE(I) .NE. 0 ) THEN
                  NP = NP+1
                  FUNWC(NP-1) = WSTCEN(I)*CPK(I)
                  SDUM(NP-1) = SCEN(I)
                 END IF

              END IF

50          CONTINUE

            CALL SPLINE(SDUM,FUNWC,NP,COB,COC,COD)
            SUMINT = 0.0
```

```
            CALL INTGRL (SDUM,FUNWC,NP,COB,COC,COD,SUMINT)
            VOL(I) = WVCOF*SUMINT
            TVOL = TVOL+VOL(I)

100         CONTINUE

            AVOLR = TVOL/NST


            IF (RNUM .NE. 0 .AND. ITL .NE. 1) GO TO 300
            DV = 0.0
            DO 200 I = 1,NST
             DV = DV+VOL(I)
               VOLIN(I) = VOL(I)
200         CONTINUE
            AVOLIN = DV/NST

            WRITE(6,*)' Initial average volume of the streamtube = ',AVOLIN

300         RETURN
            END
```

```
C-----------------------------------------------------------------------
C       SUBROUTINE SPLINE :
C              CALLED FROM SUBROUTINE VOLUME AND DETERMINES COEFFICIENT
C       FOR THE CUBIC SPLINE INTERPOLATER.
C-----------------------------------------------------------------------


        SUBROUTINE SPLINE (XENT,A,N,B,C,D)

        REAL XENT(0:17),A(0:17),H(0:17),ALPHA(0:17),L(0:17),
     1  MU(0:17),Z(0:17),C(0:17),B(0:17),D(0:17)
        INTEGER N,NM1,I


        NM1 = N-1
        DO 100 I = 0,NM1
         H(I) = XENT(I+1)-XENT(I)
100     CONTINUE

        DO 200 I = 1,NM1
          ALPHA(I) = 3.0*(A(I+1)*H(I-1)-A(I)*(XENT(I+1)-XENT(I-1))+
     1               A(I-1)*H(I))/(H(I-1)*H(I))
 200    CONTINUE

        L(0) = 1.0
        MU(0) = 0.0
        Z(0) = 0.0

        DO 300 I = 1,NM1
         L(I) = 2.0*(XENT(I+1)-XENT(I-1))-H(I-1)*MU(I-1)
         MU(I) = H(I)/L(I)
         Z(I) = (ALPHA(I)-H(I-1)*Z(I-1))/L(I)
300     CONTINUE

        L(N) = 1.0
        Z(N) = 0.0
        C(N) = Z(N)

        DO 400 I = NM1,0,-1
         C(I) = Z(I)-MU(I)*C(I+1)
         B(I) = (A(I+1)-A(I))/H(I)-H(I)*(C(I+1)+2.*C(I))/3.0
         D(I) = (C(I+1)-C(I))/(3.*H(I))
400     CONTINUE

        RETURN
        END
```

```
C-----------------------------------------------------------------------
C       SUBROUTINE INTGRL :
C              THIS SUBROUTINE COMPUTES THE INTEGRAL OF AN EQUATION
C       OBTAINED FROM A CUBIC SPLINE.
C-----------------------------------------------------------------------

        SUBROUTINE INTGRL(X,F,N,B,C,D,SUM)

        REAL X(0:17), F(0:17), B(0:17), C(0:17), D(0:17)
     &  ,SUM
        INTEGER N, J


         DO 100 J = 0,N-2
          SUM = SUM+F(J)*(X(J+1)-X(J))+(B(J)*(X(J+1)-X(J))**2)/2.0
     &    +(C(J)*(X(J+1)-X(J))**3)/3.0+(D(J)*(X(J+1)-X(J))**4)/4.0
100      CONTINUE

        RETURN
        END
```

```
C-----------------------------------------------------------------------
C       SUBROUTINE FRONT :
C              THIS SUBROUTINE COMPUTES THE X & Y COORDINATES FOR THE
C       FRONT LOCATIONS OF THE TRACER SLUG.
C-----------------------------------------------------------------------
C
        SUBROUTINE FRONTA

        INTEGER NST,NISO(100),JL(100),JR(100),NH,ICNS(100)
        COMMON /COMNST/NST,NISO,JL,JR,NH,ICNS
        REAL XVAL(100,2500),YVAL(100,2500)
        COMMON /XYCOORD/XVAL,YVAL
        INTEGER NS(100)
        COMMON /NPOINTS/NS
        REAL TVAL(100,2500),TBT(0:100)
        COMMON /TIMEV/TVAL,TBT

        SMIN = 1000.0
        DO 10 I = 1,NST
          IF (ICNS(I) .NE. 0 ) GOTO 10
          IF ( TBT(I) .LT. SMIN ) THEN
            NM = I
            SMIN = TBT(I)
          END IF
10      CONTINUE
        N = 15
        SINC = SMIN/N
        SB = SINC
        DO 30 J = 1,N
          DO 20 I = 1,NST
          IF (ICNS(I) .NE. 0 ) GOTO 20

            IK = 1
            IF (IK .GE. NS(I)) IK = 1
            IF (SB .LT. TVAL(I,IK)) GO TO 14
            IF (SB .LE. TVAL(I,IK+1)) GO TO 16
14          IK = 1
            JK = NS(I)+1
15          KC = (IK+JK)/2
            IF (SB .LT. TVAL(I,KC)) JK = KC
            IF (SB .GE. TVAL(I,KC)) IK = KC
            IF ( JK .GT. IK+1) GO TO 15
16          DS = (SB-TVAL(I,IK))/(TVAL(I,IK+1)-TVAL(I,IK))
            XTP =DS*(XVAL(I,IK+1)-XVAL(I,IK))+XVAL(I,IK)
            YTP =DS*(YVAL(I,IK+1)-YVAL(I,IK))+YVAL(I,IK)
20        CONTINUE
          SB = SB+SINC
30      CONTINUE

        CLOSE(UNIT=11)

        RETURN
        END
```

```
C-----------------------------------------------------------------------
C       SUBROUTINE DVEL :
C              THIS SUBROUTINE CALCULATES X & Y COORDINATES ALONG STREAM
C       LINES, VALUES OF POTENTIALS AND DARCY VELOCITY ON CORRESPONDING
C       POINTS. THESE VALUES WILL BE USED LATER FOR LINEAR INTERPOLATION.
C       ROUTINE ALSO COMPUTES VALUES OF THE LONGITUDINAL & TRANSVERSE
C       DISPERSION COEFFICIENTS.
C-----------------------------------------------------------------------

        SUBROUTINE DVEL(AD,AP,Q,BB,LAML,LAMT,NST,PARAME,PHI,PK)

        REAL VXVAL(100,2500),VYVAL(100,2500),VVAL(100,2500)
        COMMON /COMVXY/VXVAL,VYVAL,VVAL
        REAL XVAL(100,2500),YVAL(100,2500)
        COMMON /XYCOORD/XVAL,YVAL
        REAL DLVAL(100,2500),DTVAL(100,2500),HVAL(100,2500)
        COMMON /DLDTHV/DLVAL,DTVAL,HVAL
        INTEGER NS(100)
        COMMON /NPOINTS/NS
        REAL SVAL(100,2500),PVAL(100,2500)
        COMMON /DISPRES/SVAL,PVAL
        REAL V1(0:152,0:152),V2(0:152,0:152),DX(0:152,0:152)
     &       ,DY(0:152,0:152),HPOT(0:152,0:152)
        COMMON /GRIDV/V1,V2,DX,DY,HPOT
        COMMON /SATWITH/SW,H
        REAL SIGH(0:100)
        COMMON /ANGLES/SIGH
        INTEGER QINT(100)
        COMMON /FLOWST/QINT
        REAL SLAST(100),PLAST(100)
        COMMON /LASTV/SLAST,PLAST
        REAL TVAL(100,2500),TBT(0:100)
        COMMON /TIMEV/TVAL,TBT
        REAL POTEN(0:152,0:152),X1(0:152,0:152),X2(0:152,0:152)
        COMMON /LOCALG/X1,X2
        COMMON/NUMG/NX,NY

        REAL XLAST(100),YLAST(100),ICOUNT(100)
        REAL LAML,LAMT
        REAL K(152,152),KVAL(100,2500)



        DO 30 I =1,NX
          DO 30 J = 1,NY
            READ(10,*)N,X1(I,J),X2(I,J),V1(I,J),V2(I,J),HPOT(I,J)
            DX(I,J) = 1.0
            DY(I,J) = 1.0
30      CONTINUE
        CLOSE(UNIT=10)

        DO 40 I =1,NX
          READ(3,*)(POTEN(I,J),J=1,NY)
40      CONTINUE
        CLOSE(UNIT=3)
```

```
      DO 41 I =1,NX
        READ(4,*)(K(I,J),J=1,NY)
41    CONTINUE
      CLOSE(UNIT=4)

      DO 45 I = 0,NX+1
        V1(I,0) = -V1(I,2)
        V1(I,NY+1) = -V1(I,NY-1)
        V2(I,0) = -V2(I,2)
        V2(I,NY+1) = -V2(I,NY-1)
45    CONTINUE

      DO 46 I = 0,NY+1
        V1(0,I) = -V1(2,I)
        V1(NX+1,I) = -V1(NX-1,I)
        V2(0,I) = -V2(2,I)
        V2(NX+1,I) = -V2(NX-1,I)
46    CONTINUE

      PI = 3.141592654
      TBT(0) = 0.0
      SIGH(0) = 0.0
      H2 = 90.0/(NST+1)


      ANGLE = 0.0
      VMAX = 0.0
      DO 100 I = 1,NST
       I1 = I
       ANGLE = ANGLE+H2
       SIGH(I) = ANGLE*PI/180.0
       DS = SIGH(I)-SIGH(I-1)
       QINT(I) = 5.615*Q*(SIGH(I)-SIGH(I-1))/(2.*PI)
       SVAL(I,1) = 1.42
       XVAL(I,1) = SVAL(I,1)*COS(SIGH(I))
       YVAL(I,1) = SVAL(I,1)*SIN(SIGH(I))
       XP = XVAL(I,1)
       YP = YVAL(I,1)

       CALL LOCATE(XP,YP,NI,NJ)

         T1 = (XP-X1(NI,NJ))/(X1(NI+1,NJ)-X1(NI,NJ))
         U1 = (YP-X2(NI,NJ))/(X2(NI,NJ+1)-X2(NI,NJ))
       KVAL(I,1) = (1.-T1)*(1.-U1)*K(NI,NJ)+T1*(1.-U1)
     &             *K(NI+1,NJ) +T1*U1*K(NI+1,NJ+1)
     &             +(1.-T1)*U1*K(NI,NJ+1)
       VXVAL(I,1) = (1.-T1)*(1.-U1)*V1(NI,NJ)+T1*(1.-U1)
     &             *V1(NI+1,NJ) +T1*U1*V1(NI+1,NJ+1)
     &             +(1.-T1)*U1*V1(NI,NJ+1)
       VYVAL(I,1) = (1.-T1)*(1.-U1)*V2(NI,NJ)+T1*(1.-U1)
     &             *V2(NI+1,NJ) +T1*U1*V2(NI+1,NJ+1)
     &             +(1.-T1)*U1*V2(NI,NJ+1)


       VVAL(I,1) = SQRT(VXVAL(I,1)**2+VYVAL(I,1)**2)
       PAR = KVAL(I,1)*PARAME
       DTX = VXVAL(I,1)/PAR
       DTY = VYVAL(I,1)/PAR
```

```
      HVAL(I,1) = SQRT(DTX**2+DTY**2)
      DLVAL(I,1) = LAML*VVAL(I,1)
      PVAL(I,1) = -((1.-T1)*(1.-U1)*POTEN(NI,NJ)+T1*(1.-U1)
     &             *POTEN(NI+1,NJ) +T1*U1*POTEN(NI+1,NJ+1)
     &             +(1.-T1)*U1*POTEN(NI,NJ+1))
      XLAST(I) = AD-.1
      YLAST(I) = AD-.1
      TVAL(I,1) = 0.0
      ICOUNT(I) = 0
      DO 50 J = 2,2500
       I2 = J

       IF ( J .LE. 60 )THEN
        DELT = .0001
        GO TO 101
       END IF

       IF ( SVAL(I,J-1) .GE. 5.0 ) THEN
         DELT = .4/VVAL(I,J-1)
       ELSE
         DELT = .03*(1./VVAL(I,J-1))
       END IF

       IF ( DELT .GE. .3) DELT = .3
       IF ( XVAL(I,J-1) .GE. (AD-.2) .OR. YVAL(I,J-1)
     &      .GE. (AD-.2) ) DELT = .03/VVAL(I,J-1)

101    SVAL(I,J) = SVAL(I,J-1)+VVAL(I,J-1)*DELT

       IF ( XVAL(I,J-1) .LE. (AD-.1) ) THEN
         XVAL(I,J) = XVAL(I,J-1)+VXVAL(I,J-1)*DELT
       ELSE
         XVAL(I,J) = XVAL(I,J-1)
       END IF

       IF ( YVAL(I,J-1) .LE. (AD-.1) ) THEN
         YVAL(I,J) = YVAL(I,J-1)+VYVAL(I,J-1)*DELT
       ELSE
         YVAL(I,J) = YVAL(I,J-1)
       END IF

       TVAL(I,J) = TVAL(I,J-1)+DELT
       XP = XVAL(I,J)
       YP = YVAL(I,J)
       CALL LOCATE(XP,YP,NI,NJ)
        T1 = (XP-X1(NI,NJ))/(X1(NI+1,NJ)-X1(NI,NJ))
        U1 = (YP-X2(NI,NJ))/(X2(NI,NJ+1)-X2(NI,NJ))
        KVAL(I,J) = (1.-T1)*(1.-U1)*K(NI,NJ)+T1*(1.-U1)
     &              *K(NI+1,NJ) +T1*U1*K(NI+1,NJ+1)
     &              +(1.-T1)*U1*K(NI,NJ+1)
       IF ( MOD(J,10) .EQ. 0 ) THEN
        ICOUNT(I) = ICOUNT(I)+1
       END IF

         IF ( NI .EQ. 1 .OR. NJ .EQ. NY-1 ) THEN
         IF ( NI .EQ. NX-1 .OR. NJ .EQ. 1 ) THEN
           CALL VELINTP(I1,I2,PI,NI,NJ,AD,AD)
           GO TO 20
```

```
          END IF
          END IF

          VXVAL(I,J) =(1.-T1)*(1.-U1)*V1(NI,NJ)+T1*(1.-U1)*V1(NI+1,NJ)
     &                +T1*U1*V1(NI+1,NJ+1)+(1.-T1)*U1*V1(NI,NJ+1)
          VYVAL(I,J) =(1.-T1)*(1.-U1)*V2(NI,NJ)+T1*(1.-U1)*V2(NI+1,NJ)
     &                +T1*U1*V2(NI+1,NJ+1)+(1.-T1)*U1*V2(NI,NJ+1)
20        IF ( XVAL(I,J-1) .GE. (AD-.1) ) THEN
          VXVAL(I,J) = VXVAL(I,J-1)
          END IF

          IF ( YVAL(I,J-1) .GE. (AD-.1) ) THEN
          VYVAL(I,J) = VYVAL(I,J-1)
          END IF

          VVAL(I,J) = SQRT(VXVAL(I,J)**2+VYVAL(I,J)**2)
          IF (VVAL(I,J) .GT. VMAX ) VMAX = VVAL(I,J)

          PAR = KVAL(I,J)*PARAME
          DTX = VXVAL(I,J)/PAR
          DTY = VYVAL(I,J)/PAR
          HVAL(I,J) = SQRT(DTX**2+DTY**2)
          PVAL(I,J) = -((1.-T1)*(1.-U1)*POTEN(NI,NJ)+T1*(1.-U1)
     &                *POTEN(NI+1,NJ)+T1*U1*POTEN(NI+1,NJ+1)+(1.-T1)
     &                *U1*POTEN(NI,NJ+1))
          CRIT1 = BB/(LAML*VVAL(I,J))
          CRIT2 = BB/(LAMT*VVAL(I,J))

          IF (CRIT1 .LE. .0013 ) THEN
            DLVAL(I,J) = LAML*VVAL(I,J)
          ELSE
            DLVAL(I,J) = BB+LAML*VVAL(I,J)
          END IF

          IF (CRIT2 .LE. .0013 ) THEN
            DTVAL(I,J) = LAMT*VVAL(I,J)
          ELSE
            DTVAL(I,J) = BB+LAMT*VVAL(I,J)
          END IF

          IF ( XVAL(I,J) .GE. XLAST(I) .AND.
     &         YVAL(I,J) .GE. YLAST(I)    ) THEN
             SLAST(I) = SVAL(I,J)
             PLAST(I) = PVAL(I,J-1)
             TBT(I) = TVAL(I,J)
             GO TO 60
          END IF

50        CONTINUE
60        DBT = ABS(TBT(I)-TBT(I-1))
          NS(I) = J
          WRITE(6,*)'I=',I,' N=',NS(I),' T=',TBT(I)
     &             ,' S=',SVAL(I,J-1),' P=',PLAST(I),' DBT=',DBT
100     CONTINUE

        DO 150 I = 1,NST
          IF ( I.GE.26 .AND. I.LE.30 ) THEN
C         WRITE(7,*)ICOUNT(I)
```

```
          DO 125 J = 1,NS(I)

            IF ( MOD(J,10) .EQ. 0 ) THEN
C              WRITE(7,*)XVAL(I,J),'  ',YVAL(I,J)
            END IF

125         CONTINUE
           END IF
150       CONTINUE

C         CALL FRONTA

1000      FORMAT(2X,' NI ',2X,' NJ ',3X,' XP ',4X,' YP ',2X,' S ',4X,
     &          ' V1 ',8X,' V2 ',4X,' VVAL',4X,'HVAL',//)
2000      FORMAT(1X,I3,1X,I3,1X,F7.3,1X,F7.3,1X,F7.3,1X,F8.3,1X,F8.3,
     &          1X,F9.3,1XF10.5)
          CLOSE(UNIT=7)


          RETURN
          END
```

```
C-----------------------------------------------------------------------
C       SUBROUTINE VELINTP:
C       INTERPOLTATES VELOCITIES, PRESSURES ETC. THE GRID BLOCKS
C       CONTAINING WELLS.
C-----------------------------------------------------------------------


        SUBROUTINE VELINTP(I1,I2,PI,NI,NJ,AD,AP)

        REAL VXVAL(100,2500),VYVAL(100,2500),VVAL(100,2500)
        COMMON /COMVXY/VXVAL,VYVAL,VVAL
        REAL XVAL(100,2500),YVAL(100,2500)

        COMMON /XYCOORD/XVAL,YVAL
        REAL DLVAL(100,2500),DTVAL(100,2500),HVAL(100,2500)
        COMMON /DLDTHV/DLVAL,DTVAL,HVAL
        REAL V1(0:152,0:152),V2(0:152,0:152),DX(0:152,0:152),
     &       DY(0:152,0:152),HPOT(0:152,0:152)
        COMMON /GRIDV/V1,V2,DX,DY,HPOT
        REAL SIGH(0:100)
        COMMON /ANGLES/SIGH
        COMMON/NUMG/NX,NY

        DOUBLE PRECISION ANGH,ANGT,ANGL,A1,A2,A3,B1,B2,B3,A,B

        ANGH = 45.*PI/180.0
        ANGT = 90.*PI/180.0
        ANGL = SIGH(I1)

        IF ( NI .EQ. 1 .AND. NJ .EQ. 1 ) THEN

          A1 = V1(NI+1,NJ)*DX(NI+1,NJ)
          B1 = HPOT(NI+1,NJ)*DX(NI+1,NJ)
          A2 = SQRT(V1(NI+1,NJ+1)**2+V2(NI+1,NJ+1)**2)*SQRT
     &         (DX(NI+1,NJ+1)**2+DY(NI+1,NJ+1)**2)
          B2 = HPOT(NI+1,NJ+1)*SQRT(DX(NI+1,NJ+1)**2+DY(NI+1,NJ+1)**2)
          B3 = HPOT(NI,NJ+1)*DY(NI,NJ+1)
          A3 = V2(NI,NJ+1)*DY(NI,NJ+1)

          IF ( ANGL .LE. ANGH ) THEN
            A = A1+(1.4142*A2-A1)*ANGL/ANGH
            B = B1+(1.4142*B2-B1)*ANGL/ANGH
          ELSE
            A = A3+(1.4142*A2-A3)*(ANGT-ANGL)/ANGH
            B = B3+(1.4142*B2-B3)*(ANGT-ANGL)/ANGH
          END IF

          VVAL(I1,I2) = A/(SQRT(XVAL(I1,I2)**2+YVAL(I1,I2)**2))
          VXVAL(I1,I2) = VVAL(I1,I2)*COS(ANGL)
          VYVAL(I1,I2) = VVAL(I1,I2)*SIN(ANGL)
          HVAL(I1,I2) = B/(SQRT(XVAL(I1,I2)**2+YVAL(I1,I2)**2))

        END IF

        IF ( NI .EQ. NX-1 .AND. NJ .EQ. NY-1 ) THEN
```

```
      A1 = V2(NI+1,NJ)*DY(NI+1,NJ)
      B1 = HPOT(NI+1,NJ)*DY(NI+1,NJ)
      A2 = SQRT(V1(NI,NJ)**2+V2(NI,NJ)**2)*SQRT(DX(NI,NJ)**2
     &       +DY(NI,NJ)**2)
      B2 = HPOT(NI,NJ)*SQRT(DX(NI,NJ)**2+DY(NI,NJ)**2)
      A3 = V1(NI,NJ+1)*DY(NI,NJ+1)
      B3 = HPOT(NI,NJ+1)*DY(NI,NJ+1)

      IF ( ANGL .LE. ANGH ) THEN
        A = A1+(1.4142*A2-A1)*ANGL/ANGH
        B = B1+(1.4142*B2-B1)*ANGL/ANGH
      ELSE
        A = A3+(1.4142*A2-A3)*(ANGT-ANGL)/ANGH
        B = B3+(1.4142*B2-B3)*(ANGT-ANGL)/ANGH
      END IF

      VVAL(I1,I2) = A/SQRT((AD-XVAL(I1,I2))**2+(AD-YVAL(I1,I2))**2)
      VYVAL(I1,I2) = VVAL(I1,I2)*COS(ANGL)
      VXVAL(I1,I2) = VVAL(I1,I2)*SIN(ANGL)
      HVAL(I1,I2) = B/SQRT((AD-XVAL(I1,I2))**2+(AD-YVAL(I1,I2))**2)

    END IF

    RETURN
    END
```

```
C-----------------------------------------------------------------------
C       SUBROUTINE CENTER :
C               THIS SUBROUTINE COMPUTES THE VALUES OF VARIABLES AT THE
C       CENTER ISOCONCENTRATION LINE BY INTERPOLATION.
C-----------------------------------------------------------------------

        SUBROUTINE CENTER

        INTEGER NST,NISO(100),JL(100),JR(100),NH,ICNS(100)
        COMMON /COMNST/NST,NISO,JL,JR,NH,ICNS
        INTEGER NS(100)
        COMMON /NPOINTS/NS
        REAL VXVAL(100,2500),VYVAL(100,2500),VVAL(100,2500)
        COMMON /COMVXY/VXVAL,VYVAL,VVAL
        REAL SVAL(100,2500),PVAL(100,2500)
        COMMON /DISPRES/SVAL,PVAL
        REAL SCEN(100),VRCEN(100),POTCEN(100)
        COMMON /CENTRE/SCEN,VRCEN,POTCEN
        INTEGER ICONE(100),ICJR1(100),ICJR2(100),ICJL(100),ICJR(100),
     &          ICTRE(100),ICEN(100)
        COMMON /CONDITION/ ICONE,ICJR1,ICJR2,ICJL,ICJR,ICTRE,ICEN


         DO 100 I = 1,NST
          IF (ICEN(I) .EQ. 0) THEN
           IK = 1
           IF (IK .GE. NS(I)) IK = 1
           IF (SCEN(I) .LT. SVAL(I,IK)) GO TO 16
           IF (SCEN(I) .LE. SVAL(I,IK+1)) GO TO 20
16         IK = 1
           JK = NS(I)+1
18         KC = (IK+JK)/2
           IF (SCEN(I) .LT. SVAL(I,KC)) JK = KC
           IF (SCEN(I) .GE. SVAL(I,KC)) IK = KC
           IF ( JK .GT. IK+1) GO TO 18

20         DELX =(SCEN(I)-SVAL(I,IK))/(SVAL(I,IK+1)-SVAL(I,IK))

           VRCEN(I) =DELX*(VVAL(I,IK+1)-VVAL(I,IK))+VVAL(I,IK)
           POTCEN(I) =DELX*(PVAL(I,IK+1)-PVAL(I,IK))+PVAL(I,IK)
          END IF
100      CONTINUE


        RETURN
        END
```

```
C
C-----------------------------------------------------------------------
C       SUBROUTINE FRONT :
C              THIS SUBROUTINE COMPUTES THE X & Y COORDINATES FOR THE
C       FRONT LOCATIONS OF THE TRACER SLUG.
C-----------------------------------------------------------------------
C
        SUBROUTINE FRONT(T)

        INTEGER NST,NISO(100),JL(100),JR(100),NH,ICNS(100)
        COMMON /COMNST/NST,NISO,JL,JR,NH,ICNS
        REAL SVAL(100,2500),PVAL(100,2500)
        COMMON /DISPRES/SVAL,PVAL
        REAL XVAL(100,2500),YVAL(100,2500)
        COMMON /XYCOORD/XVAL,YVAL
        REAL C(100,17),S(100,17)
        COMMON /COMCS/C,S
        INTEGER NS(100)
        COMMON /NPOINTS/NS

        REAL DX, XT
        INTEGER IK, JK, KC, I

        AREA = 90000.0
        Q = 600.0
        H = 12.0
        PHI = .26
        SW = .55

C       WRITE(8,*)NST
        DO 10 I = 1,NST
           IK = 1
           IF (IK .GE. NS(I)) IK = 1
           IF (S(I,1) .LT. SVAL(I,IK)) GO TO 11
           IF (S(I,1) .LE. SVAL(I,IK+1)) GO TO 13
11         IK = 1
           JK = NS(I)+1
12         KC = (IK+JK)/2
           IF (S(I,1) .LT. SVAL(I,KC)) JK = KC
           IF (S(I,1) .GE. SVAL(I,KC)) IK = KC
           IF ( JK .GT. IK+1) GO TO 12
13         DX = (S(I,1)-SVAL(I,IK))/(SVAL(I,IK+1)-SVAL(I,IK))
           X =DX*(XVAL(I,IK+1)-XVAL(I,IK))+XVAL(I,IK)
           Y =DX*(YVAL(I,IK+1)-YVAL(I,IK))+YVAL(I,IK)
C          WRITE(8,*)X,' ',Y
10      CONTINUE

C       WRITE(8,*)NST
        DO 30 I = 1,NST
           IK = 1
           IF (IK .GE. NS(I)) IK = 1
           IF (S(I,NISO(I)) .LT. SVAL(I,IK)) GO TO 16
           IF (S(I,NISO(I)) .LE. SVAL(I,IK+1)) GO TO 20
16         IK = 1
           JK = NS(I)+1
18         KC = (IK+JK)/2
```

```
            IF (S(I,NISO(I)) .LT. SVAL(I,KC)) JK = KC
            IF (S(I,NISO(I)) .GE. SVAL(I,KC)) IK = KC
            IF ( JK .GT. IK+1) GO TO 18
20          DX = (S(I,NISO(I))-SVAL(I,IK))/(SVAL(I,IK+1)-SVAL(I,IK))
            X =DX*(XVAL(I,IK+1)-XVAL(I,IK))+XVAL(I,IK)
            Y =DX*(YVAL(I,IK+1)-YVAL(I,IK))+YVAL(I,IK)
C           WRITE(8,*)X,' ',Y
30        CONTINUE

          VPD = (5.615*Q*T)/(AREA*PHI*H*SW)
          WRITE(8,*)'* PORE VOLUME =  ',VPD

          RETURN
          END
```

```
C-----------------------------------------------------------------------
C       SUBROUTINE LOCATE:
C       EVALUATE THE INDEX OF THE REGULAR GRID BLOCKS WITH RESPECT TO
C       THE POSITIONS OF STREAMLINES.
C-----------------------------------------------------------------------

        SUBROUTINE LOCATE(X,Y,J,I)

        REAL X1(0:152,0:152),X2(0:152,0:152)
        COMMON /LOCALG/X1,X2
        COMMON/NUMG/NX,NY

        JL = 0
        JU = NX+1
10      IF(JU-JL .GT. 1)THEN
          JM = (JU+JL)/2
          IF ((X1(NX,1) .GT. X1(1,1)) .EQV. (X .GT. X1(JM,1))) THEN
            JL = JM
          ELSE
            JU = JM
          END IF
          GO TO 10
        END IF

        J = JL

        JL = 0
        JU = NY+1
20      IF(JU-JL .GT. 1)THEN
          JM = (JU+JL)/2
          IF ((X2(1,NY) .GT. X2(1,1)) .EQV. (Y .GT. X2(1,JM))) THEN
            JL = JM
          ELSE
            JU = JM
          END IF
          GO TO 20
        END IF

        I = JL


        RETURN
        END
```